ODESSA ASTRONOMICAL PUBLICATIONS

Volume 17 (2004)

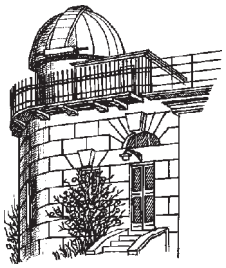

Odessa
«AstroPrint»

FOREWORD

This issue of the "Odessa Astronomical Publications" collects up the articles that were presented at the International jubilee scientific conference "Astrophysics and cosmology after Gamov: theory and observations" that has been devoted to the 100th anniversary of George Gamov (1904 – 1968). The conference was held in Odessa (Ukraine), in that city where George Gamov was born, in the period from 8 to 14 August 2004. The conference was organized by I. I. Mechnikov Odessa national University. It is that University where George Gamov started his high education.

Together with Odessa national University the following organizations took part in the conference preparation: Euro-Asian Astronomical Society (Moscow), Ukrainian Astronomical Association (Kiev), Odessa Astronomical Society, Department of astronomy, Department of theoretic physics and Research Institute "Astronomical Observatory" of I. I. Mechnikov Odessa national University. The SOC was headed by Prof. G. S. Bisnovaty-Kogan, while the Memorial and Local organizing committees – by rector of Odessa University – Prof. V. A. Smyntyna.

The scientific program of the conference included seven main sections and two affiliated sections: 1. Memorial Meeting. 2. Cosmology and Gravitation. 3. Large-Scale Structure of the Universe. 4. Gravitational Lenses in the Universe. 5. Neutron Stars and Black Holes. 6. Nucleosynthesis in Stars, Starbursts and Interstellar Medium. 7. High Energy Astrophysics. Among affiliated sections there were: 1. Small Bodies of the Solar System. 2. Astronomy in Odessa. The Memorial part of the conference was devoted to the Gamov's life, his scientific, pedagogical and popularization activity.

About 200 scientists from 18 countries of the America, Asia and Europe participated in the conference. More that 100 scientific talks were delivered there (20 of them were the plenary talks). The total number of the poster presentations was about 30. In the conference resolution it was noted that the Gamov conferences are very productive. The present conference was the third one (the first Gamov conference was held in 1994, and the second one – in 1999). It was decided to establish a good tradition for the future to organize the Gamov's conferences every three years at the regular base. We hope to see participants of the next conference in 2009.

According to the SOC decision the publication of the Gamov's conference proceeding was divided into two parts. The first part consists of the invited talks and reviews. They are published by Cambridge Press as a separate issue (Eds. Prof. G. S. Bisnovaty-Kogan and S.A. Silich). The rest of the contributions are presented here, in this Volume 17 of "Odessa Astronomical Publications".

V. G. Karetnikov

CONTENTS

Karetnikov V. G.
Foreword ... 2
Contents ... 3

Gamow memorial international conference "ASTROPHYSICS AND COSMOLOGY AFTER GAMOW – THEORY AND OBSERVATIONS"

Ryabov M.I.
Gamow's year in Odessa ... 5

Bezdenezhnyi V.P.
The histogram of Pulsars' periods distribution ... 8

Bezdenezhnyi V.P.
Nuclear isotopes and magic numbers ... 11

Bienaym'e O., Mishenina T., Kovtyukh V., Soubiran C.
Chemical and dynamical evolution in the Solar neighbourhood ... 19

Cernobai V.
G. Gamow and calculability problems of the world constantants and the life code ... 21

Dryomova G.N., Svechnikov M.A., Tutukov A.V.
Blue stragglers as a mersing product of low-massive main sequence binaries with detached components ... 25

Dugin N.A., Kuznetsova I.P., Razin V.A.
Flux density absolute measurements of Supernova Remnants using two-temperature blackbody calibration standard ... 28

Elyiv A.A., Hnatyk B.I.
The time delay of extragalactic cosmic rays in the Galactic magnetic field ... 30

Kolesnik S.Ya., Dobrovolsky A.V., Paltsev N.G.
Determination of pole and rotation period of not stabilized artificial satellite by use of model "diffuse cylinder" ... 33

Koshkin N.I., Paltsev N.G.
The set of methods and algorithms for the remote photometric and coordinate monitoring of cosmic objects ... 36

Kovtyukh V.V., Wallerstein G., Andrievsky S.M.
Discovery of two lithium Cepheids in the Galaxy ... 39

Kravetz R.O., Litvinenko O.A., Panishko S.K.
Temporal variations of ionospheric scintillation index on cosmic radiosources observations at decametric wave range ... 42

Maksyuta N.V.
Fractal model of the Universe ... 45

Marchenko V.V., Hnatyk B.I.
Relativistic shock break out at the surface of Hypernova star ... 48

Markina A.K., Skoblikova L.Ya.
Statistical characteristics of hyperbolic orbits meteors ... 51

Mikhalchuk V.V.
Determination of planetocentric coordinates of albedo details on surface of the spherical planet and some points of the illuminated part of planet's visible disk under various phase angles from ground telescopic observations 54

Miroshnichenko A.P.
Evolution Effects for Quasars and Galaxies with Jet Structure 58

Nazarova L.S., Bochkarev N.G., Gaskell C.M., Klimek E.S.
Evaluation of the disk presence in AGNs 61

Nykytyuk T.V., Mishenina T.V.
Tte magnesium abundance in the thin and thick disk of the Galaxy 63

Ostrovskiy N.V.
Physical Model of the Orbital Movement of the Jupiter Satellite Sinope 67

Popov A.M., Smolyakov M.N.
Inflation Theories and Plank Mass Problem 70

Prigara F.V.
Induced Radio and X-ray Emission from an accretion disk 73

Shakun L.S., Motrich V.D., Melykjants S.M.
Calculate method of the twilight sky brightness in the Solar vertical, stipulated by a multiple scattering of a sunlight 78

Shatsova R.B., Anisimova G.B.
Natural modeling of galactic and extragalactic structures 82

Sirotkin F. V.
Two scenarios of mass exchange in close binary systems consisting of the low mass pre-main sequence stars 84

Smirnov V.A.
The wave principle of the distribution of substance in Solar system 91

Smirnov V.A.
Radiation of spectra of meteor 93

Solonovich A.P., Bryukhanov I.S., Sergey I.M.
Searches of the Periods and Definition of Variability Types of New Variable Stars TX Crv, DP Cam, IRAS 17583+5150 96

Sukhov P.P., Movchan A.I., Koshkin N.I., Korniychuk L.V., Strakhova S.L., Epishev V.P.
Some results of the photometry of GEO objects 99

Tsivilev A.P., Sorochenko R.L., Cortiglioni St., Poppi S., Montebugnoli St.
Primordial helium abundance by RRL: new result 103

Udovichenko S.N.
Photometric investigation of XX CYG 106

Vasil'eva S.V., Gopka V.F., Yushchenko A.V., Andryevsky S.M.
Abundances of *r*-process elements in the photosphere of red supergiant star PMMR23 in Small Magellanic Cloud 109

Yasinskaya M.P., Dragunova A.V.
Interstellar absorption in some directions 113

Yushchenko A.V., Gopka V.F.
Stellar abundance. From quantity to quality? 116

GAMOW'S YEAR IN ODESSA

M.I. Ryabov

Chairman of Odessa Astronomical Society

In 2004 we celebrated 100th anniversary of great physicist and astrophysicist of XX century, corresponding member of USSR Academy of science, professor G.A.Gamow.

G.Gamow was born in Odessa on March 4, 1904, in teachers' family. Their roots were connected with significant events in Ukrainian and Russian history. Mother's side (A.A.Lebedintseva) was presented by the superior priesthood. His grand-father Arseniy Lebedintsev was Odessa cathedral archpriest and Chairman of Kherson ecclesiastic society. By father's side there were military people. Another grand-father was Army Commander in Kishinev.

G.Gamow graduated from Odessa gymnasium and continued his education in Odessa University. At the same time he was working as calculator in astronomical observatory.

Then he graduated from St.-Petersburg University and started to work in Leningrad, Cambridge, Copenhagen, Paris. For a long time he was working as professor in Cambridge University, USA.

G.Gamow achieved great results in quantum mechanics, atomic and nuclear physics, astrophysics, cosmology, biology and history of physics. He was working with such famous scientists of XX century as A. Einstein, N. Bor, E. Reserford, Maria Kyjury, L. Landau.

Among his main scientific achievements are creation of alpha and beta decay, use of nuclear physics for explaining the star evolution theory. G.Gamow worked out the theory of "hot Universe" - basis of nowadays cosmology explaining the Universe creation theory.

G.Gamow was the first who could decipher the genetic code. He was an eminent popularizer of science. In 1994 and 1999 large-scale international conferences were carried out. They were devoted to the 90th and 95th anniversary of Gamow. After these events the Public Garden after Gamow appeared.

At the February session of Scientific Unit of Odessa National University professor V.Smyntyna declared about carrying out "Gamow's Year" in Odessa. Also there was told about setting up an annual "Gamow's scholarship" for the best students in astronomy and physics, and about issue of Jubilee Gamow's medal.

Program "Gamow's Year" was announced on TV and mass-media. Firstly the ceremonial session was carried out in the House of Scientists. Professor V.Smyntyna opened the evening. Dr. M.Ryabov, Dr. A.Andrievsky, Prof. I.Andronov, Prof. S.Andrievsky, Prof. A.Zhuk advanced with reports. Professor I.L.Gamow (Rector of Russian-Pridnestrivsky University) spoke about Gamow's family history. After the musical ensemble "Lyra"had perfprmed the memoril party was over.

Regional and municipal conferences "Modern astronomy in school education" were also devoted to Gamow's anniversary. They were carried out by support of the Regional and municipal government of education in Odessa.

Second Municipal conference was held on 18th of March in the House of Scientists. Regional conference was carried out in Assembly Hall of Odessa national university in April. Professor S.Andrievsky, I.Andronov, assistant professor M.Ryabov, A.Khalevin, scientific workers L.Kudashkina and V.Marsakova took part in it. A Resolution supporting astronomical education in Odessa and Odessa region was set up.

At every faculty throughout 2003-2004 and 2004-2005 academic years lectures were delivered - "Universe around us" explaining the nowadays scientific picture of the world. Great contribution in it had been made by G.Gamow.

International scientific conference "Astrophysics and Cosmology after Gamow - theory and observations" (8-14 August 2004) was held at Odessa National University. Chairman of SOC was professor G.S.Bisnovatyi-Kogan (Russia). Vice-chairmen SOC were professor A.Zhuk (ONU, Odessa) and professor S.Silich (Mexico, Ukraine). Among members of Scientific and Memorial committees were such famous astrophysicist as professor I.Novikov (Denmark), professor A.Cherepashchuk (Russia), P.Gonsalez-Dias (Spain), R.Terlevich (Mexica), V.Rudenko (Russia), I.Gamow (USA), Ya.Yatskiv (Ukraine).

Conference worked in 8 sessions. Chief of the Memorial meeting was professor A.Chernin (Russia). Chief of the session "Large-scale structure of the Universe and gravitational lenses In Universe" - professor B.Novosjadly (Lvov, Ukraine). Session "Neutron stars and black holes" - professor M.Porokhov (Moscow, Russia). Session "NucleoSynthesis in stars, stars creation, interstellar space" - pro-

fessor N.Bochkarev (Moscow, Russia). Session "Astrophysics of high energies" - professor B.Gnatyk (Kyiv, Ukraine). Session "Small solids in solar system" - professor K.Churyumov. Session "Astronomy in Odessa" - professor V.Karetnikov (Odessa, Ukraine). Conference was opened by rector of ONU professor V.Smyntyna. Famous scientists and participants of the conference were awarded with Gamow's medals.

Many letters with wishes of future successful work were sent to SOC and LOC orgcommittee. The most important congratulation was from the Presidium and Department of physics and astronomy of Ukrainian National academy of science (UNAS), sent by Vice-President of NAS Academician A.Naumovets and academician-secretary V.Loktev.

Participants of the conference were greeted by: President of Ukrainian Astronomical Association (UAA), Academician of UNAS Ya.Yatskiv, Vice-president of European Astronomical Society, corresponding member of RAS, Prof. A.Cherepashchuk, chairman of International Bureau of Euro-Asian Astronomical Society Prof. N.Bochkarev, Russian General Consul in Odessa F.Dovzhenyuk, Academician-secretary of Georgian Academy of science Prof. D.Lominadze. President of UAA Ya.Yatskiv presented to ONU the certificate of naming a minor planet "Gamow".At the memorial Session were presented 10 reports and 3 video reports were presented: About 200 scientists from 18 countries participated in the conference. The majority was from Ukraine and Russia. Representatives of USA, France, Spain, Germany, Poland, Slovakia, Serbia, Italy, Mexico, Japan, Byelorussia, Kazakhstan, Turkmenistan, Denmark, Georgia and Great Britain were presented too. At the plenary session were presented 20 reports, connected sections of cosmology and astrophysics, in which Gamow worked. And the most important thing is that there appeared and new directions of observations. At the 7 scientific sessions 80 oral reports and 30 poster reports were presented. Results of the conference work will be observed in special edition "Conference Transactions" by the Cambridge Press publisher and in the magazine "Odessa Astronomical Publications".

Participants of the conference have met with mayor of Odessa R.Bodelan. During this meeting questions of science development and organizing Gamow's centre with Planetarium were discussed. Conference was held in "Gamow's style" - with surprises and unexpectedness.

The weather was fine and favorable for the guests of the city. This was demonstrated during traditional "sea beach session".

Gamow's conferences are carried out 3rd time in every 5 years and have their special traditions. Between them Gamow's summer schools take place: "Astronomy and beyond: Astrophysics, Cosmology and Astrobiology". Its organizers were: Astronomical Observatory and Chair of Astronomy of Odessa National University, Ukrainian Astronomical Association, Euro-Asian Astronomical Society, Odessa Astronomical Society. Chairman of the conference organizing committee was Rector of ONU V.A.Smyntyna. Vice-chairmen - Prof. V.G.Karetnikov and Dr. M.Ryabov. I.Chernishova, S.Melikyants, A.Pilipenko took part in Secretariat Gamow's Conference and Gamow Summer School in different years. All problems were solved by the orgcommittee with help of employees of Astronomical Observatory and Department of Astronomy of ONU. Carrying out the conference became possible thanks to all the pro-rectors and departments of ONU.At the end of the conference participants adopted the Resolution.

Resolution of International Scientific Conference: "Post Gamow's Astrophysics and Post-Gamow's Cosmology", devoted to 100th anniversary of G.Gamow

Participants of the conference presenting 17 countries of Europe, America and Asia, paid a tribute of respect to scientific achievements of G.Gamow, which were always created on the junction of different sciences and sections of astrophysics, cosmology and biology.

G.Gamow was the first to use quantum mechanics for explaining alpha decay. With E.Teller he worked out the theory of beta decay, at first constructed the star evolution theory, based on nuclear energy, and showed the role of the neutron in the explosion of supernova and new stars.

G.Gamow offered the model of "Hot Universe". With R.Alfer and R.Kharman calculated the theory of Universe creation and predicted the existence of Relict Radiation. He also worked out the system of information code of DNK protein molecule and deciphered the genetic code.

These theories are the basis of today's science. Ideas and methods used by G.Gamow anticipated the main directions of science development in XX and XXI centuries.

G.Gamow made a great contribution to science popularization, published many popular scientific books, and for this he was rawarded with the prestige international YUNESKO prize. And today this work of his is vitally important for the influx of youth in science, for popularization of physics and astronomy at schools and institutes.

G.Gamow worked in many international centers of Europe and USA (Leningrad, Cambridge, Copenhagen, Paris, Washington, Colorado, Copenhagen, Gettingen), but in his scientific style always assisted "Odessa roots" - features of the city, where he was born and studied.

Participants of the conference think it necessary:

1. To thank Astronomical Observatory and Department of Astronomy of ONU after Mechnikov and Odessa Astronomical Society for organizing and carrying out the international scientific conferences, devoted to the memory of G.Gamow in 1994, 1999, and especially in 2004 - in the year of his 100th anniversary.

2. To consider the International Gamow's scientific conferences "Astrophysics and Cosmology after Gamow" as traditional and to carry out them every 5 years in Odessa.

3. To support the proposals about organizing an International Gamow's Scientific-Educational Centre with Planetarium on the territory of astronomical observatory.

4. To support the proposals about organizing in Odessa the International Gamow's Fund for development science and education.

5. To appeal to institutes and universities of those countries, where G.Gamow worked, to International physics and astrophysics societies with information about carrying out the conference with proposal to support organizing an International Gamow's Scientific-Educational Centre and Odessa International Gamow's Fund.

6. To appeal to President of Ukrainian National Academy of science and to President of Russia Academy of science about issue of annual academic Gamow's medal, awarded for scientific achievements in theoretical physics and astrophysics.

7. To support an annual carrying out the International Gamow's summer astronomical school: "Astronomy and beyond: Astrophysics, Cosmology and Astrobiology" for young scientists, students and graduates (on the basis of ONU).

8. To welcome carrying out in Odessa regional and municipal teachers' conferences "Today's Astronomy in school education" for development astronomical education in schools.

9. To support the proposal of Astronomical observatory and Chair of astronomy of ONU about creation Summer astronomical Center for Odessa region schools (on the basis of Astronomical station Kryzhanovka).

10. To support proposal of ONU about setting up a memorial plague on the house, where G.Gamow was born, and memorable token in the City Public Garden named after G.Gamow in Odessa.

On discussion

THE HISTOGRAM OF PULSARS' PERIODS DISTRIBUTION

Vladimir P. Bezdenezhnyi
Department of Astronomy, Odessa National University
T.G.Shevchenko Park Odessa 270014 Ukraine
astro@paco.odessa.ua

ABSTRACT. In considering of the distribution of periods for pulsars taken from Smith (1979) and GCVS (1976) data 20 peaks are found: at 0.672 sec, 0.450 sec, 0.403 sec, 0.270 sec, 0.191 sec and other smaller peaks. Identifications and comparison with the distribution of periods for δ Scuti stars are carried out.

Key words: Stars: pulsars, δ Scuti, RR Lyrae, Cepheids.

In Table 1 a histogram of pulsars' periods distribution (n=105 stars) based on the data taken from the book "Pulsars" by Smith (1979) is presented.

The intervals of periods ΔP are taken as 0.05 sec. For control we give a histogram with intervals ΔP=0.1 sec (see Figure 1). In Table 2 and in Figure 2 the same histograms based on the data (n=147 stars) taken from "Third supplement to the third edition of the General Catalogue of Variable stars" (Kukarkin et al., abbreviation: GCVS, 1976) are given.

Table 1: The histogram of pulsars' periods distribution (n=105 stars)

ΔP	n_{puls}	ΔP	n_{puls}
0.00-0.05	1	1.20-1.25	4
0.05-0.10	1	1.25-1.30	4
0.10 0.15	0	1.30-1.35	1
0.15-0.20	6	1.35-1.40	3
0.20-0.25	4	1.40-1.45	1
0.25-0.30	4	1.45-1.50	0
0.30-0.35	3	1.50-1.55	1
0.35-0.40	7	1.55-1.60	1
0.40-0.45	6	1.60-1.65	0
0.45-0.50	6	1.65-1.70	1
0.50-0.55	5	1.70-1.75	0
0.55-0.60	5	1.75-1.80	0
0.60-0.65	2	1.80-1.85	0
0.65-0.70	8	1.85-1.90	1
0.70-0.75	6	1.90-1.95	0
0.75-0.80	3	1.95-2.00	1
0.80-0.85	4	2.00-2.05	0
0.85-0.90	1	2.05-2.10	0
0.90-0.95	1	2.10-2.15	1
0.95-1.00	0	2.15-2.20	0
1.00-1.05	2	2.20-2.25	1
1.05-1.10	2	2.25-2.30	1
1.10-1.15	0	2.30-2.35	1
1.15-1.20	1	3.70-3.75	1

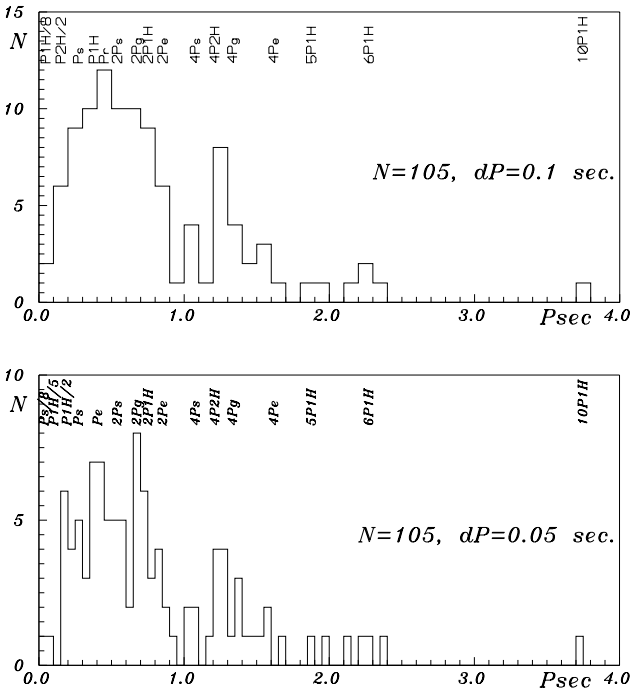

Figure 1: The distribution of pulsars' periods based on the data of the sampling according to Smith (1979).

We used intervals ΔP=0.02 sec for control of our results too. On the base of our analyses of these histograms 20 peaks (maxima) at the following periods P_i and frequencies f_i corresponding to them are obtained (see Table 3). As it can be seen from figures and Table 3, the highest peaks are: P_{11}=0.672 sec, P_8=0.403 sec, P_9=0.448 sec, P_6=0.270 sec and P_5=0.191 sec. The ratios of the periods show that all periods are commensurable (often - multiple ones), as in the case of pulsating stars: δ Sct, bimodal Cepheids, RR Lyrae and other types. The histogram of pulsars' periods distribution is similar to one of δ Scuti stars

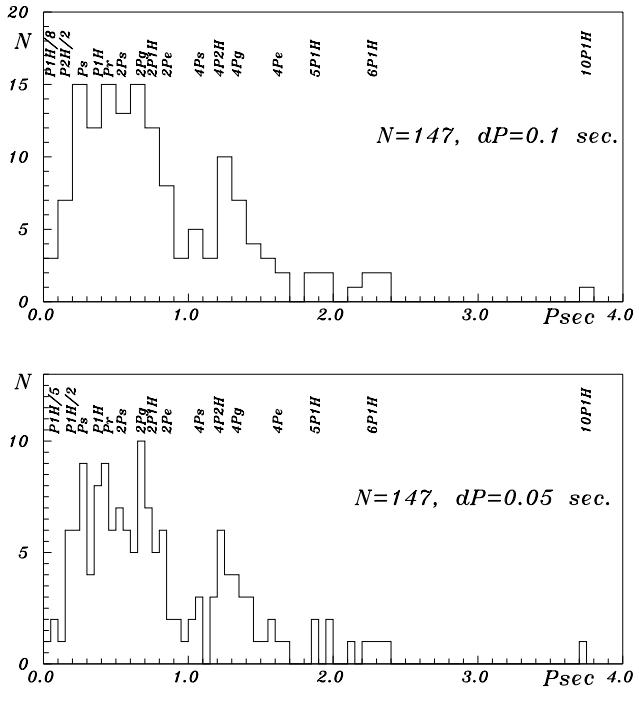

Figure 2: The distribution of pulsars' periods based on the data of the sampling according to GCVS (1976).

(Bezdenezhnyi, 1994b).

We can see five sequences of multiple periods. The first sequence is: $P_7 = 8P_2 = 5P_3 = 2P_5 = P_{12}/2 = P_{18}/5 = P_{19}/6 = P_{20}/10$. Eight periods are connected with multiple relation, and moreover the period P_7 is favoured one. We accept it for the main period and make up the ratios of every period P_i to the period P_7. The second sequence is: P_6=8P_1= $P_{10}/2$=$P_{14}/4$. And three more multiple relations are: $4P_8$=2P_{13}= P_7, P_{15}=8P_4 and 2P_{11}=P_{16}. Only period P_9 has no multiple ones in this table. Thus, we have five groups of periods, inside of wich multiple relations take place. The primary periods are: P_7, P_6, P_8 and $P_{11}/2$ (because period P_{11} lies between two double periods P_{10}=2P_6 and P_{12}= 2P_7. We add two periods P_9 and 2P_4 to these primary ones as the period P_4 lies beside half period P_5. These six periods give us chance to make identifications as in the case of pulsating stars. We accept period P_7 as P_{1H} one - the first overtone of some fundamental period that is not seen in our histograms. The last column of Table 3 contains possible interpretations of these peaks.

From our list of periods we have probable identifications: P_6=P_s, P_8=P_e, P_9=P_r and $P_{11}/2$=P_g. These are periods introduced by the author earlier (Bezdenezhnyi, 1994a, 1994b, 1997) for RR Lyr -type and δ Sct stars. And period 2P_4 is identified as P_{2H} (the second overtone). At such identifications the theoretical ratios k_{theor}= P_i/P_{1H} are given in the fifth column of Table 3. The observed P_i/P_7 ratios are close

Table 2: The histogram of pulsars' periods distribution (n=147 stars)

ΔP	n_{puls}	ΔP	n_{puls}
0.00-0.05	1	1.20-1.25	6
0.05-0.10	2	1.25-1.30	4
0.10 0.15	1	1.30-1.35	4
0.15-0.20	6	1.35-1.40	3
0.20-0.25	6	1.40-1.45	3
0.25-0.30	9	1.45-1.50	1
0.30-0.35	4	1.50-1.55	1
0.35-0.40	8	1.55-1.60	2
0.40-0.45	9	1.60-1.65	1
0.45-0.50	6	1.65-1.70	1
0.50-0.55	7	1.70-1.75	0
0.55-0.60	6	1.75-1.80	0
0.60-0.65	5	1.80-1.85	0
0.65-0.70	10	1.85-1.90	2
0.70-0.75	7	1.90-1.95	0
0.75-0.80	5	1.95-2.00	2
0.80-0.85	6	2.00-2.05	0
0.85-0.90	2	2.05-2.10	0
0.90-0.95	2	2.10-2.15	1
0.95-1.00	1	2.15-2.20	0
1.00-1.05	2	2.20-2.25	1
1.05-1.10	3	2.25-2.30	1
1.10-1.15	0	2.30-2.35	1
1.15-1.20	3	2.35-2.40	1
–	–	3.70-3.75	1

Table 3: Results of identifications of pulsars' periods

i	P_i(sec)	f_i(1/sec)	P_i/P_7	k_{theor}	ident.
1	0.033	30.303	0.087	0.089	$P_s/8$
2	0.047	21.277	0.124	0.125	$P_{1H}/8$
3	0.075	13.333	0.199	0.200	$P_{1H}/5$
4	0.150	6.667	0.397	0.400	$P_{2H}/2$
5	0.191	5.236	0.506	0.500	$P_{1H}/2$
6	0.270	3.704	0.715	0.711	P_s
7	0.3775	2.649	1	1	P_{1H}
8	0.403	2.481	1.068	1.067	P_e
9	0.448	2.232	1.187	1.185	P_r
10	0.538	1.859	1.425	1.422	$2P_s$
11	0.672	1.488	1.780	1.778	$2P_g$
12	0.750	1.333	1.987	2	$2P_{1H}$
13	0.801:	1.248	2.122	2.133	$2P_e$
14	1.075	0.930	2.848	2.844	$4P_s$
15	1.210:	0.826	3.205	3.200	$4P_{2H}$
16	1.332:	0.751	3.528	3.556	$4P_g$
17	1.616:	0.619	4.281	4.264	$4P_e$
18	1.875	0.533	4.970	5	$5P_{1H}$
19	2.270	0.441	6.010	6	$6P_{1H}$
20	3.745:	0.267	9.920	10	$10P_{1H}$

to theoretical ones from multiplicity viewpoint. In 19 cases of 20 the observed period ratios are different from theoretical ones within 0.03.

Thus, similarly to pulsating stars, the periods of pulsars are close to periods P_{1H}, P_{2H}, P_r, P_e, P_g, P_s and multiple to them ones. It is curiously that fundamental period P_f is absent in this range.

References

Bezdenezhnyi V.P.: 1994a, *Odessa Astron. Publ.,* **7**, 55.

Bezdenezhnyi V.P.: 1994b, *Odessa Astron. Publ.,* **7**, 57.

Bezdenezhnyi V.P.: 1997, *Odessa Astron. Publ.,* **10**, 95.

Kukarkin B.V., Kholopov P.N. et al.: 1976, *Third Supplement to the third edition of the General Catalogue of Variable Stars,* Nauka, Moscow, 324.

Smith F.G.: 1979, Pulsars, Moscow, 256.

NUCLEAR ISOTOPES AND MAGIC NUMBERS

V.P. Bezdenezhnyi

Astronomical observatory, Odessa National University
T.G.Shevchenko Park, Odessa 65014 Ukraine, *astro@paco.odessa.ua*

Dedicated to D.I.Mendeleev's 170-th anniversary, to the 135-th anniversary of Periodic Law discovery and to G.A.Gamov's 100-th anniversary

ABSTRACT. In addition to the formulas (1) and (2) from work of the author (Bezdenezhnyi, 1999, hereafter Paper I) alternative formulas (3)–(6) are derived for description of two sequences of magic numbers. Their properties are described. Dependences of some physical parameters as a function of the number of chemical element (Z), number of neutrons (N) and the mass number (A) are analysed. It is shown that magic numbers of protons (Z) and neutrons (N) are displayed in them. The concept of magic mass numbers (A) is proposed, and it is shown that they are also present in some dependences. The list of magic and twice magic (on Z and N) elements is extended, as well as the list of twice magic ones on A and Z or N. We propose to refer a nucleus that contains magic numbers of protons and neutrons to thrice magic nucleus if their sum is a magic number too. It is suggested that during the decay of "double -uranium" super-nucleus one of three twice magic elements (X(112,168), Y(126,184) and Z(168,258) or Z'(168,240)) predicted (in Paper I) will be formed fragment accompanying in areas of twice magic nuclei: Yb(70,112), Sn(50,70) and S(16,16) respectively.

Key words: nuclear astrophysics, r-, s-processes, Mendeleev's periodic system, isotopes, magic numbers

1. Introduction

As is generally known from nuclear physics (Mukhin, 1974), atomic nuclei containing certain numbers (2, 8, 20, 28, 50, 82, 126) of protons (P) or neutrons (N) show an enhanced stability that makes them distinguished among other nuclei neighbouring them. They are named as magic nuclei (isotopes of chemical elements), and the numbers of their protons and neutrons are called "magic numbers". Their explanation lies in the envelope nucleus model, in which the nucleons form the filled envelopes separately for P and N. According to the model of nucleus envelopes the nucleon energy levels with close values of energy are grouped into series far apart from each other which are called nucleon envelopes. According to the Pauli principle, a certain number of nucleons of a given kind can be placed on each envelope. Whenever an envelope is filled, it corresponds to the magic nucleus formation with the respective magic number. Nucleon envelopes of protons and neutrons are filled independently. The simultaneous filling up of proton and neutron envelopes is followed by a corresponding formation of particularly stable twice magic nucleus. At the same time the saturation of forces of nuclear interaction is attained - a high value of nuclear package (mass defect).

In previous author's work (Paper I), the Table (117.8) from "Quantum Mechanics" (Landau and Lifshits, 1963) has been analysed and two recurrentformulas have been found connecting all the set of magic numbers and corresponding to their two sequences - large and small ones:

$$M_i = M_{i-1} + \sum J(i-2) + J(i), \text{where i=1, 2,...} \quad (1)$$

$$m_{i-2} = M_i - J(i), \text{where i = 3, 4,...} \quad (2)$$

The numeral values, counted up on these formulas, are the following:

M_i: 2, 6, 14, 28, 50, 82, 126, 184, 258, 350, 462, ...
m_i: - - 8, 20, 40, 70, 112, 168, 240, 330, 440, ...

In that way, new magic numbers: 6, 14, 40, 70, 112, 168, 240, 258, 330, 350, 440, 462 were added to the before known ones. Numbers of neutrons 16, 96, 114, 152, appearing in the literature, are not magic ones: three from them are numbers of alpha-particle configurations, and 114 is a difference of magic numbers 184 and 70. The quantity of the nuclei referred to magic and twice magic ones was increased in connection with the increasing of the quantity of magic numbers. The author added (6,6), Si(14,14), Ni(28,28), Zr(40,50) Sn(50,70) to the previously known twice magic nuclei of isotopes: He (2,2), O(8,8), Ca(20,20), Pb(82,126). All of them have high peaks in abundance curve of isotopes (Figure 1 from author's quoted work according to Lang's (1978) data). Small double peaks in the well known curve

of elemental abundances (Zyuss and Yuri) at magic numbers of neutrons 28, 40, 70, 112 have been added to double peaks of r-, s-processes of neutron capture at magic numbers 50, 82, 126. They convincingly confirm an existence of these two capture processes.

2. New results

Recently the author added the nuclei of isotopes Si (14,20), Ca (20,28), Ni (28,40), C (6,8), O (8,6), He(2,6) to twice magic ones. It is logically to name three last isotopes, and also Ca(20,20) and Si(14,14) as thrice magic nuclei, as they have simultaneously magic numbers of protons (Z) and neutrons (N) and their sum (mass number A=Z+N) is a magic number too. Magic mass numbers (for example =258) also are proved in the plots of dependences of some physical parameters.

Combining both sequences in one series, we have the first 20 magic numbers: 2, 6, 8, 14, 20, 28, 40, 50, 70, 82, 112, 126, 168, 184, 240, 258, 330, 350, 440, 462. Taking the differences between neighbouring values, we get series of 19 members: 4, 2, 6, 6, 8, 12, 10, 20, 12, 30, 14, 42, 16, 56, 18, 72, 20, 90. It is easily to notice that this series consists of two sequences of numbers - odd D_{2n-1} and even D_{2n}, the members of which are described by the following formulas:

$$D_{2n-1} = 2(n+1), \text{where n = 1, 2, ..., 10} \qquad (3)$$

$$D_{2n} = n(n+1), \quad \text{where n = 1, 2, .., 9} \qquad (4)$$

Thus, every subsequent member is expressed through previous one by formulas:

$$M_1 = 2, \qquad (5)$$

$$M_{i+1} = M_i + D_i, \quad \text{where i = 1, 2, 3, ...} \qquad (6)$$

are determined as $i = 2n$ or $i = 2n - 1$ for n in formulas (3) and (4). For example, at $n = 1$ D_{2n-1} $= D_1 = 2(1 + 1) = 4$ and $M_2 = M_1 + D_1$=2+4=6, D_{2n}=D_2=2 and M_3=M_2 + D_2=6+2=8 and etc.

In the model of nucleus with nucleon orbits, the Quantum Mechanics calculations for rectangular potential well give (Table 21, Enrico Fermi, 1951) the total numbers of filled states for closed shells: 2, 8, 20, 40, 70, 112, 168, ... Numbers 40, 70 and 112 coincide with those obtained by the author (Paper I), but the numbers 6, 14 and 28 are not present in this table. The numbers 2, 8, 20, 50, 82, 126 were referred to the magic ones, because nuclei with such number of protons or neutrons appeared especially steady and these numbers are confirmed by experiment. However, other numbers of nucleons in the closed shells become apparent in the experiment.

It will be shown in present work that magic numbers 6, 28, 40, 70, 112, 168, 184, 240, referred by author, also become apparent in experimental dependences between the physical parameters of isotopes. So, in Figure D2 taken from Luc Valentin's (1986), the effects of shells and magic numbers are superimposed upon the smooth dependence of binding energy as a function of the mass number (A) at N=28 and 50, Z=50, N=82 (marked there) and at twice magic nucleus Pb(82,126), but also distinct peaks are seen (Figure 1) at the twice magic O(8,8), thrice magic Si(14,14), twice magic (on A and N or Z): N=28 (A=50), Z=40 (N=50), Z=50 (N=70), Z=50 (N=82), Z=70 (N=82) and Z=112 (N=126). Noticeable declinations of the theoretical curve for binding energy from the experimental values for the lightest nuclei (Figure 4.3, Luc Valentine, 1986) are also explained by the effect of magic numbers: at A=4 (Z=N=2) and A=12 (Z=N=6).

The physicists discuss daring ideas of producing new nuclei by fission of super-heavy unstable nucleus of the "double- uranium" type R(184,292) obtained by bombardment of uranium target with ion U(92). The fission usually occurs in the fragments of unequal masses. Therefore, at this fission new transuranium elements can arise as well as new isotopes lighter than uranium.

Owing to this we had to extend the boundaries of Table 2 (Paper I). The following terms of both sequences of magic numbers: M_{10}=350, M_{11}=462 and m_8=330, m_9=440 were calculated by formulas (1) and (2). As a result of this, it is suggested that the super-nucleus may decay into one of four mentioned above twice magic isotopes X(112,168), Y(126,184) and Z(168,258) or Z'(168,240) plus fragment in areas of twice magic nuclei Yb(70,112), Sn(50,70) and S(16,16) respectively. It could serve as a test for presence of these unobserved twice magic isotopes by means of analysis of those fragments.

3. Properties of magic numbers

1) All magic numbers are even.
2) They fit to the recurrent formulas (1)-(2) or (3)-(6).
3) They are the sums of two or three other magic numbers: 8=2+6, 14=6+8, 20=6+14, 28=20+8, 50=40+8+2 (or 50=28+14+8); 70=50+20, 82=40+28+14, 112=70+28+14 (or 112=70+40+2), 126=112+14; 168=126+40+2 (or 168=126+28+14); 184=168+14+2 (or 184=126+50+8); 240=184+50+6 (or 240=168+70+2); 258=112+126+20, 330=184+126+20 (or 330=168+112+50), 350=330+20 (or 350=184+126+40), 440=350+82+8 (or 440=350+50+40), 462=350+112.
4) Multiplicities among magic numbers: eight from the first twenty magic numbers are multiple to the magic number 14: 28, 70, 112, 126, 168, 350, 462; eight magic numbers are multiple to the number ten: 20, 40, 50, 70, 240, 330, 350, 440. The numbers 70 and 350 can be met in both multiplicities; remaining six numbers are multiple too: 2 and 82=241, 6 and

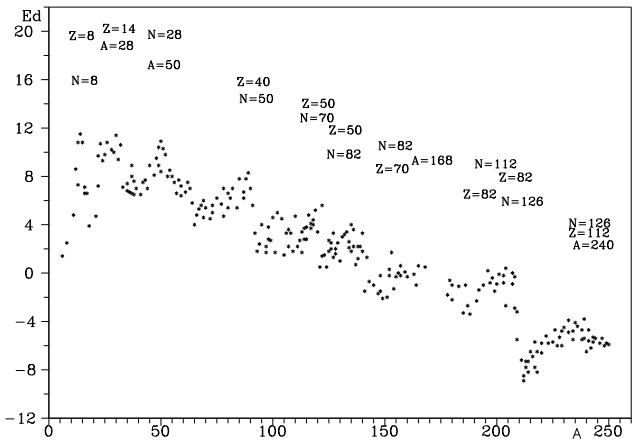

Figure 1: The effects of magic numbers in the dependence of binding energy as a function of the mass number A.

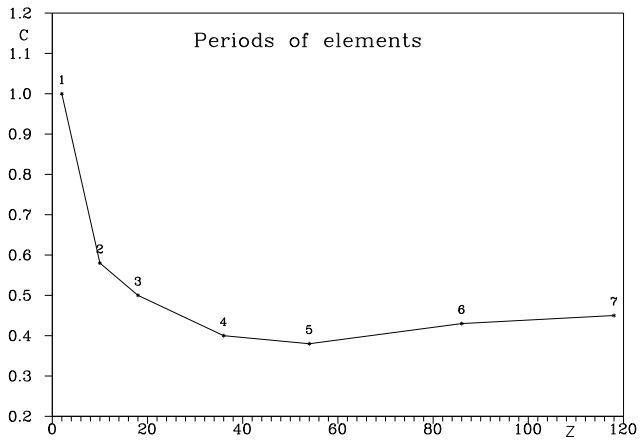

Figure 2: The dependence of C-ratio as a function of the maximal value of Z for every period of chemical elements.

258=643, 8 and 184=823. Besides, the numbers 23, 41 and 43 are the prime ones.

5) Numbers multiple to magic are also developed in dependences of physical parameters: 12, 16, 32, 56, 80, 164 et al.

6) In Figure 2 dependence of ratio (C) of the mean value of magic numbers on Z to similar ones on A for every period of chemical elements is shown as a function of the maximal value of Z for this period. Minimum C-values in the fifth period is seen.

4. Appearances of magic numbers in dependences of physical parameters

a). Behaviour of the packing factor.

Aston (1948) chose the oxygen atom 16 as the most appropriate standard. And percent deviation of masses of other atoms from an integer on this scale, shown in tenthousandth, was adopted by a packing factor. The graphical dependence of the packing factor (taken from Aston's (1948) data on isotopic weights) as a function of proton number shows a presence of magic numbers Z=2, 6, 8, 20, 28, 40, 50, 70 and 82. There is a minimum on the smoothed curve of the packing factor at Z=28 (Figure 3).

b). Dependence of neutron excess on atomic number.

Dependence of atom isotopic number (A-2Z) or neutron excess (N - Z) as a function of atomic number (Z) is shown in Figure 4. A connection of peak positions (local maxima and minima) with magic numbers can be seen. Local minima (N-Z) are seen at the magic numbers of protons: 2, 6, 8, 14, 20, 28, 40, 112, and also near the numbers of the alpha-particle configurations Z: 44, 60, 84 and 108. Local maxima are present at magic Z: 70 (weak) and 82, at the numbers of the alpha-particle configurations Z: 4, 12, 24, 36, 52, 56, 100 and at Z=114. Extrema of a small

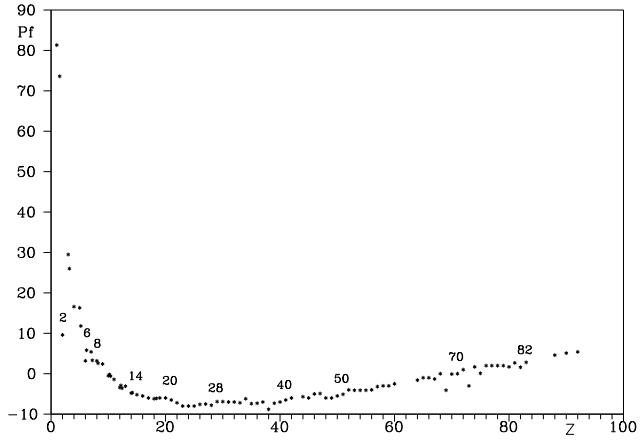

Figure 3: The dependence of the packing factor as a function of proton number Z.

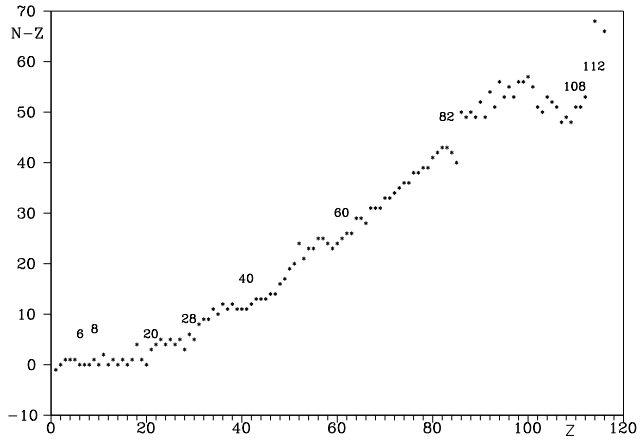

Figure 4: The dependence of neutron excess (N-Z) as a function of atomic number Z.

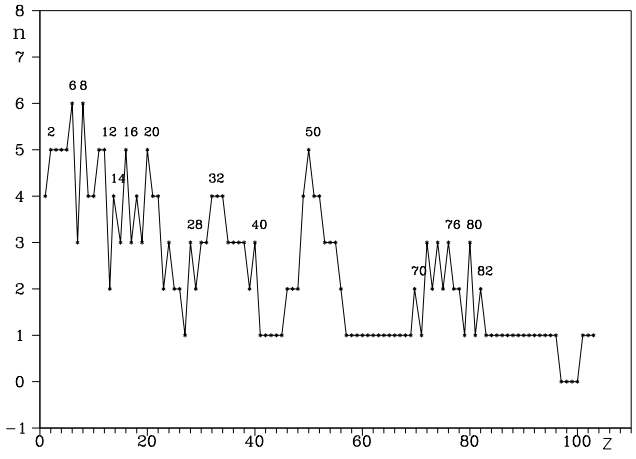

Figure 5: The dependence of total quantity of magic numbers for every chemical element as a function of Z.

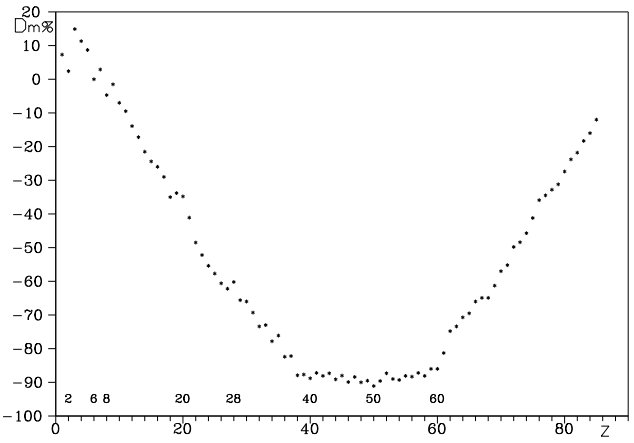

Figure 6: The dependence of the parameter $Dm_{\%}$ as a function of Z.

amplitude at the magic numbers of neutrons are seen in a similar dependence (N-Z) as a function of neutron number (N). A weak effect is also seen at magic mass numbers A: 6, 8, 14, 40, 50, 82, 126, 168 and 258.

c). Analysis of the dependences between isotopic mass excess and the mass number.

On the plots based on the data from Luc Valentine (1986), the four characteristic points can be considered: A_{min} and A_{max} are the left and the right borders of the range of isotopes as a function of the mass number for every element; the point of the mass number $A_{min(dm)}$ at minimum of the mass excess (dm) and corresponding minimal value of dm_{min}; the point $A_{\%}$ for isotope with maximal abundance ratio and the value $Dm_{\%}$ corresponding to it. About 17 % of A_{min} values coincide with magic numbers, for A_{max}, $A_{min(dm)}$ and $A_{\%}$ these coincidences are 19 %, 34 % and 30 % respectively. There are about 20 % of coincidences of numbers $A_{min(dm)}$ and $A_{\%}$. The plot of the dependence of total (on Z, N and A) quantity (n) of magic numbers for every chemical element as a function of its number Z is derived in Figure 5. There are peaks at the magic numbers Z = 2, 6, 8, 14, 20, 28, 40, 50, 70, 82, and also at the numbers of α-particle configurations: Z=12, 16, 24, 32, 72, 76, 80. In Figure 6 the dependence of $Dm_{\%}$ as a function of Z is shown: effects of the magic numbers Z = 2, 6, 8, 20, 28, 40, 50 and the numbers of α-particle configurations at Z=60=20+40 are seen. In Figure 7 the dependence of the parameter $Dm = dm_{max}$ - dm_{min}, giving the limits of the changes of dm for this isotope, as a function of Z is present. There are peaks at the magic numbers Z: 2, 6, 8, 14, 20, 28, 40, 50 and 82. There are also peaks at Z = 11, 37, 55, 87 for the elements of the first period (alkaline metals) and at the numbers of the α- particle configurations: Z = 24, 80, 84, 100 and at Z=90. Dividing Z for each element on its mass number $A_{\%}$, corresponding to the most

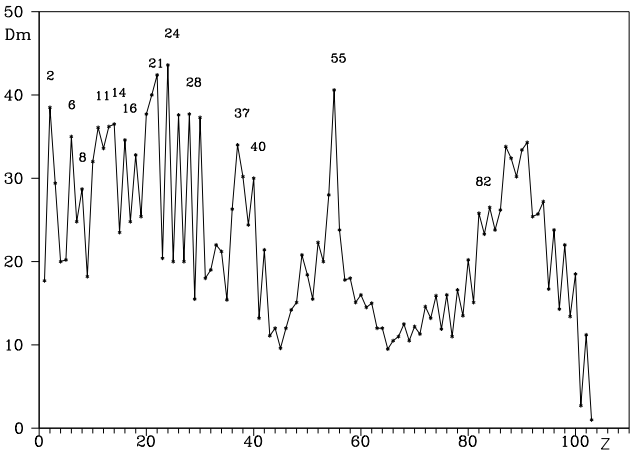

Figure 7: The dependence of the parameter Dm as a function of Z.

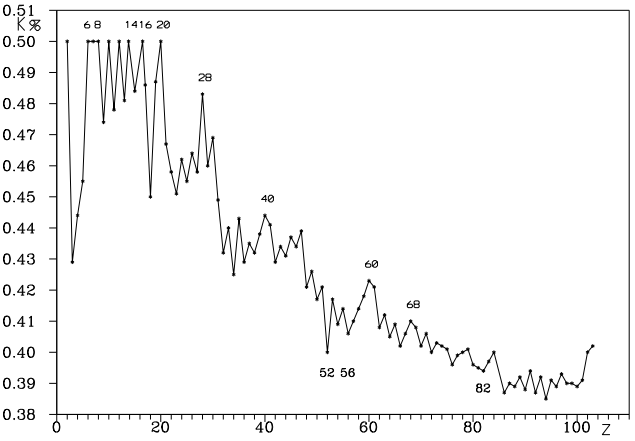

Figure 8: The dependence of the coefficient $k_{\%}$ as a function of Z.

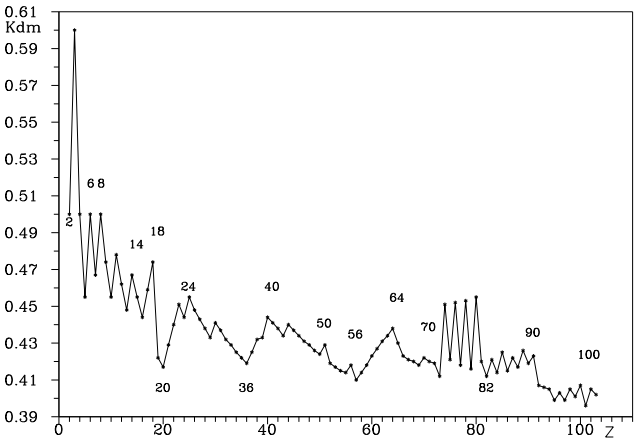

Figure 9: The dependence of the coefficient k_{dm} as a function of Z.

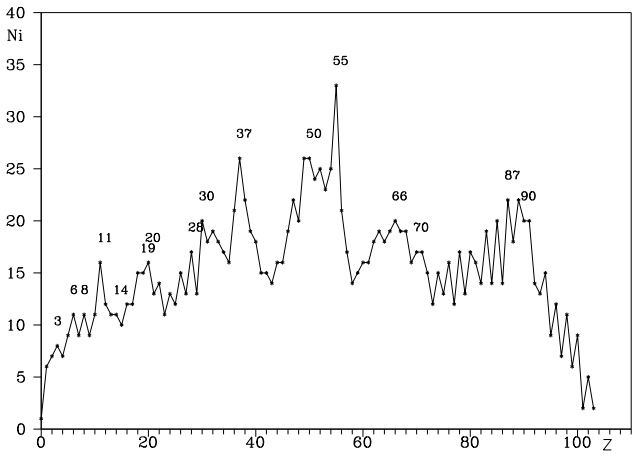

Figure 10: The dependence of quantity of isotopes (N_i) for each element as a function of its number Z.

abundant isotope, we get the coefficient $k_{\%}$. In Figure 8 the dependence of this coefficient ($k_{\%}$) as a function of Z is shown. In this Figure magic numbers Z: 6,8, 14, 20, 28, 40, 70, 82 are seen as well as the numbers of the α-particle configurations Z: 12, 16, 52, 56, 60, 68. In Figure 9 the dependence of a similar coefficient (k_{dm}) corresponding to the minimum of dm is shown. The magic numbers Z: 2, 6, 8, 14, 20, 28, 40, 50, 70. 82 and the numbers of the α-particle configurations Z: 36, 56, 64 and even numbers Z: 18, 90 are seen too.

In Figure 10 the dependence of quantity of isotopes (N_i) for each element as a function of its number Z is present. The magic numbers Z = 6, 8, 20, 40, 50, 70 and the sums of magic numbers: 30=28+2 and 90=40+50 are shown. Besides, peaks for all alkaline metals (at Z = 3, 11, 19, 37, 55, 87) are clearly expressed. They can be also seen on the dependence of A_{min} as a function of Z. For the elements of IA group (alkaline metals) the recurrent formulas for Z are the following:

Table 1: Calculations of Z_i for alkaline metals

i	1	2	3	4	5	6	7	8
n	1	2	2	3	3	4	4	5
D_i	2	8	8	18	18	32	32	50
Z_i	1	3	11	19	37	55	87	119

Table 2: Calculations of Z_i for noble gases

i	1	2	3	4	5	6	7
n	2	2	3	3	4	4	5
D_i	8	8	18	18	32	32	50
Z_i	2	10	18	36	54	86	118

$$Z_1 = 1,\ Z_{i+1} = Z_i + D_i,\ D_i = 2 \times n^2, \qquad (7)$$

where i = 2n-2 or i = 2n-1, i=1, 2, ..., 8, n=1, 2,..., 5.

Numerical results are given in Table 1. Similar results for the VIIIB elements (noble gases) are shown in Table 2. They are derived from the formulas (8).

$$Z_1 = 2,\ Z_{i+1} = Z_i + D_i,\ D_i = 2 \times n^2, \qquad (8)$$

where i = 2n-3 or i = 2n-2, i=1, 2, ..., 7, n=2, 3, 4, 5.

The model of atomic shells explains also the increased stability of the noble gases. Dependence of ionization potential (P_i) as a function of Z (Figure 11) gives the maxima of peaks at Z=2, 10, 18, 36, 54, 86 (for the noble gases) and minima at Z = 1, 3, 11, 19, 37, 55, 87 for alkaline metals.

d). Spin of the ground state of nucleus (I).

The behavior of the mean (on Z, N and A) spins of the basic state ($< I >$) of the nuclei is analysed. Spins (I) are taken from Luc Valentine's Table (1986). There are pulse groups of peaks within the areas of

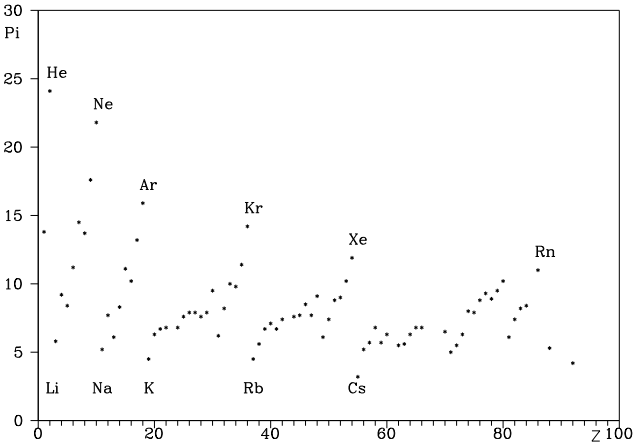

Figure 11: The dependence of ionization potential (P_i) as a function of Z.

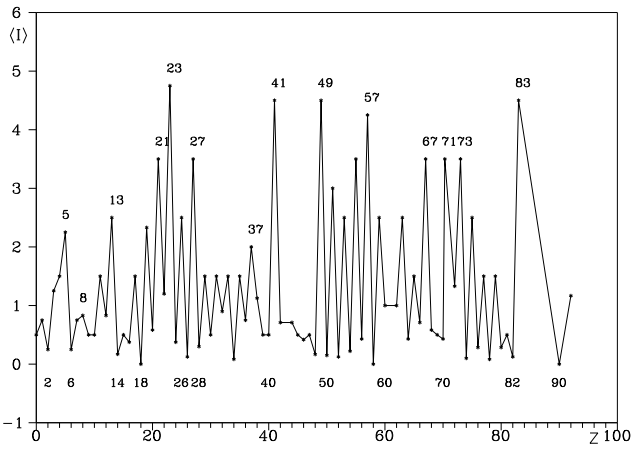

Figure 12: The dependence of the mean (on Z, N and A) spins of the basic state ($< I >$) of the nuclei as a function of Z.

magic numbers Z and N, and also A (less expressed). Apart from the rare cases, the spins of the ground state of nuclei (I) have small or zero values at even, α-particle configurations and magic Z, N and A. It testifies to the spherical, less deformed nuclear shells (see, e.g., Sobiczewski, 1996). But we do not agree that the numbers 108, 114 and 162 mentioned in that work should be considered as magic ones. Thus, the element Hs(108,162) is not only twice magic, but moreover it is not simple magic one. And the element Uuq(114,184) is not twice magic one but it is just simple magic one (the neutron number N=184)!

At the odd values of Z, N, and A (especially at the values differ by unit from magic and α-particle configurations ones) there are maximal peaks of $< I >$-values (Figure 12). There are minima at magic Z: 2, 6, 14, 20, 28, 40, 50, 70, 82 (local maximum is at Z=8) and at α-particle configurations Z: 52, 60, 64. There are also minima at magic N: 2, 6, 8, 14, 20, 28, 40, 50, 70, 82, 112, 126 and at α-particle configurations N: 12, 16, 24, 36, 44, 48, 56, 60, 68, 80, 84, 88, 96, 100, 108, 120, 144.

5. On the mass scale standard

The new atomic mass unit (carbon scale) was accepted in 1960 as 1/12 part of the carbon mass isotope with the mass number 12. It is equal to 1.66×10^{-24} g $= \frac{931481keV}{c^2}$. This unit differs very small from the previous one (oxygen scale), but it is more appropriate for measuring of the masses by the mass-spectroscopy method, since carbon has much more different compounds than oxygen.

There was a time when Gamov made an attempt to introduce isotope of helium He (2, 4) as a standard for the mass scale identical both in physical and chemical respects. But helium is not a simple element, its isotope He (2, 3) has been discovered with the relative abundance 0.0001. Besides, the density of helium is difficult to measure, and in addition it is too close to the beginning of the scale for the aims of mass-spectroscopy.

For physical purposes it appears substantial for the unit of mass to be related with a certain simple atom. Such simple atoms could belong to elements not having more than one stable isotope, e.g. beryllium, sodium, aluminum or phosphorus. But deviations of their masses from integer numbers vary from 0.01 to 0.03; that is significantly larger than for hydrogen (0.0079) and helium (0.0026). From the author's point of view, fluorine F (9, 19) is more appropriated for these purposes. It has also one stable isotope, and mass deviation for it is only 0.0016, that only slightly exceeds that for oxygen isotope O (8, 8): 0.0006. A packing factor for fluorine is negligible and can be taken as zero. Moreover, fluorine is chemically identical to such elements as chlorine and bromine, which are not simple elements; however, these have been used as convenient auxiliary standards to determine atomic weight of silver, which is not simple element either. The fluorine ions can be easily obtained in mass- spectroscopy by using gaseous fluorinated boron. Molecules of hydrocarbons are very suitable to make measurements of the masses by the method of doublets, therefore the atoms of hydrogen, deuterium and carbon C (6, 12) adopted as additional standards as well.

As it known, the neutral atomic oxygen O (8, 8) with mass number 16 was used before as the basic standard for comparison of atomic masses by different physical and chemical methods (oxygen scale). This standard was adopted when oxygen was considered as a simple element. When the isotopes of oxygen O17 and O18 were discovered, it became evident that the adopted unit of mass differs from the classic chemical unit: 1/16 of the average atomic weight of oxygen. However, even after this, the chemical standard was kept as the previous one because the masses of many elements were rather close to integer numbers in its scale. And from the chemical point of view, the discovery of isotopes is not a very complicated matter to measure the atomic weight. Many chemists considered that advantages of a new scale could hardly compensate the inconveniences connected with the changes of atomic weights commonly adopted. But nevertheless, the new scale was accepted!

By the way, the isotope O16 is the twice magic nucleus, its proton and neutron numbers are equal to the magic number 8. It has the smallest deviation of the mass from the integer number due to this, hasn't it? And that isotope O16 is so abundant on the Earth, cradle of humanity. And it is so needed for the Life! The Earth's atmosphere contains 21% of oxygen and 78% of nitrogen (Seaborg and Valens, 1966). The Earth's crust consists of 46.6% of

oxygen. And this despite of the fact that our Universe consists of 99% of hydrogen and helium, and all the rest elements (including oxygen) represent just 1%!

6. Mendeleev and Gamov

When engaged in the problem of abundance of chemical elements and their isotopes, magic and twice magic nuclei (Proceedings of the Memorial conference devoted to the 95-th G.A. Gamov's anniversary, Odessa, 1999 and present work), the author paid an attention the names of two great scientists - D. I. Mendeleev (1834 - 1907) and G.A. Gamov (1904 - 1968) and he was staggered by surprising parallels in the lives of these great people. As is seen from the given above dates of their lives, Gamov was born 70 years later than Mendeleev and died approximately 60 years after the death of the great chemist.

Both giants of thought lived and worked in Odessa for some time, the memorial plaques are witnesses of this fact: the one is on the wall of the National University building, another one is on the wall of the Richelieu lyceum, wherein Mendeleev used to teach. Further, the activity of both scientists was related to Petersburg, and what is more both genii manifested themselves in science very early. At the age of 35 Mendeleev discovered the Periodic Law. This enabled him to create the periodic system of chemical elements, and on its basis to predict the existence of some chemical elements, that were not known at that time. That was a fundamental work both in area of chemistry and physics, that apparently deserved the Nobel prize. However, it is rather strange, neither Mendeleev, nor Gamov (though because of different reasons) were not awarded with it.

At the age of 24 Gamov explained the origin of α-decay of isotopes - one of the most enigmatic problems of nuclear physics of that time. The velocities of nuclear reactions are calculated on the basis of this theory. Both of them have left an eternal trace in the investigation and discovery of the fundamental natural laws of matter, which the Universe consists of.

Both of them are versatile scientists, talented educational specialists, and popularizers of science. Mendeleev published over 500 works on chemistry, physics, metrology, aeronautics, agriculture, economics and enlightenment for the people, developed an industrial method of oil fractioning, and invented quite a new kind of smokeless powder. And Gamov was the most talented pedagogue as well, he himself was able not only to enjoy his favorite physics, but also to instill this feeling in his students, listeners of his numerous lectures, and also to the readers of his articles and popular books. For all that he was awarded with Calling prize of UNESCO. And the scope of his researches is striking: from purely theoretical works on cosmology, nuclear physics and astrophysics, genetics to the applied works at the most powerful explosion phenomenon (the thermonuclear explosion), and that is a real grandiosity as compared with gunpowder!

Both scientists are of a nobiliary origin. Mendeleev was born in the family of director of Tobol'sky Gymnasium which he graduated afterwards. Gamov's Father graduated from Odessa (Novorossiysky) University and then taught Russian and literature in one of Odessa private boy schools and in Odessa higher school. One of Gamov's uncles (maternal side) graduated from Odessa University, chemistry faculty. The discovery of poisonous (for fishes) layer of carbonic combination at the bottom of the Black Sea belongs to him," - wrote Gamov (1970) in his autobiography. In 1928 Gamov after studying a year at the physics-mathematics faculty of Odessa University began studying in Petersburg University which he graduated before the appointed time - in three years. In 1928 while being a post-graduate student of the second course he was recommended by the University as a probationer to the well-known Göttingen University. It was there that Gamov made his classic work on α-decay, and became a man of the world renown as a physicist-theorist.

In 1859 after obtaining his master's degree at the age of 25 Mendeleev went abroad for two years assignment. Mendeleev was not only a great scientist but also a progressive public person. Being Professor of St.-Petersburg University (1865 - 1890), he resigned protesting against the students' oppression. At the age of 42 being the luminary of world science Mendeleev was elected as a corresponding member of St.-Petersburg Academy of Sciences. In 1880 he was nominated as an Academician but failed to be voted. The public protested against that sharply.

Gamov was much luckier in this respect. At the age of 28 (in 1932) he was elected nearly unanimously (with the record count 42:1) as a corresponding member of Academy of Sciences of the USSR. He was the youngest member of the Academy. And in spite of such a great success he did not come back to his motherland in 1933. It was almost an escape! And he did not say good-bye! In1938 Academicians had to expel Gamov from the Academy under the government pressure. Indeed, extraordinary personalities cannot be attested according to the conventional public standard!

Under these conditions Gamov displayed a great flair and forethought! It was on the eve of political public purges, confessions and self-accusations, just before the shattering of science and culture! The horrible period of Solovki, Siberian camps and mass repressions! He realized that his nobiliary origin and friendship with "bourgeois" physicists would be remembered to him, and first of all his independence,

intellectuality, his sparkling wit, a love for freedom and scientific creation.

If he had not made that step, we would not have a chance of speaking about Gamov as a creator of Hot Universe theory (or Big Bang theory), and about his prediction of microwave radiation, that was discovered in 1965 (15 years after his prediction) at Gamov's live, and about Gamov's pioneer work on finding the clue to solve the structure of universal genetic code (1953), when genetics itself as a science was considered as "a sale whore of imperialism" in his homeland. But the fate placed everything in the place. Already at the time of his life Gamov enjoyed recognition of his scientific achievements and predictions, tasted nectar of immortality!

Just the same words can be said about Mendeleev - they both are classics of science!

Acknowledgement. The author would like to thank S.M. Andrievsky for his editing of this English text.

References

Aston F. W.: 1948, *Mass spectra and isotopes,* Moscow.

Bezdenezhnyi V.P.: 1999, *Odessa Astron. Publ.,* **12**, 166.

Fermi Enrico: 1951, *Nuclear Physics,* Moscow.

Gamov George: 1970, *My World Line. An Informal Autobiography,* New York.

Landau L.D., Lifshits E.M.: 1963, *Quantum Mechanics,* Moscow, **1**, 523.

Lang K.R.: 1978, *Astrophysical formulae,* **2**, 14.

Mukhin K.N.: 1974, *Experimental Nuclear Physics,* Moscow, **1**, 48.

Seaborg G.T. and Valens E.G.: 1966, *Elements of the Universe,* Moscow, 226.

Valentine Luc: 1986, *Subatomic Physics: nuclei and particles,* Moscow, **1**.

Sobiczewski A.: 1996, *Physics Uspekhi 39,* 885-889.

CHEMICAL AND DYNAMICAL EVOLUTION IN THE SOLAR NEIGHBOURHOOD

O. Bienaymé[1], T. Mishenina[2], V. Kovtyukh[2], C. Soubiran[3]

[1]Strasbourg Observatory, France, *bienayme@astro.u-strasbg.fr*
[2]Odessa Observatory, Ukraine
[3]Bordeaux Observatory, France

ABSTRACT. We measure the surface mass density of the galactic disk in the solar neighbourhood using two samples of red clump stars, we also determine the thin and thick disk chemical properties. High resolution spectral data of red clump stars towards the NGP have been obtained with the spectrograph Elodie at OHP for Tycho-2 selected stars. Nearby Hipparcos red clump stars were also observed with the Elodie spectrograph.

Keywords: Stars: abundances and kinematics – Galaxy: stellar populations.

1. Introduction

This paper is the extension of the previous works published by (Soubiran et al., 2003) and (Siebert et al., 2003) to probe the properties and the distribution of red clump stars within 100 pc from the sun and at larger distances towards the north galactic pole.

2. The survey

To study the kinematics properties of the galactic disk and to determine the vertical force perpendicular to the galactic plane, we measure the vertical spatial distribution and the vertical velocity distribution of a test stellar population. As far as possible, this test population must be homogeneous and unbiased with selection criteria independent of velocities and distances. It must also be in a stationary state. For this purpose, we use a sample of red clump stars, extending to larger distances from the galactic plane the NGP sample previously analysed in (Soubiran et al., 2003; Siebert, 2003).

This sample is built from a preliminary list of red clump candidates, a list based on the Tycho-2 star catalogue (Hög et al., 2000) for which we select all stars in a restricted range of colour ($B-V$ within 0.9 and 1.1) in two fields in directions close to the North Galactic Pole. This preliminary list is dominated by red clump stars: our high resolution spectroscopic observations allow to determine the absolute magnitudes and to confirm and separate the red clump stars from other stars. We have also improved the local counterpart sample of red giants by measuring and determining the radial velocities and metallicities for a complete set of 203 Hipparcos red clump stars.

2.1. The Hipparcos red clump stars

We select the 203 nearby red clump Hipparcos stars with a parallax larger than 10 mas, an equatorial latitude larger than -20 deg, a $B_J - V_J$ Johnson colour within $0.9 - 1.1$ (the Johnson magnitudes being determined from the Tycho-2 B_T and V_T magnitudes applying Eq. 1.3.20 from (ESA SP-1200):

$$\begin{aligned} V &= V_T - 0.090\,(B_T - V_T) \\ B - V &= 0.850\,(B_T - V_T)\ , \end{aligned} \qquad (1)$$

and an absolute magnitude $M_{\rm Vj}$ within $0. - 1.3$. Most of these stars were observed with the echelle spectrograph Elodie in February 2003, October 2003 and February 2004 at the Observatoire de Haute Provence (France). The signal to noise ratios range from 150 to 200. We have measured and determined their radial velocity, the atmospheric parameters (Teff, log g, microturbulent velocities Vt, [Fe/H]), and abundances of some elements. The abundances of Fe, Ca, Si, and Ni have been determined from equivalent widths under LTE approximation whereas abundances of Mg have been determined under NLTE approximation using equivalent widths of 4 lines and profiles of 5 lines.

2.2. NGP K giants

The distant K giant sample is drawn from the Tycho-2 star catalogue. We have applied the same criteria given in (Soubiran et al., 2003) to build the list of red clump candidates, just extending the limiting apparent magnitudes to fainter stars. In summary, we have extracted from the Tycho-2 catalogue, stars in two fields

close to the north galactic pole. The first field is circular with a 10 deg radius and is centered towards the galactic direction $b = +90$ deg. The second field is also circular (radius 15 deg) and centered on the galactic direction ($l = 35.5$ deg, $b = +80$ deg) (we have removed stars close to the Coma open cluster direction, $l = 221$ deg, $b = 84$ deg, inside a 4.5 deg radius circle). The total area effectively covered by our samples is 720 square degrees.

From these two fields, we select stars with a $B_J - V_J$ colour within $0.9 - 1.1$. For the first field we keep stars with an apparent magnitude V_J within 7 and 10.6 and for the second one with V_J within 7. to 9.5. About 500 candidates have been observed with the echelle spectrograph Elodie at OHP with a median S/N ratio of 20. This low S/N is sufficient to obtain the stellar parameters, $T_{\rm eff}$, gravity and [Fe/H] metallicity, and also the absolute magnitude by comparison and fitting to high resolution spectra within the TGMET library (Katz et al., 1998). The determined absolute magnitudes are then used to identify the real red clump giants and remove the dwarfs and subgiants.

3. Discussion

Nearly 700 Tycho-2 stars have been observed in the solar neighbourhood at distances smaller than 100 pc or in a 720 square degree field in the direction of the North Galactic Pole. Absolute magnitudes, effective temperatures, gravities and metallicities have been estimated, as well as distances and 3D velocities. Abundances of Fe, Si and Ni have been determined from equivalent widths under LTE approximation, whereas abundances of Mg have been determined under NLTE approximation. Most of these stars are clump giants and span typical distances from 0 pc to 800 pc to the galactic mid-plane. This new sample, free of any kinematical and metallicity bias, is used to investigate the vertical distribution of disk stars.

The old thin disk and thick disk populations are deconvolved from the velocity-metallicity distribution of the sample and their parameters are determined. The thick disk is found to have a moderate rotational lag with respect to the Sun with a mean metallicity of [Fe/H] $= -0.48 \pm 0.05$ and a high local normalization of $15 \pm 7\%$. We also determine both the gravitational force law perpendicular to the Galactic plane and the total surface mass density and thickness of the Galactic disk. The surface mass density of the Galactic disk within 800 pc derived from this analysis is Σ ($|z|$ <800 pc) = 76 Msun pc^{-2}.

The thickness of the total disk mass distribution is dynamically measured for the first time and is found to be 390 pc in relative agreement with the old stellar disk scaleheight. All the dynamical evidences concerning the structure of the disk (its local volume density - i.e. the Oort limit-, its surface density and its thickness) are compatible with our current knowledge of the corresponding stellar disk properties. This result implies that the dark matter component of our Galaxy cannot be distributed in a flat or disk-like component but must be distributed in a round halo.

References

Soubiran C., Bienaymé O., Siebert A.: 2003, *A&A*, **398**, 141.

Siebert A., Bienaymé O., Soubiran C.: 2003, *A&A*, **399**, 531.

Hög E., Fabricius C., Makarov V.V.: 2000, *A&A*, **355**, 27.

The Hipparcos and Tycho Catalogues: 1997, *ESA SP-1200*, Vol. 1-17.

Kovtyukh et al.: 2004, in preparation.

Mishenina et al.: 2004, in preparation.

Katz D., Soubiran C., Cayrel R. et al.: 1998, *A&A*, **338**, 151.

G. GAMOW AND CALCULABILITY PROBLEMS OF WORLD CONSTANTS AND THE LIFE CODE

V. Cernobai

Astrointeroptic Plus, Kishinev, Rep. of Moldova
e-mail: astro@mail.md

ABSTRACT. Developing the George Gamow ideas, the fine structure and the life code calculation possibility, resulting from fundamental principles of quantum logic, the Galois field $GF(257)$ and combinatorial configurations on the tetrahedron, is shown.

Keywords: world constants, genetic code, quantum logic.

The origin and perhaps, the fundamental physical constants variability in time have been engrossed the G. Gamow's imagination and directed his efforts in the last years of his life. The great questions, left without answer, relate to the connections between the elementary particles masses and, also, to the very big numbers, representing the relations between nuclear, electrical and gravitational forces. Gamow considered these numbers could not appear as the result of a primary fortuity and they could be obtained from topological or theoretical set considerations. He believed in the final simplicity of the theory, that one day must explain these numbers (Ulam, 1970).

In one of his last letters to his son, Gamow writes that his paper with the variable e^2 will appear in the number of Phys. Rev. Letters dating from September, 25, but the storm-clouds appear on the horizon. In a number of Ap. J. Letters (July 1967) Maarten Smidt and others analyze a quasar spectra $3C = 191$ and get that, although the red shift has the factor 3 (more exactly, $2,945 \mp 0,001$), the fine structure constant $\alpha (= e^2/hc)$ "changes" only with the factor $0,98 \mp 0,05$, i.e. does **not** change at all.

But since we do not know **what are** quasars, it is difficult to say what does it mean (Gamow, 1994).

In paper (Cernobai, 1971) we have proposed a trivalent logic use for describing the electron interference. We have put forward the idea that a Planck's constant value in unities $e = 1$, $c = 1$ can be explained by the decrease of 256 truth tables for conjunction and disjunction and of 8 truth tables for negation to a single triplet of these functions for a bivalent logic.

It can sound paradoxically, but the classical logic looks to be the most quantum object. Its universality extends even to the introducing the measure for aleatory phenomenons. The response to the eternal question "to be or not to be" in many different environments is given by a coin throwing. But the coin, in addition to its two sides, has thickness, and therefore it exists the third possibility – it drops on the edge, no matter how small would be this probability.

Exactly the existence of the third logical possibility – non-determination – could serve for a logical description of the elementary particles interference phenomenon. This idea realization needs a serious analysis of the most fundamental notions and an adequate language development for description and measuring of a new, apparently ephemeral, logical notion – the non-determination.

We have proposed these ideas development in (Cernobai, 2002a). In fuzzy logic, proposed by Zadeh, any logic function takes values on the interval [0,1], while the logic functions can be an infinity for any operations. This refers to the connection between x and the $x^{\ominus}$ negation.

"The subtraction on a circumference" presents a particular attention for the connection with a quantum mechanics and for other uses:

$$x^{\ominus} = \sqrt{1 - x^2}.$$

We can unite x and $x^{\ominus}$ in a complex number $l = x + ix^{\ominus} = \sin\alpha + i\cos\alpha$.

We use the same trigonometric parametrization for building the logical operations such as conjunction, disjunction and implication.

In fuzzy logic there exist more definitions (an infinity) for every operation of negation, conjunction and disjunction, but for passing to the limit case of a bivalent logic, these operations must satisfy Morgan's laws:

$$(x_1 \vee x_2)^{\ominus} = x_1^{\ominus} \wedge x_2,$$
$$(x_1 \wedge x_2)^{\ominus} = x_1^{\ominus} \vee x_2.$$

Further we will show that a fuzzy logic based on the complex numbers algebra we have proposed in (Cernobai, 2001) satisfies this law.

Also, it is important to find physical conditions, when the non-deterministic logic takes place. The following argumentations show some limits of this kind.

Non-deterministic conditions are discussed for an electron interference experiment on two slits within an absorbent screen. It is shown that the non-determination caused by the relativity theory is $\triangle t \sim d/c$, where d is the distance between the slits, c is the velocity of light in vacuum and the energetic speed is $\triangle\varepsilon \sim e^2/d$, where e is an elementary electron charge. So the non-deterministic action is $\triangle t \triangle\varepsilon \sim e^2/c$ (Cernobai, 1971). This non-determination makes necessary the trivalent logic application (Cernobai, 1971) or, more generally, the discrete fuzzy logic application for description the interference in a quantum mechanics.

The non-determination in the quantum mechanics expresses by Planck's constant, that to within a coefficient coincides with $e^2/c : \hbar \approx 137e^2 = \frac{1}{\alpha} \cdot \frac{e^2}{c}$, where $e \approx \frac{1}{137}$ is a constant of the fine structure. It is discussed the possibility of the constant calculation using some combinative principles connected with the passing from the multidimensional fuzzy logics (fuzzy generalizations of the multivalent logics) to the classic ones.

These reasons explain to some extent the connection between the composition laws of a quantum phenomenons extension and the composition laws of probabilities, emphasized by R. Feynman in many times.

If we introduce three basic vectors in the three-dimensional logical space:

$$f = \begin{pmatrix} 1 \\ 0 \\ 0 \end{pmatrix};\ ? = \begin{pmatrix} 0 \\ 1 \\ 0 \end{pmatrix};\ t = \begin{pmatrix} 0 \\ 0 \\ 1 \end{pmatrix},$$

then we can show easily that they are eigenvectors of a matrix

$$\nu_3 = \begin{pmatrix} 1 & 0 & 0 \\ 0 & 0 & 0 \\ 0 & 0 & -1 \end{pmatrix} = \frac{1}{2}\lambda_3 + \frac{\sqrt{3}}{2}\lambda_8 =$$

$$= \frac{1}{2}\begin{pmatrix} 1 & 0 & 0 \\ 0 & -1 & 0 \\ 0 & 0 & 0 \end{pmatrix} + \frac{1}{2}\begin{pmatrix} 1 & 0 & 0 \\ 0 & 1 & 0 \\ 0 & 0 & 2 \end{pmatrix}$$

with eigenvalues $+1$, 0 and -1, correspondingly, where λ_3 and λ_8 are Gell-Mann's matrixes, known from the elementary particles physics (Cernobai, 1995).

Those 256 matrixes of the trivalent logic, numbered from 1 to 256 with bivalent representations of their elements:

$$C_1 = \begin{pmatrix} 0 & 0 & 0 \\ 0 & 0 & 0 \\ 0 & 0 & t \end{pmatrix};\ C_2 = \begin{pmatrix} 0 & 0 & 0 \\ 0 & 0 & 0 \\ 0 & 1 & t \end{pmatrix};$$

$$C_3 = \begin{pmatrix} 0 & 0 & 0 \\ 0 & 0 & 0 \\ 1 & 0 & t \end{pmatrix};\ C_4 = \begin{pmatrix} 0 & 0 & 0 \\ 0 & 0 & 0 \\ 1 & 1 & t \end{pmatrix};\ \ldots$$

can be organized in 128 complex matrixes

$$Z_k = C_k + i(C_{256} - C_k).$$

They form, together with fuzzy negations represented by Gell-Mann's matrixes $\lambda_1 - \lambda_8$ and with the unity matrix E basic operations of the trivalent fuzzy logic and can be named with the numbers of a field Z_{137} from 1 to 137. It is important that the roots of the equation $x^{137} - 1 = 0$ are algebraically calculable, because a regulate polygon with 136 sides can be built using the compasses and ruler, since $136 = 2^3 \cdot 17$ and 17 is a number of Fermat-Gauss type.

In our paper (Cernobai, 2002b) we have paid attention to the problem of passing to limit from a discrete space-time with a finite number of symmetry groups to an unique continuum.

This problem does not produce big complications in non-relativistic quantum mechanics, because for the time ordering, representing an one-dimensional operation, the iterative Dedekind's process based on sequence of irrational numbers corresponds to the approximation with irrational numbers. However, for the case of space ordering there exists a finite number of 230 discrete transformations groups, called Fyodorov groups, which make an ambiguous transition to the limit to the same point (vacuum); this fact produces a non-determination. We do not exclude the fact that an exit from this difficulty may be found in the general principle of the statistical mechanics: the initial system states averaging and the final states summation. It is obvious, exactly like in the case of a genetic Gamow's triplet, that some transformations would turn out to be equivalent ones, and this fact would decrease the groups number from 230 (for the case of three-dimensional space) to a smaller number. Calculating the average, we may need to apply some particularities of the theory structure based on multidimensional logics or on fuzzy logics, that allow a description within grates theory also.

G. Gamow also emphasized the fundamental role of the "discrete", quantum, combinatorial concept in modern science: "The nature is sly, but the existent amino acids number is still equal to the number of triplets that can be composed from four different elements. It is possible that one day we will see why it is so." (Gamow, 1968).

From the fundamental mathematical structures Kepler has noted the golden section and its connection with Platonic bodies: "There exist two regulate bodies, the dodecagon and the icosagon; the first of them is bounded by regulate pentagons and the second one by equilateral triangles, but these ones are adjacent one to another such that some pentahedral spatial angles are created. The building of these bodies and especially of a pentagon itself is impossible without that proportion, called by contemporary mathematicians a divine one. It is built in such a way that two minor terms of

this infinite proportion add up to the third term, and any two of the last terms being summed, give the next term, and this proportion maintains ad infinitum. It is impossible to bring a numerical example, where would be written out all the terms. However, as far as we will go from the unity, our example will become more complete. Let both of two minor terms will be numbers 1 and 1 (you can consider them as being unequal ones). Adding them we get 2. Adding to 2 the biggest minor term we get 3, and adding to 3 number 2 we get 5. Then, adding to 5 number 3 we get 8, adding to 8 number 5 we get 13, adding to 13 number 8 we get 21. The ratio of number 5 to 8 is approximately equal to the ratio of number 8 to 13, and the ratio of number 8 to 13 is approximately equal to the ratio of number 13 to 21.

In the image and likeness of this continuing proportion by itself is created, as I assume, the constructive force, and by this constructive force the authentic symbol of a pentagonal figure is embodied in a flower. I omit all other considerations I could adduce in the support of what has been said in these very pleasant discussions. They would require a special place. And here I brought them only as an example, so that we would be more versed and better prepared for the hexagonal snow figure study" (Kepler, 1982).

For his part, H. Weyl emphasizes the symmetry role in the fundamental notions forming: "As I can appreciate, all "a priori" affirmations of the physics have the symmetry as source" (Weyl, 2003). And further: "...every time you having to do with some object S provided with structure, you try to define its automorphisms group, i.e. a group with elements representing transformations that do not change all structural relations".

Operations of addition, subtraction, multiplication, division and extraction of the square root are the algebraic operations that are geometrically realizable by using *the compasses and ruler.* Exactly because of this, the regulate triangle, pentagon and 17–gon can be built using the compasses and ruler; for each of these cases the automorphisms group is a cyclic group, its order being some power of number 2:

$$3 = 2^1 + 1, \;\; 5 = 2^2 + 1, \;\; 17 = 2^4 + 1,$$

$$257 = 2^8 + 1, \; 65.537 = 2^{16} + 1.$$

Thereupon, let us consider automorphisms of Platonic bodies and, first of all, the tetrahedron automorphisms. The tetrahedron considered as a simplex, i.e. the most elementary regulated polyhedron of a three-dimensional space, contains the following elementary polyhedrons: four triangles (faces), six edges, four vertexes, forming a set of 16 elements with itself and the nullity set. The set of all sets, composed from these 16 elements, is 2^{16} and formes an algebraic group of the tetrahedron with the operation of inclusion; it is a group of tetrahedron automorphisms.

Let us paint the faces in four different arbitrary colours, e.g. in blue, yellow, green, red. Each edge has two colours and each vertex has three colours. Let us distribute three balls between the tetrahedron faces; such a distribution can be made in $4 \times 4 \times 4 = 64$ different ways. Every time we will associate the ball with an edge in such a way that each ball will situate on different edges for every distribution. This is possible, because in the case when maximum three balls are situated on a face, one single face is associated with each side. Every distribution will give us a combination of six edges by three: $C_6^3 = 20$, attributing every time to each ball the colour of one single face. In order to avoid the uncertainty of a ball coloration, let us make the next projection of tetrahedron: we dissect it from a vertex and so we obtain four triangles in the plane. For example let us consider that we have made the projection on a green base of the tetrahedron; so we have made a spontaneous rule violation. We will cut each of the three vertexes of lateral triangles and one vertex of the interior triangle. Paint each edge in two complementary colours and distribute the edges in the form of a matrix 3×4. Here, we deal with the second rule violation; in our case one edge and more exactly, the one that belongs to the red colour face, has the same complementary colour with the green colour of the base situated in the center.

$$A \times \begin{pmatrix} b \\ y \\ g \\ r \end{pmatrix} = \begin{pmatrix} b_r & y_b & g_b & r_y \\ b_g & y_g & g_r & r_g \\ b_y & y_r & g_y & r_b \end{pmatrix} \times \begin{pmatrix} b \\ y \\ g \\ r \end{pmatrix}.$$

Let us put each of the three balls on a separate line. We will give the value 1 to the places where the balls intersect with columns, and the value 0 to other matrix elements. Multiplying this matrix by a vector-column with four coordinates of colours, we obtain a vector with three colour components every time.

Taking into account the restrictions between the matrix elements caused by their connections on the tetrahedron, we obtain 20 matrixes reflecting 20 combinations (by three of six) of the tetrahedron edges. One of them is expressed by three equivalent matrixes, and this degeneration is connected with non-determination of the vertex with three colours, opposed to the base. Other two contain two synonyms each, caused by symmetry violation in the last phase of the figure splitting. We establish the fact that, with precision of colour marking, the 20 obtained vector-triplets together with their synonyms correspond with 20 triplets of amino acids studied by G. Gamow. The colour symmetry of 20 Gamow invariants $C_4^3(r)$ is a latent symmetry.

Other triplets generated by this matrix encode the same 20 elements. The same thing takes place for

other three projections on the bases with other three colours. In this way we obtain $4 \times 64 = 256$ triplets. To each of the 256 triplets it corresponds a matrix of order 3×3 from 256 matrixes, obtained by excluding the fourth column from the matrix A, where g_r is fixed and other elements have values 0 or 1. We recognize the definition of conjunction in the trivalent logic in these matrixes. In order to identify these matrixes and their respective triplets, we associate to each of the matrixes a nonzero root of an equation $x^{257} = x$. The set of polynomials in a finite field Z_{257} of the order 257^n is a finite one, and forms a Galois field $GF(257^n)$, the polynomial roots being periodical with the period $257^n - 1$ (Birkgoff and Barti, 1976).

References

Ulam Stanislav M. Introduction to the G. Gamow's book "My world line". 1970, New York.

Gamow G. My world line. 1994, Nauka, Moscow (in Russian).

Cernobai V. About the interference experiment, The thesis work: 1971, Dubna.

Cernobai V. Application of fuzzy logic in Feynman's formulation of quantum mechanics, Proceedings of Int. Conf.: 2002a, Târgu-Mureş, România.

Cernobai V.A. Fuzzy logic based on the algebra of the complex numbers and the mechanical quantum logic, Proc. of Int. Conf. CNF: 2001, Iaşi, p.22.

Cernobai V. The bivalent and trivalent logic in quantum mechanics, algebras SU(2) and SU(3) in the logical space and the optoelectronic computers (in Romanian), Proc. of Symposium SIOEL-95: 1995, Bucureşti.

Cernobai V. Causality principle and the problem of divergences liquidation from the Feynmann's diagrams, Proc. of Int. Conf. "The path integrals from quarks to galaxies": 2002b, Antwerpen, Belgium.

Gamow G. Combinatorial principles in genetics. The applied combinatorial mathematics: 1968, Mir, Moscow (in Russian), p. 289–308.

Kepler I. On the hexagonal snowflakes: 1982, Nauka, Moscow (in Russian).

Weyl G. The symmetry: 2003, Moscow (in Russian).

Birkgoff G., Barti T. The modern applied algebra: 1976, Mir, Moskva (in Russian).

BLUE STRAGGLERS AS A MERGING PRODUCT OF LOW-MASSIVE MAIN SEQUENCE BINARIES WITH DETACHED COMPONENTS

G.N.Dryomova[1], M.A.Svechnikov[1] and A.V.Tutukov[2]

[1]Ural State University, Yekaterinburg, Russia, *e-mail: G.N.Dryomova@mail.ru*
[2]INASAN, Moscow, Russia, *e-mail: atutukov@inasan.rssi.ru*

ABSTRACT. In the framework of magnetic braking formalism the evolutionary chain describing the sequential evolutionary transitions of the low-massive detached close binaries into "$short-periodic$" $RS\ CVn$-type systems and then into $W\ UMa$-class contact stars with the final stage of the single objects of Blue Stragglers-type was reconstructed. This problem was solved with the use of extensive observation materials. The relations of statistics and lifetimes obtained for systems participating in evolutionary chain serve as an evidence for genetic relationship of given objects.

Keywords: close binaries, $W\ UMa$-type, magnetic braking, Blue Stragglers.

1. Introduction

The possibility of the formation of late spectral class contact systems known as $W\ UMa$-type stars from the detached binaries with low masses and belonging to the Main Sequence (MS) was proposed in the early sixties last century.

The timescale of this evolutionary transition is determined by Angular Momentum Loss (AML) process due to magnetic braking of the donor star. The law of deceleration of the spin rotation with the age for solar-like single stars found by Scumanich in 1972 (Skumanich, 1972) and written as $V_{rot} \sim \alpha/t^{1/2}$ serves as an empirical basis for this evolutionary scenario and quantitative estimation of the efficiency of the Magnetic Stellar Wind (MSW). As an evidence for MSW in the contact systems one may point out to:

- coronal activity recorded in X-rays, near and far IR- and *Radio*-ranges;
- presence of the *dark spots* in the photosphere;
- strong *chromospheric emission*;
- sudden *jumps* of the orbital period.

The magnetic braking process in the binaries in contrast to single stars leads to orbital AML as a result of the tidal interaction between the components. Magnetic braking is produced by the interaction of the stellar wind emanating from the star with the surface magnetic field. It tends to keep the spin rotation of the donor synchronous to its orbital revolving. Using the simple formulas for orbital and spin angular momenta:

$$J_{orb} = M_1 \cdot M_2 \cdot (M_1 + M_2)^{-1/2} \cdot A^{1/2} \cdot G^{1/2} \quad (1)$$

$$J_{spin} = (M_1 \cdot {R_1}^2 + M_2 \cdot {R_2}^2) \cdot V_{rot}/R \quad (2)$$

and following the synchronization condition $\frac{J_{spin}}{dt} = \frac{J_{orb}}{dt}$ one can express the time having the sense of the timescale of AML in the binary:

$$\tau = 3 \cdot 10^6 \cdot A^5 \cdot R^{-4} \cdot M_1 \cdot (M_1 + M_2)^{-2}. \quad (3)$$

It is a well-known expression for estimation of the orbital AML for binary system which was first derived by Iben and Tutukov in 1983 (Iben & Tutukov, 1984). Returning to the question of magnetic braking one should note that an extensive convective envelope and radiative core are necessary structural elements for effective MSW. It means that the mass range has to be rigorously determined within the limits $0.3 \div 1.5 M_\odot$.

The study of the merging process in such low-massive Detached Main Sequence (DMS) close binaries in the timescale of the orbital AML due to magnetic braking allows to explain the origin of the single objects of Blue Stragglers-type (BS) populating the stellar clusters older than $2 \cdot 10^9$ yrs (Stryker, 1993).

So, on the basis of extensive observation data taken from the (Svechnikov & Kuznetsova, 1990) the evolutionary relationship of the close binaries of considered classes was revealed and presented in the form of evolutionary chain $DMS \Rightarrow$*short-period* $RS\ CVn \Rightarrow W\ UMa \Rightarrow BS$.

2. $M_1 - A$ diagram and precursors of BS-objects

The $M_1 - A$ diagram occupies the central place when studying the evolution of low-massive close binaries. Namely in this diagram the deficiency of the short-periodic DMS with $M_1 \leq 5M_\odot$ and $A \leq 10R_\odot$ was first noticed by Svechnikov (Svechnikov, 1969). This domain was named as "*forbidden triangle*" and explained by Tutukov (Popova et al., 1982a) via accretion regime of the close binary formation.

Fig.1 presents in $M_1 - A$ diagram the distribution of the close binaries of DMS, pre-contact, $W\ UMa$ and Contact systems of Early spectral class (CE) types taken from catalogue (Svechnikov & Kuznetsova, 1990). Lets try to identify in this plane the domain occupied by the "precursors" of the contact systems under the assumption that MSW is driving force for the components approaching.

Mentioned above accretion regime of the close binaries formation imposes restrictions on the star sizes and semi-major axis. Thus the minimum possible value of the semi-major axis at the fixed primary mass separating the detached binary zone from contact one may be written in the next form:

$$A_{min}/R_\odot \sim 6 \cdot (M_1/M_\odot)^{1/3} \qquad (4)$$

It is a low boundary of the sought domain found from considerations that the radii of newly formed stars have not to be less than $3R_\odot$ otherwise they merge at the Hayashi stage (Popova et al., 1982a).

Also it is well known that the evolution of low-massive binaries is described by orbital AML timescale which is much more shorter than nuclear timescale. At the same time if masses of both components are less than $1.5M_\odot$ such binary will expend its orbital angular moment two times as intensive. Therefore from the relation connecting the lifetime of the primary component within MS-band and characteristic time of orbital AML we found the upper boundary of the "*feeding zone*" for contact systems submitting to power dependence:

$$A_{min}/R_\odot \sim 7.67 \cdot (M_1/M_\odot)^{0.42} \qquad (5)$$

It should be noted that binaries with $M_1 > 1.5M_\odot$ also might be "parents" for contact systems. But in this case the satellites have to be responsible for magnetic braking and their masses ought be less than $1.5M_\odot$. Then from the equalization of satellite timescale of spin AML to the nuclear timescale of the primary component one can derive the law of the right boundary:

$$A_{min}/R_\odot \sim 11.58 \cdot (M_1/M_\odot)^{-0.58} \qquad (6)$$

The left boundary is obtained for reasons of restriction of the contactization timescale by Galaxy age adopted as 15 Gyrs and may be presented in linear form:

$$A_{min}/R_\odot \sim 7.25 \cdot M_1/M_\odot \qquad (7)$$

The intersection of these four boundaries forms the *trapezium*-like domain occupied by detached binaries, which may evolve into contact one (see Fig.1).

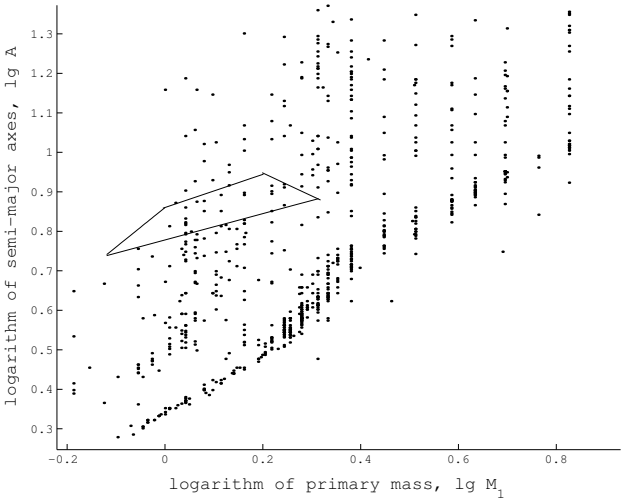

Figure 1: Distribution of the close binaries taken from (Svechnikov & Kuznetsova, 1990) in $M_1 - A$ diagram.

Concerning the possible mechanisms of the filling the "*forbidden triangle*" zone one may emphasize the following:

1. satellite magnetic braking;
2. *Algol*-mechanism for far evolved systems;
3. disintegration of the multiple and mainly triple systems when they collide.

3. Testing $DMS \Rightarrow W\ UMa \Rightarrow BS$ scenario

If it were adopted that all single stars of BS-type in old globular clusters are the product of merging contact systems due to MSW one might theoretically estimate their formation frequency. For that one may use the birth-rate function (Popova et al., 1982b) of the close binaries in the entire Galaxy reconstituted on the basis of observational data of Sun neighborhood:

$$d\nu^3 = 0.2 \cdot d(lgA/R_\odot) \cdot (M_1/M_\odot)^{-2.5} \cdot d(M_1/M_\odot) \cdot dq. \qquad (8)$$

Supposing all potential parents of BS-stars are enclosed into *trapezium*-like area and setting $q \sim 1$, $\Delta\ lgA/R_\odot \sim 0.1$ and $\Delta M_1 \sim 0.75 \div 2M_\odot$ one may found that BS-objects are formed at a frequency ~ 0.01 per year. Knowledge of mean age of BS (2.5 Gyrs) allows to determine their average number $N_{BS} \sim 25 \cdot 10^6$.

Nevertheless it would be more suitable to evaluate not the absolute BS number but the weighted over the Horizontal Branch (HB) stars number. Since indicated

systems have fixed lifetime ($\sim 10^8$ yrs) and BS age is a function of mass the ratio of last to the first may be considered as a measure of their formation frequencies. So to form the typical HB-star with $1M_\odot$ the satellite is to be within $10^3 \div 10^6 R_\odot$. Then their ν_{HB} and N_{HB} in our Galaxy may be estimated as ~ 0.6 per year and $\sim 60 \cdot 10^6$ respectively.

Thus the sought ratio of these numbers N_{BS}/N_{HB} is evaluated as ~ 0.4 that is very close to observed estimate equal to 0.3 (De Angeli & Piotto G., *astro-ph/0303292*). It is evident that observed value of N_{BS}/N_{HB} is well reproduced by magnetic braking process in AML timescale under all residual uncertainty of input parameters.

The more massive DMS-stars with $M_1 \sim 3M_\odot$ have not MSW and may revolve with top velosities. This fact in the absence of other braking mechanisms of the rotation may leads to formation of the deccretion disks and to beginnings of the planetary systems.

References

Skumanich A.: 1972, *Aph. J.*, **171**, 565.

Iben I., Tutukov A.: 1984, *Astron. J*, **284**, 719.

Stryker L.: 1993, *PASP*, **105**, 1081.

Svechnikov M., Kuznetsova E.: 1990, *Catalogue of the approximate photometric and absolute elements of the eclipsing variables*, Yekaterinburg, **1, 2**.

Svechnikov M.: 1969, *Catalogue of the orbital elements, masses and luminosities of the close binaries*, Scientific Notes, **5**, N 88.

Popova E., Tutukov A., Yungelson L.: 1982a, *Letters in Astron. J*, **8**, 297.

Popova E., Tutukov A., Yungelson L.: 1982b, *A&SS*, **88**, 155.

De Angeli F., Piotto G.: *astro-ph/0303292*.

FLUX DENSITY ABSOLUTE MEASUREMENTS OF SUPERNOVA REMNANTS USING TWO-TEMPERATURE BLACKBODY CALIBRATION STANDARD

N. A. Dugin, I. P. Kuznetsova, V. A. Razin

Radiophysical Research Institute (NIRFI),
Nizhny Novgorod, Russia, *razin@nirfi.sci-nnov.ru, dugin@nirfi.sci-nnov.ru*

ABSTRACT. The two-temperature standard of noise radio emission consisted of two identical "black" disks with different temperatures is used to increase the accuracy of absolute measurements of cosmic source radio emission flux densities. A brief description is given to the construction of the measuring facility at the RAO NIRFI "Staraya Pustyn′", the measurement procedures and data processing with taking into account apparatus and methodical factors. The results are given of the absolute measurements made in 2003 of the radio emission flux densities of SNRs Cassiopeia A and Taurus A and the radio galaxy Cygnus A at frequencies 2829 and 8834 MHz.

Radio emission flux density absolute measurements of cosmic sources are of principle importance since they permit to measure energetic and associated parameters of astronomical objects.

The method of "blackbody" disks has been designed and thoroughly developed at the Nizhny Novgorod (Gorky) Radiophysical Research Institute (RRI) to carry out flux density absolute measurements of cosmic radio sources. The substance of the method is in radio telescope calibration by noise radio emission of an artificial radiation standard which is a metallic disk covered by a radio-absorbing material; the standard has the radio emission brightness temperature equal to that of the environment.

An essential step in the development of the "blackbody" disk method has become a possibility to place disks in the antenna Fresnel zone and overfocusing the antenna by displacing the feed from the dish focus; the calculation of diffraction corrections; an application of two identical standards with different temperatures (Dugin, 2002; Dugin, 1993). The increase of accuracy in this case is achieved due to the elimination of calculations of the atmosphere temperature behind the disk and diffraction effects that permits to widen the application range of the method (see for details Dugin et al., 2004a; 2004b; 2004c). The calibration of radio sources by the "blackbody" disk method had been carried out at NIRFI since 1960-s and were cut off in the end of 1980-s. In 2002–2003 the facility to carry out flux density absolute measurements of cosmic sources in the frequency bands of 3 and 10 GHz (in which the first measurements of Cassiopeia A, Taurus A and Cygnus A radio emission flux densities were made in autumn 1952 (Plechkov & Razin, 1956)) was reconstructed and upgraded at the NIRFI Radioastronomical Observatory "Staraya Pustyn′" (100 km to south from city of Nizhny Novgorod). The continuation of the observational series at different frequencies with new technical equipment is essential for getting more accurate data on the time variations of radio emission of SNRs Cassiopeia A and Taurus A that is significant to study the physical processes in the supernova remnants. At the resumption of work on the radio source calibration a task was set to attain an extremely small inaccuracy of absolute measurements.

The facility consists of a 7-m fully-steerable parabolic antenna and a two-temperature calibration standard mounted on a 25-m tower 100 m apart from the radio telescope. The maximum heating temperature of one of the disks is about 55° C. Receivers at 2829 MHz (wavelength 10.6 cm) and 8834 MHz (wavelength 3.4 cm) have the sensitivity threshold 0.1 K at the time constant 1 s. The data processing is made by PC Omnibook XE3100.

During the preparation and carrying out the experiments we have developed a procedure of absolute measurements of cosmic sources radio emission flux densities using two-temperature blackbody calibration standard. The problem of measuring with high accuracy the disk temperature difference proved to be rather complicated. We approved several ways of measurements which finally allowed to find the mean temperature of the heated disk with an accuracy of about 0.1° . A comparative analysis of calibration results using two-temperature calibration standard according to the developed technique and one disk according to the traditional one has shown that the calibration error by

two-temperature standard is 3–5 times less especially at the unstable absorption in the atmosphere. Besides, the application of the two-temperature standard permits to measure some of the correction coefficients and also increases accuracy and reliability of the absolute measurements of the cosmic radio sources flux densities. The advantages of the two-temperature standard will be more visible at the lower frequencies where it is practically impossible to take into account the diffraction corrections for small sizes of disks and their low position above the ground level.

To increase the measurement accuracy we have developed the way of determining the mean error of antenna pointing on the source by radio telescope drive systems directly from the data of conducting measurement series. The correction of the measured signal value by the error of antenna tracking is actual for any precision observations in shortwave bands.

In the process of measurements we used such a way of signal registration when no changes are introduced in the radiometer adjustment, and the computer memory stores the full information on the radio telescope reaction to the actions made. This allows to register continuously the changes in the atmosphere absorption and to introduce the corresponding corrections in the signal values by the developed algorithm. Such a procedure of taking into account the absorption variations during the measurements significantly widens the temporal frames of precision observations at short waves in the middle latitudes where the number of cloudless days is relatively small.

The series of observations of radio sources Cassiopeia A, Taurus A and Cygnus A at two given waves were made in summer and autumn 2003. The following values of SNR radio emission flux densities were obtained at $\lambda = 10.6$ cm: Cassiopeia A — 1059.0 ± 9.3 Jy, Taurus A — 698.1 ± 17.2 Jy. The flux density of the stable source Cygnus A was 666.6 ± 12.5 Jy. Flux density ratios of Cassiopeia A/Cygnus A and Taurus A/Cygnus A are equal, respectively, to 1.59 and 1.047 with errors 2.1% and 3.1%.

Measurements at the wavelength 3.4 cm gave the following values of SNR radio emission flux densities: Cassiopeia A — 416.4 ± 8.6 Jy, Taurus A — 471.2 ± 8.4 Jy. The flux density of the stable source Cygnus A was 163.0 ± 5.1 Jy. Flux density ratios of Cassiopeia A/Cygnus A and Taurus A/Cygnus A are equal, respectively, to 2.55 and 2.89 with errors of about 3%.

Spectral indices α ($S_\nu \sim \nu^{-\alpha}$) of the studied radio sources in the frequency band $(3 \div 10)$ GHz are the following:

Cygnus	$\alpha_{\rm Cyg} = 1.24 \pm 0.03$,
Cassiopeia	$\alpha_{\rm Cas} = 0.82 \pm 0.02$,
Taurus	$\alpha_{\rm Tau} = 0.34 \pm 0.01$.

These results are in a good agreement with those obtained at RAO "Staraya Pustyn′" in previous decades:

$\alpha_{\rm Cyg} = 1.28 \pm 0.06$ in the wavelength band 2–9 cm,
$\alpha_{\rm Cas} = 0.82 \pm 0.03$,
$\alpha_{\rm Tau} = 0.32 \pm 0.03$.

Next series of measurements was made in spring 2004 when we got the error of relative measurements of radio source flux densities less than 1% and that one of absolute measurements of about 2% at both operating frequencies. Strong enough short-term changes of SNR fluxes require regular (1–2 times a year) observations of SNR and calibration sources to reveal peculiarities in their radiation spectra.

References

Dugin N. A.: 2002, *Izv. Vuzov. Radiofizika*, **65**, 2.

Dugin N. A.: 1993, *ISEM-93, Abstract of 2nd Conf.*, Beijing.

Dugin N. A., Kuznetsova I. P., Razin V. A.: 2004a, preprint NIRFI/484.

Dugin N. A., Kuznetsova I. P., Razin V. A., Troitskij N. R.: 2004b, preprint NIRFI/485.

Dugin N. A., Kuznetsova I. P., Serkin A. G., Chernikova S. O., Boyarinov V. A.: 2004c, preprint NIRFI/486.

Plechkov V. M., Razin V. A.: 1956, *Proceedings of the Fifth Meeting on the Questions of Cosmogony, 9–12 March 1955, radio astronomy, AS USSR*, M., p. 430–435.

THE TIME DELAY OF EXTRAGALACTIC COSMIC RAYS IN THE GALACTIC MAGNETIC FIELD

A. A. Elyiv, B. I. Hnatyk
Astronomical Observatory of the Taras Shevchenko
Kyiv National University, Kyiv, Ukraine
e-mail: elyiv@observ.univ.kiev.ua

ABSTRACT. We investigate the propagation of extragalactic cosmic rays (ECRs) in the regular component of the Galactic magnetic field. Especially we numerically calculate the expected time delay of ECRs due to curvature of trajectories. The maps of time delay depending on energy and arrival directions of ECRs have been constructed. We show that regular component of Galactic magnetic field increases the time delay up to 700 kyr for low-energy part ($E \geq 3 \times 10^{17}\, eV$) of ECRs. This value is noticeably larger than the expected time delay in a random (turbulent) component of the Galactic magnetic field. Both regular and turbulent components of Galactic magnetic field do not modify considerably ECR flux and spectrum at energy $E \geq 10^{18}\, eV$.

Keywords: cosmic rays: general – Galaxy: magnetic fields.

1. Introduction

Transition from Galactic to extragalactic component in total flux of cosmic rays is still a point at issue (Berezinskii et al., 1990; Berezinskii et al., 2004). As it is argued in (Berezinskii et al., 2004) extragalactic cosmic rays (ECRs) are expected to dominate in the total flux of cosmic rays at energy $E \geq 1 \times 10^{18}\, eV$ and are comprised predominantly of protons. Galactic and extragalactic magnetic fields affect the trajectories and propagation time of ECRs and can considerably change the total flux and spectrum of ECRs (Sigl et al., 2004; Parizot, 2004). For example, it is expected that the random extragalactic magnetic field and both regular and random components of Galactic magnetic field considerably increase the time-in-flight of low energy part of ECRs outside and inside Galaxy - up to the energy loss time scale, which can result in suppressing of ECR flux (low-cut filter (Parizot, 2004)). In our work we analyse the influence of the Galactic magnetic field on the time delay of ECRs. For symmetric and asymmetric models of regular component of the Galactic magnetic field (Han&Qiao, 1994; Sofue&Fujimoto, 1983; Tinyakov&Tkachev, 2002) we numerically calculate the maps of time delay depending on energy and arrival directions of ECRs. We estimate also the time delay created by random (turbulent) component of the Galactic magnetic field and show that both regular and turbulent components of the Galactic magnetic field do not modify considerably ECR flux and spectrum at energy $E \geq 10^{18}\, eV$.

2. The Galactic magnetic field model

Galactic magnetic field consists of a regular and a random (turbulent) components. Both components have similar amplitudes ($B_{reg} \approx 3 \times 10^{-6}\, G$ and $B_{tur} \approx 5 \times 10^{-6}\, G$ for regular and random component respectively), but different scales. Basic scale of turbulent magnetic field is of order of $l_c \sim 100\, pc$. For regular magnetic field we use model proposed in (Tinyakov&Tkachev, 2002), in which regular component traces the spiral structure, reversing (bisymmetric model) or not (axisymmetric model) field direction between spiral arms. Radial and transverse (toroidal) field components are $B_r = B(r,\theta)\sin(p)$ and $B_\theta = B(r,\theta)\cos(p)$, respectively, where $p = -8^\circ$ is the pitch angle of the local magnetic field,

$$B(r,\theta) = B(r) \times \cos(\theta - \beta \times \ln((r/R) + \phi)),$$

$\beta = 1/\tan(p)$, $\phi = \beta \ln(1 + d/R) - \pi/2$, $B(r) = B_0 R/(r\cos(\phi))$, $R = 8.5\ kpc$ is the distance from the Galactic center to the Sun, $B_0 = 1.4\ \mu G$ is the strength of magnetic field near the Sun, $d = -0.5\ kpc$ is the distance from the Sun to the position of the first field reversal (in direction to the Galactic center).

Following (Tinyakov&Tkachev, 2002) we consider bisymmetric model with halo (magnetic field extends up to $R_{max} = 20\, kpc$ from Galactic center) with two possibilities for halo field: symmetric model with parallel fields above and below the disk

$$B_{sym}(r,\theta,z) = B(r,\theta) \times \exp\left(-\frac{|z|}{h}\right),$$

and asymmetric one with anti-parallel fields: $B_{asym}(r,\theta,z) = sign(z) \times B_{sym}(r,\theta,z)$, where $h = 1.5\ kpc$ is the height scale of the disk.

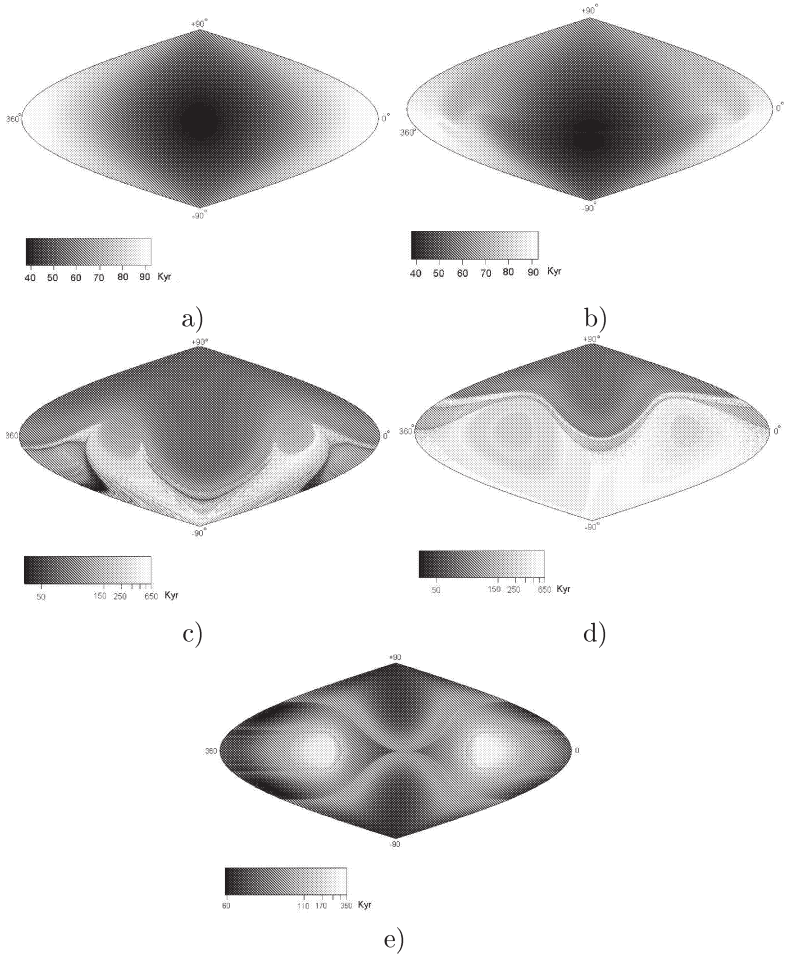

Figure 1: The propagation time maps for cosmic rays with energy $10^{20}\,eV$ (a), $10^{19}\,eV$ (b), $10^{18}\,eV$ (c), $3\times10^{17}\,eV$ (d) in the symmetric magnetic field and with energy $3\times10^{17}\,eV$ in the asymmetric magnetic field (e).

3. The maps of the propagation time

We assume that extragalactic cosmic rays are protons (Berezinskii et al., 1990; Berezinskii et al., 2004). If we eject from Earth an antiproton (a particle with the proton mass but with opposite to proton electric charge) in arrival direction of proton from ECR flux, antiproton will restore the original proton trajectory.

Therefore, we eject antiprotons with certain energy in the all possible directions from the Earth, and calculate trajectories and the propagation time of antiprotons from Earth to the edge of the Galactic magnetic field (and vice versa for cosmic ray protons).

In Fig.1(a) we show the propagation time for protons with energy $E = 10^{20}\,eV$. As the distance from Earth to the Galactic center is 8.5 kpc, the propagation time changes in the range from 37 to 93 kyr. Due to the fact that at such a high energy protons move practically rectilinearly, the time delay (as a difference between propagation time for proton and photon for given direction) in this case is practically absent.

With decreasing of energy of ECRs the propagation time increases (Fig.1(b-e)) and reaches a saturation for 10^{17}eV - 10^{18}eV at a maximum value of order of 650 kyr, i.e., the maximum value of time delay is $T_{max} \sim 600\,kyr$. The main reason for the limited value of time delay is the regular character of the Galactic magnetic field considered.

4. Turbulent component of the magnetic field

Larmor radius $r_L = E/eB_{tur}$ of ECR proton with energy $E \geq 3 \times 10^{17}\,eV$ in magnetic field $B_{tur} = 5 \times 10^{-6}\,G$ is considerably larger than basic scale of turbulent magnetic field $l_c = 100\,pc$. Therefore, penetrating in the turbulent Galactic magnetic field ECRs move initially quasi-rectilinearly with the random small-angle scattering, resulting in the r.m.s. deflection angle θ over a distance r (Sigl et al., 2004)

$$\theta \sim 40^{\circ}(\frac{E}{10^{18}\,eV})^{-1}(\frac{r}{1\,kpc})^{1/2}$$

and the time delay

$$\tau \sim 0.38(\frac{E}{10^{18}\,eV})^{-2}(\frac{r}{1\,kpc})^{2}\,kyr$$

For all directions out of Galactic plane ECRs with $E \geq 10^{18}\,eV$ can penetrate Galactic disk and reach Earth in ballistic regime without considerable flux suppression. The transition to diffusive regime takes place at distances where $\theta \sim \pi$ or $r_{dif} \geq 2\,kpc$ at energy $E \geq 3 \times 10^{17}\,eV$. Since $r_{dif} \geq h$, diffusive regime does not affect considerably the time delay of ECRs.

To summarise, both regular and turbulent components of the Galactic magnetic field do not modify considerably ECR flux and spectrum at energy $E \geq 10^{18}\,eV$.

Acknowledgements. This work is supported by Ukrainian grant DFFD 02.07/00430.

References

V. Berezinskii, S. Bulanov, V. Dogiel, V. Ptuskin: 1990, *Astrophysics of cosmic rays.* Amsterdam: North-Holland, p. 534.

V. Berezinsky, S. Grigorieva, B. Hnatyk: 2004, *Astropart. Phys.*, **21**, 617.

G. Sigl, F. Miniati, T. Ensslin: 2004, preprint astro-ph/0409098.

E. Parizot: 2004, preprint astro-ph/0409191.

J. Han, G. Qiao: 1994, *Astron. Astrophys.*, **288**, 759.

Y. Sofue, M. Fujimoto: 1983, *ApJ*, **265**, 722.

P. Tinyakov, I. Tkachev: 2002, *Astropart. Phys.*, **18**, 165.

DETERMINATION OF POLE AND ROTATION PERIOD OF NOT STABILIZED ARTIFICIAL SATELLITE BY USE OF MODEL "DIFFUSE CYLINDER"

S.Ya. Kolesnik, A.V. Dobrovolsky, N.G. Paltsev

Department of Astronomy, Odessa National University
T.G.Shevchenko Park Odessa 270014 Ukraine, *astro@paco.odessa.ua*

ABSTRACT. The algorithm of determination of orientation of rotation axis (pole) and rotation period of satellite, simulated by a cylinder, which is precessing around of vector of angular moment of pulse with constant nutation angle is offered. The Lambert's law of light reflection is accepted. Simultaneously, dependence of light reflection coefficient versus phase angle is determined. The model's simulation confirm applicability of this method. Results of the calculations for artificial satellite No 28506 are carried out.

The determination of parameters of satellite movement around its centre from the photometric data is a typical reverse task of the satellite astronomy. The decision of this task allows to investigate influence of the environment factors on movement of satellite and to determine levels of these factors.

1. Choice of model

The model, accepted by us, first of all is applicable to rockets, to cylindrical satellite, which has lost stabilization after the ending of term of active work. We suggest the Lambert's law of light reflection as the elementary law which is taking into account characteristics of diffuse reflection of light. Most simple and effective model is the circular cylinder without the end faces. Such model is suitable, if the length of the cylinder in some times exceeds its diameter and the reflection of light from end faces can be neglected. The additional argument for a choice of this model is the fact, that the end faces of real rockets is not flat and does not essentially, contribute to the emission of a satellite. A more complex model having the form as the cylinder with hemispherical ends (having identical or different coefficients of light reflection) here was not considered.

2. The formulas

Further we shall consider, that the orbital elements of the satellite are known, and it is possible to calculate its place at the orbit at any time t; therefore are known the orts ε, k of "satellite-Sun" and "satellite-observer" directions; under the formula

$$\vec{b} = \frac{\vec{\varepsilon} + \vec{k}}{\mid \vec{\varepsilon} + \vec{k} \mid} \tag{1}$$

it is possible to calculate the vector $\vec{b}$ which is the bisectrix of phase angle (angle "sun-satellite-observer" designate by a symbol α).

As a result of photometric observation and their correction through extinction of light in the atmosphere is received a series of magnitudes $\{m_j\}$ at the time $\{t_j\}$. We shall transform magnitudes to intensity of light I^o, which is reflected by the satellite to the observer, under the formula

$$I^o = 278000 \cdot r^2 \cdot \exp\left(-0.921 \cdot m\right), \tag{2}$$

where r – distance up to the satellite in km. After processing, we shall receive a function of change of brightness as $I^o = I^o(t)$, where the index "o" designates, that the light curve is obtained from the observation. At a beginning of a time-scale we shall consider some moment t_0, which corresponds to the maximum of brightness and is located approximately in middle of interval of observations (is considered one passage of the satellite on the sky of the observer).

We shall consider the movement of the satellite concerning the centre of mass as precession of the its axis of symmetry (ort L) around of a moveless axis of rotation (ort Ω) with a nutation angle Θ (Fig.1).

Considering ort Ω as known, we shall construct the basis Ω, e_1, e_2 under the formulas (Fig.2):

$$\vec{e}_1 = \frac{\vec{\Omega} \times \vec{b}_0}{\mid \vec{\Omega} \times \vec{b}_0 \mid}; \quad \vec{e}_2 = \vec{\Omega} \times \vec{e}_1 \tag{3}$$

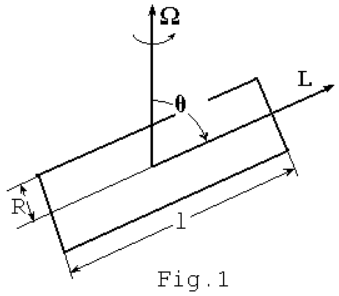

Fig.1

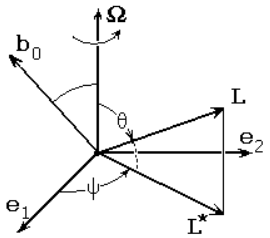

Fig.2

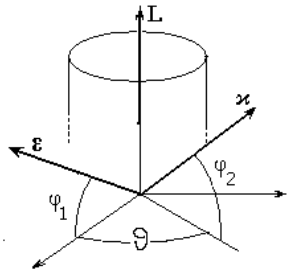

Fig.3

Here b_0 is ort b in the time t_0. Then the direction of ort L is described by the formula:

$$L = \Omega \cdot \cos\Theta + L \cdot \sin\Theta =$$

$$= \Omega \cdot \cos\Theta + [e_1 \cdot \cos\psi + e_2 \cdot \sin\psi] \cdot \sin\Theta \qquad (4)$$

where

$$\psi = \psi_0 + \omega(t - t_0); \qquad (5)$$

ω is angular velocity of the precession, ψ_0 – initial angle of the rotation. Knowing a mutual arrangement of orts ε, k, L, the sizes of model R and l, we shall calculate for a moment t under the given below formulas of light intensity I, reflected by the satellite to the observer:

$$I = I(R; l; \varepsilon; k; L(\Omega; \omega; \psi_0; \Theta; t)) \qquad (6)$$

The applied here technique of determination of a pole and rotation period of the satellite is updating of a method stated in work (Grigorevsky et al., 1979) at research of asteroids.

For various sets of parameters

$$\{\Omega, \omega, \psi_0, \Theta\} \qquad (7)$$

the theoretical curve of brightness variations $I^c = I^c(t)$ is calculated which is compared to an observable curve $I^o = I^o(t)$. For their comparison, the parameter

$$F = \sum_{j=1}^{N} \left((I^c)_j - \left(I^o_j\right) \right)^2 \qquad (8)$$

is used,which describes a degree of distinction of these curves. Let's find an optimum set of these parameters by minimizing F on parameters (7). For the calculations, the known formula for intensity of light (see, for example, McCue et al., 1971), reflected by the Lambert's cylinder was used:

$$I = \gamma l R \left\{ \frac{E}{2\pi} \cos\varphi_1 \cos\varphi_2 \left[(\pi - \vartheta)\cos\vartheta + \sin\vartheta \right] \right\} \qquad (9)$$

where E – normal illumination, created by the Sun in the vicinities of the Earth ($E = 135000$ lux), γ – factor of reflection in the Lambert's law, the angles $\varphi_1, \varphi_2, \vartheta$ are shown on Fig.3 and are functions of orts ε, k, L.

Let's designate as Φ_j expression in braces from (9) on the moment t_j; as it is impossible to determine meanings γ, l, R separately, included in (9) as product, we shall designate all this product by a symbol γ. Given factor is generally a function of a phase angle α. Considering that the given function changes rather slowly, we shall divide the interval $0° - 180°$ on 18 identical intervals, also we shall consider, what γ is constant at each of these intervals. Then the formula (8) start a kind

$$F = \sum_{k=1}^{18} \sum_{j(k)=1}^{j_k} (\gamma_k \Phi_{j(k)} - I^o_{j(k)})^2 =$$

$$= \sum_{k=1}^{18} \left(\gamma_k^2 \sum_{j(k)=1}^{j_k} \Phi^2_{j(k)} - 2\gamma_k \sum_{j(k)=1}^{j_k} I^o_j(k)\Phi_{j(k)} + \right.$$

$$\left. + \sum_{j(k)=1}^{j_k} (I^o_{j(k)})^2 \right) = \sum_{k=1}^{18} \left(a_k\gamma_k^2 - 2d_k\gamma_k + c_k \right) \qquad (10)$$

where those points enter into the sum on $j(k)$, for which the angle α gets in k-interval (certainly, for some meanings k, there is $j_k = 0$, i.e. the appropriate intervals is empty and do not bring in the contribution to the sum F). We minimize F on parameters γ_k, considering these factors by independent, for this purpose we shall write down necessary conditions of extrema:

$$\frac{\partial F}{\partial \gamma_k} = 0 \Rightarrow 2a_k\gamma_k - 2d_k = 0 \Rightarrow \gamma_k = \frac{d_k}{a_k} \qquad (11)$$

For determined $\{\gamma_k\}$, the sufficient conditions of extrema (namely-minimum) are carried out also, it follows that the square-law form (10) is positively determined. Then

$$F_{min} = \sum_{k=1}^{18} \left(a_k \frac{d_k^2}{a_k^2} - 2\frac{d_k}{a_k} d_k + c_k \right) = \sum_{k=1}^{18} \left(\frac{a_k c_k - d_k^2}{a_k} \right) \qquad (12)$$

3. Technique of minimization

The calculations which are carried out on the formulas (9)–(12), are rather simple and occupy not a lot of computing time, therefore elementary method of a rectangular grid on three parameters with a decreasing step was applied to minimization on ω, ψ_0, Θ. The optimized meanings F_{min} depend only on equatorial coordinates $\alpha_\Omega, \delta_\Omega$ of ort Ω. For these parameters, a rectangular grid (table of dependence $F_{min} = F_{min}(\alpha_\Omega; \delta_\Omega)$) is also constructed, on which directly is determined the orientation of ort Ω; optimum meanings of a nutation angle Θ, siderical period of the rotation $P = \frac{2\pi}{\omega}$ and initial angle of rotation Ψ_0 simultaneously are determined also. At $\Theta \approx 90°$, the Lambert's cylinder has the maximal brightness, when orts L, b are approximately perpendicular. The maximum appropriate to the moment t_0 has a place, when $L \approx e_1$, it follow from (3) and (4). Therefore, the initial angle ψ_0 is close to zero. We chose "with a excess" an interval $-0.6 < \psi_0 < 0.6$; if to take into account exact dependence $\psi_0(\Theta)$, the interval can be reduced. Initial meaning of angular velocity ω_0 we shall determine from observable (synodic) period of change of shine $\omega_0 = 2\pi/P_{syn}$. Let's designate through t the maximal interval between t_0 and end points of a curve of shine. Then the maximal change of angle ψ from (5), caused by a variation of angular velocity $\Delta\omega$, is those:

$$\Delta\psi = \psi_0 + (\omega_0 + \Delta\omega)\Delta t - (\omega_0 + \omega_0\Delta t) = \Delta\omega \cdot \Delta t.$$

Let $\Delta\psi < \pi$ (that is the obviously overestimated estimation). Then $\Delta\omega < \pi/\Delta t$ is maximal (and overestimated) deviation of meaning ω from ω_0.

4. Results and discussion

For check of convergence of a method the numerical experiment was carried out, in which the orbit elements of the satellite 28506 (rocket "Sich-1M", passage 05.02.2005) were used. For the arbitrary chosen orientation of rotation axis ($\alpha_\Omega = 30°, \delta_\Omega = 30°$) the theoretical light curve with siderical period = 50 sec was constructed (at $\Theta = 90°, \psi_0 = 0$). Then for this light curve, as observable, with the above described technique, the reverse task was solved and the parameters of movement of the satellite around of the centre of mass are determined. The values of $\alpha_\Omega, \delta_\Omega, P, \Theta$, were restored with high accuracy. Let's notice, that in the area $\alpha_\Omega = 210°, \delta_\Omega = -30°$ (another end of an axis of rotation, i.e. the direction opposite to a pole of rotation) also exists a minimum, however rather dim and less deep. From this follows, that the given technique allows to allocate a true direction of rotation axis by considering a parallactic effect.

The calculations for real (received from observation 05.02.2005) light curve of the satellite 28506 are carried out also. Two diametrically opposite poles of rotation are revealed: a) $\alpha_\Omega = 125°, \delta_\Omega = -12°, P = 48.15$ sec; b) $\alpha_\Omega = 308°, \delta_\Omega = +12°, P = 52.73$ sec, and to both poles correspond approximately identical values of F_{min}. Thus, in this case, the parallactic shift of maxima has not rendered essential influence on meaning of F_{min}. It is explained, first of all, that the reflection of light by surface of the satellite strongly differs from the Lambertian and contains to an essential specular component. The presence of specular component is justified by a type of the light curve, at which there are rather sharp maxima of brightness. Indirectly the presence of specular component is confirmed by the grow for the determine values of g appreciable with increase of phase angle α. In future for applying the specified technique, will be chosen a satellite, for which the dependence $I^o(\alpha)$, averaged on the period (and, if is possible, on several passages), comes closer to the theoretical dependence $I^c(\alpha)$, calculated for sphere, which reflects light according to the Lambert's law.

References

Grigorevsky V.M., Zgonjajko N.S., Kolesnik S.Ya.: 1979, *Pis'ma A.Zh.*, **5**, No 9, 482.

McCue G.A., Williams J.G., Morford J.M.: 1971, *Planetary and Space Science*, **19**, 851.

THE SET OF METHODS AND ALGORITHMS FOR THE REMOTE PHOTOMETRIC AND COORDINATE MONITORING OF COSMIC OBJECTS

N. I. Koshkin, N. G. Paltsev

Astronomical Observatory of Odessa University
T.G.Shevchenko Park Odessa 270014 Ukraine,
astro@paco.odessa.ua

ABSTRACT. The paper is devoted to elaboration of the new optimized methods, algorithms and programs for the solution of problems of the remote control of near-earth space (CS), which are related to investigation of cosmic objects (CO) based on the photometric and coordinate measurements. It is shown, that for these determination of satellite's rotation period around center of mass, the orientation of rotation axis, and also its color, polarization and others characteristics can be used. The main principles of a system of the CO identification based on their light curves are elaborated. A new algorithm of CO orbit determination using the network station data is created. Its accuracy is 3-4 grades higher than that of algorithms based on the well-known methods of celestial mechanics.

Keywords: Earth's artificial satellite, cosmic object (CO), remote control of space (CS), light curve, orbit determination.

The intensive use by world community of the space has resulted that now on different near-earth orbits there is a huge quantity of the fulfilled satellites, rockets, their fragments and waste (named by "Space debris"), representing real danger to working cosmic objects (CO), of orbital stations and is potentially dangerous to the inhabitants of the Earth.

In presented conditions the further development of near-earth space is impossible without the objective analysis of a condition of "pollution", sources of "space debris" and laws of its evolution. For the decision of these tasks the continuous *control of a space* (CS) [1] is necessary, which provides observation of the greatest possible number of cosmic objects with the purpose of reception of the most full and operatively updated multi-parametric information on current conditions in near-earth space is necessary for the decision of these problems. The volume of the information should allow to determine various characteristics CO, to draw conclusions on their form, size, status, etc. And as CO are also some kind of "trial bodies" the received information also enables to determine and specify physical parameters and state of environment of CO and to predict the further development of interaction CO with environment. I.e., the decision of CS problems is reduced to versatile research observable CO for the forecast of their flight and, probably, direction by the flight. The network of stations of the observation equipped with means of reception, processing and the analysis of the observant data is necessary for the successful decision of CS problems.

Experience shows, that most effectively problems of CS can be solved on the basis of complex use of the coordinate and not coordinate information received from observations of CO. As optical earth-based observations receive both kinds of these information about CO, the basic and the most developed now are following kinds of CS:

1. *The coordinate control* - the control of near-earth space by means of positional observations of CO with use of methods of satellite astrometry, radio ranging, laser ranging, etc. The coordinate control is primary and is based on comparison and the analysis of positions CO, that are observable and are calculated on the basis of the theory of movement, on comparison of orbital elements and their changes.

2. *The photometric control* - the control of a space by means of the analysis of the light-stream reflected by a CO-surface and measured with use photometric, spectral, polarimetric and other methods of research, widely used in astrophysics. Thus characteristic features of change of brightness of CO can be revealed, parameters and the criteria are found, allowing to estimate of grade of conformity received photometric data to properties real CO. Thus the photometric control promotes improvement of quality and reliability of identification of CO, made on a basis only the coordinate information.

It is known, that observable brightness of CO depends on many different factors. The account of influence of some geometrical and atmospheric factors on

the value of observable brightness of CO is well fulfilled, approved and stated in many papers of different authors. For the take into account of influence of some other factors it is necessary to know optical properties of CO-surface, its form, orientation, etc.

The large influence on the value of observable brightness of the artificial satellite renders absorption of light in the atmosphere of Earth, dependent besides from length of a wave. Methods of the account of distinction of instrumental and standard photometric systems are well fulfilled for stars and generalized for the artificial satellites in V.B.Nikonov's papers. Used methods of definition of extra-atmospheric brightness and color of CO are fair for all CO, taking place outside atmosphere of Earth. However, strictly speaking, application of these methods for CO moving in atmosphere, will result in overestimate of determined the values of extra-atmospheric brightness of CO.

After the account of the changing distance up to CO and the atmospheric amendments, it is possible to explain the staying observable changes of brightness by the following factors:

1) by movement of CO on the orbit and change of conditions of its illumination and the observation, connected, for example, with change of phase angle (a corner the Sun-CO-observer);

2) by CO rotation around center of mass and precession move of rotation axis;

3) by change during some time optical characteristics of a material of CO surface under action of space factors.

Besides, brightness of the some CO can contain a small-amplitude component which can be caused by the vibrations, accompanying maneuvering CO or discrete change of its form. Action of factors 2 and 3, determining CO "behavior" in the orbit and its "state", enables to carry out passive remote photometric sounding and diagnostics (or the remote control) of CO in the orbit.

The researches specify, that photometric control of CO in orbit should be based on continuous monitoring and be carried out by the following parameters:

1. By change of the period of variations of CO brightness. Angular speed of CO rotation can vary under action of atmospheric influence, pressure of the sunlight, the leak of fuel, and also at the short-term directed external influence (impact) or by a command.

2. By change of orientation in space of the axis of CO rotation, which can occur for the same reasons, as change of the period of variations of brightness.

3. By change of color, spectral and polarizing characteristics of reflected light. Their change gives the information on state of CO in the orbit and about influence on its surface of factors of near-earth space.

If observable change of CO brightness occurs because of its rotation around of the center of mass it will be periodic (quasi-periodic) and the period of CO rotation can be defined. From many methods of period search of time-series (in this case the period of CO rotation) one of the most powerful is method Lafler-Kinman (Pelt, 1980; Lafler & Kinman, 1965) and its modifications (P.N. Holopov).

The construction of dependence of CO brightness versus the value of a phase angle does not represent difficulty if exact place of CO are known, however the kind of this dependence is determined by CO form, and the calculation of real contribution of geometrical conditions of illumination into varying of brightness demands knowledge both form, optical properties, and CO orientation.

The orientation of CO is closely connected to installation of necessary operating mode of CO and its devices. Change of orientation affects on orbital drag and movement of CO, and, hence, on duration of its existence. Therefore methods of determination of CO orientation are very urgent. One's of the first papers devoted to determination of axis of rotation of rockets-carriers (RC) by means of the photometric data were the papers by V.P.Tsesevich, V.M.Grigorevsky, M.Hansburg et al. (Davis et al., 1975; Grigorevsky, 1959; Hunsburg, 1967; Kolesnik et al., 1981; Epishev, 1985).

Modern methods of determination of orientation of the rotation axis of CO, that specular reflect the light from cylindrical, conic or flat surfaces, are stated in papers of S.Ja.Kolesnik (1981), of V.P.Epishev (1985), et al. These methods also allow to draw the certain conclusions concerning design features of CO. Thus, accuracy of determination of CO orientation very much depends on accuracy of determination of parameters of its orbital movement.

More difficult problem is determination of orientation of complicated CO, which diffusely reflects (scatter) the light. Reliable algorithms of the common decision of such problem are not present. Therefore search of its decision carry out in several directions. In first, obviously simplified model of CO is considered and the problem is reduced to minimization of residuals of "calculate minus observable" brightness of CO at trial orientations of the rotation axis and sizes of model (Koshkin et al., 2003). Reliability of such decisions is for the present not so great.

On the basis of long-term experience of reception, processing and the analysis of great volume of the photometric data the system of classification of the light curves of CO is developed, allowing to automate the analysis and interpretation of the photometric data (Dobrovolsky et al., 1999; Korobko et al., 1999). On this system all light curves of CO, on presence or absence at them a periodic component, are shared into 3 classes:

- the nonperiodic light curves;
- the periodic smooth light curves;
- the periodic light curves with features.

In each of these classes, in view of specific features of the light curves, subclasses are allocated. Classification of the researched light curve to any of subclasses is carried out by its comparison with typical light curve of this subclass.

The light curves of different classes have different information content concerning characteristics of CO (dynamics of movement, features of their form, heterogeneity of covering, etc.), which cause the class of light curves and promote to identification of these CO. The most informative are light curves of 3-rd class. The light curves of 1-st class are least informative.

The developed system of classification of the light curves of CO is the important stage on the way of the decision of a inverse problem of photometry - to data acquisition about movement, the form and optical characteristics of the unknown CO. In the working catalogue over 1500 light curves concerning to more than two hundred CO is classified. These light curves are the basis of the informative data bank about CO, included in the Odessa catalogue of CO.

The opportunity of any kind of the remote control of CO depends on accuracy of the forecast of its movement, which, in turn, depends on accuracy of elements of orbits used for it. Algorithms of calculation of CO orbits based on methods of classical celestial mechanics have the essential lack and cannot satisfy the requirements of CS to accuracy of forecast of the CO positions. The analysis of movement of artificial satellite pointed, that the perturbed movement of satellite is the sum of movement of satellite occur in the plane of osculate orbit, and movement of these orbit plane that is not taken into account at all in classical methods of determination of orbits (Paltsev & Kolesnik, 2001). It requires development and creation of new reliable algorithm of determination of the CO orbit, which satisfy the requirements to accuracy of forecast of CO positions and use plenty of the coordinate information received from observation.

New algorithm of determination of CO orbit was created, admitting use of measurements received in one or several $(2 \div 5)$ close passages of CO, received by one or network of observant stations. It includes the following stages:

a) determination of primary circular (or elliptic) orbit calculated on the basis of two (three) positions of CO or according to laser measurements;

b) calculation of "Functional" - the weighed sum of squares of deviations of calculated and observed positions of CO in all arc - on the basis of algorithm of calculation of ephemeris, which take account of evolution of elements of the CO orbit;

c) minimization of "Functional" on coordinates and speed of CO in the moment t ;

d) calculation of Kepler's orbit elements of satellite on the basis coordinates and speed in the moment t.

The use of "superfluous" sets of the measurements, which were received on the long arc, results to essential reduction of influence of random errors of the primary measurements and to increase of stability and reliability of determination of the orbit by this method. Due to this there was possible use of the positional measurements of average and small accuracy. The estimations have pointed, that by use of the primary data of low accuracy ($\sim 0.1^\circ$), accuracy of semi-major axis of the orbit δa determined by this algorithm on several passages approximately on three order is higher than according to one passage, and approximately on four order is higher than by use of classical algorithms of celestial mechanics (Paltsev & Kolesnik, 2001). Such accuracy of determination of semi-major axis of the orbit was confirmed on observations of artificial satellites in 1993-2003 and on calculations of their orbits by soft "Orbita_ M" (Sheptoon et al., 1997) created on the basis of this algorithm.

References

Problem of pollution of space (space debris), *Proc. Symp. /Ed.L. Rykhlova*, Moscow: Cosmosinform, 1993. 150.

Pelt Ya.: 1980, *Frequency analysis of astronomical time series*, Tallinn: Valgus, 134.

Lafler J., Kinman T.D.: 1965, *Astron. J. Suppl. Ser.*, **11**, 100, 216-222.

Davis R.I., Wells R.C., Whipple F.L.: 1975, *Astronautically Acts, III FASCZ*, 231-237.

Grigorevsky V.M.: 1959, *Bull. of stations of optical observations of satellites*, **10**, 1-3.

Hunsburg M.: 1967, *Proc. Symp. Miami, ARL Report N 69-0078*, 42-46.

Kolesnik S.Ja., Grigorevsky V.M. et al.: 1981, *Observations of artificial celestial bodies*, **79**, 81-87.

Epishev V.P.: 1985, *A&A*, **50**, 89-93.

Koshkin N.I., Burlak N.R. et al.: 2003, *Proc. of the conf. Near-Earth astronomy-2003 /Ed.L.Rykhlova*, Russian academy of science institute for astronomy, St.-Pb., **2**, 166.

Dobrovolsky A.V., Medvedev Yu.A. et al.: 1999, *Abstracts Gamow Mem. Int. Conf. "The Universe of Gamow: Original Ideas in Astrophysics and Cosmology"*, Odessa, 117.

Korobko A.A., Dobrovolsky A.V. et al.: 1999, *Abstracts Gamow Mem. Int. Conf. "The Universe of Gamow: Original Ideas in Astrophysics and Cosmology"*, Odessa, 122.

Paltsev N.G., Kolesnik S.Ya.: 2001, *Bull. of Astronomical School*, **2**, 1, 10-16.

Sheptoon A.D., Kolesnik S.Ja., Paltsev N.G.: 1997, *Odessa Astron. Publ.*, **10**, 147-148.

DISCOVERY OF TWO LITHIUM CEPHEIDS IN THE GALAXY

V.V. Kovtyukh[1] , G. Wallerstein[2], and S.M. Andrievsky[1]

[1] Department of Astronomy, Odessa State University
T.G.Shevchenko Park, Odessa 65014 Ukraine, *val@deneb.odessa.ua*
[2] Department of Astronomy, University of Washington, Seattle, WA 98195

ABSTRACT. We report about the discovery of two lithium Cepheids in the Galaxy, based on observations made with the echelle spectrograph of the Apache Point Observatory. We have used high-resolution, high signal-to-noise spectra to determine abundances of chemical elements in 16 classical Cepheids. Only two of our program stars show a lithium line, RX Aur and YZ Aur (RX Aur has been also classified by us as a new non-radial pulsator). For the others, including the stars with [N/C]<0.2, Li is depleted up to <logN(Li)=1.0 or somewhat less. Hence it appears that mixing depletes Li before stars enter the instability strip. According to stellar models the main mixing event takes place when T_e drops below 4000 K, which is outside the red edge of the instability strip; i.e. after stars have crossed the instability strip for the first time.

Key words: Stars: abundances; stars: lithium; cepheids: non-radial pulsation; Cepheids:instability strip.

1. Introduction

The study of lithium content as a function of effective temperature, rotation and deepening of the convective zone is a key problem for our understanding of stellar convective mixing.

Cepheids have masses of roughly 3–9 $M_\odot$. Hence they are relatively young stars. After leaving the main sequence they evolve to the right in the HR diagram. In so doing they pass through the instability strip (IS). As they evolve toward even cooler temperatures they reach an effective temperature (T_e) of 4000 K, near which their convective envelopes reach down to the level at which they have depleted their lithium and scooped up material that had been subjected to the reactions of the CN cycle. After this "first dredge-up" the N/C ratio rises significantly, about a factor of 4. Since the IS does not reach T_e values as low as 4000 K, stars that are crossing the instbility region for the first time should not show the enhanced lithium abundance that is expected for stars that have mixed.

2. Observations and data reduction

The new spectra were obtained with the echelle spectrograph of the Apache Point Observatory (APO). By using a prism as cross-disperser the APO echelle covers all wavelengths from 3500 to 10 400 Å. The resolving power is about 35 000. Exposure times were usually about 10–30 minutes. We estimated the S/N ratio at the continuum level depending upon the wavelength interval to be about 80–150.

The continuum level placement, wavelength calibration and equivalent widths measurements were performed with DECH20 code (Galazutdinov, 1992).

3. The parameters and abundances

To determine the effective temperatures for our program stars we employed the method of Kovtyukh & Gorlova (2000) based on T_e – line depth relations. This technique allows the determination of T_e with an exceptional precision. It relies on the ratio of the central depths of two lines that have very different functional dependences on T_e (note that tens of pairs of lines are used in analysis). The method is independent of the interstellar reddening and only marginally dependent on individual characteristics of stars, such as rotation, microturbulence, metallicity and others.

The microturbulent velocities and gravities were found using modification of the standard analysis proposed by Kovtyukh & Andrievsky (1999). In this method the microturbulence is determined from Fe II lines (instead of Fe I lines, as used in classic abundance analyses).

Elemental abundances were calculated with the help of the Kurucz's WIDTH9 code. As usual, the reference abundances are adopted following Grevesse et al. (1996).

4. The lithium abundance in two cepheids

For a long time no classical Cepheids and supergiants were known to show a Li line. Luck (1982) found two lithium supergiants – HD 172365 and HD 174104 in the Galaxy. Luck & Lambert (1992) discovered lithium in the LMC Cepheid HV 5497.

We have detected the Li I 6707.8 Å line in two stars – RX Aur and YZ Aur. In Figs. 1, 2 we show the Li region in several spectra of RX Aur and YZ Aur, also we show this region in spectrum of usual Cepheid δ Cep without lithium line. For RX Aur the mean value of logN(Li) = 1.81 ±0.09, while for YZ Aur logN(Li) = 1.66 ±0.06. These estimates can be compared to the solar system lithium content: logN(Li) = 1.1 for the Sun and 3.3 in meteorites (Lodders, 2003). Assuming that Cepheids started with the meteoritic abundance, the bulk of the Cepheids have depleted their lithium by at least 2.3 dex while RX Aur and YZ Aur – by only 1.6 dex. According to the theory (see de Laverny et al. 2003), the lithium depletion begins when a star of about 3 $M_\odot$ reaches T_e = 6400, and lithium abundance becomes logN(Li) = 1.0 at about T_e = 5500 K. This agrees with our observation that the upper limit on logN(Li) = 1.0 for the great majority of our program stars.

The first dredge-up is expected to occur at nearly T_e = 4000 K which lies outside the IS (Petroni et al., 2003). It seems that the mixing processes that involve Li in this stars was more complicated than in the standard models.

Also RX Aur and YZ Aur have broadened spectral lines of all elements. Altogether this could be a sign that these two Cepheids are crossing the IS for the first time (Bersier & Burki, 1996). Another example of the first-crossing Cepheid is SV Vul (Luck et al. 2001). RX Aur, YZ Aur and SV Vul show the following common peculiarities:

1. The width of the spectral lines in RX Aur and YZ Aur are larger than in other Cepheids (rotation? macroturbulence? non-radial pulsation?). But it should be noted that at the same time the spectra SV Vul show sharp lines (maybe we see a polar region of SV Vul).

2. Pulsational period is about constant for RX Aur and YZ Aur or even decreasing (SV Vul), but the evolutionary calculations predict a rapid increase of period for the first-crossing Cepheids (see, for example, Bono et al. 2000, Turner & Berdnikov 2004).

Nevertheless such predictions cannot be considered as being reliably grounded and definitive. Really, just before entering the red giant phase the first crossing Cepheid suffers a sudden decrease of luminosity. During this stage its radius does not increase, on the contrary it can even decrease, causing the period decreasing. For example, observational data of Szabados (1978) testify against an observed increase of pulsational periods in the first crossing Cepheids. Standard evolutionary models do not describe adequately period changes in galactic Cepheids, as well as in Magellanic Cloud Cepheids (Pietrukowich 2001, 2002, 2003).

Our results may indicate that mixing begins long before the red giant stage. In fact the strength of convection could be much higher than it is predicted by

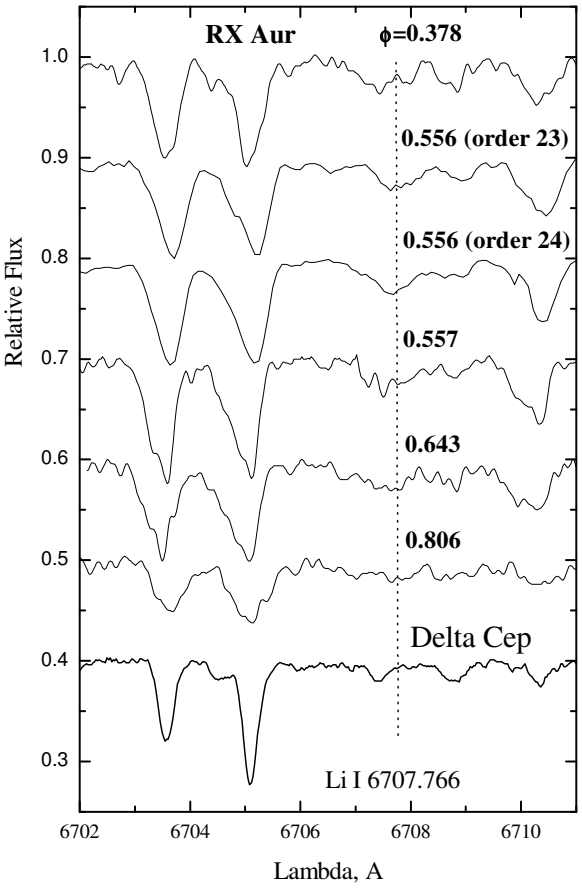

Figure 1: The Li region in RX Aur spectrum. Pulsational phases are shown. For the sake of clarity the continuum level is equally shifted. We see also unusual line profiles with small blue-shifted sharp bumps in some phases, that could be explained by non-radial pulsations excited in this Cepheid (see text for details). The resolving power is R=35000 for ϕ=0.556 and R=80000 for others phases.

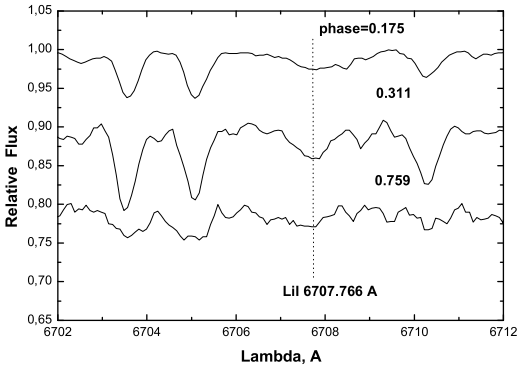

Figure 2: The same as Fig. 1, but for YZ Aur spectrum.

the standard stellar evolution theory. If one increases the convective mixing length, say, by two times, then the red giant branch appears to be shifted by several hundreds degrees towards the higher temperatures. At the same time this also shifts leftwards the region of the sharp luminosity decrease for the first-crossing Cepheids, and this region can fall on the IS (see Cordier et al. 2003). Since the both luminosity and temperature decrease within this region, this means that the Cepheid radius is about constant, and we will not be able to detect any significant period change.

5. RX Aur - a new non-radial pulsator

Unlike in the non-variable supergiants, the profiles of the Cepheids vary with phase. In the paper of Kovtyukh et al. (2003), among the 99 program stars the four unusual Cepheids were found (BG Cru, V1334 Cyg, EV Sct and X Sgr) that show interesting absorption bumps in the wings of spectral lines. Three of them (BG Cru, V1334 Cyg, EV Sct) are s-Cepheids (it is quite possible that X Sgr is s-Cepheid too). It was also noted that these four Cepheids have rather large widths of the spectral lines.

Kovtyukh et al. have suggested that the observed bumps in the line profiles in some Cepheid spectra can be considered as a combined effect of the rather high broadening (either due to rotation or macroturbulence) and a resonant interaction between the radial modes that produces the non-radial oscillations. The presence of non-radial pulsation effectively divides the visible surface of a star into sectors with different velocity fields and temperatures, and these regions redistribute the light in a rotationally broadened absorption profile to create the time-dependent bump pattern.

We have carefully re-examined available high-resolution spectra (R=80 000) of RX Aur, and found weak absorptional blue bumps at ϕ=0.557 (see Fig. 1). Note that RX Aur and X Sgr demonstrate an unusual similarity in the spectral line profiles at common phases near 0.55, where the non-radial effects are well seen. It should be noted that the effect is much more prominent in X Sgr than in RX Aur.

RX Aur has a larger period (P=$11^d.6235$) than the other five discussed Cepheids. Interestingly enough, unlike them, its pulsation amplitude is the smallest among the other 11 day fundamental Cepheids. This might be considered as additional confirmation of its status as a first-crossing Cepheid. Actually, having not reached the red giant phase, RX Aur did not experienced yet the dredge-up. Thus, it should have a smaller than ordinary Cepheids helium content, and therefore the smaller pulsational amplitude.

The total number of Cepheids with broadened lines which are known at present is 12. Only two of them, RX Aur and YZ Aur, show Li line. Five of them show obvious signs of the non-radial pulsations. The existence of the other seven Cepheids with measurable rotation but without visible bumps indicates that rotation is a necessary but not sufficient condition for an excitation of the non-radial pulsations. Looking at the common properties of the Cepheids with non-radial pulsations, one can note that among their similar features there are also small pulsation amplitude and period value that is close to the resonace between possible overtones and fundamental mode. For instance, RX Aur has its period value also near the well known 10 day resonance.

6. Summary

We discovered two lithium Cepheids in the Galaxy among more than 150 investigated program stars. These two cepheids (RX Aur and YZ Aur) show the presence of the resonance Li lines. They also show line broadening that indicates to their rather high rotation. Moreover, we conclude that RX Aur could be a non-radial pulsator.

Acknowledgements. The authors would like to thank Dr. R.E. Luck for the use of its spectroscopic data. The authors thank Drs. B. Carney and A. Fry for kindly provided KPNO spectra of RX Aur.

References

Bersier D., Burki G.: 1996, A&A **306**, 417.
Bono G., Caputo F., Cassisi S., Marconi M., Piersanti L., Tornambe A.: 2000, ApJ **543**, 955.
Cordier, D., Goupil, M.J., Lebreton, Y.: 2003, A&A **409**, 491.
De Laverny P., do Nascimento J.D.Jr, Lebre A., De Madeiros J.R.: 2003 A&A **410**, 937.
Galazutdinov G.A.: 1992, Prepr. SAO RAS **92**.
Grevesse N., Noels A., Sauval J.: 1996, ASP Conf. Ser. **99**, 117.
Kovtyukh V.V., Andrievsky S.M.: 1999, A&A **351**, 597.
Kovtyukh V.V., Gorlova N.I.: 2000, A&A **358**, 587.
Kovtyukh V.V., Andrievsky S.M., Luck R.E.: Gorlova N.I., 2003, A&A **401**, 661.
Lodders K.: 2003 ApJ, **591**, 1220.
Luck R.E.: 1982, PASP **94**, 811.
Luck R.E., Kovtyukh V.V., Andrievsky S.M.: 2001, A&A, **373**, 589.
Luck R.E., Lambert D.L.: 1992, ApJSS, **79**, 303.
Petroni S., Bono G., Marconi M., Stellingwerth R.F.: 2003, ApJ, **599**, 522.
Pietrukowicz P.: 2001, Acta Astron., **51**, 247.
Pietrukowicz P.: 2002, Acta Astron., **52**, 177.
Pietrukowicz P.: 2003, Acta Astron., **53**, 63.
Szabados L.: 1978, in.: "Stellar Phys. and Evolution. Role star Clusters Cosmogony and study galactic Struct. 1977, Budapest", 151.
Turner D.G., Berdnikov L.N.: 2004, A&A **423**, 335.

TEMPORAL VARIATIONS OF IONOSPHERIC SCINTILLATION INDEX ON COSMIC RADIOSOURCES OBSERVATIONS AT DECAMETRIC WAVE RANGE

R.O. Kravetz, O.A. Litvinenko, S.K. Panishko

Observatory URAN-4, Kharkov Radioastronomical Institute of National Academy of Sciences
Pushkinskaya str. 37 Odessa 270011 Ukraine
uran@paco.net

ABSTRACT. As show measurements cosmic radiosources have scintillations on ionospheric irregularities at decametric waves. Analysis of temporal variations of scintillation indexes was carried out on the base of observation data obtained on RT URAN-4 during 1998-2001. Daily-seasonal dependence of these indexes was investigated. The values of scintillation indexes varied with intervals from several minutes to several years, the amplitudes of such variations can reach 70 per cent from mean value.

Key words: Radiosources: scintillations; ionosphere: irregularities: electron density.

1. Introduction

At realization of radioastronomical observations in decametric wave range the essential effect appears the scintillations of compact cosmic source signals on ionospheric plasma irregularities. Basic measuring parameter reflecting the depth of scintillations is the index m determined on the formula:

$$m = \sqrt{< (I - < I >)^2 >} / < I > \qquad (1)$$

where I – intensity, measuring on the receiver's output of the radiotelescope (RT). At the certain values of the scintillation index the conditions of realization decametric radioastronomical observations can be worsened, that has an effect for results of measurements. Therefore, at realization of such observations it is important to take into account a level of ionospheric scintillation activity, which can varies with time. Ionospheric scintillations were studied in numerous investigations (for example, Crane, 1977; Aarons, 1982), but as on a state of the ionosphere renders influence set of the factors to reveal the exact formation mechanism of irregularities, resulting to scintillations, yet it is not possible, and, hence, to determine a level of scintillation activity in the given place and in the given time the further researches are required. The purpose of work is the study of temporal variations of ionospheric scintillation index, received on cosmic radiosources observations at decametric wave range.

2. Observations and technique of processing

To get the estimations of ionospheric scintillation index the observation data of powerful cosmic radiosources were used. These observations were obtained on RT URAN-4 (Galanin et al., 1989) in 1998-2002 at frequencies 20 and 25 MHz. The observations consist that for one day some passages of each source through the direction pattern of RT were recorded. Through automatic system of registration the readout from RT receivers were entered into memory of the computer with an interval 1 second. Then the data processing was spent which consist in the following. Each recording was checked visually on presence of interferences and the strongly deformed records were rejected. The theoretical direction pattern function was fitting into the record received from observations on it the amplitude of record was determined. To reduce influence of the direction pattern on the fluctuation readout level on an observable curve the segment of length 15 minutes symmetrically from the maximal value of the fitted curve got out. On this segment from an observable curve the fitted curve was subtracted. For the received sample the scintillation index from the formula (1) was calculated.

3. Results and their discussion

In the table 1 the names of observable sources, their identification and coordinates, and also average values of scintillation indexes for all considered period on two frequencies are given. All sources show the scintillations on ionospheric irregularities. The different values of scintillation indexes for different sources are caused by features of the source structures and range of angu-

Table 1:

Source	α	δ	$m20$(MHz)	M(25MHz)
3C144 Taurus A (RSN)	$05^h31^m30^s$	$21°58.4'$	0.40 ± 0.20	0.36 ± 0.20
3C274 Virgo A (radiogalaxy)	$12^h28^m18^s$	$12°40.1'$	0.36 ± 0.22	0.30 ± 0.22
3C405 Cygnus A (radiogalaxy)	$19^h57^m45^s$	$40°36.0'$	0.29 ± 0.19	0.30 ± 0.18
3C461 Cassiopeia A (RSN)	$23^h21^m11^s$	$58°33.1'$	0.24 ± 0.17	0.22 ± 0.19

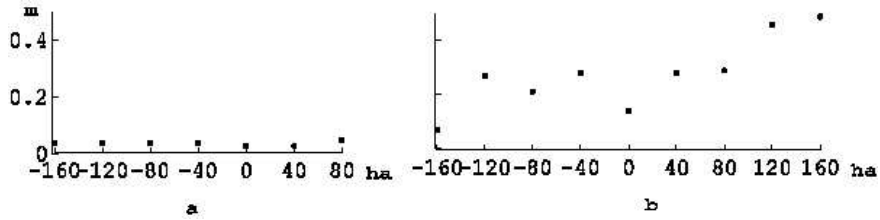

Figure 1: Variations of scintillation index on the dependence of hour angle obtained from 15-minute samples for source 3C405 in 2001 at frequency 25 MHz: a – "quiet" period, April, 4; b – "active" period, June, 4.

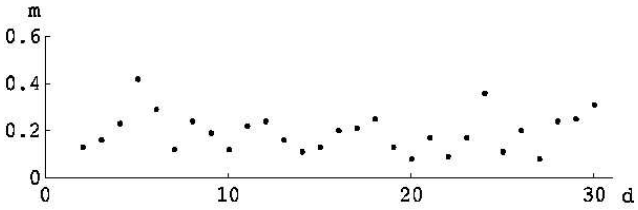

Figure 2: Daily mean scintillation index values obtained for source 3C405 in June 2001 at frequency 25 MHz.

lar heights on which they are observed. It is necessary to note, that the behavior of scintillation indexes at two frequencies is like, with that difference, that on lower frequency the level of their activity is higher, but also the level of interferences too is higher, therefore further the results of measurements on frequency 25 MHz are demonstrated, as here there are more records not deformed by interferences. As was already spoken, the state of ionosphere is influenced by set of the factors, therefore ionosphere is very changeable medium and that is reflected in behavior of a scintillation index.

Temporal scales of observed variations lay in an interval from parts of hour to several years. For the most of temporal scales of the variation values can reach 70-90 per cent from mean. The examples of scintillation index variations on time intervals day, month, 4 years are below given. In a figure 1a the plot of scintillation indexes, received on 15-minute samples within day is given which it is possible to consider "quiet". In a figure 1b the same plot, but for one of "active" days. In a figure 2 the plot of daily average values of an in-

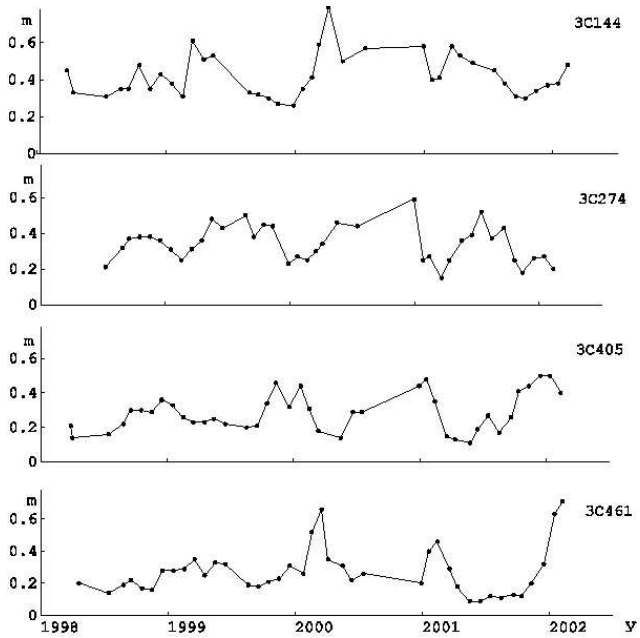

Figure 3: Monthly mean scintillation indexes obtained for four radiosources in 1998-2002 at frequency 25 MHz.

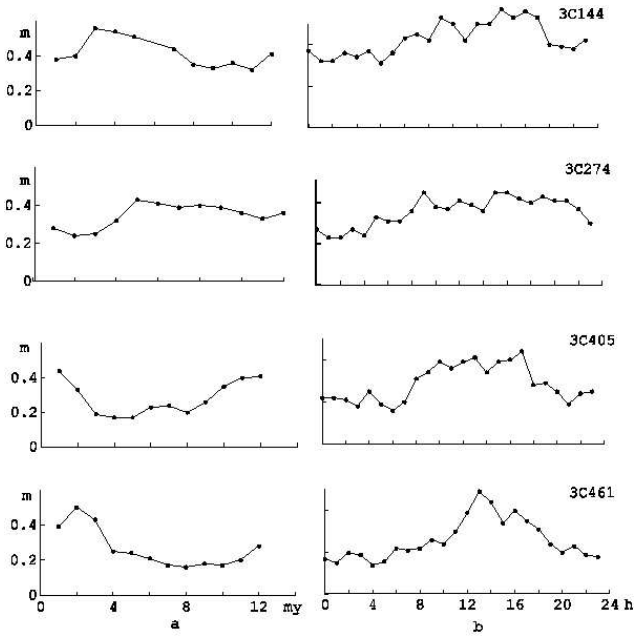

Figure 4: Mean values of scintillation indexes obtained for four radio sources on whole observation period at frequency 25 MHz: a – monthly mean, b – hour dependence.

dex m for one month for a source 3C405 is showed. Carried out before research of compact radiosources scintillations on observation data in 1987-1990 (Litvinenko & Panishko, 2000) have shown weak dependence of an scintillation index from parameters of solar and geomagnetic activity. It allows at research of various dependences in common to use the data concerning various states of ionosphere. The complexity of division of seasonal and daily dependence of a scintillation index is, that, using observation of one source, it is possible to receive the data for a time interval approximately at 5 hours, which is slowly displaced inside day, making a complete cycle for one year. That is one source gives the mixed seasonal-daily dependence. Regular character of the data, which were used in the present research, and also their performance in a digital kind, due to what exacter estimates of a scintillation index are received, allow closer to approach to the decision of this task.

In a figure 3 the plots of monthly average values of scintillation index for observed sources for all considered period are represented. The year cycle for all sources is rather well looked through, the value of variations reaches (45-70) per cent from average value. The nature of a year cycle can be determined both seasonal, and daily effect. In a figure 4a the dependences of a scintillation index from month of year is showed. Each point is the result of averaging of monthly average values for four years. The year cycle is well seen, and its phase varies from a source to a source. It testifies to a dominant role of daily dependence in the level of scintillation activity. In figure 4b the dependences of scintillation index from time of day are given, from which the increase of an index in day time and minimum at the night is visible.

4. Conclusions

If to exclude effects of solar and geomagnetic activity that is reached by averaging of a plenty of the data this research possible to established that the daily dependence is determining in seasonal-daily behavior of scintillation index. The variations of an index within one year make (45-75) per cent from average value. The minimum of scintillation activity is observed in the nighttime. These data can be considered at planning radioastronomical observations when it is necessary to take into account the influence of the ionospheric scintilations. Systematic and long-time observations of scintillation indexes allow to monitor the state of ionosphere at decametric radiowaves.

References

Crane R. K.: 1977, *Proc. IEEE,* **65**, 180.
Aarons J.: 1982, *Proc. IEEE,* **70**, 324.
Galanin V. V., Inyutin G. A., Kvasha I. M. et al.: 1989, *Kinematica i fizika nebesnykh tel,* **5**, 87.
Litvinenko O. A., Panishko S. K.: 2000, *Geomagnetizm i aeronomiya,* **40**, 116.

FRACTAL MODEL OF THE UNIVERSE

N.V. Maksyuta

National Taras Shevchenko University of Kiev, 01033 Kiev, Ukraine
maksyuta@univ.kiev.ua

ABSTRACT. In the paper for the first time from the point of view of knots theory it is considered a fractal model of the Universe. In the frames of this model it is shown that to explain its regular evolution it is necessary to adopt a conception that a physical vacuum is crystal-like. As a result it is proposed new approaches to the nature of "dark matter" and a relic radiation origin.

Keywords: Universe, fractal, trefoil, maximon, crystal, vacuum.

1. Introduction

In the given paper it is shown for the first time the model of the which evolution occurs in a regular way. Such a script proposes a crystalline space structure (see, for example, Fomin, 1990). The affirmation that space, time and motion are interconnected could be proved by such a gist: space is created by motion at a time. One of the arguments contributing to the structurization of the space under construction could be the existence of two vacua: μ-vacuum of a "dark matter" and a physical of the surrounding material world. As it is confirmed in (Gliner, 1965), a usual substance turns into μ-vacuum at a negative pressured $p = -\mu c^2$, where μ is a mass density. At the beginning of its inflation the Universe also was in a vacuum state (see, for example, Novikov, 2001; Linde, 1990), with the dimension of $l_p = \sqrt{G\hbar/c^3} \approx 1,6 \cdot 10^{-33} m$ and the density $\rho_p \approx 10^{93} g/cm^3$. Vacuum matter (inflanton) produces gravitational repulsion instead of gravitational attraction which takes place in normal conditions. Just this repulsion according to Gliner's idea gave reason for powerful impulses of giant initial spades generation of the matter inflation. To explain negative pressure this paper suggests the existence of a certain topological structure of the matter in vacuum state. From the heuristic considerations and theoretical calculations by means of knots and braid groups theory application (see, for example, Atya, 1995; Monastyrsky, 1999; Manturov, 2001) it is shown that there is a (a simple knot having a braid of σ_1^3) in the basis of a space structure. By means of the obtained "trefoil equation" and the consideration that the Universe is being constructed in a regular fractal way it is calculated a scale factor behavior coinciding with calculations by means of general relativity. Besides it is considered that "dark matter" has a cubic structure in which knots there are in turn opposite directed right-handed trefoils (further they are associated with electrons). Such a structure will be stable since repulsive forces between right-handed trefoils are compensated by the attractive forces originated in consequence with neighboring one-directed energy flows merging (the density of such vacuum coincides with ρ_p). Further on, since the trefoils (right- and left-handed) are isotopic (converted) in respect to the orientation replacement (see Manturov, 2001), similar structure should be reproduced easily in the process of the "dark matter" crystal rise which is limited by a peculiar fractal surface called a P-surface (see Turbin & Pratsevity, 1992). In the frame of this bifurcate surface in the stage of moderate inflation there occurs worlds with new crystalline vacuum which knots contain in turn one-oriented left- and right-handed trefoils. In this case vacuum structure is determined by means of a balance between attractive forces (left-handed trefoils (positrons) are attracted to right-handed trefoils (electrons)) and repulsive forces originated on account of compensation of opposite-directed energy flows between the neighbouring trefoils (just in this way it could be explained almost a zero density of electron-positron vacuum). It is also supposed that simultaneously with the rise of new vacuum it takes place a throw (channeling) of electrons in its limits from the "dark matter" regions which leads to the origin of relic radiation. This process, evidently, just lead to the moderation of the Universe regular inflation, heating it to the highest temperature. Unlike chaotic script of the Universe inflation (see, for example, Linde, 1990), the given paper deals with a regular fractal evolution of the Universe. Such a regime, first, is attractive due to the reason that now all the regions of a "dark matter" crystal space under inflation are casual-link. Just in the frames of a script of the Universe chaotic inflation of $\sim 10^{87}$ casual-unlink regions, they reveal simultaneous inflation with the possibility of $\sim \exp\left(-10^{90}\right)$ (Linde, 1990). Let's pass

to the analysis of the fractal structure of vacuum and fractal evolution of the Universe.

2. A structure of the physical vacuum and a fractal evolution of the Universe

At it follows from the above mentioned, electrons (right-handed trefoils) and positrons (left-handed trefoils) are structural units (or knots) of the space. We mean here electrons and positrons on Planck distances l_p. Consider that true electron and positron dimensions coincide with l_p and their non-screened masses are equal respectively to $m_p = \sqrt{\hbar c/G} \approx 10^{-5} g$. In other words, non-screened electrons and positrons are elementary particles with a maximum great mass of m_p named by M.A.Markov (1966). In (Markow, 1966) it is marked that gravitation interaction energy of two maximons at distance l_p equals to $W = Gm_p^2/l_p = m_p c^2$, i.e. such interaction resulted in the fact that mass defect coincides with m_p. We may say that there is an exchange between two similar maximons. They all are indistinguishable, i.e. any of them can be considered as a quantum of interaction between two others. Schematically it may be represented as left and right knots in Fig. 1a, b.

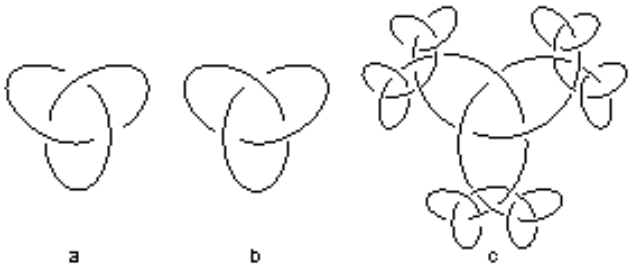

Figure 1: Left (a) and right (b) – handed trefoils, (c) – schematic representation of the process of fractal unravelling of right-handed trefoil

Thus the structure of maximon could be topologically presented as a trefoil each leaf of which is a potential maximon itself with a trefoil structure and so on and so on. Owing to maximon instability which is caused by an exact coincidence of its rest energy with the binding energy, it occurs between maximons almost at the same time (Planck time $t_P = \sqrt{G\hbar/c^5} \approx 0,5 \cdot 10^{-43} s$) non-reversible process of fractal unravelling of the trefoil structure (see Fig. 1c).

Using here a braid group B_2, generated by one oriented element σ_1, corresponding to trivial knot, the braid σ_1^2 corresponds to Hopf link, and the braid σ_1^3 corresponds to the trefoil (Atya, 1995; Monastyrsky, 1999; Manturov, 2001). We compare the equations of $\partial\vec{A}\Big/\partial t = \pm c rot\vec{A}$ with oriented trivial knots. Then Hopf link with a coefficient link +1 is compared with Maxwell equation $\partial\vec{A}_1\Big/\partial t = c \cdot rot\vec{A}_2$ and the link with a coefficient link –1 respectively with Maxwell equation $\partial\vec{A}_2\Big/\partial t = -c \cdot rot\vec{A}_1$. By the analogy to these comparisons, right- and left-handed trefoils correspond to the following systems of equations for vector fields $\vec{A}_i(\vec{r},t)$, $i = 1,2,3$:

$$\partial\vec{A}_1\Big/\partial t = \pm c \cdot rot\vec{A}_2, \partial\vec{A}_2\Big/\partial t = \\ = \pm c \cdot rot\vec{A}_3,\ \partial\vec{A}_3\Big/\partial t = \pm c \cdot rot\vec{A}_1, \qquad (1)$$

Having eliminated in the system of equations (1) the fields $\vec{A}_2$ and $\vec{A}_3$, we get the following vector equation for the field $\vec{A}$:

$$\partial^3\vec{A}\Big/\partial t^3 = -c^3 rot\Delta\vec{A}. \qquad (2)$$

Proceeding to relative units we get the following equation for the function $a(\tau)$:

$$d^3 a(\tau)/d\tau^3 = \kappa a(\tau). \qquad (3)$$

Solving the (3) at initial condition of $a(0) = 1$ and at regularity condition $a(\tau) = a(\tau + n)$, where $n = 0, 1, ...$, we get $\kappa = -8\pi^3 i$ and $a(t) = \exp(i\omega_p t)$, where $\omega_p = 2\pi\sqrt{c^5/G\hbar}$ is a Planck frequency. It is evident from here that the function $m(\tau) = |a(\tau)|^2$ in this case is equal to the unit, i.e. the scale varies.

Now instead of the derivative exponent 3 in the (3) we substitute Hausdorff-Besicovitch fractal dimension $\alpha = \ln 13/\ln 3 \approx 2,335$, characterizing a fractal growth of a crystalline vacuum of the Universe. Expediency of the transition to a fractal geometry is discussed in (Nigmatullin, 1992; Benoit, 2002). As a result we come to the following initial value problem for an arising fractional equation:

$$d^\alpha a(\tau)/d\tau^\alpha = -8\pi^3 i a(\tau) \qquad (4)$$

$$\left.\frac{d^{\alpha-1}a(\tau)}{d^{\alpha-1}a(\tau)}\right|_{\tau=0} = -4\pi^2\ ,\ \left.\frac{d^{\alpha-2}a(\tau)}{d\tau^{\alpha-2}}\right|_{\tau=0} = 2\pi i, \\ \left.\frac{d^{\alpha-3}a(\tau)}{d^{\alpha-3}a(\tau)}\right|_{\tau=0} = 1. \qquad (5)$$

As it follows from (Samko et al., 1987), the solution of the problem (4), (5) is represented in the form $a(\tau) = -4\pi^2\tau^{\alpha-1}E_{\alpha,\alpha}(z) + 2\pi i\tau^{\alpha-2}E_{\alpha,\alpha-1}(z) + \tau^{\alpha-3}E_{\alpha,\alpha-2}(z)$, where $z = -8\pi^3 i\tau^\alpha$, $E_{\alpha,\beta}(z) = \sum_{k=0}^{\infty} z^k/\Gamma(\alpha k + \beta)$ is Mittag-Leffler function. Just the scale factor in this case is a function of a relative time τ and is given by the expression $m(\tau) = \left|d^{\alpha-3}a(\tau)/d\tau^{\alpha-3}\right|^2 = \left|-4\pi^2\tau^2 E_{\alpha,3}(z) + 2\pi i\tau E_{\alpha,2}(z) + E_{\alpha,1}(z)\right|^2$. The

same dependence is represented in (Linde, 1990) but it is obtained by another way, taking into account general relativity.

Such script may take place in the following way. At the beginning the Universe being the right-handed trefoil, starts to reproduce itself spontaneously. Each leaf of the trefoil transforms into three new right-handed trefoils; they occur to be nine. Then each of these nine trefoils again reproduces three new ones; they occur to be 27. This amount of initial space quanta is packed into the initial cube of "dark matter". Further the "dark matter" crystal grows fractally since it is the most optimum way to a spherical form. Further evolution of the Universe leads to the increase of our space volume at the expense of a constant growth of a "dark matter" volume and consequently at the expense of its escape from our matter with the velocity of the light. Imaginary speaking, in the "dark matter" like in a skeleton it occurs an everlasting plaiting of the space (the space is not blowing, it is completing). Simultaneously from all sides it occurs an intervention in our space of isolated right-handed trefoils-maximons (electrons), creating the effect of relic radiation (the oscillations of our space surface layer adjoined to the "dark matter"). From the point of view of the channeling theory as expressed in (Marichev, 1987) this is a radiation of channeling particles, moving towards us at zero velocity. The relic radiation frequency is calculated by the formula $f_{\max} = \omega_P \Big/ \gamma_{\max}^{3/2}$, where $\gamma_{\max} = m_p/m_e$ is a maximum possible Lorentz factor value, m_e is an electron mass.

3. Conclusions

From the above mentioned it is evident that a fractal script of the Universe evolution undergoes following stages: fist vacuum was in a fold stage like a trefoil then it is unravelled in vacuum of a "dark matter" (the period of inflation) and at last in its interior it is originated a vacuum of a compensated electron-positron type. At the same time from the "dark matter" regions as from the source it is injacted from all the sides a noncompensated matter creating the effect of a relic radiation.

Acknowledgements. The author thanks Prof. E.G.Belokolos for the stimulated discussions.

References

Fomin P.I.: 1990, *On a crystalline structure of a physical vacuum at Planck distances. The problems of physical kinetics and physics of solid body.* Proc. of scient. papers /Edit. by A.G.Sitenko.; Acad. of Science of Ukraine. Inst. of Theor. Physics., Kiev: Naukova dumka.

Gliner E.B.: 1965, *ZhETF*, **49**, 542.

Novikov I.D.: 2001, *Vestnik RAN*, **71**, N 10, 886.

Linde A.D.: 1990, *Fhysics of elementary particles and inflation cosmology*, Moscow: Nauka.

Atya M.: 1995, *Geometry and physics of knots*, Moscow: Mir.

Monastyrsky M.I.: 1999, *Bernkhard Riman. Topology. Physics*, Moscow: Janus-K.

Manturov V.O.: 2001, *Lectures on the theory of knots and their varients*, Moscow: Editorial URRS.

Turbin A.F., Pratsevity N.V.: 1992, *Fractal maltitudes, functions, distributions*, Kiev: Naukova dumka.

Markow M.A.: 1966, *ZhETF*, **51**, N 3(9), 878.

Nigmatullin R.R.: 1992, *TMF*, **90**, N 3, 354.

Benoit B.: 2002, *Mandelbrot The fractal geometry of nature*, Moscow: Institute of Computer Investigations.

Samko S.G., Kilbas A.A., Marichev O.I.: 1987, *Integrals and derivative of a fractional order and some of their applications*, Minsk: Nauka i tekhnika.

Maksyuta N.V.: 2004, *Thesis of the report of XXXIV Intern. conf. on physics of interaction of charged particles with crystals*, Moscow: Izd-vo of Moscow university, 44.

RELATIVISTIC SHOCK BREAK OUT AT THE SURFACE OF HYPERNOVA STAR

V.V. Marchenko, B.I. Hnatyk

Astronomical Observatory of Taras Shevchenko Kyiv National University
3 Observatorna Str., Kyiv 04053, Ukraine
marv@observ.univ.kiev.ua, hnatyk@observ.univ.kiev.ua

ABSTRACT. The hydrodynamics of relativistic shock break out at the surface of Hypernova star is investigated. The characteristics of hydrodynamically accelerated external layers of star (energy spectrum of accelerated particles etc.) are estimated.

Keywords: Stars: Hypernova; gamma rays: GRB; hydrodynamics: relativistic shock waves.

1. Introduction

The gamma-ray bursts (GRBs) were discovered in the late sixties, but only detection of an optical afterglows in 1997 led to the measurement of redshifts for some long GRBs and revealed their cosmological nature (Meszaros, 2002). The first strong evidence for the connection between GRBs and SNe was provided by GRB 980425, when an unusual Type Ic supernova was seen in the error box of the GRB (Galama et al., 1998; Woosley et al., 1999). After that there were discovered another SNe that proved the GRB-SN connection – GRB 021211 (Valle et al., 2003), GRB 030329 (Stanek et al., 2003), GRB 031203 (Malesani et al., 2004).

The most popular model for long GRB is connected with death of massive star – Hypernova (Paczynski, 1998) or collapsar (MacFadyen and Woosley, 1999). In this model together with a collimated ultrarelativistic jets a mildly relativistic spherical shock break out at the surface of progenitor is expected (Woosley et al., 1999). In our work we investigate the hydrodynamics of shock break-out and determine characteristics of hydrodynamically accelerated external layers of progenitor.

2. Relativistic shock break out at the surface of star

In our work we use the CO6 model of progenitor star considered in (Woosley et al., 1999; Tan et al., 2001). It is the bare carbon-oxygen core $M_s = 6.55 M_\odot$ of $25 M_\odot$ main sequence star. The star radius is $R_s = 1.22 \times 10^{10}\ cm$.

The motion of relativistic shock wave in the outer layers of the stellar envelope can be described by an analytical approximation proposed in (Gnatyk, 1985; Berezinsky et al., 1996):

$$\Gamma_s \beta_s = (\Gamma_s \beta_s)_i \left(\frac{\rho(r)}{\rho(r_i)}\right)^{-a} \propto \left(\frac{F(r)}{F(r_i)}\right)^{-3a/4}, \quad (1)$$

where $\beta_s = u_s/c$ is the dimensionless velocity of the shock front, $\Gamma_s = \left(1-\beta_s^2\right)^{-1/2}$ is the Lorentz factor of the shock front, c is the velocity of light, $\rho(r)$ is the density of Hypernova stellar envelope as a function of distance to the center of the star r, $F(r)$ is the fraction of the stellar mass beyond the radial distance r and index "i" refers to initial values of corresponding parameters. Dimensionless parameter a is restricted by two values: $a = 0.2$ and $a = 0.232$ (Gnatyk, 1985). For outer layers of star we use a polytropic model of density distribution (Tan et al., 2001)

$$\rho(r) = \rho_0 (1 - r/R_s)^3, \quad \rho_0 = 910\ g/cm^3 \quad (2)$$

The connection between Lorentz factor of shock wave itself Γ_s and Lorentz factor of matter behind the shock γ_2 is given by the following equation (Blandford and McKee, 1976)

$$\Gamma_s^2 = (4\gamma_2 - 1)^2(\gamma_2 + 1)/(8\gamma_2 + 10), \quad (3)$$

where $\gamma_2 = \left(1-\beta_2^2\right)^{-1/2}$ is the Lorentz factor and β_2 is the dimensionless velocity of the fluid behind the shock.

The maximum value of Lorentz factor of shock corresponds to the smallest value of F at which the shock still exists in the outer layers of Hypernova star. The shock breaks out at some radius r_{max} where the dissipation of energy due to the escape of photons or other particles becomes essential (Berezinsky et al., 1996). One can show, that $F_{min} = 4\pi R_s^2 x_{int}/M_s$, where x_{int} is the interaction pathlength of photons in g/cm^2. In our calculation we use $x_{int} = 1\ g/cm^2$, therefore, $F_{min} = 1.97 \times 10^{-13}$. For initial parameters of shock wave we take their typical values from numerical calculations (Tan et al., 2001): $F_i = F(r_i) = 1.3 \times 10^{-4}$,

$\beta_{s,i} = 0.3$. In this case $\Gamma_s^{max} = 6.75\,(10.92)$ and $\gamma_2^{max} = 4.77\,(7.73)$ for $a = 0.2$ (0.232), respectively.

The temperature of the gas behind the shock front is given by (Berezinsky et al., 1996)

$$T_2(r) = \left[\frac{4}{11a_K}\,(4\gamma_2 + 3)\,(\gamma_2 - 1)\,\rho(r)c^2\right]^{1/4} \qquad (4)$$

where a_K is the constant of the energy density of radiation. When the shock reaches the surface of the star, the temperature T_2^{sur} behind it at moment of break out is given by equations (4) with $\gamma_2 = \gamma_2^{max}$ and $r = r_{max}$. The burst of radiation (gamma ray flash) emerges from the star during the shock break out, when radiation energy trapped in the shock escapes through the transparent external layer of the star. The typical energy of the photons in the burst is

$$E_\gamma^{obs} \sim \gamma_2^{max} k T_2^{sur}, \qquad (5)$$

where k is the Boltzmann constant. The corresponding values of T_2^{sur} and E_γ^{obs} for $a = 0.2\,(0.232)$ are following: $T_2^{sur} = 4.97\,(8.95) \times 10^7\ K$, $E_\gamma^{obs} = 20.46\,(59.6)\ keV$.

3. Expansion in vacuum and additional acceleration of protons

Expansion in vacuum of hot shocked plasma of stelar envelope leads to additional acceleration of matter, and final Lorentz factor is (Berezinsky et al., 1996)

$$\gamma_f = \gamma_2^b + (4 - b)(\gamma_2 - b)/\gamma_2^2, \qquad (6)$$

where parameter b is restricted by values: $b = 2.0$ and $b = 2.73$. Maximum Lorentz factor of hydrodynamically accelerated particles of star envelope is

$$\gamma_f^{max} = \left[\frac{1}{2}\left(1 + (\Gamma_s\beta_s)_i^2\left(\frac{F_i}{F_{min}}\right)^{3a/2}\right)\right]^{b/2} \qquad (7)$$

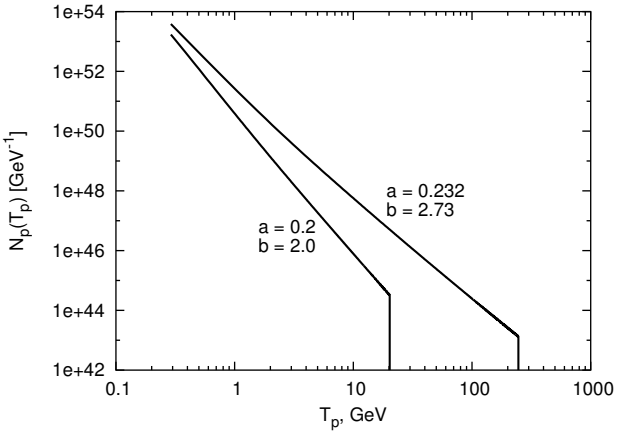

Figure 1: Differential energy spectrum of accelerated protons.

Maximum value of kinetic energy of particles (protons of mass m_p) T_p is $T_p^{max} = m_p c^2\left(\gamma_f^{max} - 1\right)$. The differential energy spectrum of protons in the whole envelope is given by

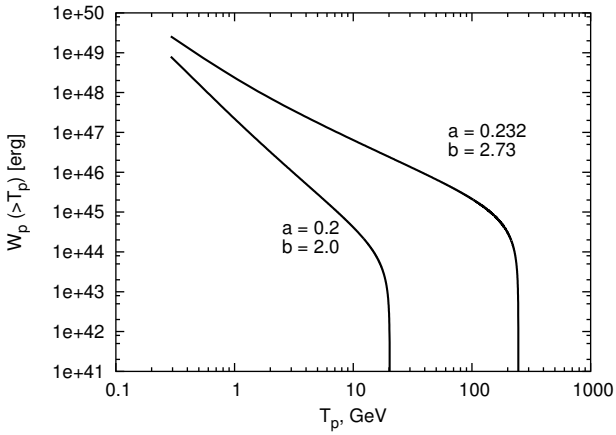

Figure 2: Integral energy spectrum of accelerated protons.

$$N_p\,(T_p) = \frac{M_s}{m_p}\,\frac{dF\,(T_p)}{dT_p}. \qquad (8)$$

It is power-low spectrum with spectral index $\delta^{diff} = 4.7\,(3.67)$ for minimum (maximum) values of a and b. The number and kinetic energy of protons with energy greater than T_p (integral spectra) are

$$N_p\,(>T_p) = \int_{T_p}^{T_p^{max}} N_p\,(T_p)\,dT_p, \qquad (9)$$

$$W_p\,(>T_p) = \int_{T_p}^{T_p^{max}} T_p N_p\,(T_p)\,dT_p. \qquad (10)$$

The differential (8) and integral (9) energy spectra are represented in Fig. 1 and Fig. 2 and parameters of hydrodynamically accelerated particles (protons) are given in Tab. 1 (T_p^{max} is given in GeV, W_p is in erg, $T_{p1} = 0.29\ GeV$, $T_{p2} = 2\ GeV$).

Table 1: Parameters of hydrodynamically accelerated protons

Parameters	$a = 0.2,\ b = 2.0$	$a = 0.232,\ b = 2.73$
γ_f^{max}	22.8	265.45
T_p^{max}	20.3	246.2
$N_p(>T_{p1})$	1.28×10^{52}	3.67×10^{53}
$W_p(>T_{p1})$	7.98×10^{48}	2.57×10^{49}
$W_p(>T_{p2})$	3.24×10^{46}	7.22×10^{47}

4. Conclusions

Relativistic shock break out at the surface of Hypernova star is accompanied by gamma ray flash and hydrodynamical acceleration of outermost layers of presupernova up to relativistic velocities. By analogy with the case of SN Ia outburst (Berezinsky et al., 1996) both the gamma ray flash and an interaction of relativistic particles with circumstellar medium can lead to signatures detectable by existing space missions.

References

Berezinsky V.S., Blasi P., Hnatyk B.I.: 1996, *ApJ*, **469**, 311.

Blandford R.D., McKee C.F.: 1976, *Phys. of Fluids*, **19**, 113.

Galama T.J. et al.: 1998, *NATURE*, **395**, 670.

Gnatyk B.I.: 1985, *Sov. Astron. Lett.*, **11**, 331.

MacFadyen A.I., Woosley S.E.: 1999, *ApJ*, **524**, 262.

Malesani D. et al.: 2004, *ApJ*, **609**, L5.

Meszaros P.: 2002, *Ann. Rev. Astron. Astrophys.*, **40**, 137.

Paczynski B.: 1998, *ApJ* **494**, L45.

Stanek K.Z. et al.: 2003, *ApJ*, **591**, L17.

Tan J.C., Matzner C.D., McKee C.F.: 2001, *ApJ*, **551**, 946.

Valle M.D. et al.: 2003, *A&A*, **406**, L33.

Woosley S.E., Eastman R.G., Schmidt P.B.: 1999, *ApJ*, **516**, 788.

STATISTICAL CHARACTERISTICS OF HYPERBOLIC ORBITS METEORS

A.K. Markina, L.Ya. Skoblikova

Department of Astronomy, Odessa National University
T.G.Shevchenko Park Odessa 270014 Ukraine, *astro@paco.odessa.ua*

ABSTRACT. We present statistical data on the distribution of orbital elements and parameters of interstellar sporadic hyperbolic meteors. We show that for some of them there is a proximity of their orbits with the Earth's orbit that can be interpreted as evidence of an existence of their interstellar origin.

Key words: meteor, orbit, hyperbolic, distribution.

In the Catalogues of Meteor Orbits (Dutch Meteor Society, photographic- and video- database from 1982 up to 2000 (Betlem, *photo@dms.web.org*; Lignie, *video@dmsweb.org*)) and MSSWG (the Meteor Science Seminar Working Group) Meteoroids Orbits (multi-station) from Yoshihiko Shigeno (photographic and TV-observations from 1953 up to 2003 (Shigeno, *cyg@nikogw.nikon.co.jp*), there are nearly 3% and 2% hyperbolic orbits of sporadic meteors respectively.

In order to reveal the peculiar characteristics of the interstellar meteors, their orbital elements and parameters of their interstellar motion have been studied by us.

Heliocentric velocity of these meteor particles slightly exceeds a parabolic limit. For 80% of meteors the excess of heliocentric velocity $dV_{\rm h} = V_{\rm obs} - V_{\rm par}$ is less than 2 km s^{-1}. Here $V_{\rm obs}$ and $V_{\rm par}$ are the observed and parabolic velocities of a meteoric particle at a distance r from the Sun ($r \sim 1$ a.u.). For a number of meteor orbits a maximum of observed distribution of their eccentricities falls within interval $e = 1.00 - 1.06$ (68%) It is demonstrated in Fig. 1. Distribution of a perihelion distance q, has a distinct maximum for $q = 0.9 - 1.0$ a.u. that is consistent with a probability maximum for meteor detecting. The second less expressed maximum is seen at $q = 0.3 - 0.4$ a.u. (about 10%, see Fig. 2).

The orbital inclination i, heliocentric interstellar velocity of a meteoric particle $V_{\rm o}$, heliocentric ecliptic coordinates of interstellar radiants λ_r, β_r and distance D of a hyperbolic orbit asymptote from the reference point are parameters of interstellar motion of a meteoric particle.

The inclination i varies from 120° to 160° for nearly 60% of hyperbolic meteors (Fig. 3). In this way their

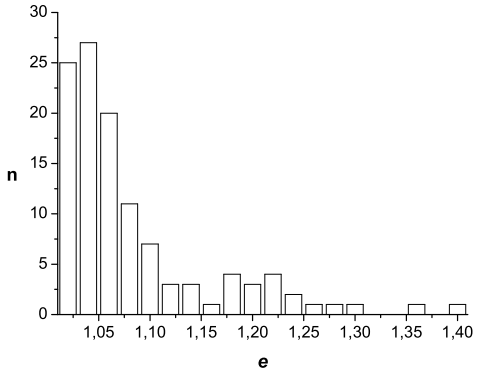

Figure 1: Distribution of the hyperbolic meteors eccentricities e.

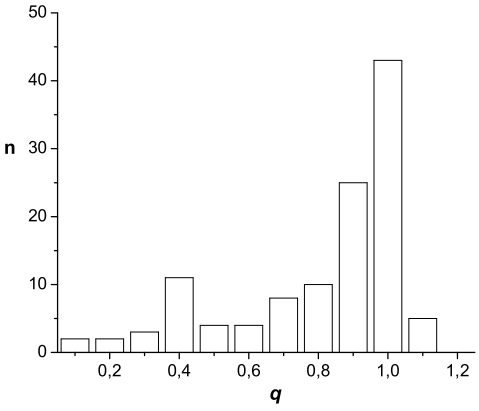

Figure 2: Distribution of the hyperbolic meteors perihelion distances q, a.u.

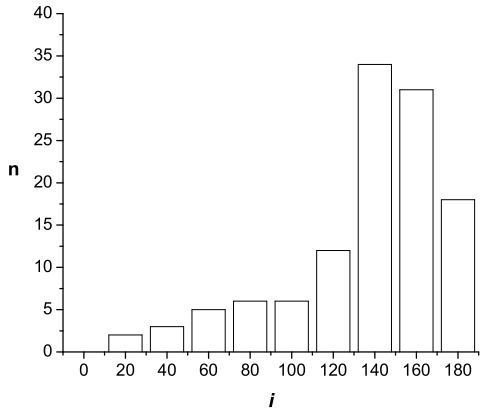

Figure 3: Distribution of the hyperbolic meteors inclinations of their interstellar trajectory i, deg.

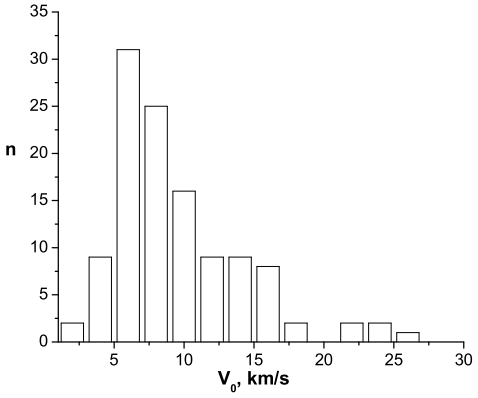

Figure 4: Distribution of hyperbolic meteors interstellar velocity $V_{\rm o}$.

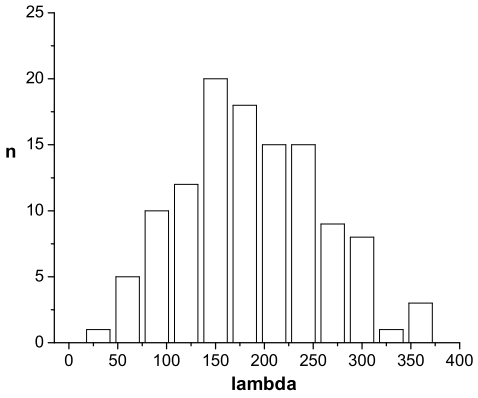

Figure 5: Distribution of ecliptic longitude λ, deg of interstellar radiants of hyperbolic meteors.

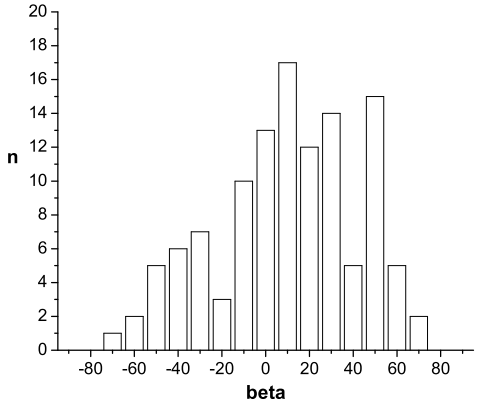

Figure 6: The same as Fig. 5 but for latitude β, deg

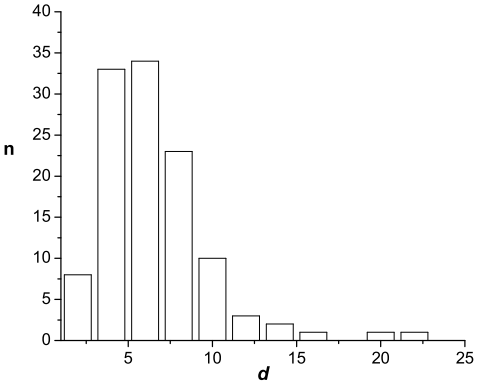

Figure 7: Distribution of hyperbolic meteors distance of asymptote from the Sun d, a.u.

orbits differ from elliptical orbits of sporadic meteors. About a half of meteor particles move at velocity $V_{\rm o}$ ranging from 4 to 8 km s^{-1} (Fig. 4). An increased concentration of interstellar radiants is observed within the region between longitudes λ_r from 90° to 240° (75%) and between latitudes β_r from −10° to 50° (65%) (Figs. 5–6) that agrees with similar distributions for typical hyperbolic orbit meteors ($dV_{\rm h} > 5$ km s^{-1}) (Kramer et al., 1998). Distribution of d value has a clear maximum between 2 and 8 a.u. (80%) (Fig. 7).

Note: r_2 (+) – the approach of meteoric particle orbit with the Earth's orbit occurred in the descending node. dr(-) – an encounter of a meteor particle with the Earth took place before its passing through the perihelion.

We also determined the necessary conditions for hyperbolic orbits of sporadic meteors to approach the Earth's orbit. Approximately 25% of the meteor orbits do not cross the ecliptic plane. For 65% of meteor par-

Table 1: Observations

Date	e	q, a.u.	i	$dV_{\rm h}$, , km s^{-1}	V_∞, km s^{-1}	λ_r	β_r	$d, a.u.$	r_2	dr
1994.03.06	1.217	0.292	44	7.2	25.6	136.2	25.9	0.9	+	–
1994.03.06	1.054	0.040	23	12.4	34.7	155.7	4.2	0.2	+	–
1996.04.22	1.008	0.497	152	0.2	3.7	294.2	27.2	7.9	+	–
1996.04.22	1.010	0.490	125	0.3	5.0	281.1	53.5	5.9	+	–

ticle orbits such an approach occurs in the descending node, and in most cases (70%) just before the meteor particle passes through the perihelion. This appears to be in a good agreement with the conclusions made in work (Kramer & Smirnov, 1999) for hyperbolic meteors with $dV_{\rm h} > 5$ km s^{-1}, and with the similar results obtained by us for hyperbolic meteor particles $dV_{\rm h} > 5$ km s^{-1} using the catalogue of transplanetary radiants (Kramer et al., 1986) based on

1) *photographic method*. 73% of meteor particles encounter with the Earth in the descending node, while for 80% of meteor paricles such encounter takes place just before perihelion;

2) *radio observations*. 67% of meteor paricles encounter with the Earth in descending node, while for 70% of meteor paricles this happens before perihelion.

According to the work (Kazantsev, 1998), some interesting hyperbolic orbits of sporadic meteor particles are given in Table 1.

As is seen from the Table 1, particles 3 and 4 have their e and q similar to those of interstellar meteors. They have been observed in the direction of the solar apex ($\lambda = 270°$, $\beta = 53°$). Thus, the given statistical characteristics of hyperbolic orbits of sporadic meteors, the heliocentric velocity of which only slightly exceeds the parabolic limit, clearly testifies their interstellar origin.

References

Hans Betlem. DMS. *photo@dms.web.org*; Marc de Lignie. DMS. *video@dmsweb.org*

Yoshihico Shigeno. MSSWG. Japan *cyg@nikogw.nikon.co.jp*

Kazantsev A.M.: 1998, *Kinem. i Fizika Nebesnykh Tel*, 82.

Kramer E.N., Markina A.K. and Skoblikova L.Ja.: 1998, *Astronomicheskiy Vestnik*, **32**, 3, 277.

Kramer E.N., Smirnov V.A.: 1999, *Astronomicheskiy Vestnik*, **33**, N 1, 85.

Kramer E.N., Shestaka I.S., Markina A.K.: 1986, Materials of the World Data Center B, 186.

DETERMINATION OF PLANETOCENTRIC COORDINATES OF ALBEDO DETAILS ON SURFACE OF THE SPHERICAL PLANET AND SOME POINTS OF THE ILLUMINATED PART OF PLANET'S VISIBLE DISK UNDER VARIOUS PHASE ANGLES FROM GROUND TELESCOPIC OBSERVATIONS

V.V. Mikhalchuk
Odessa National Maritime Academy
Didrikhsona 8, Odessa 65029 Ukraine, *phys@ma.odessa.ua, vmihalchuk@mail.ru*

ABSTRACT. The method of processing of the images of planets is based on use of auxiliary coordinate system connected with equator of intensity, is applied for determination of planetocentric coordinates of albedo details on the visible disk of the spherical planet under various conditions of its illumination. The position of a detail on the planet image is determined not relative to the center of the planet geometric disk, but relative to the center of an illuminated part of its visible disk, which permits the planetary phase influence to be excluded. By means of the given method the planetocentric coordinates of albedo details on the images of a Mercury and Mars derived from ground telescopic observations were determined.

The formulae for determination of planetocentric coordinates of some basic points of the illuminated part of the visible disk of a spherical planet, in projection onto the plane of the sky, are derived. The formulae do not require attraction of auxiliary coordinate system, in spite of the fact that they are deduced from general expressions using this coordinate system.

1. Introduction

At drawing up of maps of details of an albedo on the surface of the terrestrial planets, what their shape is spherical at first approximation, the problem of determination of planetographic coordinates of details on the images of their visible disks becomes complicated through influence of the phase, causing to appreciable damage on the visible disk. The article (Mikhalchuk, 2004a) is devoted to the solution of a considered problem. In this article the method of determination of planetocentric coordinates of any point, observable on a illuminated part of the visible disk of a spherical planet is offered.

At ground observations the equatorial planetocentric coordinate system determining a position of each point of a surface of a planet is observed on its visible disk in orthographic projection. In this coordinate system, the position of each point on the planet's surface is specified by the planetocentric latitude b and longitude l. The basic reference point is the center of the geometric disk of the planet.

The method of determination of planetocentric coordinates of center of the illuminated part of the visible disk of a spherical planet is described in article (Mikhalchuk, 2001a). From set of the points located on a illuminated part of a visible planetary disc also the greatest value for determination of planetocentric coordinates of details and for photometric measurements have some basic points located on equator of intensity (the pole of illumination, the pole of the phase, the visible center of the orthographic terminator and the mirror point), in the projection to the plane of the sky. In the contribution (Mikhalchuk, 2004b) the capability of the simplified solution of a problem about determination of planetocentric coordinates (l, b) these points is described. Let's consider the solution for two basic points: the pole of illumination and the visible center of the terminator.

2. The exception of influence of the phase angle through the auxiliary coordinate system

Let's consider the visible disk of the spherical planet illuminated by the Sun under any phase angle Φ (Figure 1). Let O is the geometric center of the planetary disk; E is the subsolar point (the pole of illumination); C is the center of the illuminated part of the planet's visible disk; F is the point of the least illumination of the disk; T is the point of intercerption direct OF with the orthographic terminator (the visible center of the orthographic terminator); the arch of the large circle

passing through the points E, C, O, T and F is the equator of intensity of the planet.

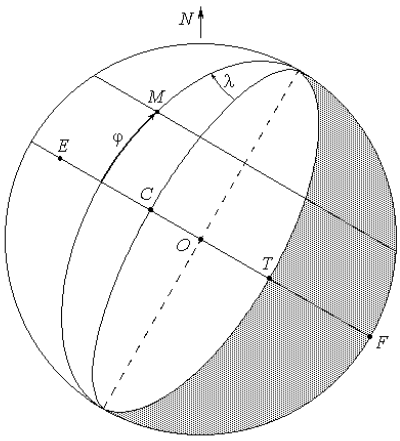

Figure 1: The auxiliary coordinate system.

In the papers (Mikhalchuk, 2004a; Mikhalchuk, 2004b) for exception of influence of a phase angle at determination of planetocentric coordinates of albedo details on surface of the planet the auxiliary spherical coordinate system (λ, φ), in which for a basic plane is adopted the plane of equator of intensity, and the poles are the orthographic horns of the disk. Origin of an auxiliary system is the the point C, which always is on the illumunated part of visible planetary disk. The arc of a large circle, passing through the orthographic horns and the point C, (mean meridian of the illuminated part of the visible disk) we shall take as an initial meridian of auxiliary coordinate system. Then the position of each point on a surface of the illuminated part of visible planetary disk will be determined by an latitude φ, is measured from the equator of intensity, and longitude λ, is measured from mean meridian westward of the planet. How is described in article (Mikhalchuk, 2004a), it is possible to find the auxiliary spherical coordinates (λ, φ) of any point on a surface of the planet (of the point M) from its relative coordinats (ξ, η).

For implementation of transition from auxiliary spherical coordinates (λ, φ) to planetocentric coordinates (l, b) we shall consider a projection of the visible disk of the spherical planet to the plane of the sky. Let $D_\oplus$ is the planetocentric declination of the Earth, P is the angle of position of the axis of rotation of the planet on the geocentric celestial sphere, Q is the angle of position of the point of the least illumination of the disk (Abalakin, 1979). The planetocentric coordinates of the point O are known and are equal (l_p, b_p), where l_p is longitude of a central meridian what is passing through center of the disk; b_p is latitude of center of the geometric disk, and $b_p = D_\oplus$. The planetocentric coordinates of the point C are equal (l_0, b_0) and are determined on the method (Mikhalchuk, 2001a). Then it is possible to determine the planetocentric coordinates (l, b) of the any point of the illuminated part of a visible planetary disk on auxiliary spherical coordinates (λ, φ) of this point through the formulae obtained in the article (Mikhalchuk, 2004a). These formulae contain the longitude $\lambda_0 = \lambda + \gamma$, where γ is the phase shift of the center of the planetary disk. The longitude λ_0 of the point M is measured from a line of the horns passing through the point O.

3. Application of the method of determination of planetocentric coordinates to drawing up of maps of the details of an albedo of the spherical planets

The planetocentric coordinates of some details of an albedo on surfaces of Mercury and Mars under their images received at ground telescopic observations (Anderson, 1997; Melillo, 2004) were determined. For processing the images of planets were taken only those, which were received at considerable phase angles.

The image of Mercury (Figure 2a) represents drawing (Melillo, 2004), received at visual observations (observer M. Frassati, telescope of diameter 203 mm). The image of Mars (Figure 2b) also represents drawing (Anderson, 1997), received at visual observations (observer Carlos E. Hernandez, telescope of diameter 200 mm). For both images the resolution equal $0.6''$.

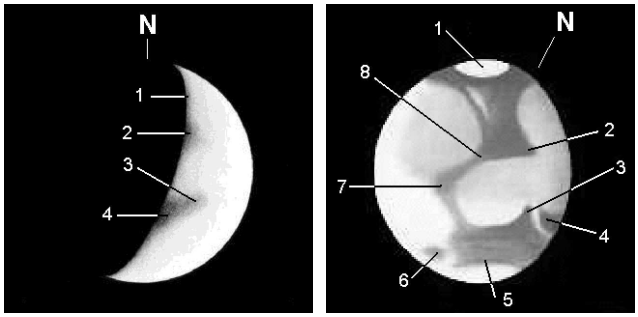

a. Mercury. b. Mars.

Figure 2: The images of visible disks of the planets.

For calculation of physical ephemerides of Mercury and Mars the elements of rotation of planets were used from article (Seidelmann et al., 2002). The visible radiuses r of planets and their the physical ephemerides at moments of observations, which are calculated on the programs of a batch (Mikhalchuk, 2001b), are given in Table 1.

On the measured relative coordinates ξ and η the auxiliary spherical coordinates λ and φ were determined through the formulae (Mikhalchuk, 2004a). During calculations the phase shift of centres of disks of planets were obtained: for Mercury $\gamma = -42.2^\circ$ and for Mars $\gamma = +5.1^\circ$. The coordinates of details on the surfaces of planets, are found as the result of application of the method (Mikhalchuk, 2004a), are listed in

Table 1: The physical ephemerides of planets

Planet	UT	r	Φ	$D_\oplus$	P	Q	l_p
Mercury	$05/05/2002, 18^h15^m$	$4''.14$	$110°.02$	$-0°.51$	$343°.03$	$72°.86$	$303°.53$
Mars	$06/01/1997, 10^h10^m$	4.22	34.79	+23.68	27.41	292.70	35.89

Table 2: The coordinates of details on the surfaces of planets

Planet	Detail	ξ	η	λ_0	φ	l	b	The name of region on the map
Mercury	1	+0.95	+0.75	$-21°.0$	$+48°.6$	$282°.5$	$+48°.1$	Apollonia
	2	+0.80	+0.45	-24.1	+26.7	279.5	+26.2	Solitudio Aphrodites
	3	+0.25	-0.10	-36.1	-5.7	267.4	-6.3	Solitudio Criophori
	4	+0.75	-0.30	-25.1	-17.5	278.4	-18.0	Solitudio Alarum
Mars	1	-0.10	+0.91	+10.4	+65.5	34.5	+89.6	The North polar cap
	2	-0.50	+0.20	-21.5	+11.5	9.9	+31.5	Deuteronilus
	3	-0.49	-0.33	-20.9	-19.3	17.9	+1.6	Margaritifer Sinus
	4	-0.80	-0.40	-39.7	-23.6	2.2	-7.2	Sinus Meridiani
	5	-0.10	-0.85	-0.1	-58.2	40.7	-34.4	Vulcani Pelagus
	6	+0.72	-0.70	+48.2	-44.4	76.0	-24.1	Nectar
	7	+0.37	-0.10	+25.2	-5.7	62.8	+17.6	Lunae Palus
	8	0.00	+0.10	+5.1	+5.7	41.2	+29.7	Niliacus Lacus

Table 2.

Comparison the planetocentric coordinates of the basic details at the images of visible disks of the Mercury and Mars, which are obtained as a result of the given method, with coordinates of the same details, which have been taken from maps of an albedo of planets of epoch 2000 (Melillo, 2004; Troiani et al., 2004), has allowed to establish, that the calculated coordinates of albedo details coincide their coordinates, which have been taken from the map, within errors of the initial images and the map.

4. Determination of planetocentric coordinates of the pole of illumination and the visible center of the terminator of the spherical planet

The formulae for determination of planetocentric coordinates of considered points should be similar to expressions for coordinates of the point C, which are obtained in articles (Mikhalchuk, 2001a; Mikhalchuk, 2004a). For points, located on equator of intensity, the latitude $\varphi = 0$. In this case from the formulae (Mikhalchuk, 2004a) we shall obtain more simplified expressions:

$$\sin b = \cos\lambda_0 \sin D_\oplus \mp \sin\lambda_0 \cos D_\oplus \cos(P-Q), \quad (1)$$

$$\mathrm{tg}(l-l_p) = \frac{\pm \sin\lambda_0 \sin(P-Q)}{\cos\lambda_0 \cos D_\oplus \pm \sin D_\oplus \sin\lambda_0 \cos(P-Q)}, \quad (2)$$

where the signs of the numerator and denominator in expression (2) coincide with the signs of $\sin(l-l_p)$ and $\cos(l-l_p)$ respectively. The formulae (1) and (2) allow to obtain the planetocentric coordinates (l, b) any point of the illuminated part of the equator of intensity.

The pole of illumination (the point E) is located on the visible planetary disk, if $\Phi < 90°$, and is on the invisible part of the planet otherwise. The longitudes of the pole of illumination are equal $\lambda = \pm\Phi - \gamma$ and $\lambda_0 = \pm\Phi$. The visible center of the orthographic terminator (the point T) has longitudes $\lambda = \pm(\Phi - 90°) - \gamma$ and $\lambda_0 = \pm(\Phi - 90°)$. Then from the formulae (1) and (2), taking into account the rule of the signs (Mikhalchuk, 2004a), and also taking into account values of longitudes λ_0, we shall obtain for the planetocentric coordinates of the pole of illumination (of the point E)

$$\sin b = \cos\Phi \sin D_\oplus - \sin\Phi \cos D_\oplus \cos(P-Q), \quad (3)$$

$$\mathrm{tg}(l-l_p) = \frac{\sin\Phi \sin(P-Q)}{\cos\Phi \cos D_\oplus + \sin\Phi \sin D_\oplus \cos(P-Q)}. \quad (4)$$

Similarly, for the planetocentric coordinates of the visible center of the orthographic terminator (of the point T), we shall obtain

$$\sin b = \sin\Phi \sin D_\oplus + \cos\Phi \cos D_\oplus \cos(P-Q), \quad (5)$$

$$\mathrm{tg}(l-l_p) = \frac{-\cos\Phi \sin(P-Q)}{\sin\Phi \cos D_\oplus - \cos\Phi \sin D_\oplus \cos(P-Q)}. \quad (6)$$

The signs of the numerator and denominator in the formulae (4) and (6) coincide with the signs of $\sin(l-l_p)$ and $\cos(l-l_p)$ respectively.

Table 3: The planetocentric coordinates of some basic points of the visible disks of planets

Planet	The point C		The point E		The point T	
	l_0	b_0	l	b	l	b
Mercury	261°.37	−0°.49	193°.51	0°.00	283°.51	−0°.54
Mars	41.49	+24.00	73.68	+21.88	339.77	+9.64

The obtained formulae (3)-(6) were applied to determination of planetocentric coordinates of the considered points of the illuminated part of the visible disks of Mercury and Mars. The results of calculations are listed in Table 3.

Because for Mercury $\Phi > 90°$, then its pole of illumination (the point E) is located on the invisible part of the planet. For Mars $\Phi < 90°$, hence, pole of illumination is on its visible disk. From Table 3 follows, what the planetocentric longitudes of the pole of illumination and the visible center of the orthographic terminator of Mercury differ exactly on 90°. It follows from what the planetocentric latitude of the pole of illumination of Mercury is always equal zero, i.e. the Sun always is positioned in the equatorial plane of the planet.

5. Conclusion

The basic results obtained in this contribution, allow us to draw the following conclusions:

1. The method of determination of the planetocentric coordinates of details on the visible disk of the spherical planet, which is allowing to exclude influence of the phase, is applied to the images of Mercury and Mars.

2. The formulae for determination of planetocentric coordinates of some basic points of the illuminated part of the visible disk of the spherical planet, lying on the illuminated part of the equator of intensity, is obtained.

Acknowledgements. The authors are thankful to anybody who has read this contribution to the end.

References

Abalakin V.K.: 1979, *Principles of Ephemeride Astronomy, M., Nauka.*

Anderson R.C.: 1997, The Mars Watch 1996-1997, *http://mpfwww.jpl.nasa.gov/mpf/marswatch.html*

Melillo F.J.: 2004, ALPO Mercury Section, *http://www.lpl.arizona.edu/∼rhill/alpo/merc.html*

Mikhalchuk V.V.: 2001a, *Astron. Vestnik,* **35**, No.1, 89-96.

Mikhalchuk V.V.: 2001b, *Odessa Astron. Publ.,* **14**, 261-264.

Mikhalchuk V.V.: 2004a, *Kinematica i fizika nebes. tel,* **20**, No.1, 76-92.

Mikhalchuk V.V.: 2004b, *Abstract Book of the Conference MAO-2004 "Astronomy in Ukraine - Past, Present and Future".- Kiev (Ukraine)*, 234.

Seidelmann P.K., Abalakin V.K., Bursa M., Davies M.E., Bergh C., Lieske J.H., Oberst J., Simon J.L., Standish E.M., Stooke P., Thomas P.C.: 2002, *Celest. Mech. and Dynam. Astron.,* **82**, No.1, 83-111.

Troiani D.M., Beish J.D., Hines D., Joyce D.P., Parker D., Schmude R.W.: 2004, ALPO Mars Section, *http://www.lpl.arizona.edu/∼rhill/alpo/mars.html*

EVOLUTION EFFECTS FOR QUASARS AND GALAXIES WITH JET STRUCTURE

Miroshnichenko A.P.

Institute of Radio Astronomy of NASU, Kharkov, Ukraine
e-mail: mir@ira.kharkov.ua

ABSTRACT. We determine the key physical characteristics of quasars and galaxies with jet structure from the observed data. The analysis of relationship of radio and optical luminosities versus the redshift for these objects is carried out. We estimate the lifetime of jet sources by different methods. Also, we study the relation of spectral indices of objects with cosmological epoch.

Keywords: jet, synchrotron radiation, characteristic age.

1. Introduction

Stream outflows from the cosmic object nuclei - jets, containing the relativictic particles, thermal plasma, magnetic field, are seeing in about 70% of radio galaxies and about 50% of quasars. The luminosity of the powerful radio sources with jets is of order $\sim 10^{42}$ erg/s, and of weak radio galaxies with jets $\sim 10^{38}$ erg/s. Linear sizes of jets are in the wide range - from some parsecs to dozens parsecs.

It is known the mean linear size of radio galaxies is decreases monotonously with the redshift, indicating on dependence of their characteristic life time from cosmological epoch (Guerra & Daly, 1998). Also radio sources observations testify, that jet propagation velocity increases with redshift (Wan et al., 2000).

At the synchrotron mechanism of jet radio emission the life time of relativistic electrons may arrive values of 10^8 years. At these characteristic times it is possible to expect the display not only the dynamic but the cosmological evolution of cosmic radio sources. So, the study of evolution relations of the key physical parameters of radio sources with jet structure is of interest.

2. Physical parameters of jet objects in our sample

In this paper the sample of radio sources with jets was considered on the basis of observed data at high radio frequencies (Bridle & Perley, 1984; Kuhr et al., 1981; Lawrence et al., 1986). In addition, we used the according data for sample objects at the optical and decametric band (Braude et al., 2003; Veron & Veron, 1991).

Our sample consists of 132 radio sources with jets, including 76 galaxies and 56 quasars. The mean sample redshift value is 0.066 ± 0.012 for galaxies, and 0.982 ± 0.110 for quasars. In whole for our sample the mean redshift value is 0.510 ± 0.063. The mean spectral index for objects with redshift $z \leq \langle z \rangle$ has value $\langle a \rangle = 0.75 \pm 0.04$, and $\langle a \rangle = 0.64 \pm 0.06$ for objects with redshift $z > \langle z \rangle$ in the given sample.

At accounts of physical parameters of objects we suppose the synchrotron mechanism of generation of optical and radio radiation of active nuclei. In this work the flat model of the Universe with parameter $q_0 = 0.5$ and the constant of Hubble $H_0 = 100\ km/s \cdot Mpc$ is used. As jets are well collimated flows, we consider, that the losses of energy of relativistic electrons on adiabatic expansion of a jet are insignificant in relation to losses of their energy on synchrotron radiation. The jets can be kept from expansion both external pressure, and own magnetic field.

For definition of a magnetic field strength of radio sources we accept a hypothesis about equipartition of energy of a magnetic field and energy of relativistic particles. Under such condition of the magnetic field strength of a radio source we find from the ratio (Ginzburg, 1987):

$$B = \left[48kA(\gamma, \nu) \frac{S_\nu}{r\varphi^3} \right]^{\frac{2}{7}}, \qquad (1)$$

where $k = 100$ (proton to electron energy ratio); $A(\gamma, \nu)$ is the tabular function; γ - index of the electron energy distribution; S_ν is the flux density at frequency ν; r is the jet distance; φ is the jet angular dimension.

The determined values B are in the range from $\sim 10^{-2}$ to 10^{-5}G, that is corresponded to known data. The mean value of the magnetic field strength is $\langle B_G \rangle = 1.37(\pm 0.99) \cdot 10^{-4}$G for galaxies and $\langle B_Q \rangle = 1.6(\pm 1.2) \cdot 10^{-3}$G for quasars in our sample. Then we estimate values of minimal total energy

$$E^{\min} = E_{rel} + E_B = \frac{7}{4}(1+k)\,A(\gamma,\nu) r^2 \frac{S_\nu}{B^{3/2}}, \quad (2)$$

and total luminosities for jet objects by using values of magnetic field strength,

$$L_{tot} = c\pi R^2 B^2. \quad (3)$$

These values are: $\langle E^{\min}\rangle_G = 3.77(\pm1.65)\cdot 10^{60}$erg, $\langle L_{tot}\rangle_G = 5.68(\pm3.23)\cdot 10^{48}$erg/s, $\langle E^{\min}\rangle_Q = 7.14(\pm2.45)\cdot 10^{60}$erg, $\langle L_{tot}\rangle_Q = 1.03(\pm0.16)\cdot 10^{49}$erg/s, respectively, for galaxies and quasars.

As we derived the characteristic size of ratio structure (mean value of object radii) $\langle R\rangle_G = 2.54(\pm0.77)\cdot 10^{23}$cm, $\langle R\rangle_Q = 2.07(\pm0.34)\cdot 10^{23}$cm, respectively, for galaxies and quasars of the sample.

We consider that the luminosity of active nuclei of jet sources L_{tot} is about value of the critical luminosity

$$L_{edd} = 1.2\cdot 10^{38}\frac{M}{M_\odot}, \quad (4)$$

which corresponds to Eddington limit at given object mass M (which is related to the Sun mass $M_\odot$). From this ratio we estimate object masses of $\langle M_G\rangle = 4.73(\pm2.69)\cdot 10^{10} M_\odot$, $\langle M_Q\rangle = 8.55(\pm1.30)\cdot 10^9 M_\odot$, respectively, for galaxies and quasars.

Basing at our data, we account the characteristic time of the synchrotron decay of relativistic electrons in jet sources:

$$t_b = \left(\frac{340 B^{-3}}{\nu}\right)^{1/2}, \quad (5)$$

where t_b is in years, B is in Gauss, ν is in MHz. This value is $\langle t_b\rangle_G = 4.39(\pm1.84)\cdot 10^6$ years for galaxies and $\langle t_b\rangle_Q = 1.44(\pm0.41)\cdot 10^6$ years for quasars at the centimeter band. At the decametric band these estimates are increase to one order, that is $\langle t_b\rangle_G \sim 5\cdot 10^7$ years, $\langle t_b\rangle_Q \sim 10^7$ years.

From the other side, we derive the minimal source age t_L as

$$t_L = \frac{E^{\min}}{L_{tot}}, \quad (6)$$

and it is $\langle t_L\rangle_G = 2.36(\pm0.72)\cdot 10^4$years, $\langle t_L\rangle_Q = 1.92(\pm0.32)\cdot 10^4$ years.

To estimate the velosity of jet propagation we used value t_L and value of radius R of a source:

$$v = \frac{R}{t_L}. \quad (7)$$

For our sample we derived the sublight velocities of jet propagation which indicate the dependence from the redshift, and the correspondent mean values are: $\langle v\rangle_G = 4.98(\pm2.14)\cdot 10^9$ cm/s, $\langle z\rangle_G = 0.07$; $\langle v\rangle_Q = 1.99(\pm0.71)\cdot 10^{10}$ cm/s, $\langle z\rangle_Q = 0.98$. It conforms with the increase of jet propagation velocity versus the redshift (Wan et al., 2000).

Assuming that object luminosity L_{tot} is due to a matter flowing, we obtained the rate of a matter flowing $\frac{dM}{dt}$ for galaxies and quasars from relation:

$$L_{tot} = \frac{1}{2}\frac{dM}{dt}v^2. \quad (8)$$

Then, the mean values of a matter flowing rate $\langle\frac{dM}{dt}\rangle$ are the next: $\langle\frac{dM}{dt}\rangle_G = 1.15(\pm0.34)\cdot 10^4 M_\odot$/year, and $\langle\frac{dM}{dt}\rangle_Q = 5.33(\pm1.04)\cdot 10^3 M_\odot$/year for galaxies and quasars, respectively. So we obtained the additional estimate of the jet object age:

$$t_M = \frac{M}{\frac{dM}{dt}} \quad (9)$$

of values $\langle t_M\rangle_G = 2.10(\pm1.67)\cdot 10^7$ years and $\langle t_M\rangle_Q = 8.23(\pm3.04)\cdot 10^7$ years for galaxies and quasars.

The value of relation of monochromatic luminosities of radio sources at low and high frequencies is of a great interest. At the first, the luminosity relation is independent from the choice of the world model. At the second, it is known from observations, the relation of object luminosities at low and high frequencies characterize the relation of luminosities of their extended (connected with jets) component and nucleus component (core).

We calculated the ratio of the monochromatic luminosities of jet objects at 25 MHz, 5 GHz and in optics. The luminosity ratio mean values for our sample are the next: $\langle\lg(\frac{L_{25}}{L_{opt}})\rangle_G = 4.40 \pm 0.20$; $\langle\lg(\frac{L_5}{L_{opt}})\rangle_G = 2.77 \pm 0.13$ for galaxies and $\langle\lg(\frac{L_{25}}{L_{opt}})\rangle_Q = 5.11 \pm 0.14$; $\langle\lg(\frac{L_5}{L_{opt}})\rangle_Q = 3.48 \pm 0.09$ for quasars.

3. Evolution relations for jet objects

The plot of our estimates of jet velocity against the redshift for sample objects indicates the correlation of this parameters (Fig.1). We have considered the relations between the magnetic field strength and the redshift and the spectral index, indicating a large dispersion of these values for jet objects. An analogous character has the relation between the object linear size and the spectral index and the redshift.

For galaxies and quasars in our sample we derived the evolution trend of luminosity ratio for decametric and optical bands (Fig.2), and for centimeter and optical bands (Fig.3). Note, that these relations indicate the smaller dispersion at the first case (see Fig.2). This corresponds to the synchrotron mechanism of the object radiation, when the radio sources evolve more rapidly at more higher frequencies with evidence of cosmological evolution. Note, that the luminosity ratio for galaxies at low redshifts has higher value then one for

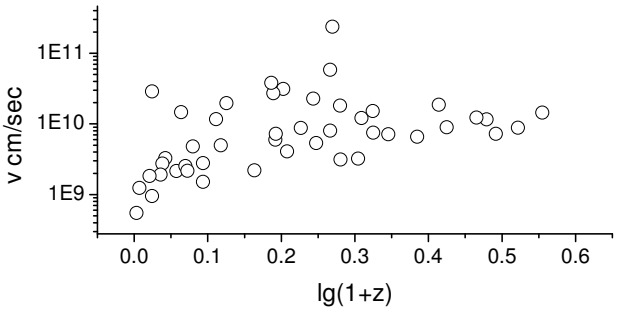

Figure 1: The jet propagation velocity against the redshift for jet objects.

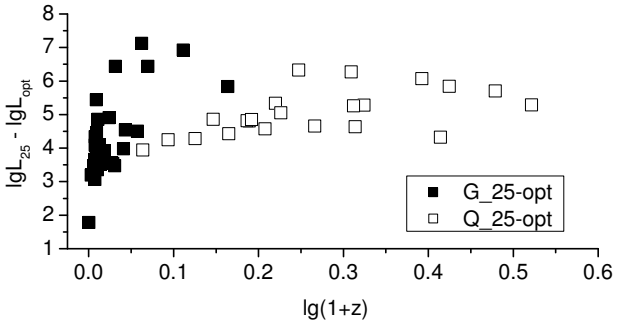

Figure 2: The ratio of luminosity at 25 MHz and optical luminosity against the redshift for jet objects.

quazars. That is, the luminosity of extended component dominates in galaxies especially.

It is interesting, that relation between the radio spectral index and the redshift for jet objects has the quasiperiodic character (Fig.4). In this plot we take the mean value of spectral indices in the redshift intervals $\Delta \lg(1+z) = 0.3$. Maybe, it is the evidence for assumption about the recurrence of activity of the quazar and galaxy nuclei.

4. Conclusions

The relation between the luminosity ratio of galaxies and quazars and the redshift corresponds to the synchrotron mechanism of radiation and indicates the cosmological evolution of object luminosity.

The evidence of correlation between the jet velocities and redshifts is derived in our sample.

The values of the jet propagation velocity received from estimate of the minimal source age points to the sublight velocity values.

The characteristic age of jet objects has the value of $10^6 \div 10^8$ years.

The relation between the ratio spectral index and the redshift for jet sources has a quasiperiodic trend.

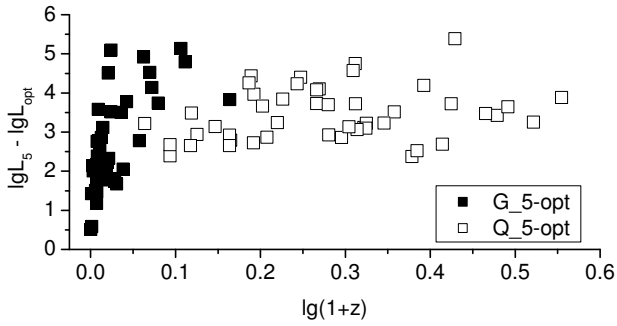

Figure 3: The ratio of luminosity at 5 GHz and optical luminosity against the redshift for jet objects.

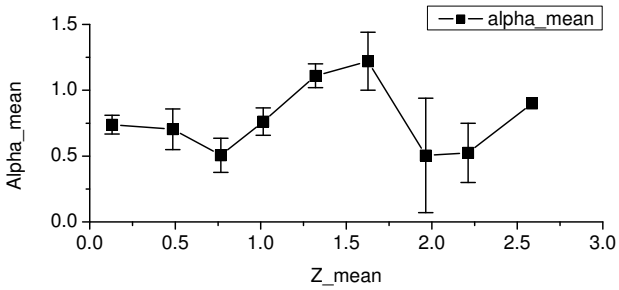

Figure 4: The spectral index against the redshift for jet objects.

References

Braude S. et al.: 1981, *Astophys. and Space Sci.*, **74**, 409.

Braude S. et al.: 2003, *Kinematics and Physics of Celestial Bodies*, **19**, 291.

Bridle A., Perley R.: 1984, *Annual Rev. of Astron. and Astrophys.*,**22**, 319.

Ginzburg V.: 1987, *Theoretical Physics and Astrophysics*, Nauka, Moscow.

Guerra E., Daly R.: 1998, *Astrophys. J.*, **493**, 536.

Kuhr H. et al.: 1981, *A catalogue of radio sources*, Max-Plank=Institute for Radioastronomie, Bonn.

Lara L. et al.: 2001, preprint NRAO No 3.

Lawrence C. et al.: 1986, *Astrophys. J.*, **61**, 105.

Veron M., Veron P.: 1991, preprint ESO No 10.

Wan L. et al.: 2000, *Astrophys. J.*, **544**, 671.

EVALUATION OF THE DISK PRESENCE IN AGNs

L.S.Nazarova [1], N.G.Bochkarev [2], C.M.Gaskell [3] and E.S.Klimek [4]

[1] EAAS, Moscow, Russia
[2] GAISH, Moscow, Russia
[3] University of Nebraska, Lincoln, USA
[4] University of Nebraska, Lincoln, USA
lsn@kzn.ru

The accretion disk emission should be inmost active galaxies. The double-peaked emission lines often used as a strong indication of the disk presence (Chen, Halpern & Filippenko, 1989: Chen & Halpern, 1989; Eracleous & Halpern, 1994). However the optical and UV spectra of double-peaked emitters obtained with HST show a dramatic difference between the double-peaked Balmer and single peaked UV line profiles. The different shape of the optical and UV lines may indicate the existence of two line-emitting regions. The detailed study of the physical conditions along the line profiles for two galaxies 3C 390.3 using optic Hβ and UV - CIV and Lα lines have been done by (Nazarova et al. 2004).

The UV and optical spectra of 3C 390.3 were taken from the AGN Watch database for the period January 1995 – January 1996. However the UV and optical spectra of NGC 5548 were obtained in 1993.The profiles of the CIV, Lα and Hβ lines have been divided into seven parts, the width of each part being equal to 2000 km s^{-1}. The core of the lines is measured between -1000 and +1000 km s^{-1}. Thus, the blue and red wings have a width of $\pm$7000 km s^{-1}. Analysis of the observed CIV/Lα along the line profiles in these galaxies is similar. The CIV/Lα ratio is small at the center $\approx$ 0.5 and grows up to $\approx$ 1 - 1.5 in the wings in both galaxies. However Lα/Hβ line ratios (Fig.1 (top)) change differently along the line profiles in these galaxies. It is low at the center of lines in NGC 5548 similar to many objects (Snedden and Gaskell, 2004) but in 3C 390.3 the Lα/Hβ ratio is higher at the center.

The modelling of the observed line ratios CIV/Lα and Lα/Hβ has been done with the photoionization code CLOUDY (version c9005; Ferland 2004), in its plan parallel version, and assuming solar abundances. The assumed spectral distribution of the central continuum taken from Dumont et al.(1998) for NGC 5548 and from Grandi et al. (1999) for 3C 390.3. The computed line ratios Lα/Hβ for given central luminosity as functions of the distance versus the electron density N_e for both galaxies are shown on Fig.1 (middle). Differing covering factors C are considered for the distributions of clouds. Three functional dependencies on the distance r have been chosen: $C \propto r^{-1}$, C = constant, and $C \propto r$. The CIV/Lα ratio do not showen here because the limited space but of course have been taken into account for estimating the physical conditions along the line profiles. From the comparison of the observed and the computed line ratios which vary across the line profiles we suggest the existing two system of clouds in both galaxies.

3C 390.3

The Lα/Hβ ratio is highest at low velocities and decreases at higher velocities. This could be accomplished with a density going from $\sim 10^{10}$ cm s^{-3} at low velocity (at the line center), up to $\sim 10^{12}$ cm s^{-3} at higher velocity (at the line wings). The CIV/Lα ratio which is low at the centre and higher at the wings may be predicted in two ways:

1. a density of $\sim 10^{7}$ cm^{-3} in the low-velocity core increasing to $\sim 10^{10}$ cm^{-3} in the higher-velocity wings, or

2. a density of $\sim 10^{13}$ cm^{-3} in the low-velocity core decreasing to $\sim 10^{12}$ cm^{-3} in the higher-velocity wings.

Of these two possibilities, the second is ruled out because the critical density of CIII] λ1909 is $\sim 10^{9.5}$ cm^{-3}, and the profile of CIII] is similar to that of CIV. Thus CIV/Lα in 3C 390.3 also implies that the wings have higher density gas. The different density ranges implied by the variation of line ratio with velocity can be reconciled, however, if we have two components, a Low Ionization Line (LIL) zone and a High Ionization Line (HIL) zone.

NGC 5548

From the comparison of the observed and computed CIV/Lα we estimated that the electron densities along the lines may change from $10^{10.5}$cm^{-3} at the wings to $10^{11.5}$cm^{-3} at the center. The observed ratio Lα/Hβ ($\approx$ 7 - 16) is small compare to the computed models accept an extremely high electron densities. Thus,

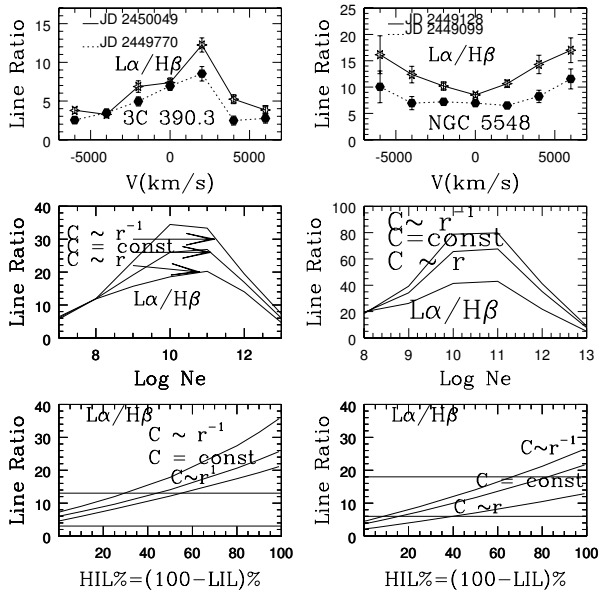

Figure 1:

there is also a contradiction between the electron densities obtained from both ratios. Let accept that the electron density obtained from the ratio of the high ionization lines CIV/Lα corresponds to the HIL zone located above an accretion disk with the electron densities $N_e \approx 10^{10-11} cm^{-3}$ while the LIL zone located in accretion disk has the electron density $N_e \approx 10^{12-13}$ cm^{-3}.

Thus, although 3C 390.3 and NGC 5548 are different, the broad-line regions could be represented by a two-component model. The two components have different locations, densities, and contributions to the line profiles. The contribution of an accretion disk (LIL region) is strong at the wings in 3C 390.3 but in NGC 5548 an accretion disk contribute to the central part of low ionization lines. Fig.1 (bottom) show the contribution of the disk component in both galaxies. The contributions from an accretion disk is less than 40% for in 3C 390.3 and is about 80-90% in NGC5548.

References

Chen K., Halpern J. P., Filippenko A. V.: 1989, *ApJ*, **339**, 742.

Chen K., Halpern J. P.: 1989, *ApJ*, **344**, 115.

Dumont A.-M., Collin-Souffrin S., Nazarova L. S.: 1998, *A&A*, **11**.

Eracleous M. & Halpern J. P.: 1994, *ApJS*, **90**, 1.

Ferland G. J. et al.: 2004, *University of Kentucky, Department of Physics & Astronomy, Internal Report.*

Grandi P., Guainazzi M., Haardt F., Maraschi L., Massaro E., Matt G., Piro L., Urry C. M.: 1999, *A&A*, **343**, 33.

Nazarova L. S., Bochkarev N. G. and Gaskell C. M.: 2004, *Ast. Ap Trans*, **24**, 000.

Snedden S. A., Gaskell C. M.: 2004, *ApJ*, submitted (ast ro-ph/0402508).

THE MAGNESIUM ABUNDANCE IN THE THIN AND THICK DISK OF THE GALAXY

T.V. Nykytyuk[1] , T.V. Mishenina[2]

[1] Main Astronomical Observatory
Ak.Zabolotnoho St. 27, Kyiv 03680, Ukraine,*nikita@mao.kiev.ua*
[2] Department of Astronomy, Odessa State University
T.G.Shevchenko Park, Odessa 270014 Ukraine, *tamar@deneb.odessa.ua*

ABSTRACT. The chemical evolution of the thin and thick disk of our Galaxy was investigated in framework of the opened model with gas inflow. It was supposed that the thin and thick disks separate chemically and spatially and have different evolution timescales. The Galactic evolution of magnesium was investigated for the thin and thick disk. The obtained results allow us that the star formation history of the thin disk is more smooth and quiet than its for the thick disk of our Galaxy.A gas infall plays an important role in an appearance of chemical distinctions of relative abundances between the thin and thick disk - a inflow rate is more intensive for the thick disk.

Key words: Galaxy: evolution; Galaxy: abundances; Galaxy: thin disk; Galaxy: thick disk.

1. Introduction

Modern studies of a kinematics and ages of a stellar population of a disk of our Galaxy allow us to talk about a presence of two distinct populations in the disk named as the thick and the thin disk. The thin and thick disks has a different spatial and temporal characteristics (Gilmore & Raid 1983, Reyle & Robin 2001, Chen 1997, Fuhrmann 1998, Bensby et al. 2003, Robin et al. 1996). A metallicity distribution function of the thin and thick disk stars of our Galaxy has peak in a different values of metallicity (Wyse & Gilmore, 1995). It is found that the thick and thin disk trends are partly overlapped in the range $-0.8 < [Fe/H] < -0.4$ but they are separated in $[\alpha/Fe]$ where α are α-capture elements (Gratton et al. 1996, 2000; Fuhrmann 1998; Bensby et al. 2003, 2004) Furthermore, later investigations show that the two disk components are also separated in [Mn/Fe] and [Eu/Ba] (r- and s-process element ratio) (Nissen et al. 2000, Prochaska & McWilliam 2000).

Thus, our goal is to make clear a causes of distinction of a chemical characteristics of the Galactic disk subsystems.

2. The model

We consider the opened two-zone model of a chemical evolution of the disk (thick and thin) of our Galaxy. It is supposed that the thin and thick disks of our Galaxy are formed independently and the infall of intergalactic gas took place in the process of their formation. We will consider the Galactic evolution of the magnesium as an application of such model.

The idea of chemical evolution of a galaxy includes not only a temporal change of heavy element content in a galactic gas but also a temporal change of mass of gas and mass concluded into stars ans stellar remains.

A star formation process in a galaxy is considered as a sequence of bursts with a population of stars formed during each burst.

The contribution of elements, synthesized by a population of stars are described by Nykytyuk (2003) in detail. It will be noted that the Mg yield in the paper of Portinari et al. (1998) was determined from yields of Woolsey and Weaver (1995) which give the underestimated Mg value (see Thomas et al., 2000). Making use of Portinari's data in the calculation of a model of chemical evolution it was found that stars formed of a matter with the initial metallicity $Z < 0.15$ give a lower Mg yield in order to have possibility to reproduce the observed data. But stars with Z=0.15 give even more higher Mg yield; because we had to lower the predicted Mg yield from the stars with 9-15 $M_{\odot}$ above by a factor of 1.5 so that the model results be in good agreement with the observation data.

The star formation rate $\psi(t)$ in thick and thin disks is described in the following way (Pilyugin & Edmunds, 1996):

$$\psi(t) \sim \begin{cases} t \cdot e^{-t/T_{top}}, & \mathrm{t} \leq T_{top} \\ e^{-t/T_{sfr}}, & \mathrm{t} \geq T_{top} \end{cases}$$

where T_{top} amd T_{sfr} are free parameters of a star formation rate.

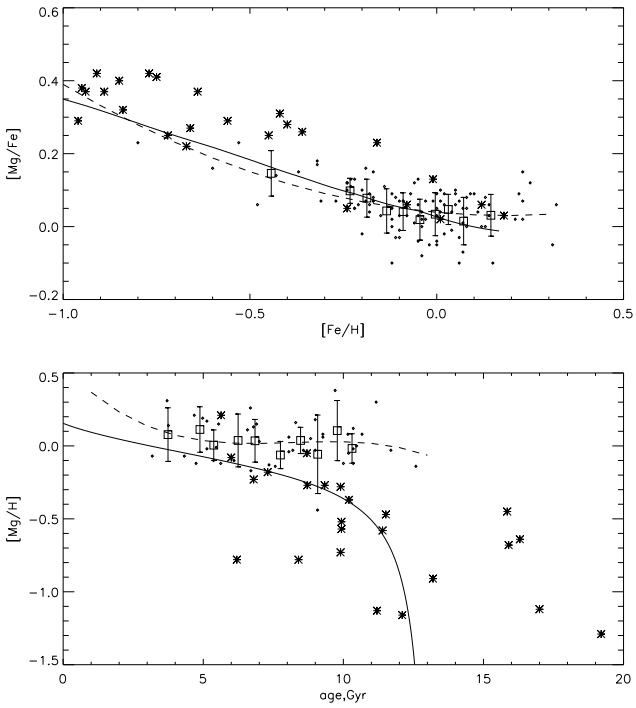

Figure 1: [Mg/Fe] vs [Fe/H] and [Mg/H] vs age diagrams for the thin disk of our Galaxy. The observed abundances of thin and thick disk stars of our Galaxy (Mishenina et al.(2004)) are marked by the small diamonds (the thin disk stars) and the asterisks (the thick disk stars). The squares are mean observed thin disk data in 10 bins with equal numbers of stars.Dashed line is curve drawn by the least-squares method in the observed data of the thin disk. The prediction for the thin disk is indicated by solid line

The star formation history is described by a set of star formation bursts whose amplitudes are derived from:

$$M_{b_i} = \int_{t_{i-1}}^{ti} \psi(t)\, dt, \qquad (1)$$

where time interval between t_i and t_{i-1} is a burst duration. It is supposed that a infall of intergalactic gas takes place on the disk during galaxy's life. According to Pilyugin & Edmunds (1996), the infall rate is described by a function

$$A(t) = a_0 e^{-t/T_{inf}},$$

where T_{inf} and a_0 are free model parameters.The accreted gas has primordial chemical composition.

The star formation histories of disk components were choosed in such a way as to order to a majority of thick disk stars has been formed 10-13 Gyr ago while thin disk stars would have ages less then 10 Gyr.

3. The results

The iron is predominantly synthesized by SNIa type (intermediate mass stars in binary systems), while α elements are synthesized by massive stars. Difference in the stellar lifes mean that α-element enrichment of interstellar medium takes place during several tens million yrs and the iron amount in the interstellar medium reachs to maximum in the first Gyr after beginning of star formation. This allows to use $[\alpha/Fe]$ ratio as an indicator of the star formation history (Matteucci, 1992). And as the $[\alpha/Fe]$ ratio of the thick and thin disk has a some distinctions we suppose that star formation histories of the disk components must be different. Therefore we will look for a such parameters of the star formation history and accretion rate whose use gives the possibility to reproduce the observed abundances of the thin and thick disk stellar population of our Galaxy.

3.1. The thin disk

Fig.1 represents the predictions of thin disk model. The ages in this paper were determined using the Bertelli (1994) isochrones. Model predictions demonstrated in Fig.1 were obtained at the following star formation parameters: $T_{top} = 1$ Gyrs and $T_{sfr} = 8$ Gyrs. The parameter T_{inf} determining the accretion rate equals 5 Gyrs. The amounts of parameters were choosed so that use of such parameters of the star formation and accretion rate would give the possibility to reproduce the observed data. It is assumed that the age of the disk of our Galaxy equals 13 Gyrs (Cowan et al., 1991).

As Fig.1 illustrates, the thin disk model with using of above-mentioned parameter values reproduces the [Mg/Fe] - [Fe/H] ratio quite well- the model track is agreed closely with the line drawn by the least- squares method through a cloud of points marked the positions of the thin disk stars on the [Mg/Fe]vs[Fe/H] diagrams. But the model don't reproduce the averaged observed data at the super-solar metallicities. The model prediction for element abundances as a function of time is noticeable worse – Fig.1 shows that the predicted abundances of the thin disk model are lower on average as compared with the Mishenina's observations.

Obtained values of parameters of the thin disk evolution are in a good agreement with parameters of the best fit model of Pilyugin and Edmunds (1996) having investigated the "age - [Fe/H]" and "age-[O/H]" ratios and the solar neighbourhood metallicity distribution function.

3.2. The thick disk

Predictions of the thick disk model are presented in the Fig.2. The following parameters of thick disk evolution were found: the star formation history $T_{top} = 1$ Gyr, $T_{sfr} = 5$ Gyrs, and the gas accretion rate $T_{inf} =$ 7 Gyr. As Fig.2 shows, solid line of the prediction of

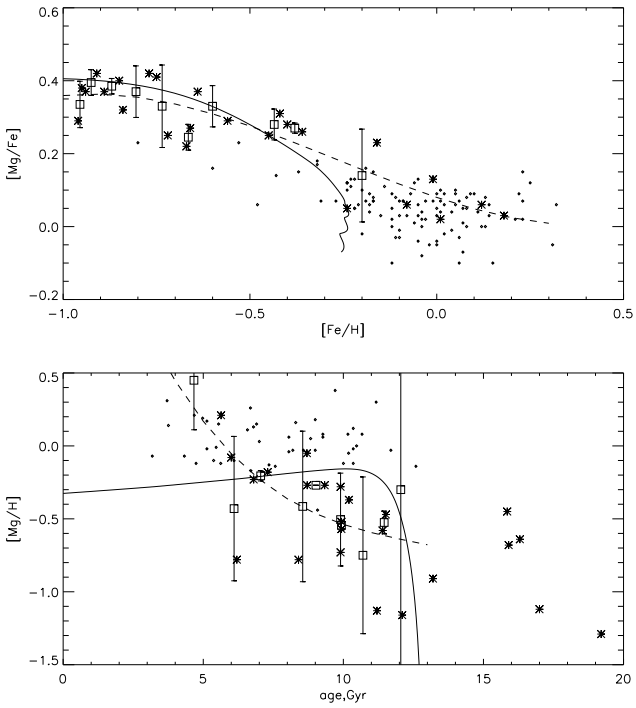

Figure 2: [Mg/Fe] vs [Fe/H] and [Mg/H] vs age diagrams for the thick disk of our Galaxy. The observed abundances of thin and thick disk stars of our Galaxy (Mishenina et al.(2004)) are marked by the small diamonds (the thin disk stars) and the asterisks (the thick disk stars). The squares are mean observed thick disk data in 10 bins with equal numbers of stars.Dashed line is curve drawn by the least-squares method in the observed data of the thick disk. The prediction for the thick disk is indicated by solid line

thick disk model is in agreement with dashed line obtained by the least-squares method from the results of observations of relative abundance of Mg of thick disk stars. Otherwise matter stands with an abundance determination as a function of time. Unfortunately, the number of stars belonging kinematically to the thin disk exceeds distinctly the number of stars belonging to the thick disk; among later there are not enough an objects for which one can surely determine the ages. Therefore, the trend in the "age - [Mg/H] " diagram for the thick disk stars is less obvious then its for the thin disk stars.

3.3. Star formation history

An index of star formation history in a model is a "gas fraction - time" relation since it indicates how fraction of a galactic gas was converted to a stars and during what time it will be.

The star formation history of the thick disk was rather quick as the majority of the thick disk stars was formed during 2 - 3 Gyrs and was almost stopped above 10 Gyrs ago (Fig.3). On the contrary, the thin

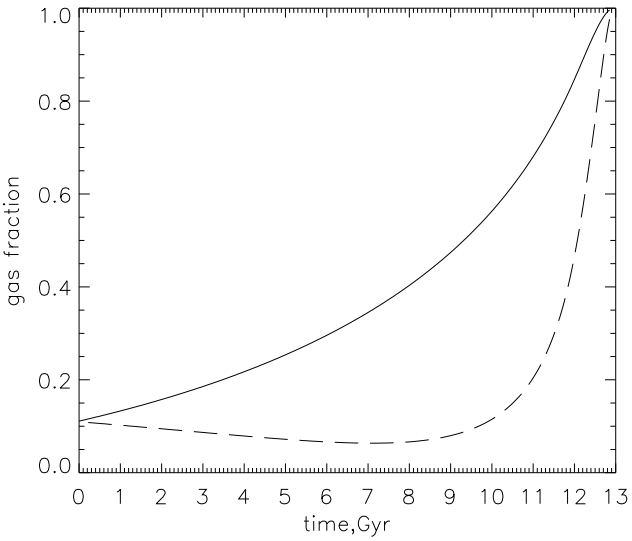

Figure 3: The gas fraction as a function of the time for thin (solid line) and thick(dashed line) disk

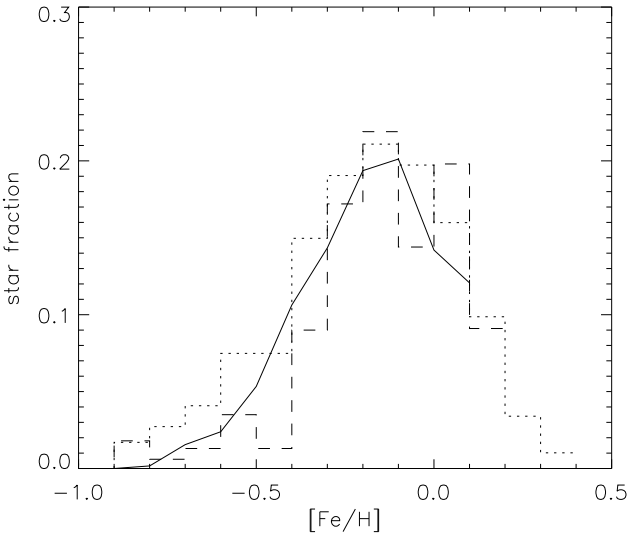

Figure 4: The metallicity distribution function. The dotted line is the observed distribution obtained by Hou et al.(1998), dashed line is the observed distribution obtained by Jorgensen (2000), solid line is the prediction of thin disk model

disk stars only begun to form 9-10 Gyrs ago, and a star formation in the thin disk gone smoothly , gradually coming to naught at our time.

It is necessary to note that the accretion of intergalactic gas have played a noticeable role in the evolution of the disk subsystems of our Galaxy. Model line of the relative abundances of the thin disk stars will change a location and approach to the thick disk star region if mass of gas infalling on the disk at the each accretion episode increases. In other words, the more massive accretion in a unit of time is characteric feature for thick disk evolution then for thin disk.

3.4. Metallicity distribution function

The prediction of model was compared with the observations of metallicity distribution function of the solar neighbourhood in Fig.4. It is known that 94 % of solar neighbourhood stars belong to the thin disk whereas remaining 6 % belong to thick disk population (Robin et al., 1996). Therefore the metallicity distribution function in Fig.4 was obtained in framework of the thin disk model. Under above-mentioned parameters of the star formation and gas accretion in the thin disk, solid line reproduces quite well the observed metallicity distribution function in the Fig.4.

4. Main results

1. It was found that the thin and thick disks has a different star formation rates. The thin disk star formation history is more smooth and quiet than its for the thick disk of our Galaxy.

2. A gas infall plays an important role in an appearance of chemical distinctions of Mg relative abundance between the thin and thick disk - a inflow rate is more intensive for the thick disk.

References

Bensby T., Feltzing S., Lundstrom I.: 2003, A&A **410**, 527.

Bensby T., Feltzing S., Lundstrom I.: 2004, A&A **415**, 155.

Bertelli G., Bressan A., Chiosi C., Fagotto F., Nasi E.: 1994, A&A Supl.Ser. **106**, 275.

Chen B.: 1997 ApJ **491**, 181.

Cowan J.J., Thielemann F.-K., Truran J.W.: 1991, ARA/A **29**, 447.

Gratton R., Caretta E., Matteucci F., Sneden C.: 1996, In Formation of the Galactic Halo...inside and out, 1996, ed. H.Morrison, A.Sarajedini (San Francisco: ASP) **92**, P. 307.

Gratton R., Caretta E., Matteucci F., Sneden C.: 2000, A&A **358**, 671.

Fuhrmann K.: 1998, A&A **338**, 161.

Gilmore G. & Raid N.: 1983, MNRAS, **202**, 1025.

Hou J., Chang R., Fu C.: 1998, Pacific Rim Conference on Stellar Astrophysics, ASP Conf. Ser. **138**, P. 143.

Jorgensen B.R.: 1997, A&A **363**, 947.

Matteucci F.: 1992, MetSAIt **63**, 301.

Mishenina T.V., Soubiran C., Kovtyukh V.V., Korotin S.A.: 2004, A&A **418**, 551.

Nissen P.E., Chen Y.Q., Schuster W.J., Zhao G.: 2000, A&A **353**, 722.

Nykytyuk T.: 2003, KFNT, **19**, 259.

Portinari L., Chiosi C., Bressan A.: 1998, A&A **334**, 505.

Pilyugin L.S., Edmunds M.G.: 1996, A&A **313**, 783.

Prochaska J.X., McWilliam A.: 2000, ApJ **537**, L57.

Reyle C., Robin A.C.: 2001, A&A **373**, 886.

Robin A.C., Haywood M., Creze M., Ojha D.K., Bienaumé O.: 1996 A&A **305**, 125.

Thomas D., Greggio L., Bender R.: 2000, The Evolution of the Milky Way: stars vs clusters, ed. by Matteucci F. & Giovanelly F., p.541.

Woosley S.E., Weaver T.A.: 1995, ApJS **101**, 181.

Wyse R.F.G., Gilmore G.: 1995, AJ **110**, 2771.

PHYSICAL MODEL OF THE ORBITAL MOVEMENT OF THE JUPITER SATELLITE SINOPE

Nikolay V. Ostrovskiy

Vyatka State University, city of Kirov, Russia
e-mail: onv1@yandex.ru

ABSTRACT. The physical models of orbital movement of heavenly body have limited application. On the one hand, it is very difficult to take into account all effects of gravitational interaction in complex systems. Therefore the physical models cannot compete on accuracy of calculation of ephemeris with statistical models. On the other hand, the known equation of world gravitation of Newton strictly corresponds only to gravitational interaction of two bodies. With its use it is impossible, for example, to explain a movement of the Moon around the Earth, as the Moon is in sphere of Sun gravitation. The similar situation exists and in case of the external satellites of Jupiter: Pasiphe and Sinope. In the given work is used the original equation for the description of gravitational interaction in system of many bodies (for system of two bodies it is converted in the Newton equation), that eliminates the known contradiction.

Keywords: celestial mechanics, generalised equation of gravitational interaction, Jupiter, Sinope.

Introduction

The physical models of orbital movement of heavenly body have limited application. On the one hand, it is very difficult to take into account all effects of gravitational interaction in complex systems. Therefore the physical models cannot compete on accuracy of calculation of ephemeris with statistical models (see, for example, Chapront&Francou, 1996). On the other hand, the known equation of world gravitation of Newton (1):

$$F_{12} = Gm_1m_2/r_{12}^2 \tag{1}$$

where: G – universal gravitational constant, m_1 and m_2 - masse of interacting bodies, r_{12} – distance between interacting bodies,

strictly corresponds only to gravitational interaction of two bodies. With its use it is impossible, for example, to explain a movement of the Moon around the Earth, as the Moon is in sphere of Sun gravitation. The similar situation exists and in case of the external satellites of Jupiter: Pasiphe and Sinope. In the given work is used the original equation for the description of gravitational interaction in system of many bodies (for system of two bodies it is converted in the Newton equation) (Ostrovskiy, 2003a):

$$\vec{F_{12}} = Gm_1r_{12}\sum m_i/\vec{r_{1i}^3}, \tag{2}$$

where: $m_i/\vec{r_{1i}^3}$ – is vector.

Equation (2) eliminates the known contradiction. This work Illustrate the use of equation (2) on example of system Sun-Jupiter-Sinope.

1. The base model

As the base for making this model was used a model earlier used for systems of two bodies (Ostrovskiy, 2003b). In the basis model a body move along a radius – vector (radial movement) and on a curve (linear movement) independently. The change of speed of a radial movement is determined by radial acceleration:

$$\vec{a}_R = \vec{a}_G + \vec{a}_C \tag{3}$$

The centrifugal acceleration is calculated on the equation:

$$a_C = v^2/r, \tag{4}$$

where: v – linear speed of a body, r – radius of curvature of a trajectory.

The acceleration of gravitation for system from two bodies is Calculated proceeding from the equation of Newton (1). The change Of speed of a linear movement is determined by change of length of a radius – vector:

$$vr = const \tag{5}$$

Step-by-step procedure is used for calculation sizes of radial Speed, lengths of a radius-vector, meanings of linear speed, and Accelerations by the equations (1), (4), (3).

The basis model for system Sun-Earth has convergence with Astrometric dates from $n \cdot 10^{-5}$ for one revolution (Ostrovskiy, 2003b) up to $n \cdot 10^{-3}$ for period of 100 years (Ostrovskiy, 2003b). For

system a Sun – Jupiter results of calculation on author's model there were are compared to others statistical methods (Ostrovskiy, 2004). The calculation was begun from perigee 1 Jun 1904. After 190 terrestrial years (11 of Jun, 2094) corner of tumbling became is according to author's model 5754.7 degree (Ostrovskiy, 2004), according to "Planeph 4.2" (Chapront&Francou, 1996) – 5770.0, according to model of The Natural Satellites Data Center (NSDC, Paris, http://www.bdl.fr/ephemeride.html) – 5762.8. Radius of orbit (m·10^{11}) – 7.40888, 7.41118 and 7.41129 accordingly. Angular velocity (sec./day) – 329.75 accordingly author's model and 329.83 accordingly Planeph 4.2. Model of NSDC does not give Value of angular velocity. Difference in corners of tumbling For System Earth-Moon for time of orbital period the Moon makes the Tumbling on 351,85 degree only (Ostrovskiy, 2003b). Bay use of the base model for System Jupiter-Sinope were are received unsatisfactory results. The Sinope orbit, described in known parameters (T=758 days, $R_{Mid} = 2.37 \cdot 10^{10}$ m, $e = 0.28$) for isolated system Jupiter-Sinope cannot exist. Two lasts example point that for reception of more exact results necessary to take into account the influence of the Sun. But account the influence of the Sun with use of Newton equation give more bad results (Ostrovskiy, 2004). For one orbital period corner of tumbling changes from 62 to 220 degree depending on initial location of satellite of Jupiter in space. By that length of orbit radius increases up to $9.7 \cdot 10^{11}$ m. This indicate that the Newton equation (1) not applicable for description of gravitational interactions in complex systems.

2. Model for system of three bodies with use of generalised equation of gravitational interaction

The equation (2) for interaction between Sinope and Jupiter gives the followed:

$$F_{12} = Gm_1 r_{12} \left[M_2/r_{12}^3 + (M_3/r_{13}^3)\cos\alpha \right], \quad (6)$$

where: 1 – the Sinope, 2 – the Jupiter, 3 – the Sun, α – a corner between radius-vector of Sinope comparatively Jupiter and radius-vector of Sinope comparatively the Sun.

The equation (6) was used for calculation of acceleration of Gravitation of Sinope. For calculation of acceleration of Gravitation of Jupiter was used equation (1). In the equation (6) Was used a normal component of Sun gravitation:

$$g_{SN} = (Gr_{JSin} M_S / r_{SSin}^3)\cos\alpha. \quad (7)$$

The tangential component of Sun gravitation:

$$g_{ST} = (Gr_{JSin} M_S / r_{SSin}^3)\sin\alpha \quad (8)$$

must use on vector of linear velocity directly, reason its offset and, hereunder, offset of satellite orbit plane. This leads to offset of line of nodes (where: $\Delta\gamma$ – change longitude of top-down node):

$$\Delta\gamma = g_{ST}\Delta t^2 / v\Delta t. \quad (9)$$

If we "start" a body on a flat circular orbit with radius, equal to average radius of Sinope orbit, its orbit gets eccentricity for one revolution depending on initial position of a body. Dependency has two minimum at initial longitude of body 20 degree relatively of Jupiter ($e = 0.060$) and at 180 degree ($e = 0.052$) and two maximum at initial longitude 90 and 270 degree (eccentricity 0.077 and 0.073 accordingly). The influence of orbit plane inclination to the ecliptics plane is various for a various situation of an nodes line. So, if an initial longitude of descending node concerning a radius-vector of the Jupiter the wound to zero, eccentricity for one revolution varies in a range from 0.051 up to 0.066. If the initial longitude of descending node equal 90 degrees, the range of change eccentricity is increased up to 0.019-0.078. The minimum corresponds to a corner of an inclination 90 degrees, and maximum – 180 degrees.

The influence of the Sun, as well as in case of the Moon, results to osculating of an orbit, as its parameters in each moment of time depend on a corner between radius-vectors of the Jupiter and Sinope. Accounts have shown, that to an orbit with average orbital Period (for 190 terrestrial years), equal 758 days and inclination Equal 150 degrees, corresponds average radius $2.52 \cdot 10^{10}$ m. Herewith average value of eccentricity of an orbit will be 0.29 (maximum 0.40), and the line of units makes a complete revolution for 29000 terrestrial days. What it was possible to calculate ephemeris of Sinope it is necessary to know rather precisely in a determined moment of time its linear and radial speeds, length of a radius – vector and situation in space.

Conclusion

Use of the generalised equation of gravitational interaction (2) allows: To explain character of interaction in system of three bodies Sun – Jupiter – Sinope.

To construct dynamic model, including the movement of the Jupiter around the Sun and movement of the Sinope around the Jupiter.

To specify orbital parameters of Sinope.

To explain osculating of orbits of the external satellites of the Jupiter.

To explain displacement perigee and rotation of units line of the Satellites at the expense of influence of the Sun.

References

Chapront J., Francou G.: 1996, ftp://cdsarc.u-strasbg.fr/pub/cats/VI/87/.

Ostrovskiy N.V.: 2003a, The collection of materials of All-Russia technological conference "Science, Manufacture, Technology and Ecology", Kirov, Vyatka state university, **4**, p. 74.

Ostrovskiy N.V.: 2003b, Natural and technical sciences, **2**, p. 22.

Serveur d'ephemerides de l'Institut de mecanique celeste et de calcul des ephemerides. URL: http://www.bdl.fr/ephemeride.html

Allen C.W. Astrophysical quantities. *Third edition*: 1973, University of London, The Athione Press.

N. V. Ostrovskiy: 2004, Electronic conference "Computer Applications in fundamental and applied Physics and Mathematics". URL: http://www.ivtn.ru

INFLATION THEORIES AND PLANK MASS PROBLEM

Popov A.M.[1] and Smolyakov M.N.[2]

[1]ASC FIAN, Moscow, Russia, *e-mail: amp@lukash.asc.rssi.ru*
[2]SINP MSU, Moscow, Russia, *e-mail: smolyakov@theory.sinp.msu.ru*

ABSTRACT. A method of producing large value of Plank mass with aids of scalar field theory is being investigated. Correspondingly, inflation models are being discussed from this point.

Special combinations of model parameters that ensure duration of inflation being greater than 60 e-foldings were derived. By means of numerical modeling we verified analytical approximations and give illustrative picture of evolution of fields and Hubble constant H for those periods of inflation, when it is not possible to perform analytical calculations.

Keywords: Cosmology, Inflation, Plank Mass, Numerical Calculations.

Introduction

Recently the problem of large value of Planck mass attracts special attention among researchers. Different models are being proposed in order to achieve effective value of Planck mass being equal to $M_{Pl} = 10^{19} GeV$ by means of special mechanisms, while real value of ${M_{Pl}}^*$ is considered rather small (e.g., in: Arkani-Hamed et al. 1998, authors attempted to solve the indicated problem with aids of compact extra dimensions).

In the present investigation authors attempted to produce correct effective value of Plank mass from smaller ${M_{Pl}}^*$ by introducing scalar field φ into the action S. One cannot argue that inflation models with appropriate corrections to Einstein equations taken into account are to be thoroughly discussed in the case. Here we tested one simple inflation model with one real scalar field with inflation potential $V = \lambda(\varphi^2 - v^2)^2$. We need to point out one's attention to the fact that scalar-tensor theories of gravitation are of great interest among researches (e.g., Faraoni, 2004), for example, well-known Brans-Dicke theory. Furthermore, there were attempts to use theories of this type even in theories of inflation (Yoshimura, 1991).

1. Model Description

As it was mentioned above, our approach is to introduce scalar field φ in the action. Thus the action S is as follows:

$$S = \int \sqrt{-g} d^4x e^{\frac{\phi}{M}} \left(\frac{1}{16\pi\hat{G}} R - g^{\mu\nu}\partial_\mu\phi\partial_\nu\phi - V(\phi) \right),$$

where

$$dS^2 = -dt^2 + a^2(t)\left(dx^2 + dy^2 + dz^2\right),$$

$$V(\phi) = \lambda(\phi^2 - v^2)^2$$

(λ, v and M are model parameters). One can see, that in the case $M_{Pl}^2 = \frac{1}{16\pi\hat{G}} e^{\frac{v}{M}}$ (at the point $\phi = 0$), or $M_{Pl}^2 = {M_{Pl}^*}^2 e^{\frac{v}{M}}$. Actions of this type (with so-called "dilaton field") were studied earlier as a solution for different problems in cosmology (see e.g., Ellis et al., 2000). The main target of the research is to find out the highest possible magnitude of ratio $\frac{v}{M}$ (and consequently the lowest value of M_{Pl}^*) that still allows inflation processes to occur in the model, and to derive the spectrum of model parameters that makes inflation last more than 60 e-foldings.

Einstein equations (and equations of motion) are:

$$\frac{3}{16\pi\hat{G}}\left(\frac{\dot{a}}{a}\right)^2 - \frac{1}{2}\left(\dot{\phi}^2 + V(\phi)\right) + \frac{3}{16\pi\hat{G}}\left(\frac{\dot{a}}{a}\right)\left(\frac{\dot{\phi}}{M}\right) = 0;$$

$$\frac{1}{16\pi\hat{G}}(\dot{a}^2 + 2\ddot{a}a) + \frac{1}{2}a^2\left(\dot{\phi}^2 - V(\phi)\right) + \frac{1}{16\pi\hat{G}} \times \times \left(a^2\frac{\ddot{\phi}}{M} + a^2\frac{\dot{\phi}^2}{M^2} + 2\dot{a}a\frac{\dot{\phi}}{M}\right) = 0;$$

$$\frac{6}{16\pi\hat{G}}\frac{1}{M}(\ddot{a}a + \dot{a}^2) - 6\dot{a}a\dot{\phi} - 2a^2\ddot{\phi} - -a^2\frac{1}{M}\left(\dot{\phi}^2 + V(\phi)\right) - a^2\frac{\delta V}{\delta\phi} = 0.$$

After some simple algebra it is convenient to transform the equations to more "familiar" form (with all terms with M grouped together):

$$\ddot{\varphi} + 3H\dot{\varphi} + \frac{1}{\sqrt{2}M}\left[V(\varphi) + \frac{\dot{\varphi}^2}{2} - \frac{3}{8\pi\hat{G}}\left(2H^2 + \dot{H}\right)\right] = 0;$$

$$3H^2 = 8\pi\hat{G}\left(\frac{\dot{\varphi}^2}{2} + V(\varphi)\right) - \frac{1}{\sqrt{2}M}3H\dot{\varphi};$$

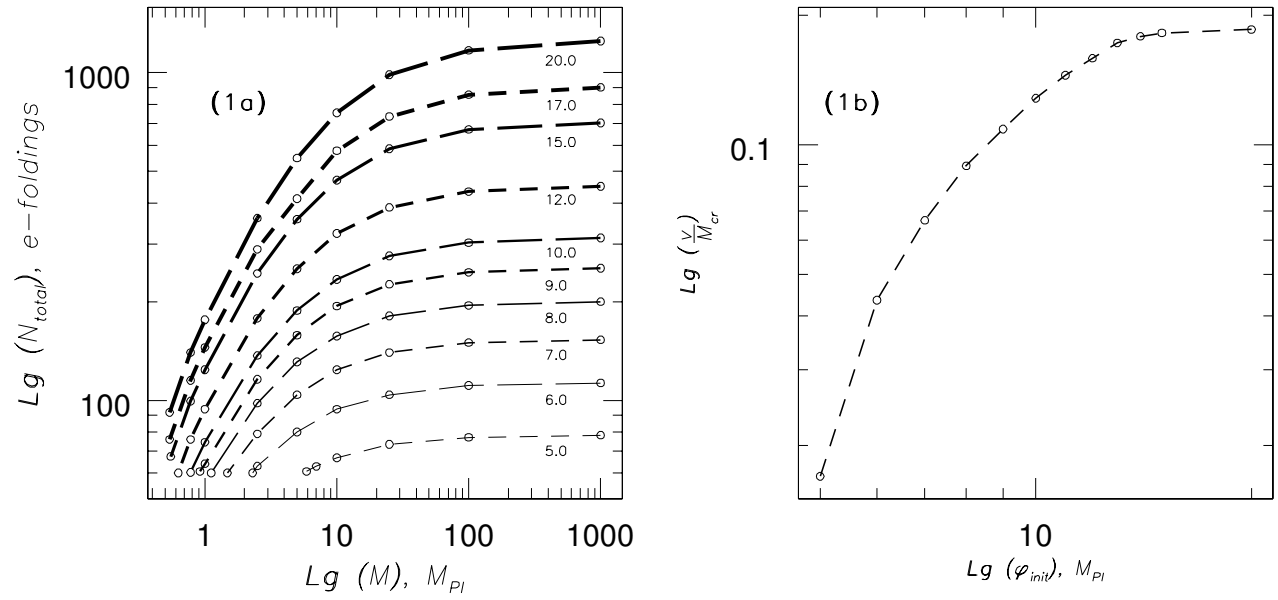

Figure 1: Fig. (1a) shows "$\varphi = \varphi_{init}$-slice" of $N_{total}(M_{cr}, \varphi_{init}), e - foldings$. Numbers to the right-side of each curve gives appropriate value of φ_{init}, M_{Pl}. Fig. (1b) shows $\frac{v}{M_{cr}}(\varphi_{init})$, which is "$N_{total} \approx 60$" slice.

$$-2\dot{H} = 8\pi\hat{G}\dot{\varphi}^2 + \frac{1}{\sqrt{2}M}\left[\ddot{\varphi} - H\dot{\varphi} + \frac{\dot{\varphi}^2}{\sqrt{2}M}\right]$$

(here $\phi = \frac{\varphi}{\sqrt{2}}$, Hubble constant H is $H = \frac{\dot{a}}{a}$). We estimate duration of inflation in "e-foldings":

$$N_{total} = \int_{t_{init}}^{t_{final}} H \quad dt.$$

2. Numerical Simulation

It is clear that one cannot solve these equations analytically (at least, not with relatively high $\frac{v}{M}$. Let's rewrite our equation set in the following manner:

$$\dot{x}_0 = x_1;$$

$$\dot{x}_1 = -a_1 V_{x_0}(x_0) - a_2 V(x_0) - a_3\tilde{x}_4^2 - 3a_4\tilde{x}_4 x_1 - a_5 x_1^2;$$

$$\dot{x}_4 = b_1 V(x_0) + b_2 x_4^2 + b_3 x_4 x_1;$$

$$\dot{x}_5 = \tilde{x}_4 x_5,$$

where

$$a_1 = \frac{32M^2\pi\hat{G}}{k}; \quad a_2 = \frac{16\sqrt{2}M\pi\hat{G}}{k};$$

$$a_3 = \frac{12\sqrt{2}M}{k}; \quad a_4 = \frac{32M^2\pi\hat{G} - 1}{k};$$

$$a_5 = \frac{8\sqrt{2}M\pi\hat{G} + 24\sqrt{2}M\pi\hat{G} + \frac{3}{\sqrt{2}M}}{k};$$

$$b_1 = 8\pi\hat{G}\frac{\sqrt{2}M + k + 1}{k}; \quad b_2 = 3\frac{2-k}{k};$$

$$b_3 = \frac{32M\pi\hat{G} - \frac{3}{\sqrt{2}M}k}{k};$$

$$k = 32M^2\pi\hat{G} + 3;$$

$$\tilde{x}_4 \equiv H = \sqrt{\frac{8\pi\hat{G}}{3}\left[\frac{x_1^2}{2} + V(x_0)\right] + \frac{x_1^2}{4M^2}} - \frac{x_1}{2M};$$

and $x_0 \equiv \varphi; \quad x_1 \equiv \dot{\varphi}; \quad x_4 \equiv H; \quad x_5 \equiv a.$

The authors performed numerical calculations by taking advantage of classical IV-order Runge-Kutta algorithm with adaptive step-correction for solving linear differential equations.

An opportunity of real-time processing and data visualization was taken into advantage to perform primary analysis of evolutionary tracks without necessity to use side-built graphics packages. This considerably reduced overall time of treatment of evolutionary tracks, since authors were able to make immediate decisions concerning applicability of sets model parameters being currently chosen.

3. Preliminary Results

In the present investigation we derived the spectrum of model parameters, that allows inflation to last 60 e-foldings or more. As a beginning, we tried to study conventional scales of energy (with Plankian

scale $10^{19}\ GeV$). It's obvious that in this case M^*_{Pl} is to be of the same order as well. The λ parameter of the model was always being chosen according to the idea that initial value of the potential V_{init} is supposed to be $V_{init} \sim M^4_{Pl}$; we fixed v parameter to $v = 0.1 M_{Pl}$.

Table 1: Critical values of M

φ_{init}, M_{Pl}	λ	V, M^4_{Pl}	M_{cr}, M_{pl}
20,00	6,250E-06	1,600E+05	0,54
15,00	1,975E-05	5,062E+04	0,55
14,00	2,603E-05	3,841E+04	0,56
13,00	3,502E-05	2,856E+04	0,58
12,00	4,823E-05	2,073E+04	0,63
11,00	6,831E-05	1,464E+04	0,69
10,00	1,000E-04	9,998E+03	0,78
9,00	1,525E-04	6,559E+03	0,92
8,00	2,442E-04	4,095E+03	1,12
7,00	4,167E-04	2,400E+03	1,50
6,00	7,720E-04	1,295E+03	2,30
5,00	1,601E-03	6,245E+02	5,90

We found that with lowering M the duration of inflation falls down as well, which makes it necessary to raise initial value of field φ_{init}. The lowest possible value of M parameter for each φ_{init} with $N_{total} \approx 60$ e-foldings is called M_{cr}; appropriate values of parameters are listed in Table 1. We built two slices of $N_{total}\,(M_{cr}, \varphi_{init})$ dependance: "$\varphi = \varphi_{init}$" and "$N_{total} \approx 60$" (see Fig. (1a)-(1b)). This allows one to easily comprehend the results given in Table 1.

One can see, that the lowest available value of M_{cr} is $M_{cr} \approx 0.54$, thus $M^2_{Pl}/M^2_* \approx e^{0.1852} \sim 1$. In general, it means, that in the boundaries of this model one cannot lessen the value of M_{Pl} by means of introducing scalar field in the action - at least, at these scales of energy. Nevertheless, it is of great interest to explore behavior of fields, Hubble constant, etc. with somewhat more realistic inflation potentials. Another subject for research is to examine lower scales of energy, thus making M^*_{Pl} of lower magnitude as well.

As an outlook for the further investigations, we are planning to perform this study for the hybrid inflation model, which includes two interacting scalar fields, thus allowing additional opportunities for fine-tuning.

Acknowledgements. Special acknowledgements to Prof. Volobuev I.P. (SINP MSU) and to Dr. Mikheeva E.V. (ASC FIAN) for their contribution to the research.

References

N. Arkani-Hamed, S. Dimopoulos and G.R. Dvali: 1998, *Phys. Lett. B*, **429**, 263.

V. Faraoni: 2004, *Phys. Rev. D*, **70**, 047301.

M. Yoshimura: 1991, *Extended Inflation and Brans-Dicke Dilaton, Proceedings of the 6th Marcel Grossmann Meeting on General Relativity*, Kyoto, Japan.

G.F.R. Ellis, D.C. Roberts, D. Solomons and P.K.S. Dunsby: 2000, *Phys. Rev. D*, **62**, 084004.

INDUCED RADIO AND X-RAY EMISSION FROM AN ACCRETION DISK

F.V. Prigara

Institute of Microelectronics and Informatics, Russian Academy of Sciences,
21 Universitetskaya, Yaroslavl 150007, Russia
fprigara@imras.yar.ru

ABSTRACT. Radio and X-ray emission from compact sources with accretion disks (active galactic nuclei, pulsars and X-ray binaries) is considered. It is shown that both radio and X-ray emission from these sources can be interpreted as emission of a hot ($T \geq 3 \times 10^7 K$) plasma in the inner part of an accretion disk or in the disk corona. Radio emission is produced by the maser amplification of thermal radio emission in a hot plasma and corresponds to the transitions between highly located energy levels (somewhat similarly to the recombination lines). The X-ray emission is either thermal radiation from dense filaments or is produced by the coherent inverse Compton scattering of radio photons in the same dense filaments. The same mechanism, which gives rise to the maser amplification at radio wavelengths, produces also laser amplification in optical in X-ray binaries.

Key words: accretion, accretion disks—radiation mechanisms: general.

Introduction

In the unified model of compact radio sources, radio emission from active galactic nuclei (AGNs) and pulsars is treated as thermal radiation from an accretion disk amplified by a maser mechanism (Prigara, 2003a). A maser amplification of thermal radio emission in continuum produces the high brightness temperatures of compact radio sources and a rapid variability of total and polarized flux density, that is characteristic for non-saturated maser sources. In particular, pulsars signals show a variability on every observable time scale up to nanoseconds (Edwards&Stappers 2003, Vivekanand 2001). The brightness temperatures of OH masers have the magnitude $T_b \leq 10^{12} K$, and those of water masers have the magnitude $T_b \leq 10^{15} K$ (Bochkarev, 1992). Compact extragalactic sources (AGNs) exhibit brightness temperatures in the range of 10^{10} K to 10^{12} K (Bower&Backer, 1998; Kellermann et al., 1998), so these temperatures have an order of magnitude of those of OH masers.

Maser amplification in continuum is closely connected with the stimulated origin of thermal radio emission. The induced origin of thermal radio emission follows from the relations between Einstein's coefficients for a spontaneous and induced emission of radiation. However, the detailed mechanism of maser amplification has been unknown so far. In this paper we show that maser amplification is produced by the inversion of the high energy level population in a hot plasma.

The unified model of compact sources can be extended to account for emission in other bands. X-ray binaries have roughly two-component X-ray spectra with a thermal blackbody component and a power law spectrum (Falcke et al., 2003). The power law spectrum in the X-ray range has been also detected in some radio pulsars, X-ray pulsars and AGNs (Chakrabarty et al., 2001). The unified model predicts photon indices of the power law spectrum in the X-ray range which may be compared with the observed indices.

1. The gaseous disk model

It was shown recently (Prigara, 2003b) that thermal radio emission has a stimulated character. According to this conception thermal radio emission from non-uniform gas is produced by an ensemble of individual emitters. Each of these emitters is an elementary resonator the size of which has an order of magnitude of mean free path l of photons

$$l = \frac{1}{n\sigma} \tag{1}$$

where n is the number density of particles and σ is the absorption cross-section.

The emission of each elementary resonator is coherent, with the wavelength

$$\lambda = l, \tag{2}$$

and thermal radio emission of gaseous layer is incoherent sum of radiation produced by individual emitters.

The condition (2) implies that the radiation with the wavelength λ is produced by the gaseous layer with the definite number density of particles n .

The condition (2) is consistent with the experimental results by Looney and Brown on the excitation of plasma waves by electron beam (Chen, 1984; Alexeev, 2003). The wavelength of standing wave with the Langmuir frequency of oscillations depends on the density as predicted by equation (1). The discrete spectrum of oscillations is produced by the non-uniformity of plasma and the readjustment of the wavelength to the length of resonator. From the results of experiment by Looney and Brown the absorption cross-section for plasma can be evaluated.

The product of the wavelength by density is weakly increasing with the increase of density. This may imply the weak dependence of the size of elementary resonator in terms of the wavelength upon the density or, equivalently, wavelength.

In the gaseous disk model, describing radio emitting gas nebulae (Prigara, 2003a), the number density of particles decreases reciprocally with respect to the distance r from the energy center

$$n \propto r^{-1}. \tag{3}$$

Together with the condition for emission (2) the last equation leads to the wavelength dependence of radio source size:

$$r_\lambda \propto \lambda. \tag{4}$$

The relation (4) is indeed observed for sufficiently extended radio sources. For example, the size of radio core of galaxy M31 is 3.5 arcmin at the frequency 408 MHz and 1 arcmin at the frequency 1407 MHz (Sharov, 1982).

2. Radio emission from the gaseous disk

The spectral density of flux from an extended radio source is given by the formula

$$F_\nu = \frac{1}{a^2} \int_0^{r_\lambda} B_\nu (T) \times 2\pi r dr \quad , \tag{5}$$

where a is a distance from radio source to the detector of radiation, and the function $B_\nu (T)$ is given by the Rayleigh-Jeans formula

$$B_\nu = 2kT\nu^2/c^2, \tag{6}$$

where ν is the frequency of radiation, k is the Boltzmann constant, and T is the temperature.

The extended radio sources may be divided in two classes. Type 1 radio sources are characterized by a stationary convection in the gaseous disk with an approximately uniform distribution of the temperature $T{\approx}const$ giving the spectrum

$$F_\nu \approx const \quad . \tag{7}$$

Type 2 radio sources are characterized by outflows of gas with an approximately uniform distribution of gas pressure $P{=}nkT{\approx}const$. In this case the equation (3) gives

$$T \propto r, \tag{8}$$

so the radio spectrum, according to the equation (5), has the form

$$F_\nu \propto \nu^{-1}. \tag{9}$$

Both classes include numerous galactic and extragalactic objects. In particular, edge-brightened supernova remnants (Kulkarni&Frail, 1993) belong to the type 2 radio sources in accordance with the relation (8), whereas center-brightened supernova remnants belong to the type 1 radio sources.

The relationship between linear size and turnover frequency in type 2 radio sources (gigahertz-peaked spectrum sources and steep-spectrum sources) (Nagar et al., 2002) is a consequence of the wavelength dependence of radio source size. The turnover frequency is determined by the equation $r_\nu = R$, where R is the radius of a gaseous disk. The same equation determines a turnover frequency for planetary nebulae (Prigara 2003a, Pottasch 1984, Siodmiak&Tylenda, 2001).

3. The unified model of compact radio sources

The unified model of compact radio sources (Prigara, 2003a) invokes an accretion disk with convection and outflows. The density profile $n \propto r^{-1/2}$used in the unified model is standard for an outflow or the convection dominated accretion flow (CDAF) models (Nagar et al., 2001). Here r is the distance from the central energy source. The temperature profile is virial, i.e. $T \propto r^{-1}$, only in active galactic nuclei (AGNs). In pulsars it has other forms. The fixed ratio of magnetic to gas pressure is inferred for AGNs, in pulsars the decouplement of magnetic and gas pressure is observed.

The unified model suggests the uniform maser amplification of thermal radio emission in continuum. In the model, the inferred brightness temperatures of radio pulsars are comparable to those of water vapor, OH and SiO masers. The unified model predicts the flat radio spectrum for a core emission from AGNs, the spectrum (9) for an outflow, and the intermediate ($0 < \alpha < 1$) values of the spectral indices for unresolved sources, depending on the relative contributions

of an outflow and accretion disk. Here $F_\nu \propto \nu^{-\alpha}$is the flux density and is the frequency.

The model includes also radiation-induced solitary waves in an accretion disk to explain the phenomena seen in pulsars (Prigara, 2004).

In the case of compact radio sources instead of the relationship (4) the relationship

$$r_\lambda \propto \lambda^2 \tag{10}$$

is observed (Lo et al., 1993; Lo, 1982). This relationship may be explained by the effect of a gravitational field on the motion of gas which changes the equation (3) for the equation

$$n \propto r^{-1/2} \tag{11}$$

The mass conservation in an outflow or inflow of gas gives *nvr=const,* where v is the velocity of flow. In the gravitational field of a central energy source the energy conservation gives

$$v = \left(v_0^2 + c^2 r_s/r\right)^{1/2} \tag{12}$$

where r_s is the Schwarzschild radius. Therefore, at small values of the radius the equation (6) is valid, whereas at the larger radii we obtain the equation (3).

It is well known that the delay of radio pulses from pulsars at low frequencies is proportional to λ^2. This fact is a mere consequence of Eq.(10), if we only assume the existence of the radial density wave travelling across the radius with a constant velocity and triggering the pulse radio emission. In this treatment the pulsars also obey the λ^2 dependence of compact source size. Note that the wavelength dependence of a pulse duration is a similar effect.

The spatial distribution of SiO, water, and OH masers (each of which emits in its own wavelength) in the maser complexes also is consistent with the λ^2 dependence of compact source size (Bochkarev, 1992; Eisner et al., 2002).

To summarize, extended radio sources are characterized by the relation (4), and compact radio sources obey the relation (10).

4. Maser amplification in compact radio sources

Recently, the energy distribution of atoms in the field of thermal black body radiation was obtained (Prigara, 2003b) in the form

$$N/N_0 = \sigma_a \omega^2 / \left(2\pi c^2\right) \left(exp\left(\hbar\omega/kT\right) - 1\right), \tag{13}$$

where N_0 is the population of the ground state E_0, N is the population of the energy level $E = E_0 + \hbar\omega$, σ_a is the absorption cross-section, $\hbar$ is the Planck constant, and T is the radiation temperature.

This distribution is valid in the range $\hbar\omega/kT \geq 1$, since in the limit $\hbar\omega/kT \to 0$ the line width is going to infinity, that indicates the violation of the one-particle approximation used by (Prigara, 2003b).

The function (13) has a maximum at $\hbar\omega_m = 1.6kT$. When the temperature exceeds the critical value of $T_0 = 3 \times 10^7 K$ (the inversion temperature), the population of the energy level E exceeds the population of the ground state E_0. Since the function (13) is increasing in the range $\omega < \omega_m$, the inversion of the energy level population is produced also in some vicinity of ω_m (below ω_m). This suggests the maser amplification of thermal radio emission in continuum by a hot plasma with the temperature exceeding the critical value T_0. Maser amplification in compact radio sources was assumed earlier by (Prigara, 2003a) based on the high brightness temperatures of AGNs. Since a hot plasma in an accretion disk is concentrated nearby the central energy source, maser amplification is characteristic for compact radio sources.

It is clear that, when the temperature of a plasma is below T_0, the radio flux is very small, and when the temperature exceeds T_0, radio emission is on. This an on-off cycle is detected in the radio pulsar PSR B1259-63 (Qiao et al., 2003). Similar is an on-off cycle in X-ray pulsars, e.g., the 35-day cycle in Her X-1. It implies that X-ray emission from X-ray pulsars is produced by the laser amplification in continuum which is quite analogues to maser amplification at radio wavelengths.

5. The photon indices of X-ray emission

X-ray binaries normally have the two most pronounced states (Falcke et al., 2003). The first one is the high/soft state dominated by the thermal blackbody emission from a thin disk. The second one is the low/hard state which is characterized by a dominant hard power-law spectrum whereas the thermal spectrum is weak or absent. The power-law spectrum is commonly attributed to an optically thin accretion flow or disk corona. However, there are other plausible origins of the power-law spectrum (Falcke et al., 2003).

The power-law spectrum in the X-ray range has also been detected in young classical pulsars, anomalous X-ray pulsars (AXPs) and soft gamma-ray repeaters (SGRs) (Chakrabarty et al., 2001). All these objects are believed to be isolated neutron stars. For AXPs and SGRs, the fallback accretion disk model has been proposed (Qiao et al., 2003). It is assumed that the accretion is fed by fallback material after the original supernova explosion.

To characterize the power-law spectrum, we introduce the photon index, Γ, defined such that photon

number flux $dN/dE \propto E^{-\Gamma}$. Since $E = h\nu$, where h is the Planck constant, $\Gamma - 1$ is the spectral index in the X-ray range.

Classical young pulsars have power-law X-ray spectra with $\Gamma = 1.1 - 1.7$ in the 0.1-10 keV band, that corresponds to the spectral indices $\Gamma - 1 = 0.1 - 0.7$. Thus, the spectral indices for these pulsars lie between 0 and 1, similar to the spectral indices of radio emission from supernova remnants (SNRs).

The X-ray spectrum of most AXPs is best characterized by a two-component spectrum consisting of a $\sim$0.5 keV blackbody emission and a steep ($\Gamma = 3 - 4$) power law spectrum, with comparable luminosities in both components (Chakrabarty et al., 2001). The spectral indices for AXPs are in the same range, $2 < \Gamma - 1 < 3$, as the spectral indices of radio emission from pulsars . The latter can be inferred by making use of the density profile of compact radio sources, similarly to the spectra (7) and (8).

Active galactic nuclei (AGNs) typically lie within a range of photon indices $\Gamma = 1.2 - 2.2$, so the spectral indices $\Gamma - 1 = 0.2 - 1.2$ are close to those of classical young pulsars, i.e. lie in the same range as the spectral indices of radio emission from extended sources.

The theory of thermal emission from a gas with account for stimulated radiation processes gives the two possibilities to explain these values of photon indices in the X-ray range. The first one is to apply the above theory to the X-ray emission from a hot, optically thin in a classical sense disk corona. If the temperature of a gas is sufficiently high, then the Rayleigh-Jeans formula (6) is still valid, and the only difference with the radio band is the order of magnitude of the density, n, required by the equations (1) and (2) to produce X-ray emission. In this scheme, the power law spectrum can be produced either by the hot inner disk corona ($\Gamma = 3 - 4$) or by the hot filaments in the thick outer disk with outflows ($\Gamma = 1 - 2$).

Another possibility is the inverse Compton scattering of radio photons from an accretion disk by the hot disk corona or the hot filaments. However, the incoherent Compton scattering is not relevant in this case, because it does not conserves the spectral indices. In fact, the final spectrum is determined mostly by the spectral energy distribution of electrons and weakly depends upon the original radio spectrum. We should assume, instead, the coherent Compton scattering to reproduce the original spectral indices of radio emission (cf. Rees, 1982). It is plausible, that both these processes, the emission of thermal radiation and the inverse Compton scattering, contribute to the observed spectra.

The coherent inverse Compton scattering of radio photons from an accretion disk is supported by a strong (one-to-one) correlation between radio oscillation events and series of spectrally hard states in GRS 1915+105 (Klein-Wolt et al., 2002). Another observational evidence for the inverse Compton scattering in the hot disk corona is that the spectral indices of radio emission from X-ray binaries correspond to the emission from an outer disk. The radio emission from the inner part of an accretion disk, which has been detected in pulsars, in X-ray binaries is absent. It suggests that this emission is converted into X-ray emission via inverse Compton scattering.

Conclusions

In this paper, we elucidate the mechanism of maser amplification in compact radio sources, which has been suggested earlier based on the high brightness temperatures of these sources. Maser amplification is produced by the inversion of the high energy level population in a hot plasma.The inversion of the level population can produce also laser amplification in optical (e.g., the high variable shifts and intensities of the weak emission lines in Sco X-1 can be attributed to the weak laser sources) and X-ray bands. An on-off cycle in radio and X-ray pulsars may be explained by the periodic changes of the emitting gas temperature from higher to lower than the inversion temperature values.

The photon indices of the power law spectra in the X-ray range are obtained similar to the spectral indices of radio emission in the unified model of compact radio sources. The only difference is the higher density of an emitting gas. However, the detected correlation between radio and X-ray emission in X-ray sources suggests that another mechanism (the coherent inverse Compton scattering of radio photons) also contributes to the observed spectra.

Acknowledgements. The author is grateful to D.A.Kompaneets, Y.Y.Kovalev, V.N.Lukash, B.E.Stern, and N.A.Tsvyk for useful discussions.

References

Alexeev B.V.: 2003, *Usp. Fiz. Nauk*, **173**, 145, *Physics-Uspekhi*, **46**, 139.

Bochkarev N.G.: 1992, *Basic Physics of Interstellar Medium*, Moscow University Press.

Bower G.C. & Backer D.C.: 1998, *ApJ*, **507**, L117.

Chakrabarty D., Pivovaroff M.J., Hernquist L.E., Heyl J.S. & Narayan R.: 2001, *ApJ*, **548**, 800.

Chen F.F.: 1984, Introduction to Plasma Physics and Controlled Fusion, **Vol. 1**, *Plasma Physics*, New York: Plenum Press.

Edwards R.T. & Stappers B.W.: 2003, *A&A*, **407**, 273.

Eisner J.A., Greenhill L.J., Herrnstein J.R., Moran J.M. & Menten K.M.: 2002, *ApJ*, **569**, 334.

Falcke H., Koerding E. & Markoff S.: 2003, *A&A*, **414**, 895.

Kellermann K.I., Vermeulen R.C., Zensus J.A. & Cohen M.H.: 1998,*AJ*, **115**, 1295.

Klein-Wolt M., Fender R.P., Pooley G.C., Belloni T., Migliari S., Morgan E.H. & van der Klis M.: 2002, *MNRAS*, **331**, 745.

Kulkarni S.R. & Frail D.A.: 1993, *Nature*, **365**, 33.

Lo K.Y.: 1982, in *AIP Proc. 83: The Galactic Center*, ed. G.Riegler & R.Blandford, New York.

Lo K.Y., Backer D.C., Kellermann K.I., Reid M., Zhao J.H., Goss M.H. & Moran J.M.: 1993, *Nature*, **361**, 38.

Nagar N.M., Wilson A.S. & Falcke H.: 2001, *ApJ*, **559**, L87.

Nagar N.M., Wilson A.S., Falcke H., Ulvestad J.S. & Mundell C.G.: 2002, in *Issues in Unification of AGNs, ASP Conf. Series 258*, ed. R.Maiolino, A.Marconi & N.Nagar, San Francisco.

Pottasch S.R.: 1984, *Planetary Nebulae*, Dordrecht: D.Reidel Reinhold Company.

Prigara F.V.: 2003a, *Astron. Nachr.*, **Vol. 324**, No. S1, Supplement: Proceedings of the Galactic Center Workshop 2002 – The central 300 parsecs of the Milky Way, ed. A.Cotera, H.Falcke, T.R.Geballe & S.Markoff, p.425.

Prigara F.V.: 2003b, *Int. J. Mod. Phys. D (submitted)*, astro-ph/0311532.

Prigara F.V.: 2004, *Phys. Plasmas (submitted)*, physics/0404087.

Rees M.J.: 1982, in *AIP Proc. 83: The Galactic Center*, ed. G.Riegler & R.Blandford, New York.

Qiao G.J., Xue X.Q., Xu R.X., Wang H.G. & Xiao B.W.: 2003, *A&A*, **407**, L25.

Sharov A.S.: 1982, *The Andromeda Nebula*, Moscow: Nauka.

Siodmiak N. & Tylenda R.: 2001, *A&A*, **373**, 1032.

Vivekanand M.: 2001, *MNRAS*, **326**, L33.

CALCULATE METHOD OF THE TWILIGHT SKY BRIGHTNESS IN THE SOLAR VERTICAL, STIPULATED BY A MULTIPLE SCATTERING OF A SUNLIGHT

L.S. Shakun, V.D. Motrich and S.M. Melykjants

Scientific research institute "Astronomical observatory" Odessa national university
T.G.Shevchenko Park, Odessa 65014 Ukraine, *spirits@tm.odessa.ua*

ABSTRACT. Use of a twilight sounding method of the Earth's atmosphere with the aim to reveal aerosols inflow to the upper and medial atmosphere needs a method of separation twilight sky brightness to the brightness of primary and secondary twilight. Method of secondary twilight brightness calculation on a declination of the logarithm of twilight sky brightness caused by a multiple scattering of sunlight is discussed. The calculation procedure of a declination of the logarithm of secondary twilight brightness on observations in solar vertical is given. The use equal declination of the logarithm of secondary twilight brightness for all viewing directions in solar vertical is proved.

Key words: remote sounding, atmospheric sounding, twilight sounding, multiple scattering

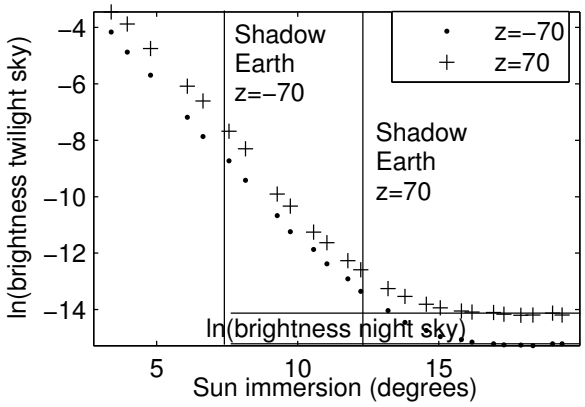

Figure 1: Observation in a solar vertical at a zenith distance 70 degrees in viewing directions on the Sun and from the Sun.

The aerosol content in the Earth's atmosphere essentially influences the processes of chemical reactions in an atmosphere and heat balance of the Earth. Present article discusses the twilight sounding method that is used for definition of the inflow and time variations of aerosol content in medial and upper Earth's atmosphere. In the twilight sounding method the brightness of the sky is measured during morning and evening twilight, and contents of an aerosol in an atmosphere is calculated on the base of quantity of a directional scattering factor. To define the directional scattering factor the discussed method uses only the brightness that is stipulated by a single scattering of sunlight (primary twilight brightness). Therefore it is necessary to split the brightness of the twilight sky into the primary twilight brightness, the brightness of the sky stipulated by a dispersion of sunlight of the higher orders (secondary twilight brightness) and the brightness of night sky. General brightness of the twilight sky is

$$B = B_1 + B_2 + B_b \qquad (1)$$

where B_1 – primary twilight brightness; B_2 – secondary twilight brightness; B_b – the night sky brightness.

To split primary and secondary twilight brightness we used, so-called, gradient method (Zaginajlo Y.I. et al. 1999). According to this method in the zone of an Earth shadow where main part of twilight sky brightness is constituted by secondary twilight brightness, the dependence of the logarithmic twilight sky brightness on immersion of the Sun under horizon at a constant zenith distance of a viewing direction can be line fitted.

In a series of works (Smoktij O.I. 1967a, 1967b) the solution for sunlight multiple scattering in the spherically symmetric exponential atmosphere was offered. We showed (Shakun L.S. 2000), that it is possible to determine the relation between the declination of the approximating line in the zone of an Earth shadow and eigenvalues in the solution for multiple scattering of light in the exponential spherical atmosphere, the above mentioned solution. Then, using analytical formulas from the solution (Smoktij O.I. 1967b), it is possible to make an extrapolation of secondary twilight brightness in the zone of small immersions of the Sun where primary twilight brightness constitutes main part of all twilight sky brightness. The accuracy

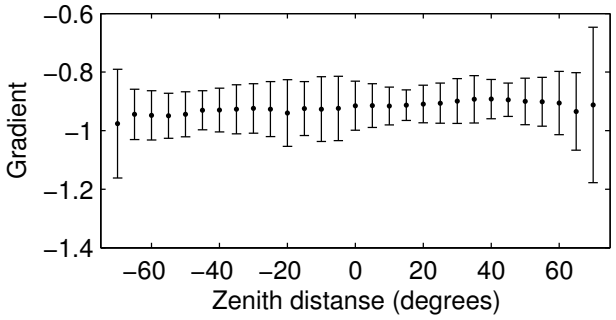

Figure 2: Declinations of fitting curves calculated separately in different viewing directions.

of calculation of secondary twilight brightness depends on accuracy of calculation of the Smoktij O.I. solution eigenvalues. Thus, it is necessary to calculate the declination of the line that approximates the secondary twilight brightness as accurately as possible. Let's call the declination of the line that approximates the secondary twilight brightness, the gradient of secondary twilight brightness.

Carrying out twilight observations in all the twilight vertical at one viewing direction it is possible to take no more than ten values of secondary twilight brightness in the Earth shadow zone. Obtained values are distributed nonuniformly on different viewing directions.

So, in the opposite of the Sun direction we can take about ten values of secondary twilight brightness, and in the direction to the Sun – one or two values. Thus, in all viewing directions the quantity of the values of secondary twilight brightness is not enough for accurate determination of declination of the approximating line (fig. 1). In the work (Shakun L.S. 2000) the gradient of secondary twilight brightness in the zone of an Earth shadow and the spectrum of Smoktij O.I. solution eigenvalues for the radiation transfer in spherically symmetric exponential atmosphere was connected with the height of an atmosphere in Smoktij's model. Most likely, this height of an atmosphere corresponds with the height of an atmosphere where an effective transfer of multiply scattered light takes place. It is logically to assume, that the height of an atmosphere where effective transfer of multiply scattered light takes place, does not depend on viewing direction. Therefore the gradient of secondary twilight brightness does not depend on viewing direction too. Really, the gradient of secondary twilight brightness differs insignificantly in different viewing directions, and in most cases this difference is less than the error of determination of the gradient of secondary twilight brightness (fig. 2). Thus, it is logically to determine the gradient of secondary twilight brightness using all the values of secondary twilight brightness. It is necessary to note, that all values of secondary twilight brightness will not lie on one line (fig. 1) because the zero-mark of the approximating line for each viewing direction varies. For simultaneous determination of zero-mark of the approximating lines and common declination of the lines it is necessary to put in special basis of the fitting functions.

The values of the secondary twilight brightness in the zone of an Earth shadow we shall fit with the following dependence:

$$\ln(B_2) = a_0 g + a_1 f_1(z) + \ldots + a_n f_n(z), \qquad (2)$$

where B_2 – the secondary twilight brightness; g – the immersion of the Sun under horizon; $f_i(z)$ – basis functions for determining the zero-mark of the approximating lines; a_0 - the gradient of secondary twilight brightness; a_i – zero-mark of the approximating lines.

At the selected viewing direction the fitting dependence should become:

$$\ln(B_2) = a_0 g + a_j, \qquad (3)$$

where j – the number of the selected viewing direction.

Thus, basis functions are defined as

$$f_j(z) = \begin{cases} 1, & where \quad z = z_j \\ 0, & where \quad z \neq z_j \end{cases} \qquad (4)$$

In order to make approximation it is necessary to allocate secondary twilight brightness from the measured twilight sky brightness. The most favorable zone to determinate the secondary twilight brightness is in the zone of an Earth shadow where primary twilight brightness can be neglected. In the zone of an Earth shadow measured brightness of the twilight sky may be represented as

$$B = B_2 + B_b + \varepsilon(B_2 + B_b) + \eta B_b, \qquad (5)$$

where B_2 – real secondary twilight brightness; B_b – real night sky brightness; ε – the relative accidental error of measurements of the twilight sky brightness; η – the relative accidental error of measurements of the night sky brightness.

In this case two types of accidental error of measurements can be distinguished. The first one is an accidental error of measurements of the twilight sky brightness as a results noise of the measuring devices and a flicker of natural atmosphere. The second accidental error, which we call an accidental measurement error of the night sky brightness, is a result of irregularity of the night sky brightness.

Except an accidental error of the night sky brightness the regular errors that depend on the way of determination the night sky brightness can be observed. The night sky brightness is being determined after the end of twilight by observations in a solar vertical. However the night sky brightness in the zone of secondary twilight domination differs slightly from the one measured on completion of twilight as a result of other orientation of solar vertical and rotation of the starry

sky around of the celestial pole. The change of solar vertical position changes the position of viewing direction relatively to the objects on horizon. Illumination produced by objects on horizon, is non-uniform, therefore the real night sky brightness during the twilight will be different. Rotational displacement of the starry sky around the celestial pole results in bias of a viewing direction relatively to stars. Both factors can become apparent as trends that difficultly take into account in practice. Therefore measuring of night sky brightness after the end of twilight can be used only for estimation of the night sky brightness.

If we obtained the estimation of the night sky brightness, let subtract it from the total twilight sky brightness. Then in the zone of the Earth shadow the logarithm of the twilight sky brightness will be

$$\ln(B) = \ln(B_2 + B_b + \varepsilon(B_2 + B_b) + \eta B_b - \tilde{B}_b) = \\ = \ln(B_2) + \ln\left(1 + \varepsilon + \frac{(\varepsilon+\eta)B_b + \delta B}{B_2}\right), \quad (6)$$

where B – the observed secondary twilight brightness; $\tilde{B}_b$ – an estimation of the night sky brightness; $\delta B = B_b - \tilde{B}_b$ – an error of estimation of the night sky brightness.

In order to adequately determinate the gradient of secondary twilight by the least-squares method the next conditions must be fulfilled

$$1 + \varepsilon + \frac{(\varepsilon+\eta)B_b + \delta B}{B_2} \approx 1. \quad (7)$$

The measured night sky brightness after the end of twilight can be represented as:

$$B = B_b + (\varepsilon + \eta)B_b. \quad (8)$$

Assuming the night sky brightness as a constant value, it is easy to receive an estimation of the night sky brightness $\tilde{B}_b$ and an estimation of a standard deviation of the values of the night sky brightness $\sigma = \sqrt{< (\varepsilon+\eta), (\varepsilon+\eta) >}$. Let's find the immersions of the Sun at which the sky brightness meets the condition:

$$\frac{B - -\tilde{B}_b}{\sigma} > n. \quad (9)$$

It is correct for these immersions, that

$$\left|\varepsilon + \frac{(\varepsilon+\eta)B_b + \delta B}{B_2}\right| < \left|\varepsilon + \frac{1}{n} + \frac{\delta B}{B_2}\right|. \quad (10)$$

In the zone of immersions of the Sun under horizon where systematic error of an estimation of the night sky brightness exceeds the secondary twilight brightness we shall see the deviation from linearity of the logarithm of secondary twilight brightness. If the error of estimation of the night sky brightness is positive than we shall see the deviation from linear dependence to larger values and in the case of negative error – to smaller values (fig. 3).

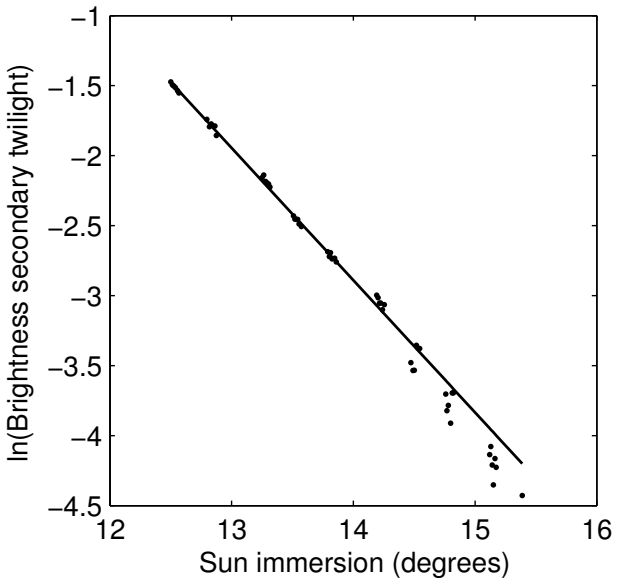

Figure 3: Approximation of secondary twilight brightness at a viewing direction on the Sun and a zenith distance 70 degrees.

As it is seen from above mentioned reasoning an error of each measuring depends on secondary twilight brightness. Therefore to adjust statistical significance of each observation and reduce the role of estimation error of the night sky brightness it is necessary to introduce the weight numbers.

Let measuring error of the device is ε_j and its standard deviation is ε; an estimation of the night sky brightness and its standard deviation are $\tilde{B}_b$ and σ accordingly. Then from the condition of equality of a standard deviation for all observations we have:

$$\left\langle w_j\left(\varepsilon_j(B_j - -\tilde{B}_b) + \sigma\right), w_i\left(\varepsilon_i(B_i - -\tilde{B}_b) + \sigma\right)\right\rangle = \\ = \varepsilon^2(B_j - -\tilde{B}_b)^2, \quad (11)$$

$$w_j^2 = \frac{\varepsilon^2}{\varepsilon^2 + \sigma^2/(B_j - -\tilde{B}_b)^2}, \quad (12)$$

where w_j – a weight number of the j twilight sky brightness.

It is evidently, that the less is the secondary twilight brightness and the higher nonuniformity of the night sky brightness the less are weight numbers.

Fig. 3 shows actual observations in a solar vertical at the constant zenith distance 70 degrees. It is seen,

that the estimation of the night sky brightness is overstated and therefore secondary twilight brightness at great immersions noticeably declines downwards from the fitting line. If observations were obtained in the entire solar vertical, then each series of measuring turns into a point with higher statistical error. That is why in case observations were made in a solar vertical it is much more difficultly to reveal overstated estimations of the night sky brightness. In this case despite of overstated estimation of the night sky brightness, good estimation of secondary twilight brightness is obtained.

Let's compare now gradients of the secondary twilight brightness, that where obtained independently for each direction (fig. 2), and the gradient of secondary twilight brightness for the same observations, but on all directions of observations simultaneously. Average gradient of the secondary twilight brightness, obtained independently for each viewing direction, is equal 0.921 at the average standard deviation 0.0089, and the general gradient of secondary twilight brightness for all viewing directions is 0.933 at a standard deviation 0.0015. Thus, the method of the general gradient of secondary twilight brightness allows reaching considerably greater statistical significance of the factor of inclination of the logarithm of the secondary twilight brightness.

At last, let's compare the directional scattering factors obtained at approximation of secondary twilight brightness in each direction separately, and the one obtained as a result of determination of a general inclination of approximation of the secondary twilight brightness (fig. 4). The directional scattering factors obtained as a result of different approximations of secondary twilight brightness for different viewing directions, contain discontinuity of scattering angle dependence that is the result of discontinuity in approximation coefficients of the secondary twilight brightness. The directional scattering factors, obtained in case of general coefficient of an inclination of the secondary twilight brightness, have better smoothness and lower statistical error. Apparently, it is the evidence of better adequacy of such directional coefficients to physical reality.

Solid line marks the directional scattering factors that were determined at the general coefficient of inclination of approximation of the secondary twilight brightness. Points mark directional scattering factors that were obtained in the case of various coefficients of inclination of approximation lines of the secondary twilight brightness.

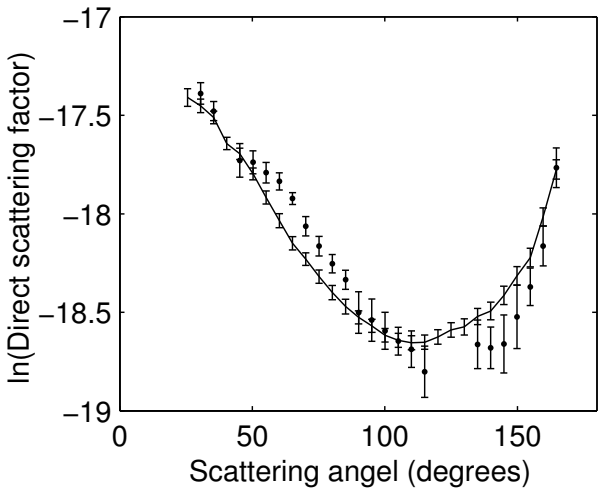

Figure 4: Directional scattering factors with a confidence interval 0.997 at height of 30 km in a wave length of 731 nm.

Thus the given procedure of determination of a general gradient of secondary twilight brightness guarantees better matching of directional scattering factors and lower statistical error. This allows preferring such method of determination of a gradient of secondary twilight brightness in the zone of an Earth shadow.

References

Shakun L.S.: 2001, *IRS 2000* Current problems in atmospheric radiation, p. 429.

Smoktij O.I.: 1967, *Fizika atmosfery i okeana*, **3**, N 3, p. 245.

Smoktij O.I.: 1967, *Fizika atmosfery i okeana*, **3**, N 5, p. 496.

Zaginajlo Y.I., Zaginajlo I.V., Motrich V.D., Melykjants S.M.: 1999, *MCAR'99*, Sbornik tezisov mezdunarodnyj simpozium stran SNG "Atmosfernaja radiacija", p. 94.

NATURAL MODELING OF GALACTIC AND EXTRAGALACTIC STRUCTURES

R.B. Shatsova and G.B. Anisimova

Rostov-on-Don Pedagogical University, Rostov-on-Don, Russia
galina@iubip.ru

ABSTRACT. The Universal Sky Net (USN) is proposed. Its elements correspond to the details of different scale structures. The examples of modeling by means of USN are cited for the system of globular clusters, for the galaxies of Local group and for the galaxies of two superclusters.

Keywords: Galaxies Superclusters: structure.

We submit into consideration the Universal Sky Net (USN). It joins such circles of coordinate systems as the ecliptical, the galactical, the Gould Belt, the supergalactical and other ones, but it have much more functions than it was before. The connections between these systems, which seemed independent before, were discovered in the frames of USN. So, the supergalactic equator Λ is orthogonal to the galactic equator MW and to the ecliptic E. The whole net is obtained by brunching of the initial dimensionless triedr E$\Lambda\Gamma$ in the poles ξ, η and others. ξ-bunch contains 4 circles over every $\pi/4$; η -bunch – 6 circles over every $\pi/6$, etc (Fig. 1).

The circles of USN one can describe by the canonical equations of such type:

tg b = tg b* sin(l-l*); where l*, b* – the coordinates of the circles knot and its inclination to the celestial equator. The numerical values of the parameters are presented in (Shatsova & Anisimova, 2003).

At present epoch ξ -pole coincides with the point of equinox, and η – with the point of solstice. But the USN is not connected with the precession as its poles are determined independently: η – is the pole of the supercluster of the galaxies. The verified correspondence of USN to the structures of all hierarchical levels of the Universe can be used for the natural modeling. The Fig. 2-5 show the examples of modeling for the similarly disposed structures. Owing to USN, the density waves parallel to E, were discovered in the nucleus of the globular cluster system, according to (Harris & McMaster Univers, 2003). The connection of two Local groups of galaxies with E and Λ is fixed, according to (Vorontsov-Velyaminov, 1972). The main elements in the Vaucouleurs supercluster became more

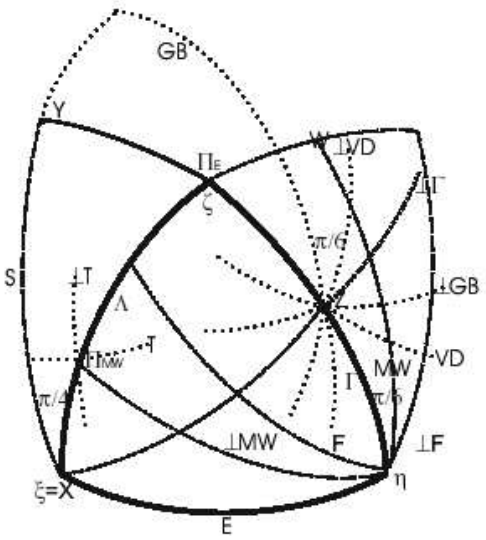

Figure 1: The Universal Sky Net near one of the octants. E- ecliptic, Π_E- ecliptic pole, MW – the Galactic plane, Π_{MW}– the Galactic pole. $\xi = \Upsilon$=(equinox), $\eta =$ (solstice), at least now. $\Gamma\perp\Lambda\perp$E; GB – the Gould belt, VD – the belt of Vacouleur – Dolidze. The spherical triangles:(E, Λ, Γ), (S, Γ, $\perp\Gamma$), (MW, Λ, $\perp$MW), etc The bunches of belts: $\xi \equiv$X(E, $\perp\Gamma$, Λ, S), η(E, $\perp$MW, Γ, MW, F, $\perp$F,...), Z(Γ, GB, $\perp$VD, $\perp\Gamma$, $\perp$GB, VD), Π_{MW}(Λ, $\perp$MW, T, $\perp$T)

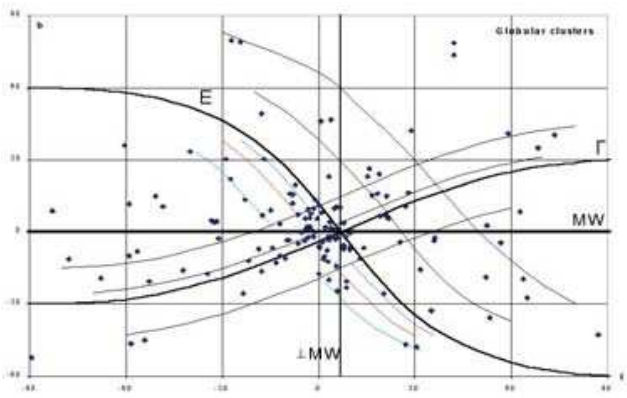

Figure 2: The distribution of the globular clusters over (Harris & McMaster Univers, 2003)

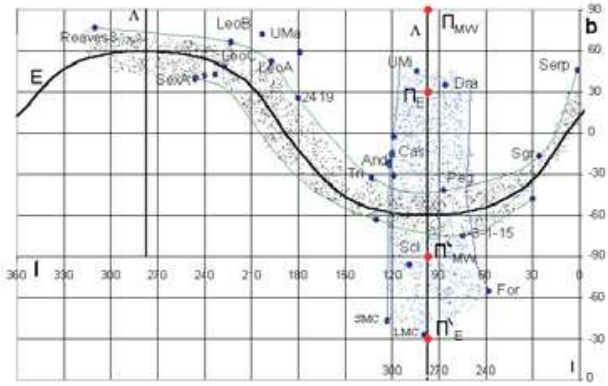

Figure 3: The Local group of the galaxies (over Vorontsov-Velyaminov, 1972)

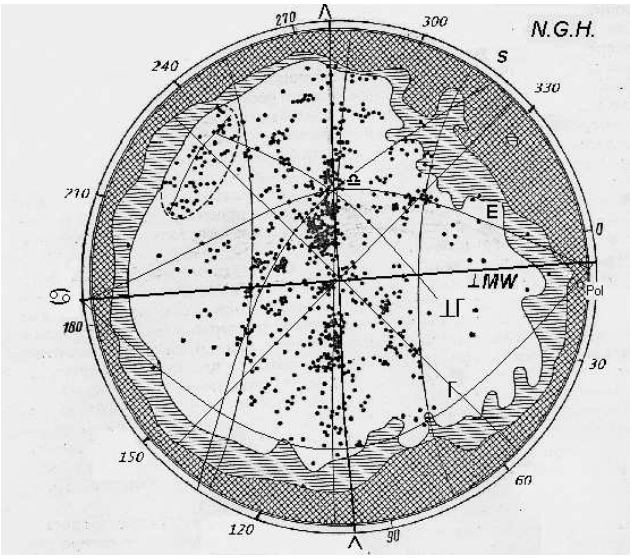

Figure 4: The supercluster of galaxies of Vaucouleurs. The galactic longitude l is along the map's border. The Vaucouleurs' net is kept for the comparison.

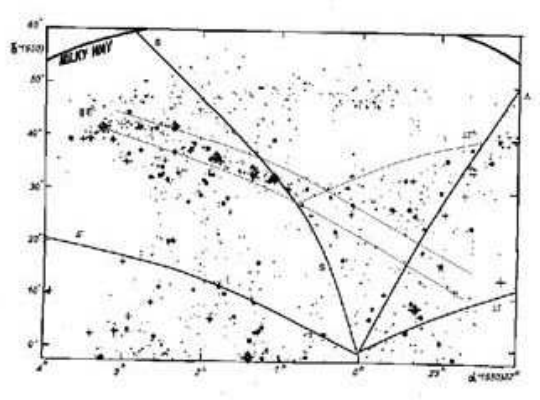

Figure 5: The supercluster in Perseus (Joeveer et al., 1977)

precisely: its equator coincides with the Λ -plane (l=97° – 277°), and the filaments – with η -bunch of meridians and with ξ -bunch of the circles. Along the filaments of supercluster of the galaxies in Perseus, according to (Joeveer et al., 1977), pass the circles of ξ -bunch and the parallel ones in the form of density waves. Unexpectedly the density of the objects in the knots of the net is observed either equal to zero or sharply overfalls from max on one side to min – on another, instead of the expected high density there (Fig. 2-5). So, the phenomenon of knots is one more dynamical indication of USN.

References

Shatsova R.B., Anisimova G.B.: 2003, *Astrofizica*, **46**, 319.

Harris W., McMaster Univers: 2003.

Vorontsov-Velyaminov B.A.: 1972, *Extragalactic astronomy*, M.

Joeveer M., Einasto J., Tago E.: 1977, Tartu.

TWO SCENARIOS OF MASS EXCHANGE IN CLOSE BINARY SYSTEMS CONSISTING OF THE LOW MASS PRE-MAIN SEQUENCE STARS

F. V. Sirotkin
Astronomical observatory, Odessa National University

ABSTRACT. In this paper, we present the results of smoothed particle hydrodynamic (SPH) simulations of mass transfer in close binary systems consisting of the low mass pre-main sequence stars. Two scenarios of mass exchange in such systems are possible. If the more massive component is closer to fill its Roche lobe than the less massive, then the binary system merges as a result of the mass exchange. The binary system can survive only in the case if the less massive component is closer to fill its Roche lobe to the beginning of a mass exchange.

Key words: computational fluid dynamics, close binary system, preMS star, mass exchange, component merging.

1. Introduction

The majority of binary systems properties are gained on the pre-main sequence stage (preMS) of their evolution. Among these properties: a wide range of the mass ratios and eccentricities in the long periodic systems. One of the possible mechanisms to acquire observable properties of zero age main sequence (ZAMS) binary stars is the mass exchange on preMS evolution stage. The very important question is an explanation of the ZAMS binary stars distribution upon their mass ratio and orbital separation.

We will show, that as a result of mass exchange in preMS binary systems either merging of their components occurs, or mass exchange in a dynamic time scale results in an increase of the orbital separation and decrease of the components mass ratio.

2. Choice of initial parameters

We consider systems with the low mass components (masses between $0.5M_\odot$ and $1M_\odot$)and effective radii of the components appropriate to the time moment, when the components are near the"birthline"(Stahler, 1988)(see Fig. 1). The "birthline"is the moment when the star has lost its envelope of infalling gas and dust.

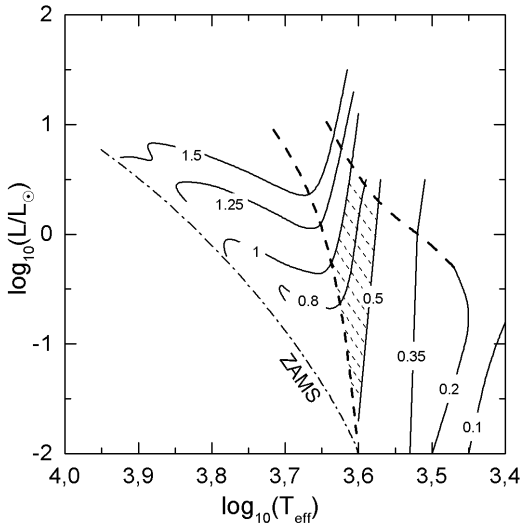

Figure 1: The theoretical pre-main-sequence tracks of Iben (1965) and Grossman and Graboske (1971), with appropriate masses (in solar units) labelled. The top dotted curve is the "birthline"(Stahler, 1988). In area between the upper and bottom dotted curves, preMS star is fully convective.

Let us designate this moment of time as t_B. At the moment t_B star of a given mass is descending a nearly vertical path. Along vertical part of the evolutionary track, the stars are fully convective, and their radii change according to this law

$$\left(\frac{R_\odot}{R}\right)^3 - \left(\frac{R_\odot}{R_B}\right)^3 = \frac{t - t_B}{t_K}, \qquad (1)$$

where R_B is stellar radius at the moment of time t_B (initial radius), t - time, t_K - Kelvin-Helmholtz time:

$$t_K \sim \frac{3}{4}\frac{GM^2}{LR}.$$

As demonstrated by Stahler (1988), radius R_B depends only upon the value assumed for accretion rate and deuterium abundance (see Fig. 2), which define

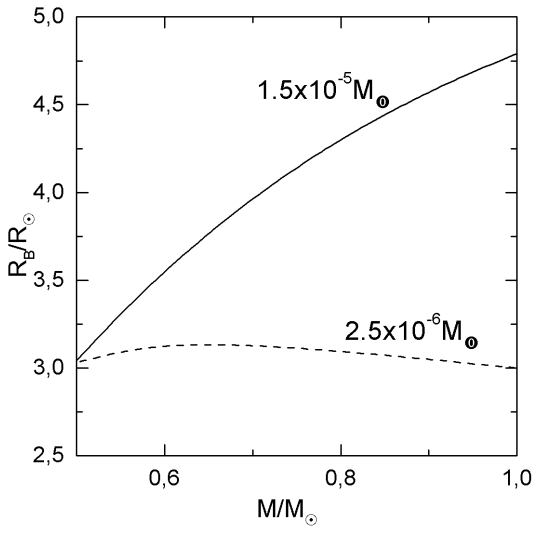

Figure 2: Mass-radius relations for the preMS stars (Stahler, 1983) located on the "birthline". Appropriate accretion rates are labelled. Deuterium to hydrogen ratio is $[D/H] = 2.5 \cdot 10^{-3}$

the energy sources of a protostar: heating through the infalling matter and deuterium burning.

Comparison between location of the theoretical "birthline" in the Hertzsprung-Russell diagram and the region where T Tauri stars are observed has allowed to Stahler (1983) to choose for an accretion rate $\dot{M} = 10^{-5} M_\odot \ yr^{-1}$ and deuterium abundance value $[D/H] = 2.5 \cdot 10^{-5}$. The mass-radius dependence for preMs stars with masses in the range from $0.575 M_\odot$ to $1.175 M_\odot$ on the "birthline"can be approximated by the following formula:

$$\frac{R}{R_\odot} = 12.6\frac{M}{M_\odot} - 8.7\left(\frac{M}{M_\odot}\right)^2 + 2.3\left(\frac{M}{M_\odot}\right)^3 - 1.4 \quad (2)$$

The applicability of the dependencies found from observations of the single preMS stars to the binary systems depends upon the accepted hypothesis of the binary system formation. If one to assumes that the binary system was formed through fragmentation of the protostellar cloud during its dynamical collapse, it is necessary to take into account effects connected with closeness of components, and these dependencies are probably not applicable to the short periodic systems. If one assumes, that the components of the binary system were formed independently, and binary system was formed as a result of collision , then these dependencies can be applicable.

The probability of a binary system components to merge grows with degree of the filling by components of their Roche lobes. The Eq. (1) shows, that stellar radii rapidly decrease, and the probability of a binary system to merge should be much higher for the stars situated at the beginning of the preMS stage (i.e. occupying the region closer to the "birthline").

The orbital separation at which the components are close to fill their Roche lobes in the chosen range of the component masses is $12 R_\odot$. Thus we consider here the systems for which the probability of the component merging is very high.

3. Method

In the case of polytropic equation of a state:

$$P = K\rho^\gamma, \quad (3)$$

where γ is the ratio of specific heats (in present calculations $\gamma = 5/3$), K is the entropy function, the equation of motion of a compressible fluid can be written in the form:

$$\frac{\partial \rho}{\partial t} + \nabla \cdot (\rho \vec{v}) = 0 \ , \quad (4)$$

$$\rho \frac{\partial K}{\partial t} + \rho(\vec{v} \cdot \nabla)K = -\frac{\gamma - 1}{\rho^\gamma}\Im \ . \quad (5)$$

$$\frac{\partial \vec{v}}{\partial t} + (\vec{v} \cdot \nabla)\vec{v} = -\frac{1}{\rho}\nabla P - \vec{F}, \quad (6)$$

where ρ is the density, $\vec{v}$ the velocity, P pressure, and the $\Im$ the energy loss function which comprises all nonadiabatic sources and sinks of energy.

In SPH (Lucy, 1977; Gingold & Monaghan, 1977), these equations of motion are solved using Lagrangian formulation in which the gas is partitioned into fluid elements. A subset of these fluid elements are selected and represented by particles. In SPH these subset is chosen so that the particle mass density is proportional to the fluid density, ρ. This means that ρ can be estimated from the local density of particles at later times if the system is updated according to the equations of hydrodynamics.

Since the number of particles is finite, it is necessary to introduce a "smoothing"procedure to interpolate between them to represent the fields as continuous quantities. If each particle has a mass m_j then the SPH-smoothed density is given by

$$\rho(\vec{r}) = \sum_{i=1}^{N} m_i W(|\vec{r} - \vec{r}_i|, h), \quad (7)$$

where h_i is the smoothing length, and $W(r, h)$ is the smoothing kernel which satisfies the following conditions:

$$\int W(r - r', h)dr' = 1, \quad (8)$$

$$\lim_{h \to 0} W(r - r', h) = \delta(r - r'). \quad (9)$$

The calculations presented here were performed using the Gaussian kernel

$$W(r, h) = \frac{\exp(-r^2/h^2)}{\pi^{3/2} h^3}, \quad (10)$$

In the implementation used here the components of a binary system have their own fixed smoothing length. The primary component is described by N_p particles with smoothing length h_p and mass $m_p = M_1/N_p$. The secondary component is described by N_s particles with smoothing length h_s and mass $m_s = M_2/N_s$, $N_s = N - N_p$, where N is the total number of particles. For this case the SPH form of the equation (7)

$$is\rho_i = \sum_{j=1}^{N} m_j W_{ij}, \tag{11}$$

$$W_{ij} = W(r_{ij}, h_i)/2 + W(r_{ij}, h_j)/2 \tag{12}$$

where ρ_i is the smoothing density at the point $\vec{r}_i$, and $r_{ij} = |\vec{r}_i - \vec{r}_j|$.

SPH form of the equation (4) is the following

$$\frac{d\vec{v}_i}{dt} = -\sum_{j=1}^{N} m_j \left(\frac{P_i}{\rho_i^2} + \frac{P_j}{\rho_j^2}\right) \cdot \nabla_i W_{ij} - \\ -G\sum_{j=1}^{N} \frac{M(r_{ij})}{r_{ij}^2}\frac{\vec{r}_{ij}}{r_{ij}} + \vec{a}_i^{visc} \tag{13}$$

$$M(r_{ij}) = 4\pi m_i \int_0^{r_{ij}} r^2 W(r,h) dr,$$

where G is the Newtonian gravitation coinstant. The second term in equation (13) is the gravitational forces, $\vec{a}_i^{visc}$ is the viscous forces. The standard artificial viscosity is employed (Monaghan, 1992):

$$\vec{a}_i^{visc} = \sum_{j=1}^{N} m_j \Pi_{ij} \nabla_i W_{ij}, \tag{14}$$

where

$$\Pi_{ij} = \frac{-\alpha\mu_{ij}c_{ij} - \beta\mu_{ij}^2}{\rho_{ij}} \tag{15}$$

$$\mu_{ij} = \begin{cases} \dfrac{\vec{v}_{ij}\cdot\vec{r}_{ij}}{h(r_{ij}^2/h^2 + \eta^2)}, & \vec{v}_{ij}\cdot\vec{r}_{ij} < 0 \\ 0, & \vec{v}_{ij}\cdot\vec{r}_{ij} \geq 0 \end{cases} \tag{16}$$

and $\vec{v}_{ij} = \vec{v}_i - \vec{v}_j$,$\vec{r}_{ij} = \vec{r}_i - \vec{r}_j$, $c_{ij} = c_i - c_j$ is the average speed of sound of particles i and j, $h_{ij} = (h_i + h_j)/2$, $\rho_{ij} = (\rho_i + \rho_j)/2$. The numerical simulation is performed with constant $\alpha = 0.5$, $\beta = 1$, $\eta = 0.001$.

Ignoring any sources of entropy other than artificial viscosity, the smoothed equation (5) for the entropy function K is

$$\frac{dK_i}{dt} = \frac{\gamma - 1}{2\rho_i^{\gamma-1}} \sum_{j=1}^{N} \Pi_{ij} m_j \vec{v}_{ij} \cdot \nabla_i W_{ij} \tag{17}$$

The solution of the equations (11), (13), (17) is determined by a choice of the initial conditions. We establish the initial conditions in such way that at the initial moment of time the binary components are in the state near the stationary equilibrium. The construction of such initial conditions can be divided into three steps:

- The first step is the construction of internal structure of each component as a star in the state of hydrostatic equilibrium.
- The second step is to take into account rotation of each component and tidal forces operating beetwen them.
- The last step is coordinate transformation and establishing of the initial speed of particles.

At the first step the models were constructed by laying particles down randomly and then solving equation (13) in the presence of frictional dumping to achieve a stationary equilibrium (Gingold and Monaghan, 1977).

At the second stage we take into account rotation and tidal forces. For each binary component the tidal forces were estimated considering another companion as a point mass.

At the last step we make transformation of coordinates. For the primary component this transformation of coordinates can be written as follows':

$$\vec{r}_i = \vec{r}_i + \vec{r}_{cm_1}\ ,\ \vec{v}_i = \vec{\Omega}\times\vec{r}_i\ ,\ i = 1...N_p, \tag{18}$$

and for the secondary one:

$$\vec{r}_i = \vec{r}_i + \vec{r}_{cm_2}\ ,\ \vec{v}_i = \vec{\Omega}\times\vec{r}_i\ ,\ i = N_p + 1...N, \tag{19}$$

where $\vec{r}_{cm_1}$ is the primary component's center of mass, $\vec{r}_{cm_2}$ is the secondary component's center of mass. The initial angular velocity $\vec{\Omega}$ was set in units of the Keplerian angular velocity $\vec{\Omega}_K$:

$$\vec{\Omega} = k_\Omega \vec{\Omega}_K, \quad |\vec{\Omega}_K| = \sqrt{\frac{GM}{A^3}} \tag{20}$$

were A is the orbital separation, $M = M_1 + M_2$. In close binaries, the tidal distortion of a star by its companion gives rise to a perturbation of the external gravitational field which in turn causes a secular motion of the line of the apses (Stern, 1939):

$$\frac{d\omega}{dt} = \left(\frac{R_1}{A}\right)^5 \Omega_K q k_2 15(1-e^2)^{-5}\left(1 + \frac{3e^2}{2} + \frac{e^4}{8}\right) \tag{21}$$

where $q = M_2/M_1$ is the mass ratio, e is the orbital eccentricity, ω is the longitude of the periastron. The apsidal-motion constant k_2 depends on the internal structure of the star and measures the extent to which mass is concentrated towards the stellar center. For the preMS stars along their vertical part of the evolutionary track the apsidal-motion constant is typically of the order of $10^{-1} - 10^{-2}$. For systems with circular orbits this means that the angular velocity higher than

the Keplerian angular velocity (i.e. $k_\Omega > 1$). To estimate parameter k_Ω one can use the following formula

$$k_\Omega = 1 + \frac{0.22q^{7.71}}{32.13q^{7.46} + \ln(1+q^{6.48})}. \qquad (22)$$

This formula is correct in case if the orbital eccetntriciry is zero, the primary component fill its Roche lobe, the secondary component is point mass and the ratio of specific heats γ equals to 5/3.

4. Results

Models were created by a method described above with component masses in the range from $0.575M_\odot$ to $1.175M_\odot$, with the parameter k_Ω in the range from 0.95 to 1.01. The mass of the binary system equals to $1.75M_\odot$ and the initial orbital separation equals to $12R_\odot$ for all the models. For the description of each component 3000 points were used. Models were divided into two groups.

The initial stellar radii of the models of group "B"obey the law (2). For these models

$$\frac{R_1}{R_1^e} > \frac{R_2}{R_2^e}, \qquad (23)$$

where R_1^e and R_2^e are the Roche lobe equivalent radii of the primary (more massive) and secondary component, R_1 and R_2 are the equivalent radii of the primary and secondary component respectively. The Roche lobe equivalent radius is the radius of the sphere having the volume which is equal to the Roche lobe volume. The component equivalent radius is the radius of the sphere having the volume which is equal to the component volume.

The initial stellar radii of the models group "A"do not obey the law (2). For these models:

$$\frac{R_1}{R_1^e} < \frac{R_2}{R_2^e}, \qquad (24)$$

and R_2/R_2^e for the group "A"is equal to R_1/R_1^e for the group "B". Stellar radii quickly decrease according to the Eq. (1). More massive stars collapse faster. Thus, there can be a situation at which less massive component of the binary system can be closer to fill its Roche lobe, than the more massive component. For all the models initial stellar radii are smaller than the corresponding Roche lobe:

$$\frac{R_1}{R_1^e} < 1, \qquad \frac{R_2}{R_2^e} < 1. \qquad (25)$$

Twenty models were created for each group.

Group "A ". For these models the result of mass transfer depends upon initial angular velocity of the system. The range of value k_Ω, where mass transfer exists, is narrower for the mass ratio close to unit. Let us consider this on an example of one model.

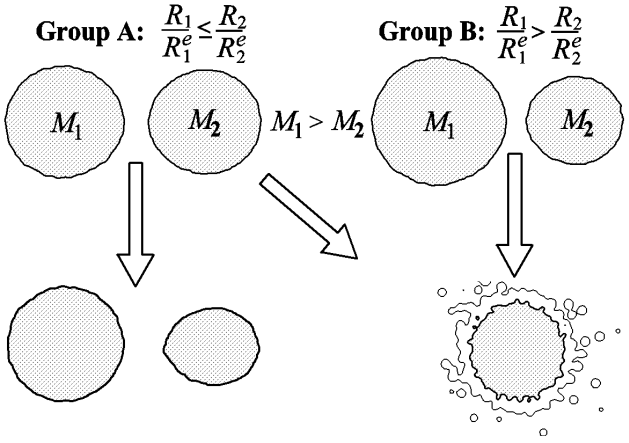

Figure 3: Flowchart of the mass transfer for the preMS close binaries. Letters "A"and "B"corresponds to the groups of the models.

Initial density distribution for the model with initial parameters $M_1 = 1.075$, $R_1 = 4.81$, $R_1/R_1^e = 0.95$, $M_2 = 0.685$, $R_2 = 3.96$, $R_2/R_2^e = 0.97$ are presented in Fig. (4a), (4d). Initial period of this system is 3.63 days and initial mass ratio $q = M_2/M_1$ is 0.63. In the range of values of k_Ω from 0.95 to 1.005, the orbital separation decreases as a result of kinetic energy dumping on nonequilibrium tides. Less massive component begins to overflow its Roche lobe, and mass transfer begins (see Fig. (4b), (4e)) correspondenly. Orbital separation increases as a result of mass transfer, and mass transfer respectively finishes. Final mass ratio and orbital separation depend upon initial parameters, but orbital separation increases and mass ratio decreases for any initial parameters for which mass transfer in this group exists. For example, in case of the value $k_\Omega = 0.97$ the final value of orbital separation is $16R_\odot$ and value of the mass ratio is 0.17. For the value $k_\Omega = 1$ the final value of orbital separation is $14.5R_\odot$ and the value of the mass ratio is 0.28 (see Fig. (4c), (4f)). The components merge which the value $k_\Omega < 0.95$.

Group "B ". If the mass transfer began, the models of this group merge always. For model with initial parameters $M_1 = 1.075$, $R_1 = 4.93$, $R_1/R_1^e = 0.97$, $M_2 = 0.675$, $R_2 = 3.87$, $R_2/R_2^e = 0.95$ initial density distribution presented in Fig. (5a), (5d). This model differs from the previous one onnly on the components radii. And this difference is small, but for this model if there is a mass transfer then components merge always.

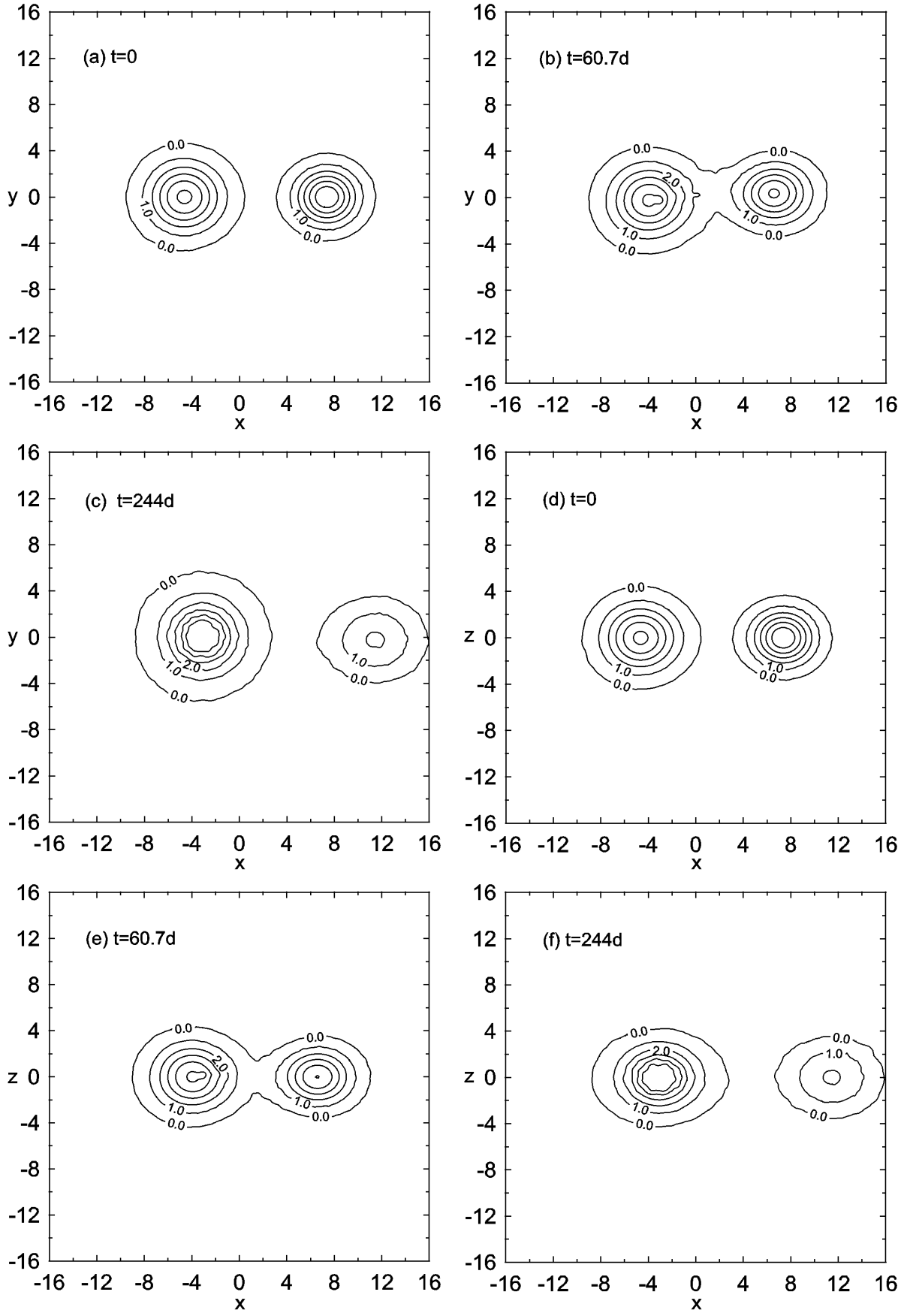

Figure 4: Model A. The density contours in the orbital plane (a,b,c), and in the XOZ plane(d,e,f) for the moments of time labeled. $M_1 = 1.075$, $R_1 = 4.81$, $R_1/R_1^e = 0.95$, $M_2 = 0.685$, $R_2 = 3.96$, $R_2/R_2^e = 0.97$, $k_\Omega = 1$, $M_2/M_1 = 0.615$. Distances are given in terms of $R_\odot$. Density is given in terms of $3\pi(M_1/R_1^3+M_2/R_2^3)/8$

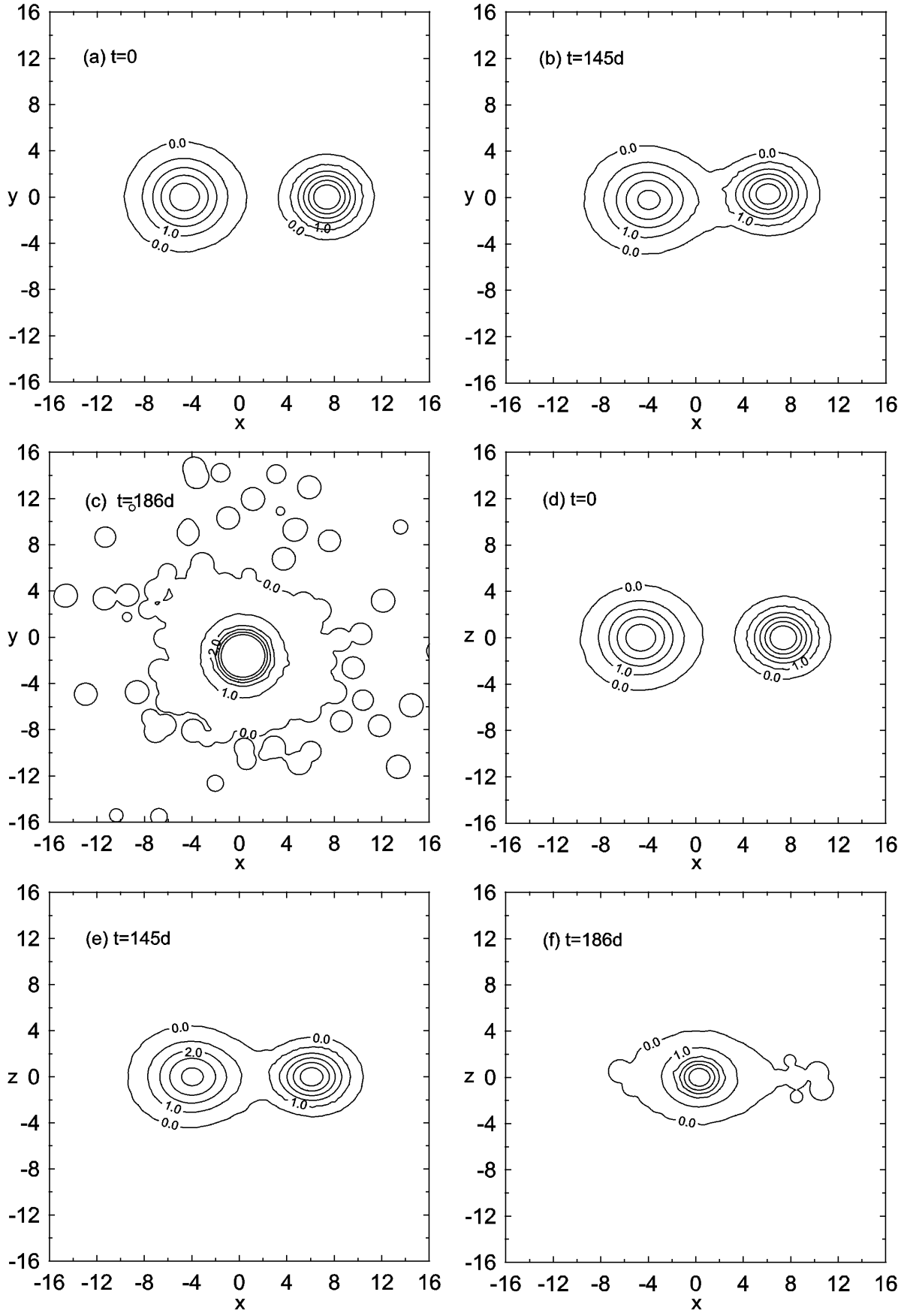

Figure 5: Model B. The density contours in the orbital plane (a,b,c), and in the XOZ plane (d,e,f) for the moments of time labeled. $M_1 = 1.075$, $R_1 = 4.93$, $R_1/R_1^e = 0.97$, $M_2 = 0.675$, $R_2 = 3.87$, $R_2/R_2^e = 0.95$, $k_\Omega = 1$, $M_2/M_1 = 0.615$. Distances are given in terms of $R_\odot$. Density is given in terms of $3\pi(M_1/R_1^3 + M_2/R_2^3)/8$

5. Conclusion

- In the case if the more massive component is closer to fill its Roche lobe, the components merge always.
- In the case if the less massive component closer to fill its Roche lobe, the mass transfer can occur in a dynamic time scale.
- The orbital separation increases, and the mass ratio decreases as a result of the mass transfer.
- Probability of existence of preMS close binary systems with the less massive component which closer to the filling its Roche lobe higher, than systems where the more massive component closer to fill its Roche lobe.
- The number of the preMS close binary systems should decrease for the mass ratio close to unit.

The basic conclusions are correct for other part evolutionary track, for which the assumption about fully convective stellar interior is correct.

References

Iben I.: 1965, *Ap. J.*, **141**, 993.
Gingold R.A., Monaghan J.J.: 1977, *MNRAS*, **181**, 375-389.
Grossman A.N. and Graboske H.C.: 1971, *Ap. J.*, **164**, 475.
Lucy L.B.: 1977, *Astron. J.*, **82**, 1013.
Monaghan J.J.: 1992, *Annu. Rev. Astron. Astrophys.*, **30**, 543-74.
Stahler S.W.: 1983, *Ap. J.*, **274**, 822.
Stahler S.W.: 1988, *Ap. J.*, **332**, 804-825.
Stern T.E.: 1939, *MNRAS*, **99**, 451.

THE WAVE PRINCIPLE OF THE DISTRIBUTION OF SUBSTANCE IN SOLAR SYSTEM

V.A. Smirnov

Academy of Communication of Ukraine, *smirnovw@tm.odessa.ua*

ABSTRACT. The wave principle of planet system formation and systems of satellites of Jupiter, Saturn and Uranus in Solar system is considered.

The opinion about the wave nature of substance' distribution in Solar system comes out of fundamental book of J.Kepler "Welt Harmonik" (Kepler, 1939; Smirnov & Shvets, 1987). In this book by J.Kepler the musical proportions are united with geometrical means of building Plato's inscribed and described figures. From this construction of geometrical figures in the scales of Solar system J.Kepler receives the method of the detecting of the distances of planets from Sun, when the orbits of planets are equal with geometrical figure built accordingly inscribed or described around another.

The definition of the planets' orbits according to the constructed "Plato' figures" is geometrically possible in case of existence of common measure for these geometrical constructions, how λ – the length of wave.

Proportions, received by J.Kepler, are possible in the case of formations of standing waves in the space of Solar system, when the place of the formation of planets conforms the main surfaces of standing waves having as the source the central luminary of Solar system. Similarly in experiments of Chladni, during the formation of standing wave on the planes of fluctuating plate scattered along its particles are collecting together, getting from points which fluctuate with maximal amplitude, to the points, the amplitude of fluctuations of which is equal to zero, filling in the main lines (Smirnov, 1999a).

If we will consider the Central luminary of the planet' system or their satellites as a source of "gravitational waves" which are reflected from the environment with less density on the borders of system in the period of its initial evolution then the standing wave with crests and nodes in definite points along the direction of its distribution.

If we would mark the co-ordinate, along which the wave through r will form, then, for one-dimension standing wave the co-ordinates of main points correspond to points defined from the condition:

$$Y = \frac{2n+1}{4} \cdot \lambda,$$

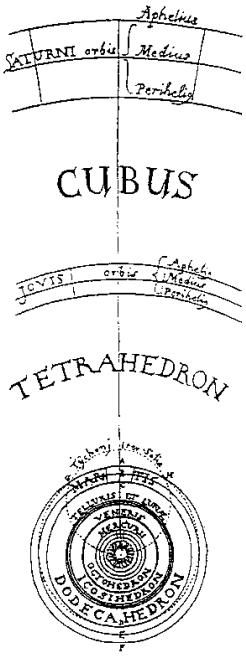

Figure 1: Planet orbit construction according to J.Kepler from book "Harmony of Universe"

Table 1:

Satellite Of Jupiter	True distance from Jupiter 10^3 km	Calculated distance 10^3 km from Jupiter
5	181	
Io	422	$181+\lambda=422$
Europa	671	$181+2\lambda=661$
Ganymede	1070	$181+4\lambda=1141$
Callisto	1883	$181+7\lambda=1861$
6	11476	$181+47\lambda=11461$
10	11700	$181+48\lambda=11701$
7	11737	$181+48\lambda=11701$
12	21200	$181+88\lambda=21301$
11	22600	$181+93\lambda=22501$
8	23500	$181+97\lambda=23461$
9	23600	$181+98\lambda=23701$

Table 2:

Saturn' satellite	The true distance from Saturn 10^3 km	Calculated distance 10^3 km from Saturn
Janus	159	159
Mimas	186	$159+\lambda=186$
Enceladus	238	$159+3\lambda=240$
Tethys	295	$159+5\lambda=294$
Dione	377	$159+8\lambda=375$
Rhea	527	$159+14\lambda=537$
Titan	1222	$159+39\lambda=1212$
Hyperion	1483	$159+49\lambda=1482$
Iapetus	3560	$159+126\lambda=3561$
Phoebe	12950	$159+474\lambda=12957$

In this formula n - whole numerals 0, 1, 2,... In such condition for the length of gravitational wave we receive significance 0.52 AU (Smirnov, 1999b).

Presuming the length of standing wave equal $\lambda = 240 \cdot 10^3$ km for the system of satellites of Jupiter we can receive the result, similar to the following information (Table 1).

If we will admit as the "common measure" the length of characteristical standing wave for Saturn $\lambda = 27 \cdot 10^3$ km, then the distances of the Saturn' system of satellites display the same wave regularity (Table 2).

If we will admit the effective length of wave for the system of Uranus' satellites equal to $\lambda = 62 \cdot 10^3$ km then we can receive the picture of the nodes of standing wave, in which these satellites were formed.

References

Kepler J.: 1939, *Welt-Harmonik*, Munchen-Berlin, 403.

Smirnov V.A.: 1999a, *Astronomical and Astrophysical Transaction*, **18**, 521–532.

Smirnov V.A., Shvets V.A.: 1987, *Music Theory Question in Johannes Kepler's "Harmony of the World"*, DEP. N1029-B87, Odessa.

Smirnov V.A.: 1999b, in: *Proceedings of Gamow Memorial International Conference "The Universe of Gamow: Original Ideas in Astrophysics and Cosmology", Odessa*, 31.

RADIATION OF SPECTRA OF METEOR

V.A. Smirnov

Academy of Communication of Ukraine, *smirnovw@tm.odessa.ua*

ABSTRACT. The characteristics of meteor's, flares by the mechanism cascade radiation are investigated.

1. History of an issue

The first period of researches of meteor's spectra was a period of visual observations by A.S. Herschel before receiving the first spectrograms, achieved by S.N. Blajko in 1904 and 1907 (Smirnov, 1994). The results of meteoric spectra studies within the second period has been examined in the early 60 *s* by P. Millman (1906-1990) in his work "The General Survey of Meteor Spectra". Peter Millman, originally from missionary's family, took after his parents the "mission" – the organization of spectral meteor's researches development in various countries. Besides his regularly publishing of the lists of meteor's spectrograms made all over the world, he also dispatched his works to many young researchers and was actually their teacher. (For example, published in 1962 work in Odessa University, volume 152, page 55 – 60, by Vladimir A. Smirnov "Photometry of two spectra of meteors using a method of A. Cook and P. Millman"). Appeared, that the spectrum of a meteor is not only a function of a chemical structure, but also of velocity, or rather, reserve of meteoroids kinetic energy. It was visible from the fact that the spectrum of high-speed streams of Perseids, Orionids, Leonids belonged to an Y-type. The meteors of low-speed streams – Geminis and Giacobinid – belonged to an X-type. Also appeared, that the lines more than 120 multiplet's of the iron, on 10 multiplet's of the ionized iron each, magnesium, calcium, oxygen were identified, bands of molecular and line of the ionized nitrogen. A significant abundance of the spectral lines have given the sodium, chromium, manganese, nickel, cobalt, carbon, lithium, barium, strontium, hydrogen and also ions of magnesium, oxygen, silicon, and aluminum. More than 10 head cants of band's FeO, MgO, CaO, CN, C_2, CO, CH, CO^+ etc. The application of methods of star photometrics and spectrophotometrics to the meteoric spectra and especially photographic traces in integrated light was burdened by a plenty of regular errors. This was considered in details in the book of an author (Smirnov, 1994) of the star image of the same brightness. The same concerns also to the receiving of spectra, when any "spectral line" represents monochrome image of a meteor, as the meteor spectrograph work in a mode of expectation of a meteor flight and fix a meteor in all his volume. Spectrophotometrical analysis of a spectrogram, made by *A.* Cook and P. Millman (1955) does not raise an objection: by them the densities of radiating atoms and ions were determined as a result of absolute spectrophometry of the monochrome images in a state of "spectral bands" and "lines". However, the usage of a method of growth curve construction, and defining the self-absorption in volume of meteor's radiation by means of photometric profiles of the same imaginary "lines", is not correct.

2. The physical theory of meteors in historical aspect

The determination of the equations solutions of meteor physics clearly requires the separation according to the spatio-temporal principle (Smirnov, 1994; 1997; 2000; 2001). Otherwise one runs into contradictions upon interpreting of the actual conservation laws for the task of following the evolution of the meteor phenomenon in space and time. If dt the time interval, where $S(t)$ – cross-section of meteoroid, $\rho(H)$ is the atmospheric density at altitude H, and $v(t)$ is the velocity of the meteoroid with mass $m_{\downarrow}$, Γ is the coefficient of resistance, characterizing the momentum transfer to the atmospheric particles passing the meteoroid , then, the "equation of braking " of the physical theory of meteors is represented by the following formula:

$$m_{\downarrow}\frac{d\nu}{dt} = -\Gamma S\rho\nu^2 \qquad (1)$$

In the last equation all the parameters except the empirically determined velocity and accelerations, are unknown. Also the laws of the evolution of these parameters with gradual penetration of the meteor into more dense layers of the atmosphere are unknown. Apart from this, the meteoroid mass mv is supposed to be independent from the time t in disagreement with any model of the evolution of the meteor phenomenon. Equation (4) was used again for the determination of the "dynamic masses" of meteors (Bronshten, 1981).

However, V.A.Bronshten noted in his studies that the value of the velocity being dependent on the time serves for the determination of the momentary significance of the meteoroid mass. In other words, it will admit the application of equation (1) for the case of a stationary ("momentary") meteor mass. Obviously, the application of the "equation of braking" of the meteor stipulates a stationary "dynamical" mass. Analogously, the application of the equation below of mass loss stipulates the condition of a stationary velocity V, which disagrees with the actual flight of the meteoroid. Here, the mass loss in turn defines the momentary significance of the velocity. In the third equation of physical theory – the "equation of emission" photometric data deliver the observed intensity I of meteor radiation being related with the loss of kinetic energy τW, where coefficient τ characterizes the conversion of kinetic energy of the meteoroid into radiation upon disintegration of the body by some $m(t)$. Meteor radiation emerges from the plasma generated as a consequence of the meteoroid's interaction with the atmosphere along its trajectory. The theory of meteor radiation is a physical theory of non-equilibrium, chemically active plasma. One cannot solve equation for the intensity I in integral light uniquely for the evolution of the meteor phenomenon. For every meteor, the coefficient t as well as its mass m are unknown as disintegration of each individual meteoroid. Therefore, the "photometric mass" generally differs from the "dynamical mass" obtained from (1). The absolute spectrophotometry of meteors allows determining the intensity of such monochromatic images in absolute units for every moment of the flight of the meteor. If we neglect induced emission and self-absorption in these lines, the radiation intensity emitted in a certain moment and in a unit volume of particles is determined by the total exposure of the film

$$I_{ik} = N_i A_{ik} h\nu_{ik}, \tag{2}$$

where N is a concentration of radiating particles, A_{ik} is the Einstein probability coefficient of the transition i, k, and $h\nu_{ik}$ is the energy of the quantum. (The astronomical application of (9) requires an additional factor of $1/(4\pi)$). Therefore, A.Cook and P.Millman (1955) used spectral line intensities determined in absolute units for the determination of the number of radiating atoms in the meteor spectrum. The intensity of monochrome radiation of the meteor image can be described by the sum

$$I_{ik} = I_{shock} + I_{casc}, \tag{3}$$

where I_{shock} is defined by the direct shocks of meteor plasma shock particles with electrons. I_{casc} is defined by cascaded transitions. Calculating the total power being radiated by the meteor it is needed to sum up the intensities at various wavelengths, in various time intervals, and of various area parts through which the radiation passes, in absolute units. In other words, the determination of the power P implies the calculation of the triple integral.

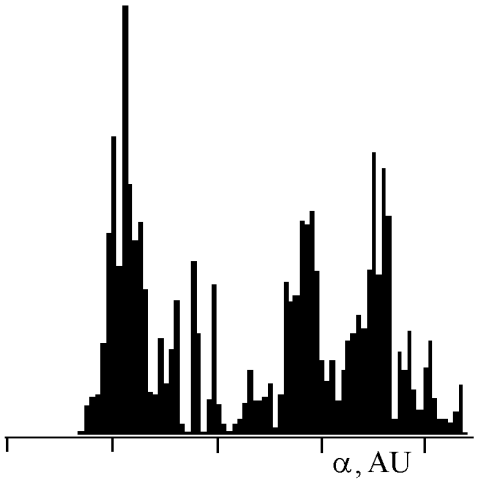

Figure 1: The distribution of the shower meteor orbits semi-major axis.

$$P = \int_{\lambda_1}^{\lambda_2} \int_{t_1}^{t_2} \int_{S} I d\lambda dt ds, \tag{4}$$

Practically, at the expense of averaging the meteor's monochromic radiation powers, the obtained intensities refer to wavelength intervals, time intervals, and an area chosen for the radiation model, for example, a sphere with 100 km radius. In this approach, we have to adopt that the radiation of spherically symmetric meteor emission takes place at 100 km distance from the camera lens. During the certain period of time t the concentration of particles in every point of the meteor path varies according to the law, described by the solution of kinetic equation (Biberman et al., 1982):

$$N(t) = N_e(t) \left(27.10^{-23} \frac{N_0^2}{T_0^{9/2}} t_0 \left[\left(\frac{t}{t_0} \right)^{0.4} - 1 \right] \right)^{1/2}, \tag{5}$$

where N_{e0}, N_0, t_0, T_0 initial values of electron concentration, of plasma particles concentration, of time and temperature.

3. Phenomenological description of meteor

The physical processes accompanying development of the meteor phenomenon proceed in various timescales. For example, frequently appearing double final flares in meteors of a Perseid's stream occur

within the time, which is smaller than 0,05 seconds. However, the transmission of energy for evaporation of 1 gram of meteoroid requires much more time. Thus can be explained the significant inertness in meteors movement and independence of light streams of meteor plasma from the mechanical changes in meteoroid's structure. On the early stage of expanding all the relaxation process in plasma occurs swiftly, and gas is considered to be in the thermodynamic equilibrium. Further on, at the lower temperature in expanding ionization and dissociation processes are retarded, more energy is being consumed. However, the velocities of inverse processes, recombination, in particular, depend on density, temperature, time. The events of ionization can be neglected in this case. The process is secured only due to the recombination and subsequent cascade transition. The meteor penetrates into the dense of atmosphere layers, the density of energy flux of interaction between it and atmosphere particles (they may be considered as immovable) increases and achieves its value and may lead to radiation similar to the "laser" scenario. The task – the mechanism of a characteristic double flare of a meteor stream.

References

Biberman L.M., Vorobjev V.S., Yakubov I.T.: 1982, *The Kinetics of Non-equilibrium Low-temperature Plasma*, Moscow: Science.

Bronshten V.A.: 1981, *The physics of meteor phenomena*, Moscow: Nauka, 416 p.

Cook A.F., Millman P.: 1955, *Ap. J.*, **121**, No 1, 250-270.

Smirnov V.A.: 1994, *The Spectra of Transient Atmospheric Luminous Phenomena: Meteors*, Moscow: Physico-Mathematical Literature.

Smirnov V.A.: 1997, *Planetary and Space Science*, **45**, 847-851.

Smirnov V.A.: 2000, *Proceeding IMC Frasso Sabino*, 47-58.

Smirnov V.A.: 2001, *Proceedings of the International Meteor Conference*, Pucioasa, Romania, 88-95.

SEARCHES OF THE PERIODS AND DEFINITION OF VARIABILITY TYPES OF NEW VARIABLE STARS TX CRV, DP CAM, IRAS 17583+5150

A.P. Solonovich, I.S. Bryukhanov, I.M. Sergey

Amateur group of variable stars observers "Betelgeuse",
the Republic Center of Technical Creativity of Pupils,
220023, Belarus, Minsk, Makaionak street, 12,
betelgeize_astro@mail.ru

ABSTRACT. Measurements of brightness of stars TX Crv, DP Cam, IRAS 17583+5150 opened in "IRAS" and "HIPPARCOS" experiments are carried out using negatives of the Odessa observatory. Proposed types of these stars: TX Crv – type ISB(?), DP Cam – type ISB, IRAS 17583+5150 – type SRB (SRC).

Key words: Variable Stars.

History of research

Analysis of photo-electric measurements series of "HIPPARCOS" experiment allow Roger W. Sinnott to inform in electronic version of magazine "Sky & Telescope" that new variable stars TX Crv and DP Cam are of EA type (Sinnott, 2000a; 2000b). The same assumption has stated also by Sergey E. Gur'yanov in the magazine "Zvezdochet" (2000). During the measurements of brightness of stars TX Crv, DP Cam using negatives of the Odessa observatory authors used identification cards and stars of comparison from magazines "Sky and Telescope" and "Zvezdochet". At the time of work with these stars Ivan S. Bryukhanov discovered optical variability of the star Tyc 2 3523 1519 1 or alternatively IRAS 17583+5150 or else IRC+50275 or HD 164645.

TX Crv

Eye estimations of Ivan S. Bryukhanov of brightness of the star TX Crv (HIPP 58579, spectrum G0) carried out using Neiland-Blazko method on 238 photographic plates, also 88 measurements of brightness of the star TX Crv based on "HIPPARCOS" experiment data were used in investigation. It was not revealed eclipses of the star on negatives of the Odessa observatory – amplitude of fluctuations of brightness of the star TX Crv – $8.0^m - 8.3^m$ in V rays within the range of errors.

According to "HIPPARCOS" experiment data (amplitude of fluctuations of brightness of the star TX Crv – $8.0^m - 9.5^m$ in V rays) 6 casual decreases of TX Crv shine were registered which can not be eclipses of TX Crv in any way:

2448217.1970 H. J. D.	8.922 in V rays
2448294.8591	9.334
2448622.4628	8.830
2448983.1108	9.548
2449014.4785	8.972
2449024.8111	9.150

As a result of search of the period using Lafler-Kinman method Ivan S. Bryukhanov was not established the period of fluctuations of brightness of the star. Authors assume that TX Crv either a constant star, or a variable star of ISB type.

Long and exact photo-electric and visual measurements of TX Crv shine are required for confirmation or refutations of changeability type.

DP Cam

Eye estimations of Ivan M. Sergey of brightness of the star DP Cam (HIPP 22498, spectrum 7) carried out using Neiland-Blazko method on 445 photographic plates, also 171 measurements of brightness of the star DP Cam based on "HIPPARCOS" experiment data were used in investigation. Ivan M. Sergey was not revealed eclipses of the star on negatives of the Odessa observatory – amplitude of chaotic fluctuations of brightness of the star DP Cam – $10.0^m - 10.9^m$ in V rays.

According to "HIPPARCOS" experiment data (am-

plitude of fluctuations of brightness of the star DP Cam – $9.9^m - 11.6^m$ in V rays) 2 casual decreases of DP Cam shine were registered which can not be eclipses of TX Crv in any way:

2448018.7527 H. J. D.	11.642 in V rays
2448180.9388	11.005

As a result of search of the period using Lafler-Kinman method Ivan S. Bryukhanov was not established the period of fluctuations of brightness of the star. Authors assume that DP Cam is a variable star of ISB type. Fast sinusoidal or chaotic changes of DP Cam shine are appreciable (Fig. 1, 2, 3).

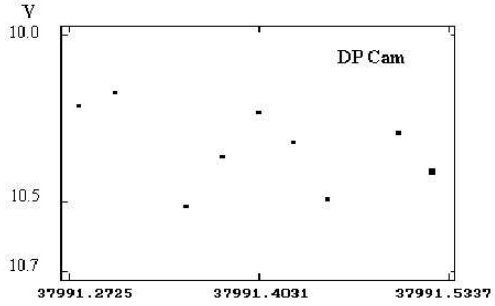

Figure 1: 2437991 J.D. The Odessa photograph collection

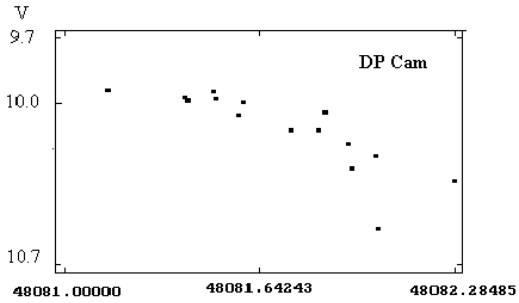

Figure 2: "HIPPARCOS" 2448081-2448082

Long and exact photo-electric and visual measurements of DP Cam shine are required for confirmation or refutation of variability type.

IRAS 17583+5150

Ivan S. Bryukhanov has opened optical variability of the star Tyc 2 3523 1519 1 (or alternatively IRAS 17583+5150 or else IRC+50275 or HD 164645) (spectrum Mc) on negatives of the Odessa observatory. Measurements were carried out only on negatives of the Odessa observatory where the maximal amplitude of

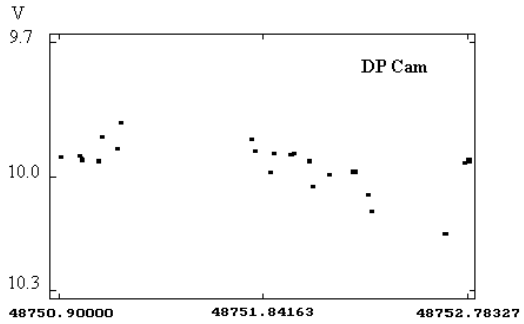

Figure 3: "HIPPARCOS" 2448750-2448752

fluctuations of shine of the star – $7.4^m - 8.9^m$ in V rays. Map and stars of comparison in a visual range for IRAS 17583+5150 (Fig. 4):

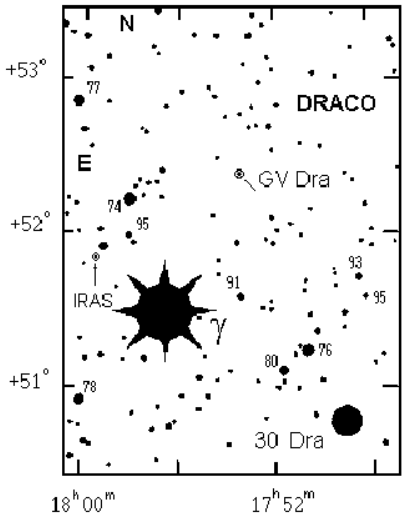

Figure 4: Map and stars of comparison IRAS 17583+5150 and GV Dra (Sinnott, 2000a; 2000b)

Eye estimations of Ivan S. Bryukhanov of brightness of the star IRAS 17583+5150 carried out using Neiland-Blazko method on 567 photographic plates. Search of period or cycles of fluctuations of star's shine was carried out by Ivan S. Bryukhanov using Lafler-Kinman method.

Series of measurements of star's shine are divided by the author into 3 intervals: early observations from 2436432 to 2441898 JD, amplitude of fluctuations from 8.1^m up to 8.9^m magnitude; observations from 2442243 to 2448184 JD, amplitude of fluctuations from 7.4^m up to 8.7^m magnitude; late observations from 2448391 to 2449221 JD, amplitude of fluctuations from 7.9^m up to 8.7^m.

Early observations show cycles 3386, 3320, 406.5(?) and 58.8 days. Observations from 2442243 to 2448184 JD with the big amplitude show cycles 56.2, 388(?),

48.7 days, 1497–1500 days. Late observations show cycles only 11 and 17 days. Fluctuations of star's shine in this period are produce chaotic effect most likely because of small quantity of measurements – only 28 points.

3 best diagrams of shine fluctuations of star IRAS 17583+5150 in V rays (figures 5, 6, 7) are given below:

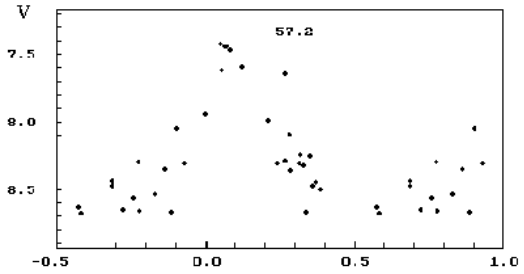

Figure 5: IRAS 17583+5150 2441573-2445879 J.D.

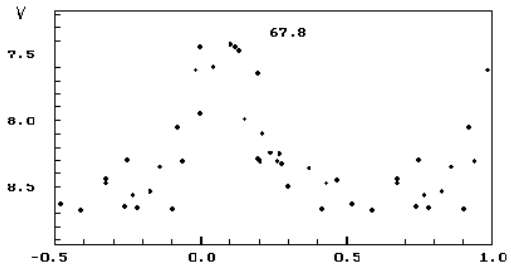

Figure 6: IRAS 17583+5150 2441573-2445879 J.D.

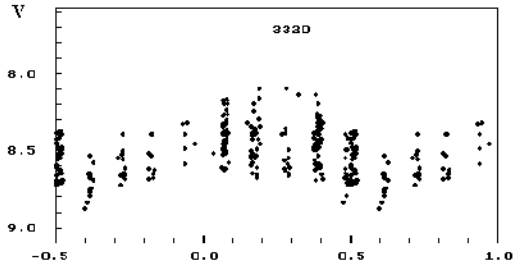

Figure 7: IRAS 17583+5150 2346432-2441898 J.D.

Acknowledgements. We are thankful to Samus Nikolai Nikolaevich and Hryshel Maksim Aleksandrovich for consultations and help in work.

References

Gur'yanov S.E.: 2000, *Zvezdochet*, **4**.
Lafler J., Kinman T.D.: 1965, *Ap. J. Suppl.*, **11**, 216.
Sinnott R.W.: 2000a, *http://skyandtelescope.com/observing/objects/variablestars/article_291_1.asp.*
Sinnott R.W.: 2000b, *http://skyandtelescope.com/observing/objects/variablestars/article_292_1.asp.*

SOME RESULTS OF THE PHOTOMETRY OF GEO OBJECTS

P.P. Sukhov[1], A.I. Movchan[1], N.I. Koshkin[1], L.V. Korniychuk[1], S.L. Strakhova[1], V.P. Epishev[2]

[1] Department of Astronomy, Odessa National University
T.G.Shevchenko Park Odessa 65014 Ukraine,
deepsky@tecom.odessa.ua, astro@paco.odessa.ua

[2] Laboratory of Space Researches, Physical Department, Uzhgorod National University,
St. Dalcka 2, Uzhgorod 88000 Ukraine, *space@univ.uzhgorod.ua*

ABSTRACT. Odessa Astronomical Observatory participated in the photometric observations of the GEO objects from June to September 2004. The photometric observations of the GEO objects were carried out at Observatory Station in Mayaky. For the observations 50 cm telescope Cassegrain was used. During the observations 7 light curves was obtained.

Key words: geostationary orbit (GEO), GEO objects, light curve.

The large number of artificial GEO objects and risk of its collision are needed the regular monitoring of Near Earth Space (Konovalenko at al., 2003). At June-September 2004 in Odessa Astronomical Observatory, simultaneously with positional observations, the photometric observations of the some GEO objects were organized. The ephemerides were given by MAO Academy of Science of Russia (Pulkovo). The photometric observations were obtained at the 50 cm Cassegrain telescope, in its focus is located electrophotometer with receiver of the radiation FEU-79. The optic-mechanical block and broadband amplifier are designed by A.I.Movchan. During the observations 7 light curves of such GEO objects: 98029, 95035, 95099, Cosmos-X was received. The observed data are given in the table 1.

The photometric light curves are presented on fig. 1-8. Besides integral light the observations were obtained in filters B and V. The analysis of given results and searching of the period were made by means of software package, including Fourier-analysis. The obtained periods of change of the brightness are given in the table. Figure 1 shows the changes of the brightness of GEO object 98029. They were got 21.06.04 during nearly hour. The brightness of GEO object, after the calculation of the absorption in atmosphere and adductions to one distance, is 8.2 magnitude and shows the small variations with typical time around 22.0 minutes, that is possible caused by precession of axis rotation. The fragment of the light curve GEO object 95035 is given on fig. 2, it shows the change of the brightness with period of 1.06 sec. In different dates GEO object 95099 reveals such periods: P_0 = 32.87 sec (28.07.04), P_0 = 32.61 sec (16.08.04), P_0 = 32.22 sec (14.09.04). The value P_0 = 97.5 sec (28.07.04) and P_0 = 98.0 sec (16.08.04) is, possibly, the value of the precession rotation period of the satellite. This is seen from presented fragment of the light curve on fig. 5. As to object "Cosmos-X", the observed change of the brightness, in our view, is not caused by proper rotation of the object, but periodic moving of the solar battery panels for Sun. The calculation of orientation of panels, which reflect light as a mirror, for to mirror flashes from curves of change of the brightness GEO object "Cosmos - X" for 12.09.04 shows that its movement occurred, practically, in plane of the ecliptic. So, direction of normal in the event of the first flash – α = 176.96°, δ = 4.94°, the second – α = 179.22°, δ = 4.96°. The absence of the mirror flash 14.09.04 is explained simply. An observation of the satellite began well later, than 12.09.04. And orientation for forming the mirror flash became unfavourable. The first maximum on this light curve under the conditions of luminosity corresponds for the third maximum on the light curve for 12.09.04. The change of the brightness superposing on mirror flashes with the period 44-47 sec is caused probably by hit mirror "bunny", which moves on panels of the solar battery, on gaps between separate sections of battery. More exactly estimation is possible in the case of colourimetric observations of this GEO object. The orientation of the panels of the last GEO object is fairly well saved relatively to Sun, though it slowly ($\sim$ 1.2 degree overnight) moves on orbit. During the first flash the angle of inclination of the panels to Sun was 6.5°, during the second one 8.7°. The minimum inclination of the panels to Sun was $\sim$ 5.0°. This is a classical inclination of the panels to Sun in active GEO object. It is known that positional observations allow to separate the objects on groups depending on character of the motion relative to the observer on surface of the Earth (Hernandez & Jehn, 2004). On the other hand the photometry of GEO objects allows to classify

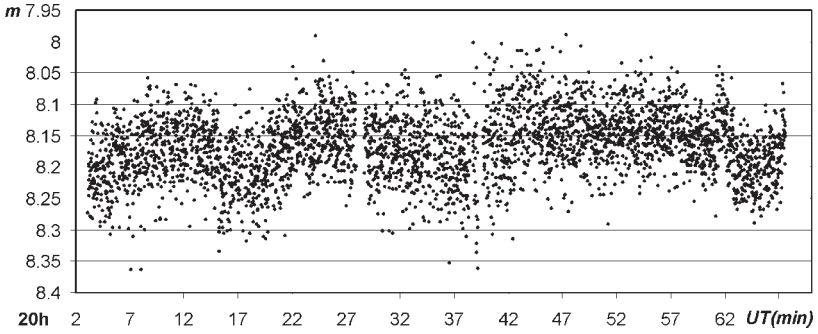

Fig. 1: CO 98029 21.06.04 $UT_o=20^h03^m05^s$ (integral light)

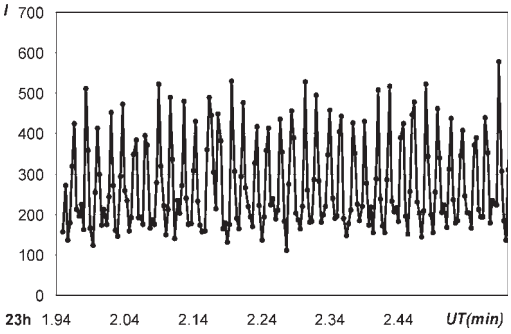

Fig. 2: CO 95035 20.07.04
$UT_o=23^h01^m56^s$ (V-filtr, fragment)

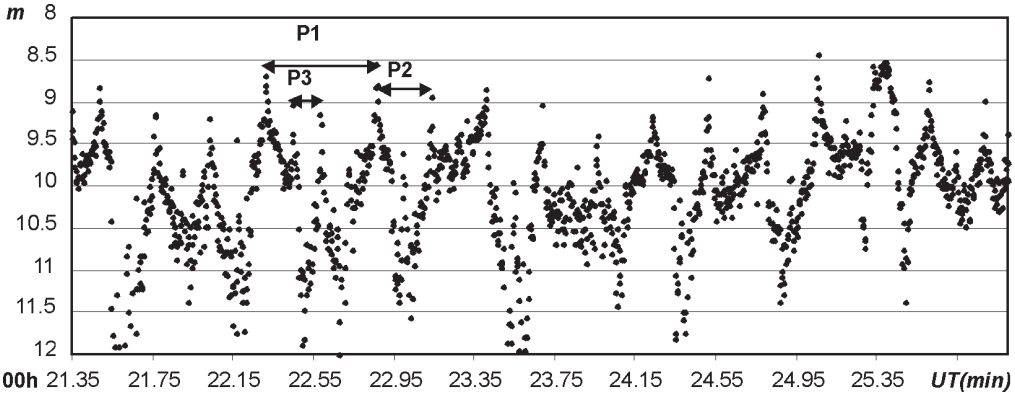

Fig. 3: CO 95099 28.07.04 $UT_o=00^h18^m02^s$ (integral light, fragment)

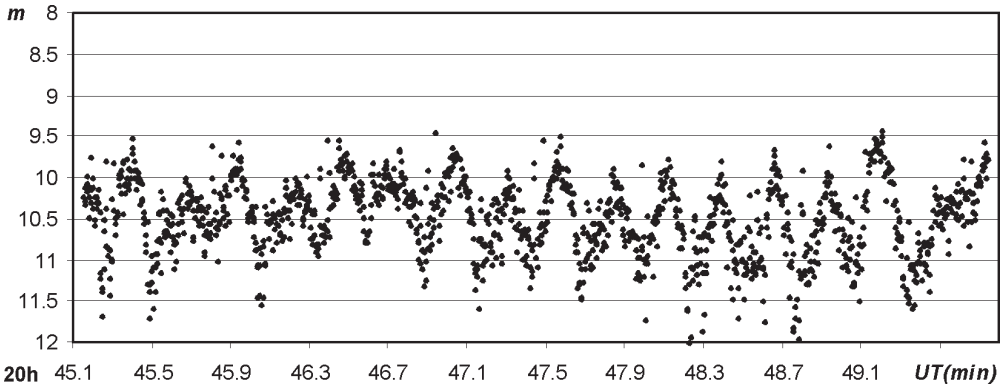

Fig. 4: CO 95099 16.08.04 $UT_o=20^h45^m09^s$ (integral light, fragment)

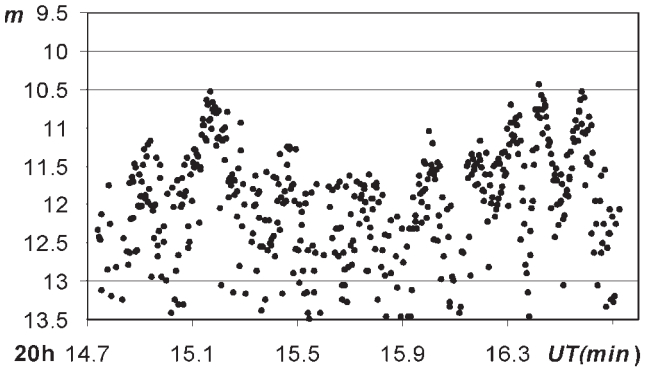

Fig. 5: CO 95099 16.08.04 $UT_o=20^h14^m07^s$
(B-filtr, fragment)

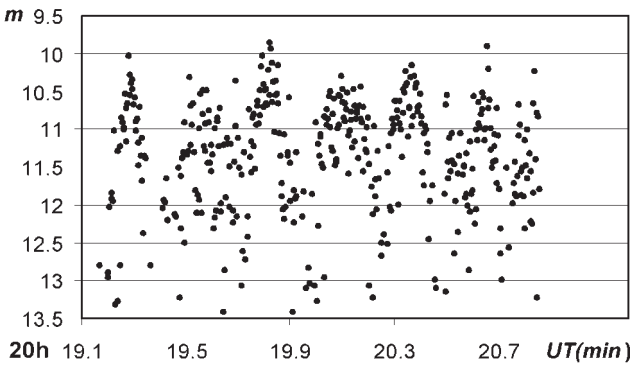

Fig. 6: CO 95099 16.08.04 $UT_o=20^h19^m17^s$
(V-filtr, fragment)

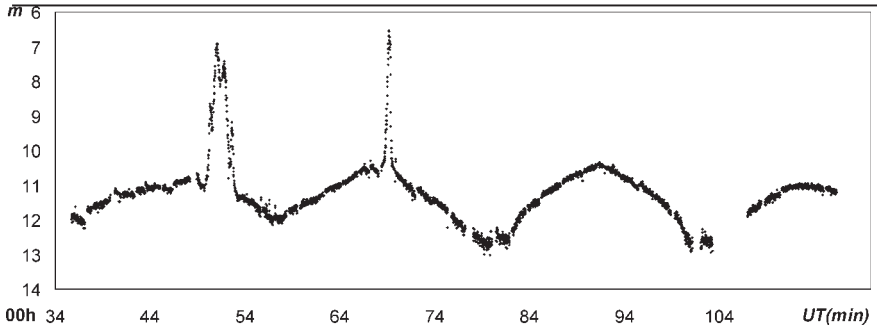

Fig. 7: CO Cosmos-X 12.09.04 $UT_o=00^h35^m42^s$

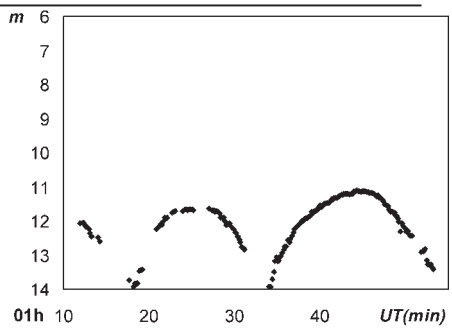

Fig. 8: CO Cosmos-X 14.09.04 $UT_o=01^h11^m56^s$

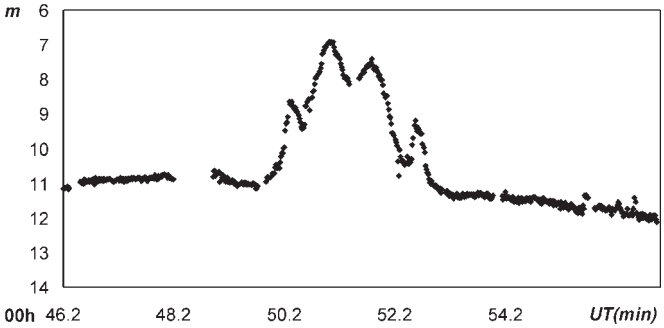

Fig. 7a: CO Cosmos-X 12.09.04 $UT_o=00^h35^m42^s$ (fragment1)

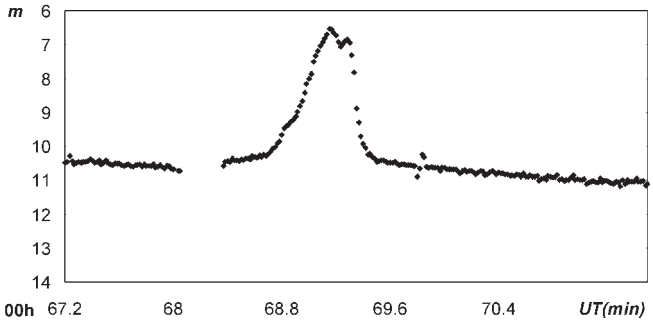

Fig. 7b: CO Cosmos-X 12.09.04 $UT_o=00^h35^m42^s$ (fragment2)

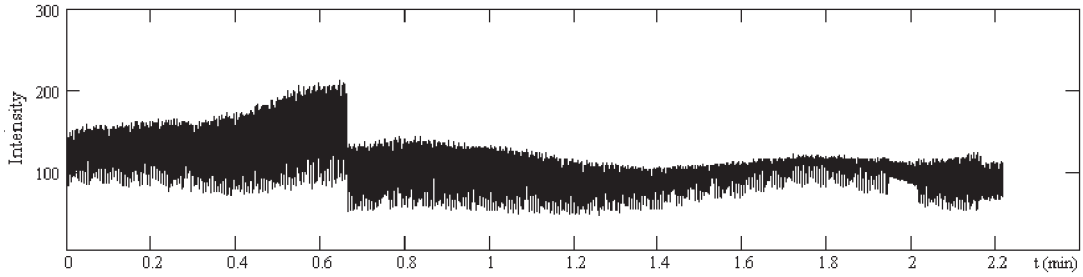

Fig. 9: The radar curves obtained for GEO object 98029 using Evpatoria RT-70=>Bear Lakes RT-64 bi-static system got by I.E.Molotov et al. 25.06.2004 on temporary interval of 2.2 minutes. Processing of the reflected radio signal was carried out in Radio-Physical Research Institute (N.Novgorod) by M.Nechaeva et al. Time to sampling radio signal – 0.016 sec. On short temporary interval period change to powers is not discovered.

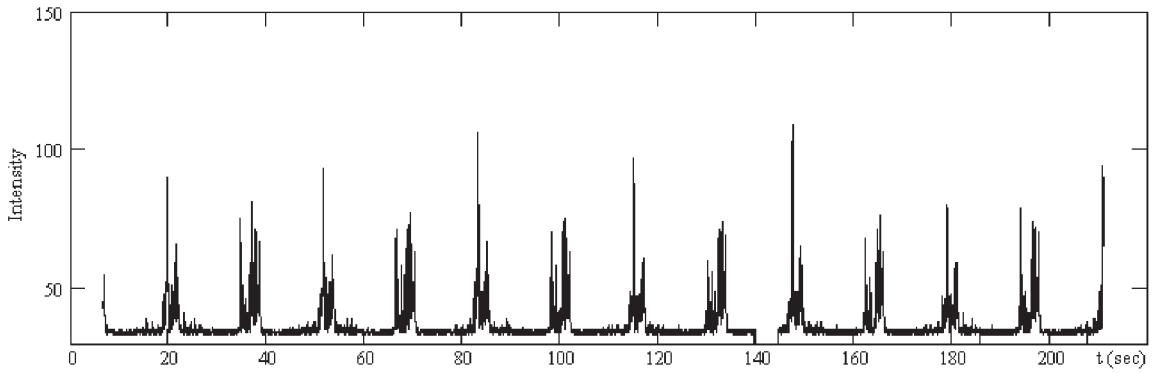

Fig. 10: The radar curves obtained for GEO object 95099 using Evpatoria RT-70=>Bear Lakes RT-64 bi-static system got by I.E.Molotov et al. 03.10.2004 on temporary interval of 3.5 minutes. Processing of the reflected radio signal was carried out in Radio-Physical Research Institute (N.Novgorod) by M.Nechaeva et al. Time to sampling radio signal – 0.016 sec. Period change of the power: P = 31.85 sec.

Table 1:

GEO objects	Date of observation	Time of observation	Longitude of the under-satellite point (deg)	Time of accumu-lation of signal (sec)	Spectral range of observa-tions	Duration of obser-vations (minutes)	Magnitude	Period of change of the brightness
98029	21.06.04	$20^h03^m05^s$	44.4E	1	Integral light	64.45	8.3^m-8.05^m	$\sim$ 22 min
95035	20.07.04	23 01 56	39E	0.2	Integral light, B, V	30.92	–	1.06sec, 0.53sec, 0.27sec
95099	28.07.04	00 18 02	42E	0.2	Integral light	10.40	12^m-8.5^m	97.50sec, 32.87sec, 16.48sec, 8.23sec
95099	16.08.04	20 14 07	14E	0.2	Integral light, B, V	30	13^m-10.5^m	98.00sec, 32.61sec, 16.36sec
95099	14.09.04	00 32 44	3.5E	0.2	Integral light	14	12.5^m-10.5^m	32.22sec, 16.11sec
Cosmos-X	12.09.04	00 35 42	2.3W	1	Integral light	80	12.8^m-6.5^m	21.5min
Cosmos-X	14.09.04	01 11 56	3.6W	10	Integral light	40	11.7^m-11.15^m	21.5min

the objects on character of the motion of the center of the masses by the methods of astrophysics, that gives important information, relating to status GEO objects, and, accordingly, the danger of approach with actively functioning objects.

On fig. 9, 10 curve changes of intensity a radio-echo GEO objects 98029 and 95099, received by I.E.Molotov et al. 25.06.2004 and 03.10.2004 on Bear Lakes RT-64, are presented. Small difference is at period object 95099 in optical and radio range possible to explain so, light curves there is integrated signal from the whole surface, but radar curves from separate details of the object. It also explicable different time of the accumulation.

References

Hernandez C. and Jehn R.: 2004, *Classification of Geosynchronous objects, ESOC*, **6**.

Konovalenko A.A., Molotov I.E., Sukhov P.P. et al.: 2003, *Proceedings of the conference Near-Earth astronomy – 2003*, Russian academy of science institute for astronomy, St.-P., **2**, 198.

PRIMORDIAL HELIUM ABUNDANCE BY RRL: NEW RESULT

A.P.Tsivilev[1], R.L.Sorochenko[1], Stefano Cortiglioni [2], Sergio Poppi [3] and Stelio Montebugnoli [3]

[1]Pushchino Observatory of P.N. Lebedev Physical Institute,
Pushchino Moscow reg., Russia
tsivilev@prao.psn.ru, soroch@lebedev.ru
[2]Istitute IASF-CNR, Bologna, Italy, *cortiglioni@bo.iasf.cnr.it*
[3] Istitute IRA-CNR, Bologna, Italy, *s.poppi@ira.cnr.it, stelio@ira.cnr.it*

ABSTRACT. New results of the Primordial Helium abundance (Y_p) measurement by radio recombination lines (RRL) observations from galactic HII regions are presented. The RRL observations were carried out with two Parabolas: RT32(λ =13.5 mm and 3.5 cm, Medicina, Italy) and RT22 (λ = 8 and 13.5 mm, Pushchino, Russia). The current value was obtained on the base of five source observations with the accurate correction for both the ionization structure and dust influence. At present, the obtained $Y_p = 25.74(\pm1.0)\%$ value seems to be higher than that suggested by optical data, allowing the presence of unknown light particles, and is in agreement with the result from cosmic microwave background asymmetry.

Keywords: Cosmology: Helium abundance: Recombination Radio Lines - ISM.

1. Introduction

Nowadays, there are several papers on the light elements production (He-4, He-3, D and Li-7) during Big-Bang Nucleosynthesis (BBN) occurred in the first 2-3 minutes of Universe. While He-3/H, D/H and Li-7/H abundances strongly depend on baryon density, the primordial He-4/H abundance dependence on baryon density is weak, since it is related to the presence of light particles as neutrinos (e.g. Yang et al., 1984) at the earlier stage, when a neutrino/proton (n/p) ratio was frozen (∼10-20 sec of Universe). Today, the number of neutrino species is known to be equal to 3 with high accuracy from accelerator experiments (Klapdor-Kleigrothaus & Zuber, 1997). Consequently, primordial helium abundance could be an indicator of some unknown light particles (Hot Dark Matter particles), if its amount would differ from BBN calculations. (Of course, the n/p ratio could depend on the rate of weak interaction too, but it was usually supposed to be as in standard physics.)

This paper presents further improvement of the RRLs Y_p measure in comparison with the previous report (Tsivilev et al., 2002).

2. Method to measure Yp by RRL

Today is clear that the systematical problems are playing a role in Y_p measurements at all wavelengths: optical, IR and radio. However the radio measurements have a remarkable feature: the radio recombination lines are originated by highly excited quantum states where the He atom has a Hydrogenic behavior, and the H and He coefficients, characterizing the levels population, are the same for the same H and He transitions. In this case the $y^+ = N(He^+)/N(H^+)$ ratio is measured directly from the ratio of He to H integral lines, since the corresponding levels population coefficients simplify each other. This is not the case for optical and IR observations, where these coefficients should be modeled. In order to increase the reliability of obtained data two radio telescopes (RT32, Medicina and RT22, Pushchino) have been used. Moreover, the achieved sensitivity allows to resolve the RRL of carbon (C) from the helium line profile, reducing also systematical problems.

Then, in principle, it's necessary to make two very important corrections: for ionization structure of HII regions and for stellar nucleosynthesis.

Ionization structure correction:

Usually, due to the difference of H and He ionization threshold, the sizes of He+ and H+ regions can be different. The correction for ionization structure ($\Delta y(IS)$) could be positive if the He^+ zone is smaller than the H^+ one, negative if the He^+ zone is larger, and zero if they coincide:

$$y = N(He)/N(H) = y^+ + \Delta y(IS).$$

To obtain it, a H and He RRL mapping of HII regions is very desirable, but a model $\Delta y(IS)$ calculation is also possible, by having two important parameters: the effective temperature (T_{eff}) of ionizing star (stars) and the amount and properties of dust inside the HII region. The dust properties are taken from Aannestad (1989) paper. Our investigations showed that Teff calibration by Pottash et al. (1979) together with the star

Source	y^+ %	$\Delta y(IS)$ %	T_{eff} K	y %	Z metallicity	Yp %
$OrionA^{**}$			~ 37000	10.2(0.8)	0.0112(.0022)	26.1(2.0)
$W3A^{**}$	9.9 (0.5)	-0.6	45000	9.3(0.5)	distant	26.1(1.6)
$M17^{**}$	11.1(1.1)	-0.7	45000	10.4(1.1)	0.0183(.0018)	24.7(2.7)
$NGC7538$	7.7(1.0)*	+1.95	$\sim 37000^*$	9.65(1.8)	distant	26.8(4.0)*
$W48$	9.6(1.3)	0.0		9.6(1.3)	$0.0183(.0019)^m$	23.3(3.3)

**) - data of the RRL mapping was also used;
distant - source at galactic distance outer than solar position;
*) - it will be further justified; m - from Galaxy Z model; for other Z see Tsivilev et al. (2002).

atmosphere models by Mihalas (1972) could be used.

Correction for stellar nucleosynthesis:

Since He4 is synthesized in stars, some of the measured helium is not primordial:

$y = y_p + \Delta y(stars)$; by atoms

or $Y = Y_p + Z * Y/dZ$; by mass

(and where $Y = 4y(1+4y)/*(1-Z)$).

To separate the Helium contribution from star nucleosynthesis two ways are proposed:

I) First way is by the observation of distant Galactic HII regions more distant than solar or Orion position from the Galactic centre, because: **a)** Observed metal abundance (Z) decreases outwards the Galaxy (i.e. Shaver et al., 1983); it can mean that interstellar matter in outer part of the Galaxy was polluted by stars nucleosynthesis products in smaller amount than that in the inner part. **b)** Hoyle&Teyler (1964) argued that the helium production in stars was small $\Delta y(stars) \sim 1\%$, ($\sim 10\%$ from stellar nucleosyntesis and $\sim 90\%$ from BBN). **c)** For simplicity, for outer part of Galaxy: $\Delta y(stars) = (0.5 \pm 0.5)\%$ (half of Hoyle&Tayler calculation) was accepted.

II) Second way uses a $Y(Z)$ dependence for the HII regions with well measured metal abundance (Z). The dY/dZ value can be taken from last accurate measurement for HII regions (in our case $dY/dZ = 2.3 \pm 1.0$ (Izotov & Thuan, 1998)). If measured value of Z is absent, it is possible to use the model Galaxy Z plot of Shaver et al. (1983), being the distance known.

3. Results

The Table reports the results of our Y_p determination. The average value is: $Yp = (25.74 \pm 1.0)\%$.

As for extragalactic radio RRL observations, it's possible to make a comparison only with 30 Doradus (LMC, Peck et al., 1997), where $y^+ = 13(2)\%$ was obtained. If one uses the max values of both IS and stellar corrections, then $Y_p = 27.2(\pm 4.3)\%$ by mass could be evaluated, which is in agreement both with our and optical Y_p, due to large errors.

However our results is in agreement with the WMAP data (Coc et al., 2004), where $Y_p = (24.79 \pm 0.04)\%$ has been obtained.

4. Summary

With respect to our previous result (Sorochenko & Tsivilev, 2000; Tsivilev et al., 2002) we obtained:

Yp = 25.74(+1.0)%,* , which is :

1) Higher than from optical measurements, but in agreement with the conclusion of CMB anisotropy experiments.

2) As for amount of unknown light particles at $\sim$ 10-20 sec, it's possible to calculate using Pagel (2000) formula, which, in turn, can be rewrite as a function only of neutrino species:

$Y_p = Y_{p,o} + 0.013(N_\nu - 3)$,

where the zero point is from WMAP data: $Y_{p,o} = 0.2479$, and an excess over established neutrino species number (=3) will be:

$\Delta N = N_\nu - 3 = 0.7 \sim 1$ for $Y_p = 25.74\%$ and $\Delta N = N_\nu - 3 = 2.3$ for 2σ upper level. *So, it means that about 1-2 unknown light particles (similar to neutrino) can exist.*

3) Nevertheless, it's worthy to note that another possibility to explain the derivation of measured Y_p from BBN value could be:

A) Pregalactic stars of the Population III ($10^2 - 10^5 M_o$) can produce ΔY up to $\sim 20\%$ (B.J.Carr, J.R.Bond and W.D.Arnet, 1984, *ApJ.*, 277, 445.) B) Variation of Physical constants: A.V.Ivanchik, A.V.Orlov and D.A.Varshalovich, 2001, *Astronomy Letters*, **27**, 615. C) Total Helium abundance was not from Big Bang Nucleosynthesis: Burbidge G. and Hoyle F., 1998, *ApJ*, **509**, L1-L3.

Note : * - Recently Izotov&Thuan (ApJ, 2004, 602, 200) presented the new value of $dY/dZ = 2.8 \pm 0.5$, consequently, a new value of Yp will be slightly lower and with slightly less error. Further it will be recalculated.

References

Yang J. et al.: 1984, *ApJ.*, **281**, 493.
Klapdor-Kleigrothaus H.V. & Zuber K.: 1997, *"Teilchenastrophysik"*, SBN 5-85504-012-7.
Tsivilev A.P., Cortiglioni S., Sorochenko R.L. et al.: 2002, *GRAVITATION & COSMOLOGY, Supplement*, **8**, 122.
Aannestad Per. A.: 1989, *ApJ*, **338**, 162.
Pottash S.R. et al.: 1979, *A&A*, **77**, 189.
Mihalas D.: 1972, *Non-LTE model atmospheres for B and O stars*, NCAR-TN/STR-76.
Shaver P.A. et al.: 1983, *MNRAS*, **204**, 53.
Hoyle F.R.S., Teyler R.J.: 1964, *Nuture*, **203**, 1108.
Izotov Yu.I., Thuan T.X.: 1998, *ApJ*, **500**, 188.
Peck et al.: 1997, *ApJ*, **86**, 320.
Coc Alain et al.: 2004, *ApJ.*, **600**, 544.
Sorochenko R.L., Tsivilev A.P.: 2000, *GRAVITATION & COSMOLOGY Supplement*, **6**, 148.
Pagel: 2000, *Phys. Rep.*, **333-334**, 433.

PHOTOMETRIC INVESTIGATION OF XX CYG

S.N.Udovichenko

Astronomical Observatory, Odessa National University
T.G.Shevchenko Park, Odessa 65014, Ukraine
udovich@farlep.net

ABSTRACT. The photometric observations of SX Phe type star XX Cyg (V=12^m, A5) were made in five nights using 48 cm reflector at the Astronomical Observatory of Odessa National University. The CCD photometer and the V filter of the UBV system was used. The variable and comparison stars monitored in the frame simultaneously. Light curves indicates a total light range 0.8 mag. A frequency analyses allow to find only one frequency of pulsating and it cause to consider this star as unique among this type. The light variation of XX Cyg can be well fitted with a single pulsation frequency during 60 years. This pulsating is in generally stable, but, there is a slight variation of period and, possibly, the light curves show, besides the primary maximum, a small bump of an amplitude of approximately 0.1 mag.

Key words: SX Phe – stars: individual (XX Cyg).

XX Cyg (V=12m, A5) – one of the well known as metal-poor and high-velocity SX Phe type star (McNamara, Feltz, 1980). The light variation was discovered by Ceraski in 1904. The period of light variation 0.134865070d, amplitude up to 1 mag (from the General Catalog of Variable Stars). The photometric observation of XX Cyg in different years show the variation of amplitude and period during a long time (Zhou at all., 2002). Szeidl and Mahdy (1981), Kiss and Derekas (2000) have published the concluding that the period of XX Cyg suffered a sudden little change and was constant otherwise.

The radial-velocity curve has a total velocity range of 37 km/s. The mean radial velocity was found to be 108 km/s. This indicated the high-velocity nature of XX Cyg (Mc.Namara and Feltz, 1980).

To study a behavior of the period change of XX Cyg, new observations were made on 5 nights of October 2001 using the CCD photometer and 48 cm reflector at the Astronomical Observatory of Odessa National University. The CCD photometer was created by author, using chip ISD015 (520x580 pixels), vacuum housing and thermoelectric (Peltier) cooler. In the observations the V filter of the UBV system was used. Two stars were chosen as comparison and check stars (comp=GSC 3948-2542, 10.0, check=GSM 3948-2105, 10.9).

Table 1: The times of maximum light XX Cyg

HJD max	O - C
2452193.2807	0.008
2452193.4144	0.003
2452196.3818	0.005
2452200.2929	0.006
2452200.4275	0.004
2452207.4403	0.003
2452208.2501	0.007
2452208.3850	0.007

The observed light curves of XX Cyg are shown in Figure 1. A preliminary analysis show that light curves indicates a total light range 0.8 mag in filter V. Possibly, the light curves show, besides the primary maximum, a small bump of amplitude of approximately 0.1 mag. The light variation of XX Cyg can be well fitted with a single pulsation frequency, but an analysis on multiple mode pulsation is carrying out.

Eight new times of maxima were determined from the individual light curves. The mean value O - C = 0.005±0.0006. To constract the updated O-C diagram, all available data from literature have been collected: (Kleissen E., 1939; Born F., Sofronievitsch H., Pohl E., 1953; Oskanjan V., 1953; Payne-Gaposhkin S., 1954; Alaniya I.F., 1954; Fitch W.S., Wisniewski W.Z, Johnson H.L., 1966; Firmanyuk B.N., 1976). The resulting diagram is plotted in Fig.2. The estimated accuracy is about 0.0006 days and correspond of dots size.

The single pulsating is in generally stable during 60 years, but slight change of period near JD=2430500 have been occured. The sudden change of period $\Delta P/P = 2x10^{-7}$. A least-squares linear fit of O-C diagram have been obtained by new formula HJD max = 2416564.4885 + 0.134865076 x E.

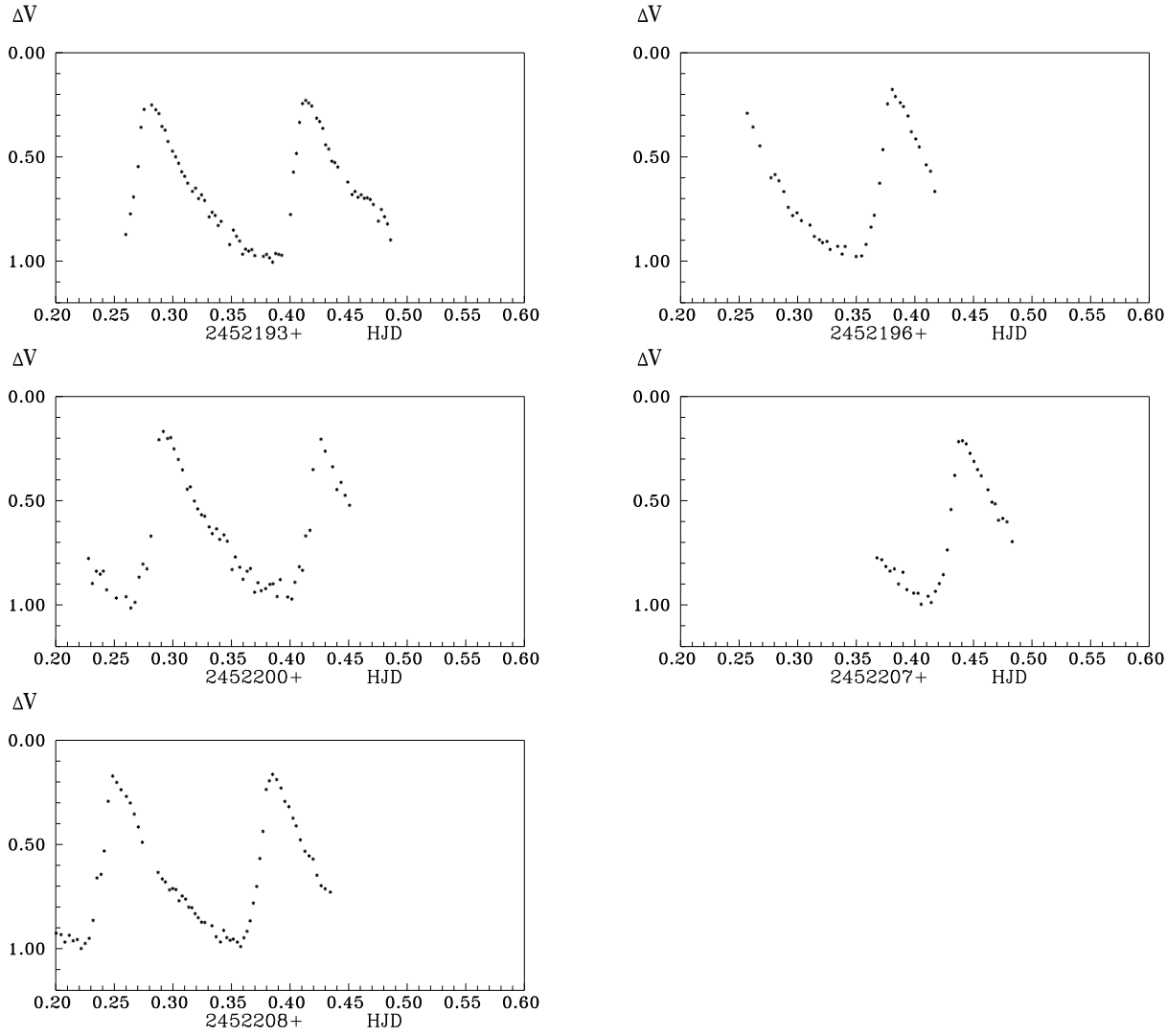

Figure 1: The light curves XX Cyg in 2001

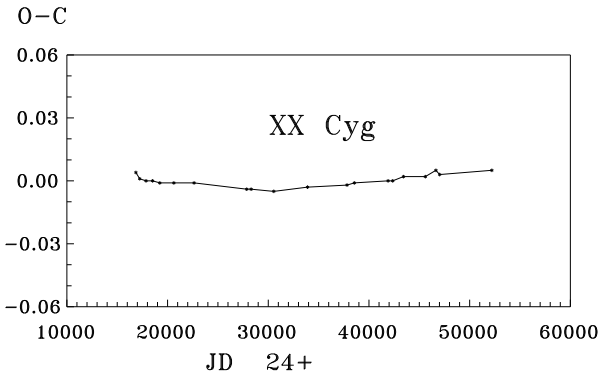

Figure 2: The mean O - C diagram of XX Cyg during 60 years

References

McNamara D.H., Feltz K. A. Jr.: 1980, *PASP*, **V. 92**, 195.

Zhou, Ai-Ying, Jiang, Shi-Yang, Chayan, B., Du, Bai-Tian.: 2002, *Astroph. Space Science.,* **V. 281**, 4.

Szeidl B., Mahdy H.A.,: 1981, *Comm. Konkoly Obs.*, No. 75.

Kiss L.L., Derekas A.: 2000, *IBVS*, No. 4950.

Kleissen E.: 1939, *Astron. Nach.*, 267.

Born F., Sofronievitsch H., Pohl E.: 1953, *Astron. Nachr.*, 281.

Oskanjan V.: 1953, *Bull. observ. astron.*, Belgrad, **V.18**, 3-4.

Payne-Gaposhkin S.: 1954, *Harvard Ann.*, **V. 113**, 3.

Alaniya I.F.: 1954, *Astron. Cyr.*, No. 981.

Fitch W.S., Wisniewski W.Z., Johnson H.L.: 1966, *Comm. of the Lunar and Planetary Lab.*, The Univer. of Arizona, 1966, **V. 5**, 71.

Firmanyuk B.N.: 1976, *IBVS*, No. 1152.

ABUNDANCES OF r-PROCESS ELEMENTS IN THE PHOTOSPHERE OF RED SUPERGIANT STAR PMMR23 IN SMALL MAGELLANIC CLOUD

S.V. Vasil'eva[1], V.F. Gopka[1], A.V. Yushchenko[2,1], S.M. Andryevsky[1]

[1]Astronomical observatory, Odessa National University, T.G. Shevchenko Park, Odessa 270014 Ukraine, *cerera_sveta@rambler.ru, gopkavera@mail.ru*

[2]Astrophysical Research Center for the Structure and Evolution of the Universe (ARCSEC), Sejong University, Seoul, 143-747, (South) Korea, *yua@odessa.net*

ABSTRACT. Detailed analysis of chemical abundances determined from high-resolution CCD-spectrogram of supergiant star PMMR23 (K5 I) in SMC is presented. The observation were obtained at 3.6 meter ESO La Silla telescope by Hill (1997). Spectral resolving power is near R=30,000. The wavelength coverage is 5050-7200 A. The abundances of iron and 15 r-, s-processes elements are found. The abundances of Cu, Zr, Mo, Ru, Pr, Sm, Gd, Dy, Er are found for the first time. The abundances of elements with atomic numbers less than 55 are deficient with respect to the Sun. The mean underabundance is near 0.7 dex. The abundances of barium and lanthanides are near solar values. The overabundances of these elements with respect to iron are in the range from 0.4 tp 0.9 dex. The abundances of heavy lanthanides are higher than the abundances of light lanthanides. The abundance pattern of PMMR23 can be fitted by scaled solar r-process distribution. The atmosphere of PMMR23 is enriched by r-process elements.

Key words: Stars: fundamental parameters; stars: abundances; stars: kinematics; stars: atmospheres; stars: individual: PMMR23; r-process nucleosynthesis; galaxies: stellar content; galaxies individual: Small Magellanic Cloud

1. Introduction

The Magellanic Clouds and our Galaxy are the members of Local Group galaxies. The Magellanic system is composed of two small irregular galaxies, the Large (LMC) and Small (SMC) Magellanic Clouds, in orbit around Galaxy. Tidal interactions between these galaxies and Milky Way have produced several high-velocity gas complexes connected to the clouds, namely the Magellanic Bridge (MB), the Magellanic Stream. The Magellanic Clouds are optimal targets for investigations of stellar formation histories in local galaxies. The Magellanic Clouds have often been used as a laboratories to test the validity of the theories of evolution of our Galaxy. These are the nearest galaxies to our Galaxy. The high resolution spectral observations of the brighest stars of these galaxies became available in the last decade.

In previous work the abundances of chemical elements in nine K-supergiants in the SMC were investigated by the method of model atmospheres (Komarov et al. 2001). High-resolution CCD-spectrograms obtained at 3.6 meter ESO telescope were used - R=30,000 for the stars with magnitudes 12.4^m-13.5^m (Hill 1997). The wavelength coverage was 5050-7180 A. It was shown that all stars have a deficit of iron from -0.4 to -0.97 dex relative to the Sun. Some differences in the abundances of the elements of α-process (Si, Ca, Ti), s-process (Y, Zr) and e-process (Sc, V, Cr, Ni, Mn) relatively to the iron abundances were found in the atmospheres of the stars in the SMC and comparison star (Sun).

In this investigation we reanalyze the abundances of iron and r-, s-processes elements in one of the stars, PMMR23 (star number 23 from the catalogue by Prevo et al. 1983), using the spectrum synthesis method for identification of the lines and for calculating the abundances.

2. Methodics

The observed spectrum of PMMR23 was compared to synthetic spectrum generated using the Kurucz's numeric code SYNTHE. URAN code (Yushchenko 1998) was used for identification of the lines in observed spectrum. The examples of the spectrum are shown in the Figs. 1, 2.

The first iteration was made with the parameters of atmosphere model taken from Hill (1997). Synthetic spectrum was calculated for the whole observed

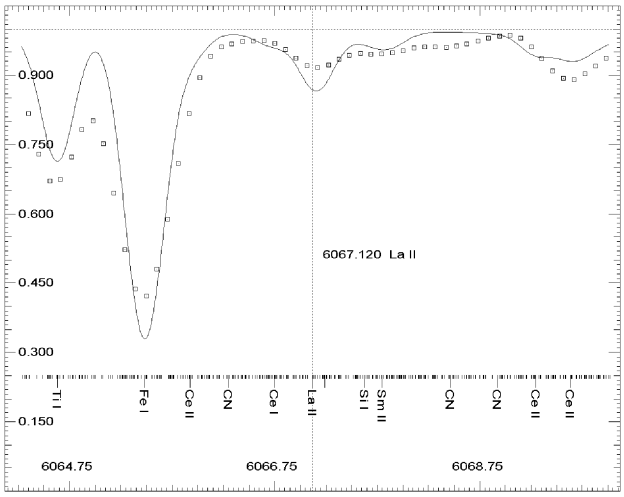

Figure 1: The example of the spectrum of PMMR23 in the vicinity of La II line 6067.12 Å . The axes are the wavelengths in angstroms and relative fluxes. The solid line is the synthetic spectrum, the open squares - observed spectrum. The positions of the lines, taken into account in the calculation of synthetic spectrum are shown in the bottom part of the figure. Part of the strong lines are identificated. Hill (1997) parameters of the atmosphere model and abundances of the elements were used for calculation of the synthetic spectrum.

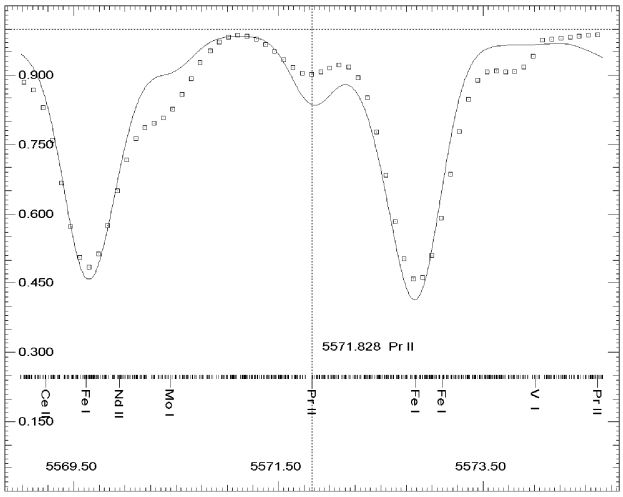

Figure 2: The same as in Fig. 1 in the vicinity of Pr II line 5571.828 Å.

wavelength region. The used list of spectral lines includes all atomic and molecular lines from Kurucz (1995), DREAM database (Biemont et al. 2002), VALD database (Piskunov et al. 1995), Hirata & Horaguchi (1995) and other sources.

This spectrum was used for identification of clean spectral lines in the observed spectrum. 88 clean lines of neutral iron and 7 lines of ionized iron were selected. Equivalent widths of these lines were used for testing of the atmosphere model. Kurucz (1995) WIDTH9 program was used for calculation of iron abundances. Hill (1997) parameters were adopted, only small change in microturbulent velocity was necessary.

The final set of atmosphere parameters is: effective temperature $T_{\rm eff}$=4200 K, surface gravity log g=0.2, microturbulent velocity $v_{\rm micro}$=3.95 km s^{-1}, the abundance of iron [Fe/H]=-0.65. The value of projected rotational velocity was estimated to be equal $v \sin i$ =3.5 km s^{-1}. This value includes all possible effects of broadening of spectral lines, for example macroturbulent velocity, magnetic broadening.

We found the numerous lines of lanthanides: La, Ce, Pr, Nd, Sm, Eu, Gd, Dy, Er in the spectrum of PMMR23. We identified also the lines of Cu, Y, Zr, Mo, Ru, Ba. The abundances were estimated using model atomosphere method with WIDTH9 program (Kurucz 1995). The next step was the calculation of abundances of these elements using the spectrum synthesis method. Kurucz (1995) SYNTHE and Yushchenko (1998) URAN codes were used for calculating of synthetic spectra and for fitting the observed spectrum by calculated one. Hyperfine and isotopic splitting data from Kurucz (1995) were taken into account for lines of Cu and Eu. More detailed description of methodic can be found in Yushchenko et al. (2005).

3. Results

The results are summarized in Table 1. The first three columns of the table are the numbers of the investigated elements, its identifications and atomic numbers. The next two triplets of columns are the abundance results of this investigation and that of Hill (1997). The relative abundances (with respect to the Sun), rms errors and number of used lines are shown in these columns. The last column is the abundances in the atmosphere of the Sun in accordance with Grevesse & Sauval (1998). The abundance on Ni from Hill (1997) is also included in the table.

The last version of database of lanthanides lines (DREAM, Biemont et al. 2002) and using the synthetic spectrum for identification of the lines permit to increase the number of investigated lines. The number of lines of heavy elements is approximately ten times exceeds the number of lines analyzed by Hill (1997). It permits us to investigate more elements and to obtain more reliable result.

The light elements are deficient in PMMR23 and the level of blocking of the spectrum by lines of these elements is not so high as in the similar stars of our Galaxy. That is why we can find more clean lines of heavy elements in the spectrum of PMMR23.

Fig. 3 shows the abundance pattern of PMMR23. The overabundances of barium and lanthanides with respect to iron are in range from 0.4 to 0.9 dex. The

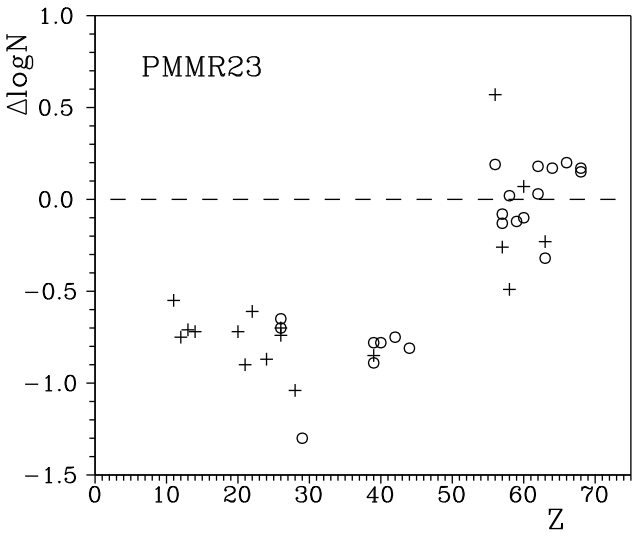

Figure 3: The chemical composition of PMMR23. The axes are the atomic numbers of the elements and relative abundances with respect to the solar values from Grevesse & Sauval (1998). The results of this paper are marked by open circles, Hill (1977) abundances – by crosses. Light elements in accordance with Hill (1997) are also shown at this picture.

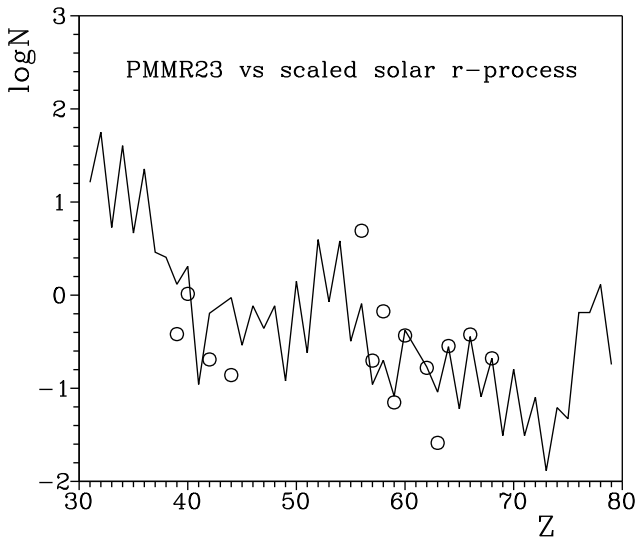

Figure 4: Comparison of the surface abundances in PMMR23 (circles) with the solar system r-abundance distribution scaled to the observed Er abundance (solid line). The solar system abundances corresponds to the photospheric determination of Grevesse & Sauval (1998) with the solar r-process distribution estimated by Burris et al. (2000)

overabundances increased with atomic number for elements after barium. Lighter r-, s- processes elements are deficient with respect to iron. All above mentioned elements exept Y, Ba, La, Ce, Nd, and Eu are identified for the first time in the spectrum of the star.

It should be noted that we detected the lines of the first spectra of La, Sm, Er. The ionization equilibrium for these elements confirms the value of surface gravity, selected from the investigation of iron lines.

4. Discussion

In this paper we confirmed the main features of abundance pattern of the star found by Hill (1997). These are the deficiency of chemical elements with atomic numbers Z<55 and near solar values of abundances for barium and lanthanides. The number of identificated lines of heavy elements is significantly higher than in previous investigations. It is the result of using the synthetic spectrum for line identification and for abundance calculations. The abundances of nine r-, s- processes elements are found for the first time. The higher precision of our results permit us to claim that the abundances of light lanthanides are usually less than the abundances of heavy lanthanides.

Supergiant stars are very young objects, so this chemical composition should reflect the present day chemical abundance of Small Magellanic Cloud. Fig. 4 shows the comparison of abundances in PMMR23 with scaled solar system r-abundance distribution. The distribution of abundances in the investigated star can be fitted by r-process distribution. It means that the interstellar gas in the place of formation of PMMR23 was enriched by *r*-process elements. Maybe it was supernovae explosion or other event.

Usually this fitting is made for halo stars of our Galaxy. In this case, in accordance with traditional Big-Bang cosmology, the number of stellar generations before the creation of investigated object is significantly less, than for young stars. In our case we can expect that PMMR23 was born in the place, where previous stellar generations were not very active. In this case the level of contamination of interstellar gase by *s*-process elements should be not very high.

The largest deviations are observed for Ba, Ce, and Eu. It should be noted that for Ba we did not take into account hyperfine and isotopic splitting of the lines. The deviations for Ce and Eu can be real, but need to be confirmed.

Recently Yushchenko et al. (2005) showed that the *r*-process in the Milky Way is not universal or more exactly the astrophysical site(s) hosting the r-process do(es) not always lead to a unique relative abundance distribution of the elements. The abundance of Eu in HD221170 (Yushchenko et al. 2005) also lower than the predicted scaled solar abundance. Maybe more complete investigation of the spectrum of PMRR23 and other supergiants observed by Hill (1997), as well as the new observations of the brightest stars in Magellanic Clouds and other galaxies will help to investigate the production of the elements in *r*-process outside of the Milky Way.

Table 1: Abundances of iron and *r*-, *s*-processes elements in PMMR23

			This work			Hill, 1997			
	Z	Ident.	$\Delta\log N$	σ	n	$\Delta\log N$	σ	n	$\log N_\odot$
1	26	Fe I	-0.65	0.13	88	-0.74	0.21	60	7.50
		Fe II	-0.70	0.07	7	-0.70	0.19	10	7.50
	28	Ni I				-1.04	0.26	10	6.25
2	29	Cu I	-1.30		1				4.21
3	39	Y I	-0.78	0.05	3				2.24
		Y II	-0.89	0.12	5	-0.85	0.21	2	2.24
4	40	Zr I	-0.78	0.19	13				2.60
5	42	Mo I	-0.75	0.01	2				1.92
6	44	Ru I	-0.81		1				1.84
7	56	Ba I	0.19	0.02	3				2.13
		Ba II				0.57	0.24	2	2.13
8	57	La I	-0.08		1				1.17
		La II	-0.13	0.13	14	-0.26	0.16	2	1.17
9	58	Ce II	0.02	0.14	22	-0.49	0.10	4	1.58
10	59	Pr II	-0.12	0.12	10				0.71
11	60	Nd II	-0.10	0.14	46	0.07	0.13	3	1.50
12	62	Sm I	0.18		1				1.01
		Sm II	0.03	0.22	16				1.01
13	63	Eu II	-0.32	0.02	3	-0.23		1	0.51
14	64	Gd II	0.17	0.05	5				1.12
15	66	Dy II	0.20	0.10	3				1.14
16	68	Er I	0.15		1				0.93
		Er II	0.17		1				0.93

It should be noted that in this paper we did not tried to calculate the abundances of light elements and the abundances of elements with atomic numbers higher than Z=68. Our preliminary results show that the abundance pattern of PMMR23 can be significantly more complete.

The derived abundances will be used to build the individual model of the star. The calculation of the abundances of all chemical elements using the synthetic spectrum method will be made in the next paper.

Acknowledgement. We use data from NASA ADS, SIMBAD, CADC, VALD, NIST, and DREAM databases and we thank the teams and administrations of these projects. Work by AY was supported by the Astrophysical Research Center for the Structure and Evolution of the Cosmos (ARCSEC) of Korea Science and Engineering Foundation (KOSEF) through the Science Research Center (SRC) program.

References

Biemont J., Palmeri P., Quinet P.: 2002, Database of rare earths at Mons University http: //www.umh.ac.be/˜ astro/dream.html

Burris D. L., Pilachowski, C.A., Armandroff T.E., Sneden C., Cowan, J.J., Roe H.: 2000, ApJ, **544**, 302.

Grevesse N., Sauval, A.J.: 1998, Space Science Reviews **85**, 161.

Hill V.: 1997, A&A, **324**, 435.

Hirata R., Horaguchi T.: 1995, SIMBAD Catalog VI/69.

Komarov N.S., Zgonyajko N.S., Vasil'eva S.V.: 2001, Kinematisc and Physics of Selectial Bodies, **17**, 471.

Kurucz R.L.: 1995, ASP Conf. Ser., **81**, 583.

Piskunov N., Kupka F., Ryabchikova T., Weiss W., Jeffery C.: 1995, A&AS, **112**, 525.

Prevo L., Martin N., Maurice E., Rebeirot E., Rousseau J.: 1983, A&AS, **53**, 255.

Yushchenko A.V.: 1998, Proc. of the 29th conf. of variable star research, Brno, Czech Republic, November 5-9, 201.

Yushchenko A., Gopka V., Goriely S., Musaev F., Shavrina A., Kim C, Kang Y. W., Kuznietsova J., Yushchenko V.: 2005, A&A, **430**, 255.

INTERSTELLAR ABSORPTION IN SOME DIRECTIONS

M.P.Yasinskaya, A.V.Dragunova

Astronomical Observatory, Odessa National University
T.G.Shevchenko Park, Odessa 65014, Ukraine
astro@paco.odessa.ua

ABSTRACT. Interstellar absorption has been researched towards Kapteyn Areas KA-64, KA-65, KA-86, KA-87, KA-88, KA-98 by the method of a colour excess. The star magnitudes V and colour indexes (B-V) of stars were received by the employees of Odessa Astronomical Observatory Yasinskaya etc. (Odessa Astron. Publ., 2000, v.13, p.4). The stars of all spectral classes had been used for determination of quantity of interstellar absorption. The received curves of absorption have allowed to estimate the density of an absorption substance in explored directions. The results are presented in a graphical view. The random error of determination of complete visual absorption for KA-64, KA-86, KA-88 is $\pm 0^m.10$, for KA-65 is equal to $\pm 0^m.09$, for KA-87, KA-98 - $\pm 0^m.11$. The random error of determination of distance for all areas is 110 pc on the first kiloparsec. At the distance of 2 kpc the random error increases up to 220 pc.

Key words: Galaxy, interstellar absorption, Kapteyn Aries.

The classical method of a colour excess of stars was used to study the allocation of interstellar absorbing substance in the Galaxy. This method allows - simply and reliably - to determine quantity of complete interstellar absorption on all distance up to the star using the data of a photometry in two photometric systems (in our case it is systems B and V). The catalogues of stars magnitudes and colour indexes are initial materials for examinations by this method. The catalogue of B- and V- magnitudes of 4437 stars from Kapteyn Areas 64, 65, 86, 87, 88, 98 (Yasinskaya et al. (2000)) has been used in this work. The photographic material for researched Kapteyn Areas was obtained by M.S.Kazanasmas, L.A.Zavershneva and L.Ph.Tomak with the help of unaberrational Schmidt camera of Abastumany Astrophysical Observatory in 1981 - 1988. The filter Schott GG11 with the film A -600 (V- magnitudes) and filter Schott GG13 with the film A-500 (B-magnitudes) were used for reception of the Johnson-Morgan B-,V-magnitudes. The photometric processing of the received photographic material was made using micro-photometer. Three films were used to make measurements for every star. The mistake of a field of the Schmidt camera was not taken into account, because it does not exceed $0^m.01$ at distance $2^o20'$ from the centre of a photosnapshot, where the photometry of stars was carried out. The standard technique was applied for calculations of stellar magnitudes. The random errors of B- and V- magnitudes are less than $\pm 0^m.04$. The area of each Kapteyn square makes 15,9 square degrees. The equatorial coordinates of areas at the epoch 2000.0, Galactic coordinates l, b, and also the quantity of stars N, which were examined in each area, are indicated in the Table 1. The interstellar absorption was explored by the method of colour excess according to main relation: $A_V = RE_{B-V}$. A_V - complete visual absorption, E_{B-V} - colour excess, which is determined by the difference E_{B-V}=(B-V)-$(B-V)_0$, where (B-V) - observed colour index of a star, $(B-V)_0$ - normal colour index, which have not been burdened by interstellar absorption. Coefficient R, that translates a colour excess in complete visual absorption, was considered as a stationary value 3.0. The normal colour indexes of stars were taken from Fitzgerald's publication (1970). The dependence of complete visual absorption A_V from distance r in parsecs was calculated by the formula: lg r=0.2(V+5-M_V-A_V). The values of absolute magnitudes of stars M_V by Straizys et al.(1982) were used for evaluation of photometric parallaxes of stars (r). The spectral classes and classes of a brightness of stars for Kapteyn Areas were received by Bartaya R.A. (Abastumani astrophysical Observatory, private communication), and also were taken from the literature. The stars of all spectral classes were used for determination of quantity of interstellar absorption. The root mean squared errors of determination of absorption σ_{A_V} and the distance σ_r for one star are $\pm 0^m.23 \div \pm 0^m.38$, and $\pm$2pc $\div$ $\pm$970pc. Received relationships of absorption A_V from distance r at the chosen directions are shown in Figure 1. The calculations have shown, that the random errors of determination of complete visual absorption for KA-64, KA-86, KA-88 are $\pm 0^m.10$; for KA-65 there are equal to $\pm 0^m.09$, for KA-87, KA-98 - $\pm 0^m.11$. The random error of determination of distance for all areas is 110 pc on the first kiloparsec.

Apart 2 kpc the random error is incremented up to

Table 1: Equatorial and Galactic coordinates of the Kapteyn Areas

Name of Kapteyn Area	α	δ	l	b	N, quantity of stars
KA-64	$20^h\ 02^m.0$	$+30^o16'.1$	$67^o.1$	$+0^o.1$	475
KA-65	$21^h\ 02^m.6$	$+30^o32'.8$	$75^o.3$	$-10^o.8$	425
KA-86	$18^h\ 15^m.0$	$+15^o00'.0$	$42^o.6$	$+14^o.6$	396
KA-87	$19^h\ 15^m.0$	$+15^o11'.0$	$48^o.9$	$+2^o.0$	345
KA-88	$20^h\ 14^m.0$	$+15^o26'.0$	$56^o.5$	$-10^o.7$	440
KA-98	$06^h\ 52^m.0$	$-\ 0^o15'.0$	$213^o.1$	$+0^o.3$	345

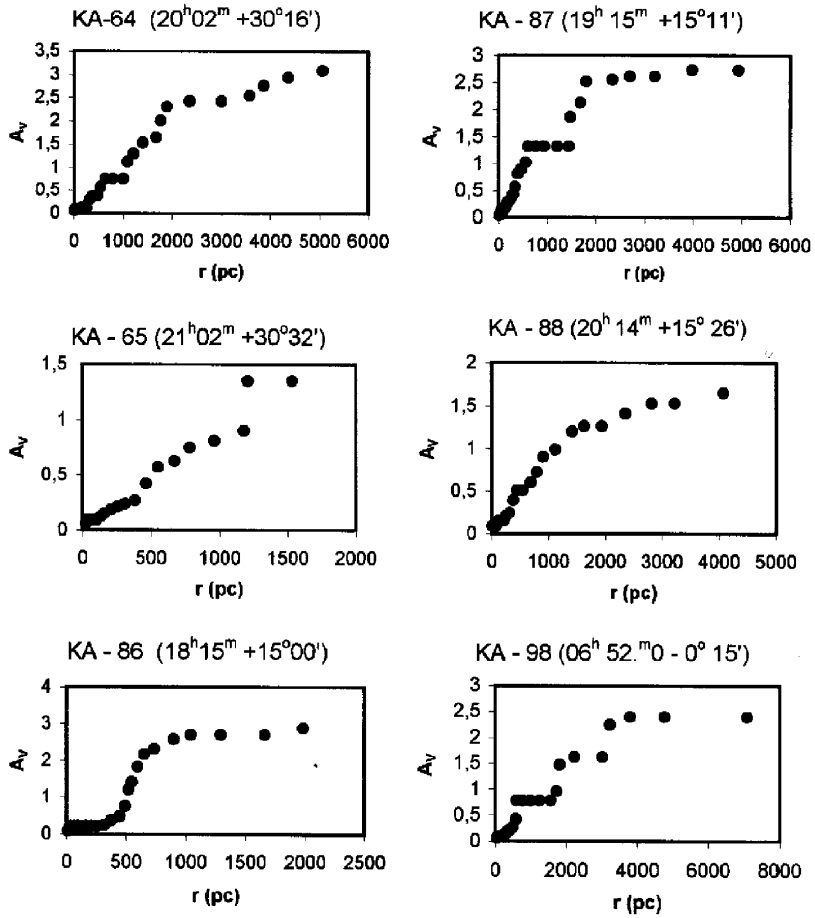

Figure 1: The mean absorption relationships at the chosen directions.

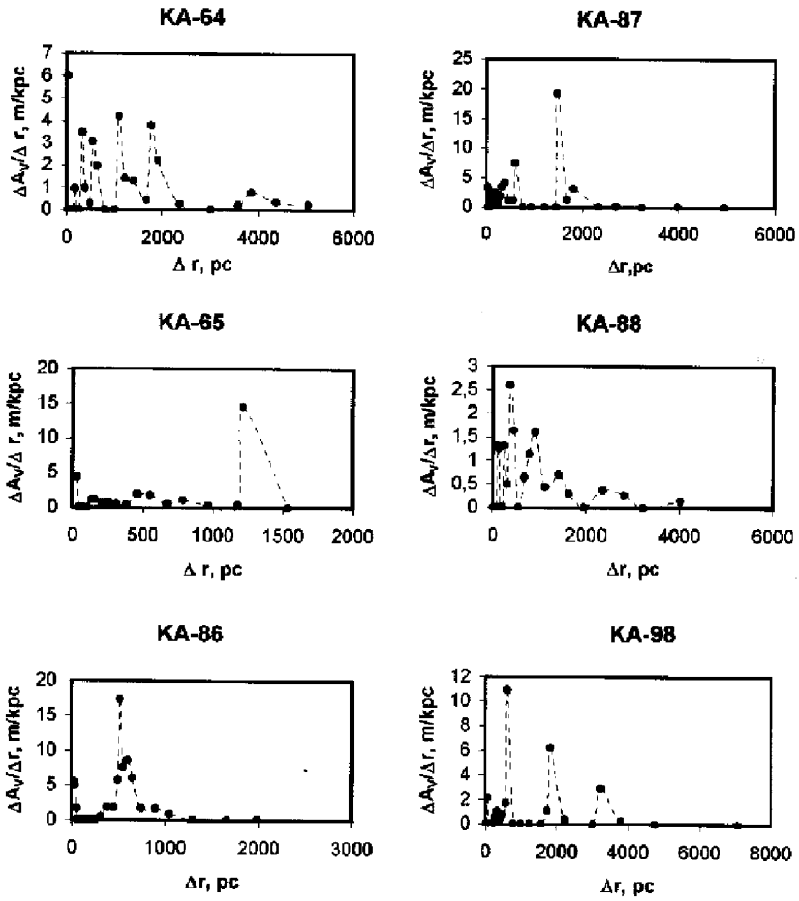

Figure 2: Distribution of the interstellar absorption matter.

220 pc. The obtained curves of absorption allow to estimate the density of an absorbing substance in explored directions. The results are presented in Figure 2, where Δ_{A_V}/Δ_r is the density of an absorbing substance on 1 kpc, Δ_r - the distance interval. The analysis of received results permits to make the following deductions. In a direction KA-64, KA-65, KA-86, KA-88 apart 300 pc from the Sun the absorption misses. In a direction KA-87 the absorption becomes noticeable from distance 200 pc, and in a direction KA-98 the absorption is not observed almost up to 500 pc. It is impossible to consider the dust clouds, which appear on this distance, to be real because of the major errors in quantities of complete visual absorption and distances. The absorbing matter is distributed very nonuniformly, and forms the clouds. The ground mass of the dust concentrates in the galactic plane. So, in directions of KA-64 (b = $+0^o.07$), KA-87 (b = $+2^o.0$), KA-98 (b = $+0^o.3$) the dust clouds are observed on distances, twice bigger, than in directions KA-65 (b = $-10^o.8$), KA-86 (b = $+14^o.6$), KA-88 (b = $-10^o.7$).

The dense clouds of absorption substance are observed at the distances, which exceed the half-thickness of dust layer, equal 100 pc, mean for the Galaxy. So, in direction of KA-65 apart 1200 pc from the Sun the dust cloud with density 14.52 m/kpc is situated under a galactic plane apart 225 pc. And in a direction of KA-86 apart 500 pc from the Sun the dense cloud is observed apart 130 pc above a galactic plane. Increase of absorption discontinues in all explored directions, if the beam of sight goes out in space between spiral sleeves.

References

Yasinskaya M.P., Tomak L.Ph., Zavershneva L.A., Dragunova A.V.: 2000, *Odessa Astron. Publ.,* **13**, 4.

Fitzgerald M.P.: 1970, *Astron. Astropys.,* **4**, 234.

Straizys V., Kuriline G., Yodinskene E.: 1982, *Bull. Vilnius Astron. Obs.,* **60**, 9.

STELLAR ABUNDANCES. FROM QUANTITY TO QUALITY?

Yushchenko A.V.[1,2], Gopka V.F.[2]

[1]Sejong University, Seoul, Korea
yua@arcsec.sejong.ac.kr, yua@odessa.net
[2]Odessa National University, Odessa, Ukraine
gopkavera@mail.ru

ABSTRACT. We present the overview of chemical compositions of the atmospheres of seven stars with the most detailed abundance patterns – the Sun, Przybylski's star, HD221170, Sirius, Procyon, ζ Cyg, δ Sct. The abundance pattern of the Sun is 73 chemical elements, for other stars (except HD221170) – more than 50 elements. A big quantity of known abundances permits to find a qualitatively new results. The lines of radioactive elements with short decay-time are found in the spectrum of Przybylski's star – Tc, Pm, and elements with atomic numbers $84 \leq Z \leq 99$. The abundances of heaviest elements in old halo star HD221170 permit us to show that it is not correct to use the ratio's of radioactive elements for determination of the age of the stars. The abundance patterns of barium star ζ Cyg and Sirius A can be explained by mass transfer in the binary system. The chemical composition of Procyon is solar, only Te is overabundant by 0.5 dex. Te is located at one of the peaks of r-process in the standard abundance pattern. The abundance pattern of δ Sct appears to be similar to that of δ Del type stars.

Keywords: stars: abundances, stars: individual (HD48915, HD61421, HD101065, HD172748, HD202109, HD221170), nucleosynthesis.

1. Introduction

The solar abundance pattern is 73 chemical elements (Grevesse&Sauval, 1998; Gopka et al., 2001). Some other well-determined abundance patterns are those for peculiar Przybylski's star – 57 elements (Cowley et al., 2000; Cowley et al., 2004; Shavrina et al., 2003), two halo stars: GS22892-05 – 57 elements (Sneden et al., 2003) and GS31082-001 – 56 elements (Aoki et al., 2003; Sneden et al., 2000), Procyon – 55 elements (Yushchenko&Gopka, 1996a; 1996b) HgMn star χ Lupi – 51 elements (Leckrone et al., 1999), and the prototype of mild barium stars ζ Cyg– 51 elements (Yushchenko et al., 2004a). In this review we will show the abundance patterns and main astrophysical results obtained for the Sun, Przybylski's star, halo star HD221170, Sirius, ζ Cyg, Procyon, and δ Sct. The discussion is based on our recently published papers and new results for Przybylski's star (HD101065), δ Sct, and Sirius. The use of spectrum synthesis for all stages of spectra processing, from continuum placement and line identification to the abundance calculations permits us to obtain these results.

2. The Sample

Sun. The review (Grevesse&Sauval, 1998) includes the abundances of 71 elements. The abundance of As was found in (Gopka et al., 2001). The meteoritic value for Th (Grevesse&Sauval, 1998) is used for the Sun. The abundances of Se, Br, Kr, Te, I, Xe, Cs, Ta, Re, Hg, Bi and all radioactive elements are unknown, upper limit is known for U. Fig. 1a is the solar abundance pattern.

Przybylski's star. All heavy elements show large overabundances in the atmosphere of this roAp star. The lines of Tc and Pm were identified in (Cowley et al., 2004). We found the abundance of Tc (log N(Tc)=4 in the scale log N(H)=12), and identified the lines of all radioactive elements with atomic numbers (Z) from 84 to 99, except 85 (At) and 87 (Fr) (Gopka et al., 2005). Z<92 elements can be explained by natural decay of Th and U. Z>92 elements can exist due to neutron capture reactions in the layers of the atmosphere with overabundances of Th and U. Spallation reaction, accretion can be used to explain this phenomena. Fig. 1b shows the abundances of 62 elements in Przybylski's star based on (Cowley et al., 2000; Shavrina et al., 2003) and our values for Tc, Pb, Bi, Ra, Am.

HD221170. The lines of 43 elements were found in its atmosphere. (Yushchenko et al., 2005). It appears to be thorium-rich halo star. Fig. 1c shows the abundances with respect to the Sun, Fig. 1d – with respect to barium abundance and scaled Solar system r-process abundances. The comparison of HD221170 with other four Th-rich stars permits us to find that the initial ratio's of Th, U and other r-process elements in dif-

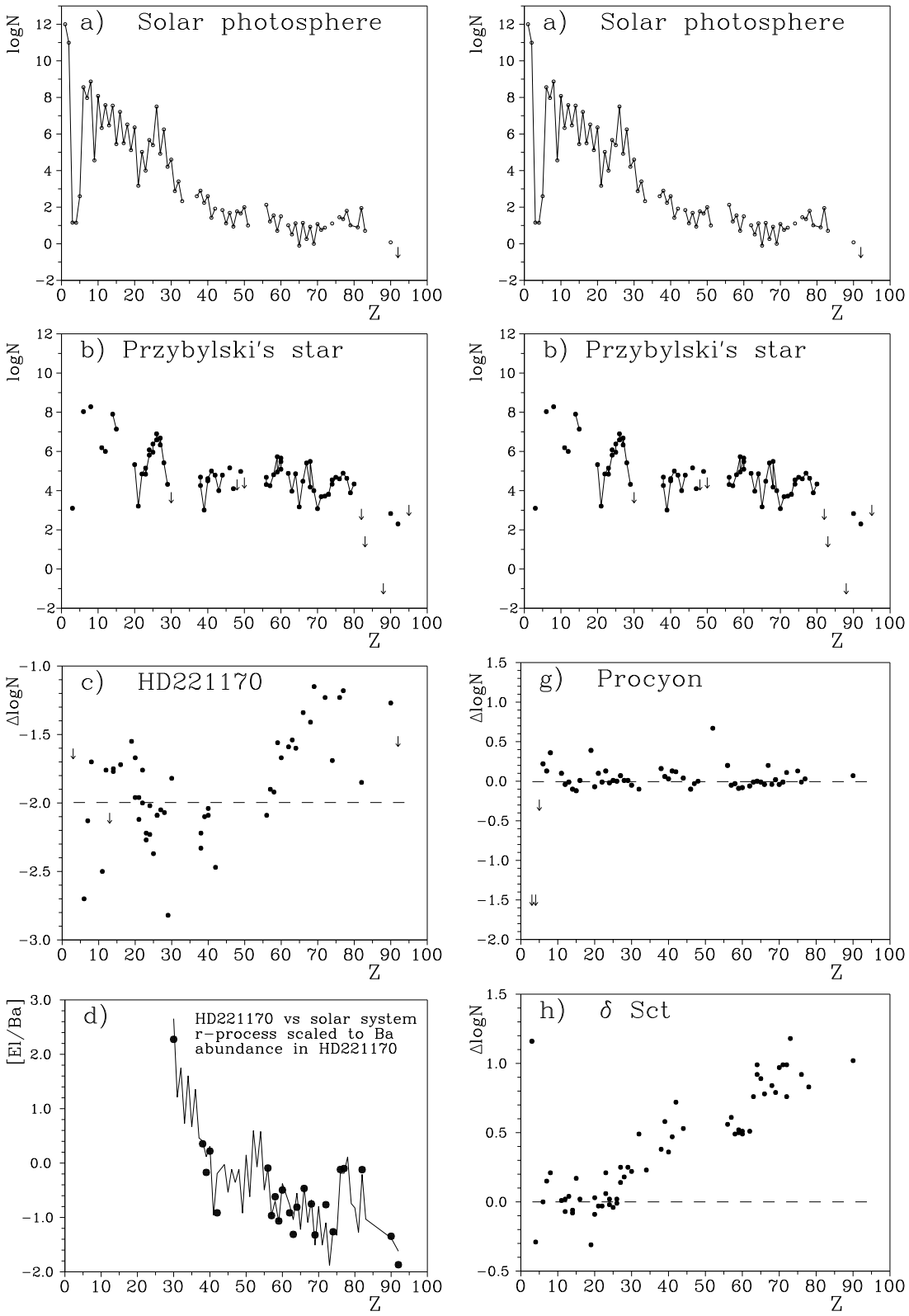

Figure 1: The abundances of chemical elements in the Sun (a), Przybylski's star (b), HD221170 (c-d), ζ Cyg (e), Sirius (f), Procyon (g), δ Sct (h). The axes are the atomic numbers and the absolute (a, b) or relative abundances: (d) – with repect to barium abundance in HD221170, (c, e-h) – with respect to solar system values.

ferent Supernova explosions were not similar. That is why it is not correct to use the abundance ratio's of radioactive and stable elements to find the ages of halo stars.

ζ Cyg, Sirius, Procyon. We found the abundances of 51 elements in ζ Cyg (Yushchenko et al., 2004a), 50 – in Sirius (Yushchenko, 1996; Gopka, 2000), and 55 – in Procyon (Yushchenko&Gopka, 1996a; 1996b). These are the binary systems with white dwarf (WD) companions. The orbital periods are 18, 50, and 40 years respectively. Mass transfer in these systems can influence on the chemical composition. WD could be a primary in the past, before loosing the great fraction of it's mass. Fig. 1e shows the chemical composition of ζ Cyg (Yushchenko et al., 2004a) and theoretical abundances which can appear due to wind accretion from WD (former AGB star). Fig. 1f is the abundance pattern of Sirius and it's approximation by the same, but scaled, theoretical curve. It is obvious that the combination of wind accretion and diffusion can explain the chemical composition of Sirius. Fig. 1g is the abundance pattern of Procyon. The abundances of heavy elements are solar. 0.5 dex overabundance of Te (Z=52) can be explained by fission of transuranium elements with Z>100 (Yushchenko&Gopka, 1996b).

δ Sct. The abundances of 49 elements were found (Yushchenko et al., 2004b). Now we can add several elements to this pattern, the final pattern will be 52-54 elements. The chemical composition of δ Sct is very similar to that of δ Del subtype stars, so it seems reasonable to change the classification of the stars in this region of HR diagram.

3. Conclusion

During the last decade the number of chemical elements investigated in the photospheres of several sharp-lined stars exceeds 50. It permits to find the qualititatively new results. Part of these results are the different production of heavy elements in different Supernova explosions (Yushchenko et al., 2005), the existence of radioactive elements in Przybylski's star (Gopka et al., 2005), the overabundance of Te in Procyon (Yushchenko&Gopka, 1996b), the explanation of the abundance pattern of Sirius as a combination of accretion and diffusion.

Acknowledgements. One of the authors (AY) was supported by the Astrophysical Research Center for the Structure and Evolution of the Cosmos (ARCSEC) of Korea Science and Engineering Foundation (KOSEF) through the Science Research Center (SRC) program.

References

Aoki W., Honda S., Beers T., Sneden C.: 2003, *Astrophys. J.*, **586**, 506.

Cowley C., Ryabchikova T., Kupka F., Bord D., Bidelman W.: 2000, *Mon. Not. Royal Astron. Soc.*, **317**, 299.

Cowley C., Bidelman W., Hubrig S., Mathys G., Bord D.: 2004, *Astron. Astrophys.*, **419**, 1087.

Gopka V.: 2000, *Kinematics Physics Sec. Bodies Suppl. Ser.*, **3**, 364.

Gopka V. et al.: 2005, *Proc. IAU Symp. 224*, Cambridge Univ. Press, 734.

Gopka V., Yushchenko A., Shavrina A., Andrievsky S., Chernysheva L.: 2001, *Kinem. i Fizika Nebesnykh Tel*, **17**, 37.

Grevesse N., Sauval A.: 1998, *Space Science Reviews*, **85**, 161.

Leckrone D., Proffitt C., Wahlgren G., Johansson S., Brage T.: 1999, *Astron. J.*, **117**, 1454.

Shavrina A. et al.: 2003, Astron. Astrophys., **409**, 707.

Sneden C., Cowan J., Ivans I., Fuller G., Burles S., Beers T., Lawler J.: 2000, *Astrophys. J.*, **533**, L139.

Sneden C. et al.: 2003, *Astrophys. J.*, **591**, 936.

Yushchenko A.: 1996, *Odessa Astron. Publ.*, **9**, 84.

Yushchenko A., Gopka V.: 1996a, *Astronomy Letters*, **22**, 412.

Yushchenko A., Gopka V.: 1996b, *Odessa Astron. Publ.*, **9**, 86.

Yushchenko A., Gopka V., Kim C., Musaev F., Galazutdinov G.: 2004a, *Astron. Astrophys.*, **413**, 1105.

Yushchenko A., Gopka V., Kim C., Musaev F., Kang F.: 2004b, preprint astro-ph/0410324.

Yushchenko A. et al.: 2005, *Astron. Astrophys.*, **430**, 255.